1994

Thiacyclophane complexes of silver(I), rhodium(I), iridium(I) and ruthenium(II).

Hilary Anne. Jenkins
University of Windsor

National Library of Canada

Acquisitions and Bibliographic Services Branch

395 Wellington Street
Ottawa, Ontario
K1A 0N4

Bibliothèque nationale du Canada

Direction des acquisitions et des services bibliographiques

395, rue Wellington
Ottawa (Ontario)
K1A 0N4

Your file Votre référence

Our file Notre référence

NOTICE

The quality of this microform is heavily dependent upon the quality of the original thesis submitted for microfilming. Every effort has been made to ensure the highest quality of reproduction possible.

If pages are missing, contact the university which granted the degree.

Some pages may have indistinct print especially if the original pages were typed with a poor typewriter ribbon or if the university sent us an inferior photocopy.

Reproduction in full or in part of this microform is governed by the Canadian Copyright Act, R.S.C. 1970, c. C-30, and subsequent amendments.

AVIS

La qualité de cette microforme dépend grandement de la qualité de la thèse soumise au microfilmage. Nous avons tout fait pour assurer une qualité supérieure de reproduction.

S'il manque des pages, veuillez communiquer avec l'université qui a conféré le grade.

La qualité d'impression de certaines pages peut laisser à désirer, surtout si les pages originales ont été dactylographiées à l'aide d'un ruban usé ou si l'université nous a fait parvenir une photocopie de qualité inférieure.

La reproduction, même partielle, de cette microforme est soumise à la Loi canadienne sur le droit d'auteur, SRC 1970, c. C-30, et ses amendements subséquents.

Canada

Thiacyclophane Complexes of

Ag(I), Rh(I), Ir(I) and Ru(II)

by

Hilary Anne Jenkins

A Dissertation
Submitted to the
Faculty of Graduate Studies and Research
through the Department of Chemistry
and Biochemistry in Partial Fulfillment
of the Requirements for the Degree
of Doctor of Philosophy at
The University of Windsor

Windsor, Ontario, Canada

September, 1994

ISBN 0-612-01406-1

Canada

Name HILARY ANNE JENKINS

Dissertation Abstracts International is arranged by broad, general subject categories. Please select the one subject which most nearly describes the content of your dissertation. Enter the corresponding four-digit code in the spaces provided.

PHYSICAL SCIENCES- CHEMISTRY- INORGANIC
SUBJECT TERM

0488
SUBJECT CODE

U·M·I

Subject Categories

THE HUMANITIES AND SOCIAL SCIENCES

COMMUNICATIONS AND THE ARTS
Architecture 0729
Art History 0377
Cinema 0900
Dance 0378
Fine Arts 0357
Information Science 0723
Journalism 0391
Library Science 0399
Mass Communications 0708
Music 0413
Speech Communication 0459
Theater 0465

EDUCATION
General 0515
Administration 0514
Adult and Continuing 0516
Agricultural 0517
Art 0273
Bilingual and Multicultural 0282
Business 0688
Community College 0275
Curriculum and Instruction 0727
Early Childhood 0518
Elementary 0524
Finance 0277
Guidance and Counseling 0519
Health 0680
Higher 0745
History of 0520
Home Economics 0278
Industrial 0521
Language and Literature 0279
Mathematics 0280
Music 0522
Philosophy of 0998
Physical 0523
Psychology 0525
Reading 0535
Religious 0527
Sciences 0714
Secondary 0533
Social Sciences 0534
Sociology of 0340
Special 0529
Teacher Training 0530
Technology 0710
Tests and Measurements 0288
Vocational 0747

LANGUAGE, LITERATURE AND LINGUISTICS
Language
- General 0679
- Ancient 0289
- Linguistics 0290
- Modern 0291

Literature
- General 0401
- Classical 0294
- Comparative 0295
- Medieval 0297
- Modern 0298
- African 0316
- American 0591
- Asian 0305
- Canadian (English) 0352
- Canadian (French) 0355
- English 0593
- Germanic 0311
- Latin American 0312
- Middle Eastern 0315
- Romance 0313
- Slavic and East European 0314

PHILOSOPHY, RELIGION AND THEOLOGY
Philosophy 0422
Religion
- General 0318
- Biblical Studies 0321
- Clergy 0319
- History of 0320
- Philosophy of 0322

Theology 0469

SOCIAL SCIENCES
American Studies 0323
Anthropology
- Archaeology 0324
- Cultural 0326
- Physical 0327

Business Administration
- General 0310
- Accounting 0272
- Banking 0770
- Management 0454
- Marketing 0338

Canadian Studies 0385
Economics
- General 0501
- Agricultural 0503
- Commerce-Business 0505
- Finance 0508
- History 0509
- Labor 0510
- Theory 0511

Folklore 0358
Geography 0366
Gerontology 0351
History
- General 0578
- Ancient 0579
- Medieval 0581
- Modern 0582
- Black 0328
- African 0331
- Asia, Australia and Oceania 0332
- Canadian 0334
- European 0335
- Latin American 0336
- Middle Eastern 0333
- United States 0337

History of Science 0585
Law 0398
Political Science
- General 0615
- International Law and Relations 0616
- Public Administration 0617

Recreation 0814
Social Work 0452
Sociology
- General 0626
- Criminology and Penology 0627
- Demography 0938
- Ethnic and Racial Studies 0631
- Individual and Family Studies 0628
- Industrial and Labor Relations 0629
- Public and Social Welfare 0630
- Social Structure and Development 0700
- Theory and Methods 0344

Transportation 0709
Urban and Regional Planning 0999
Women's Studies 0453

THE SCIENCES AND ENGINEERING

BIOLOGICAL SCIENCES
Agriculture
- General 0473
- Agronomy 0285
- Animal Culture and Nutrition 0475
- Animal Pathology 0476
- Food Science and Technology 0359
- Forestry and Wildlife 0478
- Plant Culture 0479
- Plant Pathology 0480
- Plant Physiology 0817
- Range Management 0777
- Wood Technology 0746

Biology
- General 0306
- Anatomy 0287
- Biostatistics 0308
- Botany 0309
- Cell 0379
- Ecology 0329
- Entomology 0353
- Genetics 0369
- Limnology 0793
- Microbiology 0410
- Molecular 0307
- Neuroscience 0317
- Oceanography 0416
- Physiology 0433
- Radiation 0821
- Veterinary Science 0778
- Zoology 0472

Biophysics
- General 0786
- Medical 0760

EARTH SCIENCES
Biogeochemistry 0425
Geochemistry 0996
Geodesy 0370
Geology 0372
Geophysics 0373
Hydrology 0388
Mineralogy 0411
Paleobotany 0345
Paleoecology 0426
Paleontology 0418
Paleozoology 0985
Palynology 0427
Physical Geography 0368
Physical Oceanography 0415

HEALTH AND ENVIRONMENTAL SCIENCES
Environmental Sciences 0768
Health Sciences
- General 0566
- Audiology 0300
- Chemotherapy 0992
- Dentistry 0567
- Education 0350
- Hospital Management 0769
- Human Development 0758
- Immunology 0982
- Medicine and Surgery 0564
- Mental Health 0347
- Nursing 0569
- Nutrition 0570
- Obstetrics and Gynecology 0380
- Occupational Health and Therapy 0354
- Ophthalmology 0381
- Pathology 0571
- Pharmacology 0419
- Pharmacy 0572
- Physical Therapy 0382
- Public Health 0573
- Radiology 0574
- Recreation 0575
- Speech Pathology 0460
- Toxicology 0383

Home Economics 0386

PHYSICAL SCIENCES
Pure Sciences
Chemistry
- General 0485
- Agricultural 0749
- Analytical 0486
- Biochemistry 0487
- Inorganic 0488
- Nuclear 0738
- Organic 0490
- Pharmaceutical 0491
- Physical 0494
- Polymer 0495
- Radiation 0754

Mathematics 0405
Physics
- General 0605
- Acoustics 0986
- Astronomy and Astrophysics 0606
- Atmospheric Science 0608
- Atomic 0748
- Electronics and Electricity 0607
- Elementary Particles and High Energy 0798
- Fluid and Plasma 0759
- Molecular 0609
- Nuclear 0610
- Optics 0752
- Radiation 0756
- Solid State 0611

Statistics 0463

Applied Sciences
Applied Mechanics 0346
Computer Science 0984
Engineering
- General 0537
- Aerospace 0538
- Agricultural 0539
- Automotive 0540
- Biomedical 0541
- Chemical 0542
- Civil 0543
- Electronics and Electrical 0544
- Heat and Thermodynamics 0348
- Hydraulic 0545
- Industrial 0546
- Marine 0547
- Materials Science 0794
- Mechanical 0548
- Metallurgy 0743
- Mining 0551
- Nuclear 0552
- Packaging 0549
- Petroleum 0765
- Sanitary and Municipal 0554
- System Science 0790

Geotechnology 0428
Operations Research 0796
Plastics Technology 0795
Textile Technology 0994

PSYCHOLOGY
General 0621
Behavioral 0384
Clinical 0622
Developmental 0620
Experimental 0623
Industrial 0624
Personality 0625
Physiological 0989
Psychobiology 0349
Psychometrics 0632
Social 0451

Abstract

This thesis deals with the synthesis and characterization of several Ag(I), Rh(I), Ir(I), and Ru(II) complexes of tridentate crown thioether ligands. The incorporation of a rigid xylyl group into the macrocyclic backbone causes the ligand 2,5,8-trithia[9]-*o*-cyclophane, TT[9]OC, to have an exodentate conformation in its free state, although the increased ring strain inherent in the *o*-xylyl group permits the ligand to convert to an endodentate conformation, permitting *facial* coordination at a metal atom. The ligand 5-oxa-2,8-dithia[9]-*o*-cyclophane, ODT[9]OC, may also coordinate to metal centres in a *facial* manner.

Chapters 1 and 2 serve as a study of the coordinative ability of TT[9]OC and ODT[9]OC at Ag(I). The 2:1 reaction of TT[9]OC with silver salts results in $[Ag(TT[9]OC)_2]^+$, **1-4**. X-ray diffraction studies indicate that coordination geometries depend on the counterions involved; the ligand TT[9]OC binds to silver through one, two, or all three sulphur donors. In a 2:1 reaction of ODT[9]OC with Ag(I), it was found that only the two sulphur donors coordinate to the metal in complex **5**, $[Ag(ODT[9]OC)_2]^+$. In 1:1 reactions of TT[9]OC with Ag(I), tetranuclear aggregates $[Ag(TT[9]OC)]_4^{4+}$, **6** and **7** are formed. In comparison, the ligand TT[9]MC cannot convert to an endodentate form, and complex **9**, $[Ag(TT[9]MC)]_x^{x+}$, is a polymeric complex.

The complexes $[M(COD)(TT[9]OC)]^+$, (M = Rh, Ir), **10** and **11**, are coordinatively saturated. $[Rh(COD)(TT[9]OC)]^+$ reacts with CO to form an unusual dimeric complex, $[(TT[9]OC)Rh(\mu\text{-}CO)_3Rh(TT[9]OC)]^{2+}$, **15**, but the Ir(I) analog does

not undergo the same type of substitution reaction, and $[Ir(CO)_2(TT[9]OC)]^+$, **18**, is synthesized from the reaction of $[IrCl(COE)_2]_2$ with $AgBF_4$ and TT[9]OC under CO. The products of the reactions of **10** and **11** with $NOBF_4$ decompose quickly in solution due to perturbation of TT[9]OC. The complexes $[M(COD)(ODT[9]OC)]^+$, (M = Rh, Ir), **12** and **13**, are square planar coordinatively unsaturated complexes, both of which undergo substitution reactions with CO to form $[M(CO)_3(ODT[9]OC)]^+$. Reactions with $NOBF_4$ yield products that are thermodynamically more stable that those of **10** and **11**.

The structure of complex **25**, $RuCl_2(PPh_3)(ODT[9]OC)$ shows that the crown thioether ligand is bound to the metal through all three donor atoms, and as well, the aromatic portion of the ligand is bent away from PPh_3, two conformations not previously observed for any of the thiacyclophane complexes studied previously by this group.

This work is dedicated to Ian,

the wonder dog.

I went to find the pot of gold
That's waiting where the rainbow ends
I searched and searched and searched
And Searched and searched and then--
there it was, deep in the grass,
Under an old and twisty bough.
It's mine, it's mine, it's mine at last...
What do I search for now?

Shel Silverstein

Acknowledgements

First and foremost I extend my deepest gratitude to my supervisor, Steve Loeb, for guidance and patience and all of the things for which a student is supposed to thank a boss. One's teacher is not necessarily one's friend, but he has managed both, admirably. Thanks go also to other members of the Loeb lab past and present, especially Broer de Groot, who laid some of the groundwork for my grad study, George Shimizu, and Jim Kickham, who has been a dear and much appreciated friend. The faculty and staff in the department are thanked for all of their assistance, especially Dr. Doug Stephan, Mr. Mike Fuerth, and Mr. Al Ditchburn.

I have been lucky in that my friendships have been lasting and trusting ones, and the people with whom I have shared and will continue to share friendship are in my heart always. I thank my parents, all of them, for their love and support even when they didn't know what I was doing, or why I was doing it. My siblings are sources of constant inspiration; they have taught me more about being the boss than anyone else ever could have. Thanks to the most special people in my life, to John Hilton and the wonders of e-mail, because we've gone through so much at the same time together; to Tricia Breen, frankly, for the same reasons; to Barry Klassen, who has been with me in this from the start; to Bob Berno, who has had to put up with a whole lot of insanity in the last couple of months, and who has done it cheerfully; and especially to my husband Vic, without whom this thesis would not have been completed. I know that things weren't always easy here. Finally, to my vices, The Coffee Exchange, The Upper Canada Brewing Company, and the Toronto Blue Jays...because sometimes ya just gotta get away from it all.

Table of Contents

List of Figures

List of Tables

List of Abbreviations

9S3	1,4,7-trithiacyclononane
Å	Angstrom
br	broad
°C	degrees centigrade
cm	centimetre
COD	1,5-cyclooctadiene
COE	cyclooctene
cryst syst	crystal system
d	doublet
DMF	N,N'-dimethylformamide
DMSO	dimethylsulphoxide
δ	chemical shift
diphos, dppe	1,2-bis(diphenylphosphino)ethane
Et	ethyl
eq	equivalent
F_c	calculated structure factor
F_o	observed structure factor
FTIR	Fourier Transform Infrared
fw	formula weight
g	grams

h	hours
HOMO	highest occupied molecular orbital
Hz	Hertz
IR	infrared
J	joule
K	degrees Kelvin
kJ	kilojoules
λ	wavelength
μ	absorption coefficient
m	multiplet
Me	methyl
m/e^+	mass to charge ratio
MHz	megahertz
min	minutes
mL	millilitres
mmol	millimoles
mol	moles
mp	melting point
ν	frequency
NMR	nuclear magnetic resonance
ODT[9]OC	5-oxa-2,8-dithia[9]-ortho-cyclophane
ORTEP	Oak Ridge Thermal Ellipsoid Plot

Ph	phenyl
ppm	parts per million
q	quartet
ρ	density
R	agreement factor
R_w	weighted agreement factor
s	singlet
t	triplet
T	temperature
THF	tetrahydrofuran
TT[9]MC	2,5,8-trithia-[9]-*meta*-cyclophane
TT[9]OC	2,5,8-trithia-[9]-*ortho*-cyclophane
TT[11]OC	2,5,10-trithia-[9]-*ortho*-cyclophane
X-ray	X-ray diffraction
V	unit cell volume
var	variables
Z	number of molecules in the unit cell

Chapter 1

1.1 Historical Perspective, Nomenclature

Sixty years ago the team of Meadow and Reid[1] at John Hopkins University found that the reaction of sodium ethanedithiolate with ethylene dibromide yields a rubbery foul-smelling polymer and a small amount of the cyclic hexamer 1,4,7,10,13,16-hexathiacyclooctadecane (18S6, shown in Figure 1.2). It was not until thirty years later in 1967, when Charles Pedersen's[2] seminal paper on crown ethers was written describing the syntheses, characterization, and complexation behaviour of thirty-three of these ligands that the importance of macrocyclic ligands and their complexes was realized. Crown ether chemistry grew exponentially, due to their facile syntheses and the ability to prepare derivatives. From Pedersen's crown ethers[3] to the

synthesis of cryptands by Lehn[4], to pendant arm macrocycles made by Gokel[5], to the rigid macrocycles prepared by Cram[6], to Gutsche's[7] calixarenes, to Vögtle's[8] chromogenic crown ethers, to Sauvage's catenands[9], the field is now so varied and wide that entire volumes can only scratch the surface of the available information.

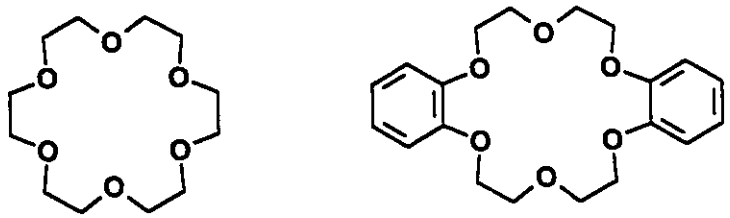

a b

Figure 1.1 Crown ethers synthesized by Pedersen: a) 18-crown-6, and b) dibenzo-18-crown-6.

More recently interest in crown thioethers has increased markedly, and the chemistry of these ligands is enjoying explosive growth. Since the report by Busch and Rosen[10] on S_4 macrocycles, several reviews have appeared detailing various aspects of thioether and crown thioether chemistry. In 1981, Murray and Hartley[11] reviewed the coordinative properties of thioether (R_2S) ligands, indicating that at the time, relatively few thioether complexes had been prepared compared to the numbers of phosphine and amine complexes. Interest in crown thioethers has increased due to four major factors: 1) the possible analogy between the coordination chemistry of thioethers and phosphines, 2) the importance of thioether coordination to the blue copper proteins plastocyanin[12] and azurin[13], 3) synthetic improvements that have made thioethers readily available in high yields, and 4) the availability of X-ray diffraction facilities, a vital tool in a field where

solution studies do not always provide unambiguous information. There are now several comprehensive reviews[14-16] on crown thioether complexes themselves, and this area of chemistry continues to grow rapidly.

Crown thioethers are named in a manner similar to that coined by Pedersen[2] for crown ethers. For example, 1,4,7,10,13,16-hexaoxacyclooctadecane, shown in Figure 1.1 is called 18-crown-6, because 1) the number of atoms in the ring is 18, 2) the ligand can surround a potassium ion, seemingly to "crown" it, and 3) there are six oxygen donor atoms in the molecule. The inclusion of substituents in the macrocyclic ring is noted at the beginning of the common name, so the ligand in Figure 1.1b is called dibenzo-18-crown-6. The extension of this nomenclature to crown thioethers is quite logical, and the ligand shown in Figure 1.2a, analogous to the crown ether in Figure 1.1, is called hexathia-18-crown-6. This naming is almost always shortened to 18S6; the numbers in the name denote ring size and number of sulphur atoms, respectively. Although it is possible that ambiguity in naming may arise due to unsymmetrical substitution of donor atoms in the ring, for crown thioether complexes this is rare and is usually remedied by an alternate naming code specific to the class of ligands.

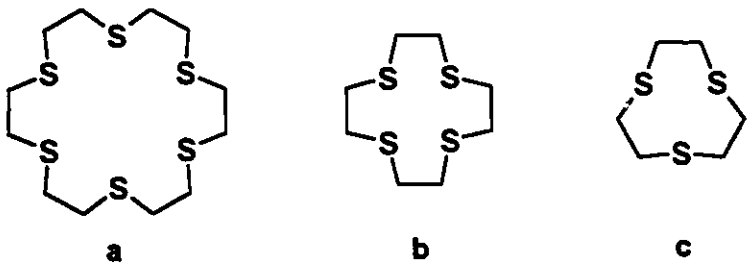

Figure 1.2 a) Hexathia-18-crown-6, or 18S6, first synthesized by Meadow and Reid. b)12S4, c) 9S3.

1.2 Synthesis

A major impediment to the study of crown thioether ligands was the lack of safe, general high-yield synthetic methods. 18S6 was prepared by Meadow and Reid[1] in 1.1% yield, and in 1974 Ochrymowycz[17] improved the yield of this ligand to 33%. However, with the improved yield came the danger in the use of an intermediate, dichloroethylene sulphide (mustard gas), a powerful vesicant. In the same paper, the synthesis of 9S3 was reported in 0.04% yield. Glass[18] improved the yield of 9S3 to 4.4% through the use of the benzyltrimethylammonium salt of the dithiolate and by using high dilution conditions, as shown in Figure 1.3.

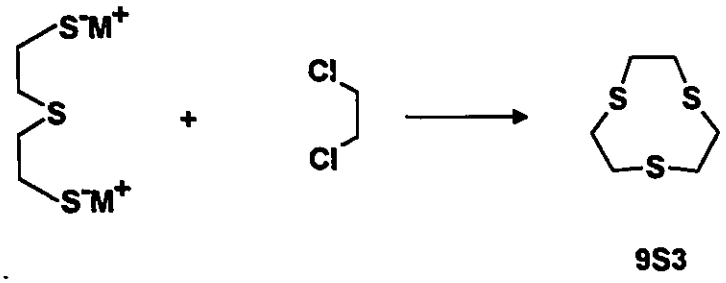

Figure 1.3 Synthesis of 9S3. Ochrymowycz: $M^+ = Na^+$; Glass: $M^+ = BzMe_3N^+$

In 1981 Buter and Kellogg[19] reported a landmark synthesis of crown thioether ligands which was straightforward and safe. The use of cesium carbonate to facilitate the ring closure step of the synthesis greatly reduces polymer formation and greatly increases the yield of the desired product. A ^{133}Cs-NMR study confirms that the cesium ion does not facilitate a template mechanism[20], but instead[14] that the Cs^+ ion promotes cyclization through weak ion pairing with RS^- in DMF, generating exceptionally nucleophilic thiolate anions. Using moderately high dilution conditions and slow addition of reactants,

intramolecular cyclization is favoured over intermolecular polymerization. Crown thioether ligands are now readily available in yields of up to 90% by this general synthetic method[21], and as well, 9S3, 10S3, 12S4, 14S4, 16S4, 15S5, 18S6 and 24S8 are commercially available[22].

There are other approaches to crown thioether synthesis which are not quite as generally applicable as Buter and Kellogg's method, however, they are certainly worth mentioning. In 1984, Sellmann and Zaph[22] reported a template synthesis for 9S3 which was in principle, catalytic and which resulted in a 60% yield of 9S3. The reaction of $Mo(CO)_3(CH_3CN)_3$ with 3-thia-pentane-1,5-dithiol yields the template intermediate $Mo(CO)_3[(SCH_2CH_2)S]_3$; reaction of this complex with ethylene bromide couples the two thiolate termini, and addition of thiol liberates 9S3. There are fewer reports of benzo-thio-crowns, but Sellmann has prepared dibenzo-hexathia-18-crown-6[24], and benzo-9S3[25] using a template mechanism. Kellogg[26] has recently reported a one step cyclization which uses a boron/aluminium alkoxide couple to yield 20S6 derivatives, a method which favours a 2 + 2 cyclization.

1.3 Ligand Conformation

The conformation of a multidentate ligand is an extremely important factor in its design. If the ligand is not predisposed to a conformation suitable for binding, it will have to undergo some kind of conformational change or changes in order to coordinate to a metal centre. In order to quantify the conformation of a particular ligand, parameters such as bond lengths and angles, or displacement from a plane within the ligand, may be

measured in order to indicate inherent strain. However, these parameters can vary widely, even for the same ligand. Dale's pioneering work in conformational studies of oxocrown ethers[27] pointed out that ligand strain is best expressed in terms of torsional angles, and that in fact, by trading strain into torsional variations, the ligand's conformation is optimized by the least expenditure in energy[27b]. Sensitive measures of the strain inherent in a molecule would be the deviations from ideal torsional angles of 60° (*gauche* placement) or 180° (*anti* placement).

The preference for *gauche* placement originates at least in part from differences in 1,4-interactions at C-S and C-C bonds. For oxocrowns, electron-nuclear attraction, or dispersion forces, between the oxygen atoms stabilizes a *gauche* arrangement. However, a thiacrown in the same conformation is destabilized due to the greater size of the sulphur atoms compared to oxygen. Alternatively, a *gauche* placement for the CCOC unit causes repulsion between the terminal protons of the unit in oxocrowns, whereas for CCSC the repulsion does not occur due to the longer C-S bond in thiacrowns. These interactions can usually dictate the conformation at a given bond in an ethyl-linked symmetrical crown thioether molecule. This is illustrated schematically in Figure 1.4.

The strong preference of CSCC and SCCS bonds to favour *gauche* and *anti* placements respectively, results in the sulphur atoms of -$SCH_2CH_2SCH_2CH_2S$- linkages pointing out of the macrocyclic ring[29,30]. De Simone and Glick referred to this conformation as exodentate[31], as opposed to the endodentate conformation of oxygen donors in oxocrown ethers. In a thorough study of a series of crown thioethers in 1987, Cooper[28] realized that the conformational preferences of the C-S and C-C bonds act in

concert to generate "bracket" S-C-C-S-C-C-S units, in which the central sulphur atom acts as a corner, as shown in Figure 1.5. These bracket units form the fundamental building blocks of crown thioethers; for example, 12S4 is composed of two such bracket units.

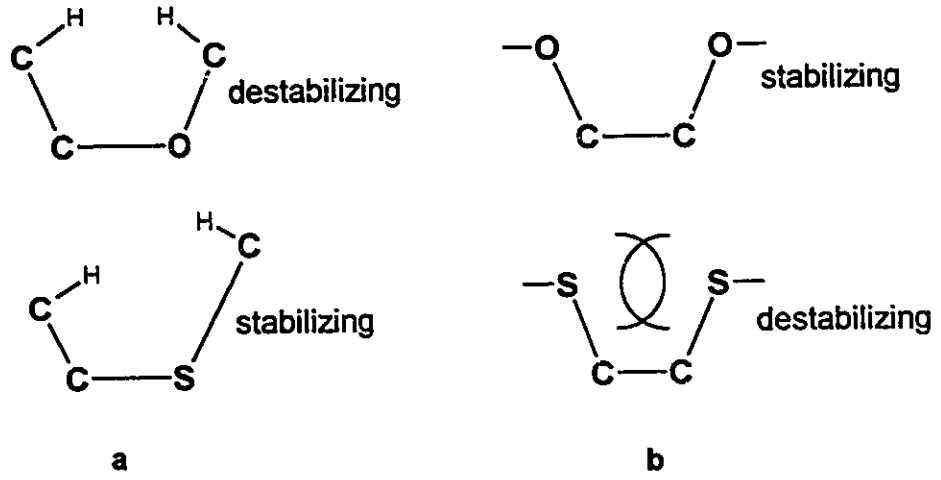

Figure 1. 4 a) 1,4-interactions in *gauche* CCEC linkages. b) 1,4-interactions in *gauche* ECCE linkages.

The ligand 9S3 crystallizes in an endodentate conformation, unlike other crown thioethers; this was shown by Glass[32] in 1980. The reason for this anomaly is the inherent ring strain in the small nine-membered ring, which results in a conformation that closely resembles that required for a metal chelation. Exodentate thioether ligands have to undergo a change in conformation to an endodentate form in order to encapsulate or cap a metal atom. However, 9S3, which is already endodentate, does not require any conformational change to bind to a metal centre. At the same time, the ligand is not easily

synthesized in yields greater than 60%, due to its inherent ring strain, and therefore the increased likelihood of formation of larger rings or polymeric materials.

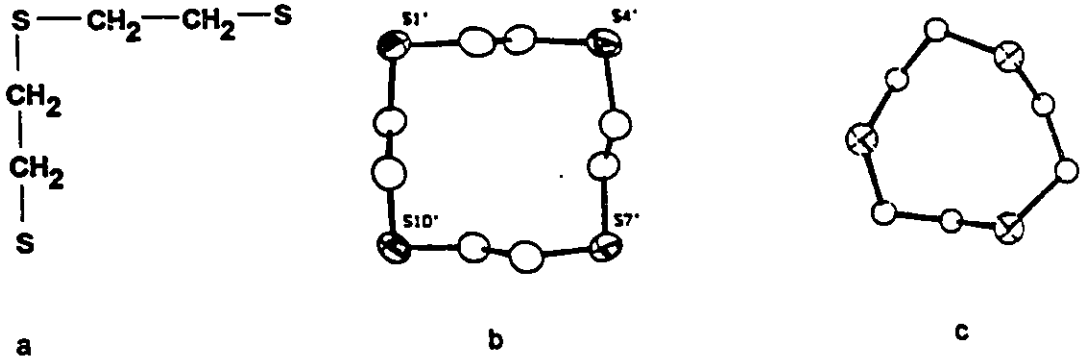

a b c

Figure 1.5 The -$SCH_2CH_2SCH_2CH_2S$- bracket unit, which resembles a right angle in projection, with the central sulphur atom at the corner. b) The ORTEP drawing of 12S4. c) The ORTEP drawing of 9S3

The fact that the endodentate conformation of 9S3 predisposes it to coordination at a metal centre has inspired intense investigations into the chemistry of metal 9S3 complexes, led by Cooper[14,15], Schröder[16], and Wieghardt[33]. The ligand exhibits tridentate *facial* coordination in a variety of environments, from tetrahedral in the complexes $[Cu(AsPh_3)(9S3)]^+$ [34] and [Ag(9S3)Cl] [35], to trigonal bipyramidal in $[Ni(9S3)(dppm)]^{2+}$ [36], and $[Rh(COD)(9S3)]^+$ [37], to a multitude of complexes with octahedral environments, including many bis-chelated complexes[14-16], as shown in Figure 1.6. 9S3 has also been observed to adapt to other metal coordination spheres in which facial coordination is not possible for the ligand. The complexes $[Pd(9S3)]^{2+}$ [38,33b], $[Pt(9S3)]^{2+}$ [39], and $[Au(9S3)]^{3+}$ [40], all show square planar geometry, where the metal atom is coordinated to two sulphur

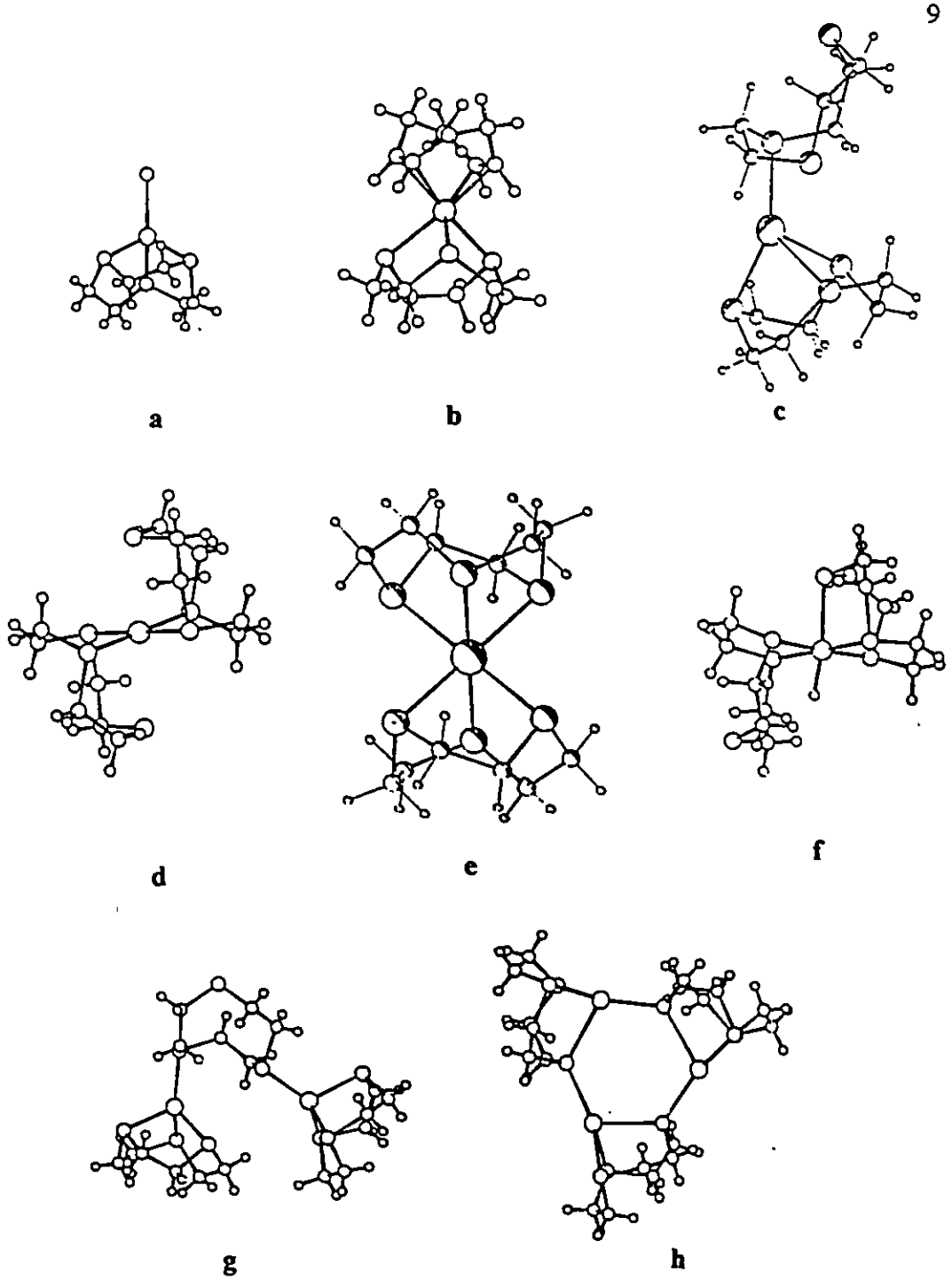

Figure 1.6 Various metal complexes of 9S3: a) Cu[CuI(9S3)], b) $[Rh(COD)(9S3)]^{+}$, c) $[Au(9S3)_2]^{2+}$, d) $[Pd(9S3)_2]^{2+}$, e) $[Au(9S3)_2]^{3+}$, f) $[IrH(9S3)_2]^{2+}$, g) $[Cu_2(9S3)_3]^{2+}$, h) $[Ag(9S3)]_3^{3+}$

donors from each ligand. The third donor atom in each case is oriented toward the metal centre, but lies outside the bonding distance. As well, two 9S3 ligands can have two different coordination modes at the same metal centre, as observed for $[Au(9S3)_2]^+$ [40], in which one ligand coordinates facially to the Au(I) centre through all three sulphur donors, and the second 9S3 ligand coordinates to the metal only through one sulphur donor, similar to $[Cu(9S3)_2]^+$ [41]. Another example of this type of coordination is in the complex $[IrH(9S3)_2]^{2+}$ [42]; one ligand coordinates *facially*, while the second binds to the metal through two sulphur donors, and the hydride ligand completes the octahedral coordination sphere. In the complex $[Ag(9S3)]_3^{3+}$ prepared by Wieghardt[43], 9S3 is bound to Ag(I) in a *facial* manner, but one of the sulphur donors also acts as a bridge to the next metal atom. As well, Cooper[44] has shown that 9S3 can bridge two independent metal centres in the complex $[Cu_2(9S3)_3]^{2+}$, in which one ligand binds to each of the metal centres through two sulphur donors and the third donor atom remains free.

Among crown thioethers, 9S3 stands alone in its remarkable ability to chelate to late transition metals. Metal complexes in unfavourable geometries or oxidation states (monomeric Rh(II), Pd(III), Pt(III), and octahedral Ag(I), Au(III), Hg(II), and low spin Co(II) anions)[14-16] often are sufficiently robust to permit isolation when coordinated to this ligand, as indicated in the survey of coordination geometries, above. The strong ligating ability of 9S3 derives from its predisposition to a suitable coordination geometry for metal binding, due to the endodentate arrangement of its donor ligands.

1.4 Bonding

The bond angles about the sulphur atom in all thioether molecules are approximately tetrahedral, consistent with sp^3 hybridization of sulphur and two lone pairs on the atom, one of which can be donated to a metal centre[11]. An alternative viewpoint is that the two lone pairs be classed as an "s-type" and a "p-type"[45]. Neither description fully accounts for the observed coordination chemistry of thioether ligands, and theoretical and structural studies suggest that thioethers possess two donor orbitals[46]. The HOMO of free thioethers is primarily 3p in character and is perpendicular to the R-S-R plane, while the second orbital, of slightly lower energy and still 3p in character, is localized along the bisector of the R-S-R angle. In the free thioether, with C_{2v} symmetry, the orbitals belong to the $1b_1$ and $2a_1$ representations respectively, but on complexation symmetry at sulphur is reduced to Cs and the donor orbitals belong to an a' representation and are free to mix. The extent to which the $1b_1$ and $2a_1$ orbitals mix can be measured by the tilt angle, α, between the M-S vector and the bisector of the R-S-R angle. If there is no mixing at all and $1b_1$ is the principle donor orbital, then a tilt angle, α, of 90° results (Figure 1.7). If the orbitals contribute equally as donors then a tilt angle of 135° results. For comparison, if sulphur is sp^3-hybridized then a tilt of 125.25° results[47].

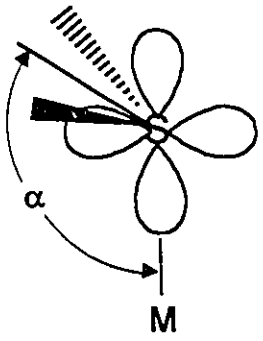

Figure 1.7 Coordinated thioether hybridization; α is the tilt angle between the M-S vector and the bisector of the R-S-R angle.

The mixing of the $1b_1$ and $2a_1$ orbitals of the free thioether upon coordination to the metal centre is described in terms of two orthogonal ligand orbitals, which are principally sulphur 3p in character. The new orbitals lie in the plane normal to the R_2S plane, bisecting the R-S-R angle. One orbital is approximately σ-donating, the other is oriented for π-donation to the metal. For 9S3, the $1b_1$-type orbitals are endodentate, whether the ligand is complexed[48] to a metal or not[32], and the molecule compensates for repulsive interactions between the sulphur atoms (see Figure 1.3) by increasing the SCCS torsion angle, which then increases the intersulphur distances and directs the sulphur lone pairs slightly away from the molecule's C_{3v} axis. When 9S3 is complexed to a metal, the M-S bonds compensate for the repulsion between sulphur atoms, and therefore the SCCS torsion angle and the intersulphur distances are shorter than in the free ligand. Overall, there is a slight trigonal distortion at the metal centre, resulting from an optimization of

orbital overlap between the thioether σ-donor orbitals with the empty π-acceptor metal orbitals[47].

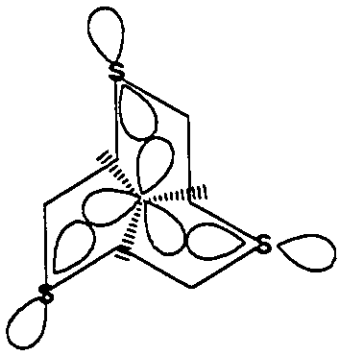

Figure 1.8 Trigonal distortion that results from optimization of orbital overlap between thioether σ-donor orbitals and empty metal π-acceptor orbitals.

1.5 Thiacyclophanes

It has been shown that 9S3 has the ability to coordinate to a wide variety of metal centres, enforcing unusual conformational geometries and/or stabilizing unusual oxidation states. The question of how the incorporation of a rigid xylyl group into the backbone of 9S3 would affect complexation to a metal, was initally approached by Vögtle[8], who reported the syntheses of trithia-*meta*-cyclophanes in 1976, in low yields (4-5%). In 1990 Loeb[49,50] reported the syntheses and improved yields of the ligands 2,5,8-trithia[9]-*ortho*-cyclophane, TT[9]OC, and 2,5,8-trithia[9]-*meta*-cyclophane, TT[9]MC, employing the cesium-mediated synthesis of Buter and Kellogg[19]. Shown in Figure 1.9 below, the *ortho*- and *meta*-S_3 ligands can be modified for various applications. The similarity of these ligands to 9S3 is obvious, and although the macrocyclic rings are

slightly larger, the incorporation of the rigid xylyl groups limits the conformational flexibility of the ligand, and provides a measure of steric control and predictability to the design of the ligands[49]. Whereas for alphatic crown thioether molecules the torsional angles dictate the conformation of the ligand, in this case the aromatic moiety could contribute to or even dictate the free ligand conformation.

The ligand TT[9]OC is exodentate in the free state, however, there is some distortion in the ring due to the constraint in the *o*-xylyl bracket. This ring strain allows for conformational flexibility in the ligand, and in fact TT[9]OC coordinates *facially* to a variety of metal atoms; such as in the complexes $Mo(CO)_3(TT[9]OC)$[49], $[Cu(PPh_2Me)(TT[9]OC)]^+$[54], and $[Ag(PPh_3)(TT[9]OC)]^+$[54]. Molecular mechanics calculations on TT[9]OC showed that the energy difference between the all exodentate conformation (70.3 $kJmol^{-1}$) and the all endodentate conformation (82.8 $kJmol^{-1}$) is not large, at 12.5 $kJmol^{-1}$, and that both conformations showed inherent ring strain[49]. In contrast, the effect of the *meta*-xylyl group in TT[9]MC is to prevent S_3 *facial* coordination by reinforcing a rigid exodentate conformation[50]. This factor prompted the preparation of 2,6,10-trithia[11]-*meta*-cyclophane, (TT[11]MC)[51]. Complexation of this ligand to Pd(II) yielded a palladated product in which all three sulphur donors as well as the carbon atom at the *two*-position of the xylyl ring participated in the square planar coordination sphere of the metal centre. The ligand TT[11]MC was the starting point for a rich variety of chemistry[52] that extends into the realm of molecular recognition[4] through simultaneous first- and second-sphere coordination to nucleobases[53].

Modification of the ligands by increasing the length of the alkyl chains or by changing the central donor atom in the macrocyclic ring expands the realm of available chemistry considerably. This thesis concentrates on the ligands TT[9]OC and its oxo-derivative ODT[9]OC in studies of their coordination chemistry to silver(I), and in studies of reaction chemistry of their Rh(I), Ir(I), and Ru(II) complexes.

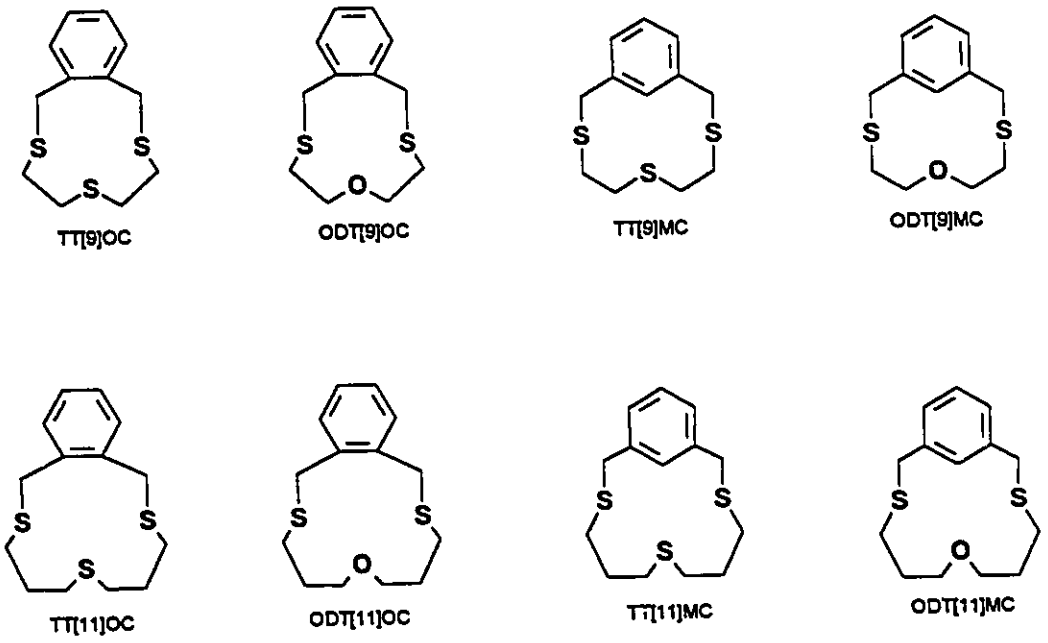

Figure 1.9 Thiacyclophane ligands.

Chapter 2

2.1 Introduction

It is known that crown thioether ligands generally favour the adoption of an exodentate conformation, in which the sulphur donor atoms are oriented out of the macrocyclic cavity[11,14-16,55]. An exception to this generality is the ligand 1,4,7-trithiacyclonane (9S3), which , due to its small size and overall rigidity, adopts an endodentate conformation[32]. This endodentate, or crown, conformation of the free ligand pre-disposes it towards facial coordination at a metal atom. In fact, it has been observed that complexation requires almost no conformational change, and therefore, it can be concluded that any thermodynamic barrier to ligand-metal binding is effectively removed. In order to synthesize a crown thioether molecule larger than 9S3 with an endodentate conformation, some inherent strain in the molecule must be included. To this end, the incorporation of xylyl rings into the macrocyclic ring can serve to either a) limit the

conformational flexibility of the macrocycle or b) introduce strain into the macrocyclic backbone, which could then result in an endodentate conformation or disposition toward such a conformation. The ligand 2,5,8-trithia[9]-*o*-cyclophane (TT[9]OC), while it is exodentate in the free state, easily converts to an endodendate conformation to act as a *facial* capping ligand in such complexes as $[Mo(CO)_3(TT[9]OC)]$[49], $[Cu(PPh_2Me)(TT[9]OC)][ClO_4]$[54a], $[Ag(PPh_3)(TT[9]OC)][ClO_4]$[54a], $[PdCl_2(TT[9]OC)]$[50], and $[Rh(COD)(TT[9]OC)][BF_4]$[56].

It has been shown previously that substitution of oxygen donors with sulphur donors in crown ethers alters the complexation properties of the macrocyclic ligand markedly[30]. With this replacement, the affinity of the crown ether macrocycles for Group 1 and 2 metal ions decreases, while affinity for transition metal ions increases. This change in complexation properties has been found to be applicable to extraction and transport of heavy metal ions such as Ag(I)[57]. In this chapter, the difference in the complexation properties to Ag(I) when a thioether sulphur atom is replaced by an oxygen donor in a crown thioether macrocycle will be investigated.

This chapter describes the synthesis and structure of the ligand 5-oxo-2,8-dithia[9]-*ortho*-cyclophane and the syntheses and structures of a series of complexes of general formula $[AgL_2][X]$, (L = TT[9]OC, ODT[9]OC) (X = ClO_4^-, BF_4^-, BPh_4^-, $CF_3SO_3^-$), in which the solid state structures vary with the type of noncoordinating anion. The variety of conformations for TT[9]OC complexes observed in the solid state and the solution behaviour of the $[Ag(TT[9]OC)_2]^+$ cations demonstrate that the metal-promoted interconversion of the ligand conformations is a low energy process for

this macrocyclic thioether ligand[58] . For ODT[9]OC, it is found that this ligand adopts only one coordination mode at the silver atom regardless of the counterion, and that the metal-ligand complex is also fluxional in solution.

2.2 Experimental

TT[9]OC[54a] and $AgBPh_4$[59] were prepared by the literature methods. $AgClO_4$, $AgBF_4$, $AgCF_3SO_3$, Cs_2CO_3, α,α'-dibromo-*o*-xylene, 3-oxapentane-1,5-dithiol, all organic reagents, and all solvents were purchased from Aldrich and used as received. All reactions were conducted under an atmosphere of N_2 using standard Schlenk techniques and all solvents were degassed prior to use. ^1H and $^{13}C\{^1H\}$NMR spectra were recorded at 300.1 and 75.4 MHz respectively on a Bruker AC300 spectrometer locked to the deuterated solvent. Infrared spectra were recorded on a Nicolet 5DX FTIR spectrometer. Elemental analyses were performed by Microanalytical Services, Delta, British Columbia, Canada. Cyclic voltammetric experiments were performed using a BAS CV-27 potentiostat with a platinum disk working electrode, a Ag/AgCl reference electrode and $[NBu_4][PF_6]$ as the supporting electrolyte. All potentials are quoted versus ferrocene/ferrocinium, Fc/Fc^+.

2.2.1 Preparation of 5-Oxa-2,8-dithia[9]-*o*-cyclophane, (ODT[9]OC)

Cesium carbonate (11.58 g, 60 mmol) was suspended in DMF (600 mL) under an atmosphere of N_2. To this mixture was added a solution of α,α'-dibromo-*o*-xylene (7.92 g, 30 mmol) and 3-oxapentane-1,5-dithiol (4.38 g, 30 mmol) in DMF (150 mL) at a rate of approximately one drop/10 sec. The temperature of the reaction was maintained at 70

°C. After addition, the mixture was cooled to room temperature and stirred for a further 12 h. The DMF was removed under vacuum and the resulting solid residue extracted with CH_2Cl_2 (200 mL). The CH_2Cl_2 fraction was extracted with 0.05M NaOH (2 x 125 mL), and then dried over anhydrous Na_2SO_4. After filtration and removal of the solvent, the solid residue was recrystallized from anhydrous ethanol. Yield: 5.8 g (80 %). $^{13}C\{^1H\}$ NMR ($CDCl_3$): δ 137.17, 130.79, 127.59 (aromatic), 72.20 (OCH_2), 33.97 (benzylic), 32.57 (SCH_2). ^1H NMR ($CDCl_3$): δ 7.20 (m, 4 H, aromatic), 4.31 (s, 4H, benzylic), 3.83 (t, 4H, CH_2O), 2.81 (t, 4 H, SCH_2). mp 140-142 °C. Anal. Calcd for $C_{12}H_{16}OS_2$: C, 59.95; H, 6.72. Found: C, 59.81; H, 6.72.

2.2.2 Preparation of $[Ag(TT[9]OC)_2][X]$; ($X = ClO_4^-, BF_4^-, BPh_4^-, CF_3SO_3^-$), (1-4)

To a solution of TT[9]OC (0.100 g, 0.390 mmol) in CH_3CN (10 mL), was added AgX (0.195 mmol). The resulting colourless solution was stirred at room temperature in the dark for 3 h. The solvent was removed under reduced pressure and the crude white product recrystallized by vapour diffusion of diethyl ether into an acetonitrile solution of the complex. **(1)**: $X = ClO_4^-$, Yield, 135 mg (96 %). Anal. Calcd for $C_{24}H_{32}AgClO_4S_6$: C, 40.02; H, 4.49; S, 26.71. Found: C, 39.98; H, 4.33; S, 26.44. **(2)**: $X = BF_4^-$, Yield, 90 mg (90 %). Anal. Calcd for $C_{24}H_{32}AgBF_4S_6$: C, 40.73; H, 4.57; S, 27.19. Found: C, 40.12; H, 4.44; S, 26.56. **(3)**: $X = CF_3SO_3^-$, Yield, 144 mg (96 %). Anal. Calcd for $C_{25}H_{32}AgF_3O_3S_7$: C, 39.00; H, 4.20; S, 29.16. Found: C, 38.88; H, 4.10; S, 28.93. **(4)**: $X = BPh_4^-$, Yield, 150 mg (91 %). Anal. Calcd for $C_{48}H_{52}AgBS_6$: C, 61.32; H, 5.59; S, 20.47. Found: C, 60.87; H, 5.32; S, 20.38. ^1H NMR (CD_3CN, cation resonances only): δ 7.28-7.41 ppm

(m, 4H, aromatic), 3.90 (s, 4H, benzylic), 2.83-2.93 ppm (m, 8H, $SCH_2CH_2SCH_2CH_2S$). $^{13}C\{^1H\}$ NMR (CD_3CN, cation resonances only): δ 136.68, 131.83, 129.21 (aromatic), 33.68 (benzylic), 33.55, 32.62 (SCH_2). ^1H NMR spectra of 3 and 4 were also recorded at 170K in $(CD_3)_2CO$: δ 7.41 (br s, 4H, aromatic), 4.12 (br d, 4H, benzylic), 3.69 (br m, 4H, SCH_2).

2.2.3 Preparation of $[Ag(ODT[9]OC)_2][BF_4]$, (5)

To a solution of ODT[9]OC (247 mg, 1.03 mmol) in CH_3CN (15 mL), was added $AgBF_4$ (100 mg, 0.514 mmol). The resulting colourless solution was stirred at room temperature in the dark for 3 h. The solvent was removed under reduced pressure and the crude white product recrystallized from vapour diffusion of diethyl ether into a CH_3CN solution of the complex. $^{13}C\{^1H\}$ NMR (CD_3CN): δ 135.53, 130.85, 128.65 (aromatic) 70.68 (OCH_2), 36.76 (benzylic), 34.69 (SCH_2). Yield, 319 mg, (92%). Anal. Calcd for $C_{24}H_{32}AgBF_4S_4O_2$: C, 42.67; H, 4.78; S, 18.99. Found: C, 42.36; H, 4.67; S, 18.74. ^1H NMR (CD_3CN): δ 7.27 (m, 4H, aromatic), 4.10 (s, 4H, benzylic), 3.73 (m, 4H, OCH_2), 2.94 (m, 4H, SCH_2).

2.2.4 General X-ray Diffraction Data Collection, Solution and Refinement

All diffraction experiments were performed on a four-circle Rigaku AFC6S diffractometer with graphite monochromatized Mo Kα radiation. Cell constants and orientation matrices for data collection were obtained from least-squares refinements using the setting angles of 25 centred reflections. The intensities of three standard reflections

were recorded periodically and showed no statistically significant changes over the duration of the data collections. An empirical absorption correction, based on ψ-scan data was applied to each data set. The data sets were processed by using the TEXSAN software package running on a SGI Workstation[60]. Refinements were carried out by using full-matrix least-squares techniques on F minimizing the function $\Sigma w(|F_o|-|F_c|)^2$, where $w = 1/\sigma^2(F_o)$ and F_o and F_c are the observed and calculated structure factors. Atomic scattering factors[61] and anomalous dispersion terms[62,63] were taken from the usual sources. Fixed H-atom contributions were included with C-H distances of 0.95 Å and thermal parameters 1.2 times the isotropic thermal parameter of the bonded C atoms. No H atoms were refined, but all values were updated as refinement continued. Summaries of crystal data, intensity collection, and structure refinement are listed in Table A.2.1, A.2.4, A.2.7, A.2.10., and A.2.13.

2.2.5 X-ray Structure Determination of 5-oxa-2,8-dithia[9]-*o*-cyclophane, ODT[9]OC

Colourless crystals of ODT[9]OC were grown by cooling a concentrated ethanol solution of the ligand to -20° C for 24 hours. A statistical analysis of intensity distributions and a determination of systematic absences were consistent with the space group *C2/c* and this was confirmed by successful solution refinement. A total of 1184 reflections were collected and 1121 unique reflections with $F_o^2 > 3\sigma(F_o^2)$ were used in the refinement. The oxygen and sulphur atom positions were determined by direct methods from the E map with the highest figure of merit and the remaining carbon atoms were located from

successive difference Fourier map calculations. In the final cycles of refinement, all non-hydrogen atoms were refined anistropically, resulting in $R = \Sigma||F_o|-|F_c||/\Sigma|F_o| = 4.11\%$ and $R_w = (\Sigma w (|F_o|-|F_c|)^2 / \Sigma w F_o^2)^{1/2} = 5.60\%$ at final convergence. A goodness of fit calculation resulted in a value of 1.91. The Δ/σ value for any parameter in the final cycle was less than 0.001 and a final difference Fourier map calculation showed no peaks of chemical significance; the largest was 0.367 e/Å^3 and was associated with the oxygen atom. Atomic positional parameters are summarized in Table A.2.2 and selected bond distances and angles are summarized in Table A.2.3.

2.2.6 X-ray Structure Determination of $[Ag(TT[9]OC)_2][ClO_4]$, (1)

Colourless crystals of $[Ag(TT[9]OC)_2][ClO_4]$ were grown by vapour diffusion of diethyl ether into an acetonitrile solution of the complex. A statistical analysis of intensity distributions and a determination of systematic absences were consistent with the space group $P2_1/n$ and this was confirmed by a successful solution refinement. 5139 reflections were collected and 1577 unique reflections with $F_o^2 > 3\sigma(F_o^2)$ were used in the refinement. The position of the silver atom was determined by the conventional heavy-atom method and the remaining non-hydrogen atoms were located from difference Fourier map calculations. In the final cycles of refinement, the silver, sulphur, chlorine, and oxygen atoms were assigned anisotropic thermal parameters and the carbon atoms were assigned isotropic thermal parameters. This resulted in $R = 7.06\%$ and $R_w = 7.58\%$ at final convergence. A goodness of fit calculation resulted in a value of 1.74. The Δ/σ value for any parameter in the final cycle was less than 0.01 and a final difference Fourier map

calculation showed no peaks of chemical significance. Atomic positional parameters are summarized in Table A.2.5 and selected bond distances and angles are summarized in Table A.2.6.

2.2.7 X-ray Structure Determination of $[Ag(TT[9]OC)_2][BPh_4]$, (3)

Colourless crystals of $[Ag(TT[9]OC)_2][BPh_4]$ were grown by vapour diffusion of diethyl ether into an acetonitrile solution of the complex. A statistical analysis of intensity distributions and a determination of systematic absences were consistent with the space group *C*2/*c* and this was confirmed by a successful solution refinement. 4058 reflections were collected and 1495 unique reflections with $F_o^2 > 3\sigma(F_o^2)$ were used in the refinement. The position of the silver atom was determined by the conventional heavy-atom method and the remaining non-hydrogen atoms were located from difference Fourier map calculations. In the final cycles of refinement, the silver, sulphur, boron atoms, and the carbon atoms of TT[9]OC were assigned anisotropic thermal parameters, whereas the carbon atoms of the BPh_4^- anion were input as rigid phenyl groups and assigned isotropic thermal parameters. The central sulphur atom, S2, of TT[9]OC displayed two-fold disorder and was successfully modelled with site occupancy factors of 72 and 28 %. This resulted in $R = 6.79\%$ and $R_w = 6.90\%$ at final convergence. A goodness of fit calculation resulted in a value of 1.86. The Δ/σ value for any parameter in the final cycle was less than 0.01 and a final difference Fourier map calculation showed no peaks of chemical significance. Selected atomic positional parameters are summarized in Table A.2.8 and selected bond distances and angles are summarized in Table A.2.9.

2.2.8 X-ray Structure Determination of $[Ag(TT[9]OC)_2][CF_3SO_3]$, (4)

Colourless crystals of $[Ag(TT[9]OC)_2][CF_3SO_3]$ were grown by vapour diffusion of diethyl ether into an acetonitrile solution of the complex. A statistical analysis of intensity distributions was consistent with the space group $P\bar{1}$ and this was confirmed by a successful solution refinement. 5622 reflections were collected and 2815 unique reflections with $F_o^2 > 3\sigma(F_o^2)$ were used in the refinement. The positions of the silver atom and four of the seven sulphur atoms were determined by direct methods from the E map with highest figure of merit. The remaining non-hydrogen atoms were located from a difference Fourier map calculation. In the final cycles of refinement, the silver, sulphur, and carbon atoms of the cation were assigned anisotropic thermal parameters and the anion was input as rigid CF_3 and SO_3 groups, each with 2-fold disorder, and overall isotropic group thermal parameters. This resulted in $R = 6.76\%$ and $R_w = 7.28\%$ at final convergence. A goodness of fit calculation resulted in a value of 2.02. The Δ/σ value for any parameter in the final cycle was less than 0.04 and a final difference Fourier map calculation showed no peaks of chemical significance. Selected atomic positional parameters are summarized in Table A.2.11 and selected bond distances and angles are summarized in Table A.2.12.

2.2.9 X-ray Structure Determination of $[Ag(ODT[9]OC)_2][BF_4]$, (5)

Colourless crystals of $[Ag(ODT[9]OC)_2][BF_4]$ were grown by vapour diffusion of diethyl ether into an acetonitrile solution of the complex. A statistical analysis of intensity distributions and a determination of systematic absences were consistent with the space

group *Cc*. A total of 2583 reflections were collected and 1501 unique reflections with $F_o^2 > 3\sigma(F_o^2)$ were used in the refinement. The positions of the silver atom and two sulphur atoms were determined by direct methods from the *E* map with highest figure of merit and the remaining non-hydrogen atoms were located from a difference Fourier map calculation. In the final cycles of refinement, all of the non-hydrogen atoms were assigned anisotropic thermal parameters. This resulted in $R = 3.05\%$ and $R_w = 3.88\%$ at final convergence. A goodness of fit calculation resulted in a value of 1.75. The Δ/σ value for any parameter in the final cycle was less than 0.001, and a final difference Fourier map calculation showed no peaks of chemical significance; the largest was 0.687 e/Å^3, and was associated with the Ag atom. Atomic and positional parameters are listed in Table A.2.14 and selected bond distances and angles are listed in Table A.2.15.

2.3 Results

2.3.1 Synthesis and X-ray Structure of ODT[9]OC

The cesium-mediated synthesis developed by Buter and Kellogg[19] is now the method of choice for the preparation of crown thioether complexes and indeed, the synthesis of ODT[9]OC is straightforward, resulting in a high yield (80%) of colourless crystalline product. The method was discussed and explained in the introductory chapter of this thesis and Equation 2.1 outlines the synthetic procedure.

The ^{1}H NMR spectrum of ODT[9]OC in $CDCl_3$ shows the expected multiplet pattern for *ortho*-aromatic substitution at δ 7.20 ppm, and a single peak for the benzylic protons at δ 4.31 ppm. The OCH_2CH_2S linkage is oberved as two well separated triplets at

δ 3.83 ppm for OCH_2 and δ 2.81 ppm for CH_2S. The $^{13}C\{^1H\}$ NMR spectrum of ODT[9]OC is straightforward, exhibiting three well defined resonances for the aromatic carbons at δ 137.17, 130.79, and 127.59 ppm, and separate resonances for the OCH_2, benzylic, and SCH_2 carbons at δ 72.20, 33.97, and 32.57 ppm respectively.

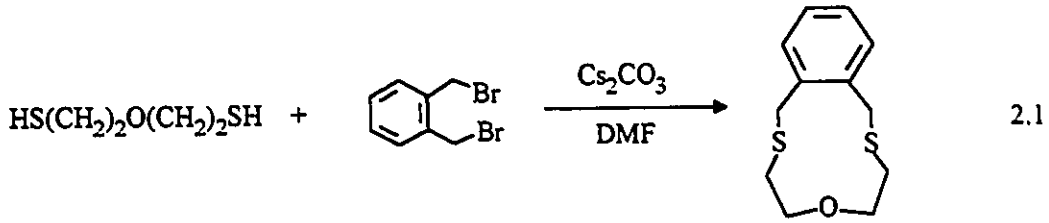

2.1

In the structure determination of ODT[9]OC, it was found that the unit cell contains four discrete molecules of the ligand. The molecule has crystallographic two-fold site symmetry. A perspective view of ODT[9]OC, indicating the atom numbering scheme, is shown in Figure 2.1a. Sulphur-carbon bond distances are 1.805(6) and 1.822(5) Å for S1-C5 and S1-C6 respectively, and the oxygen-carbon bond distance O1-C4 is 1.269(5) Å. Carbon C(sp^2) - C (sp^2) distances range from 1.363(7) to 1.414(8) Å; the C(1) - C(4) (sp^3 - sp^3) distance is 1.445(7) Å, and the C(2) - C(3) (sp^3 - sp^2) distance is 1.478(6)Å. These distances compare well to those found previously for other thiacyclophanes and mixed S, O donor macrocyclic ethers[28,49,55,57,64]. The C-C-S-C torsion angle is 161.6(3)°. A full listing of torsional angles is given in Table 2.1. The angle between the plane of the aromatic ring and the plane formed by S1, C4, C5, and O1 is 38.10°, measured as shown in Figure 2.1b.

a.

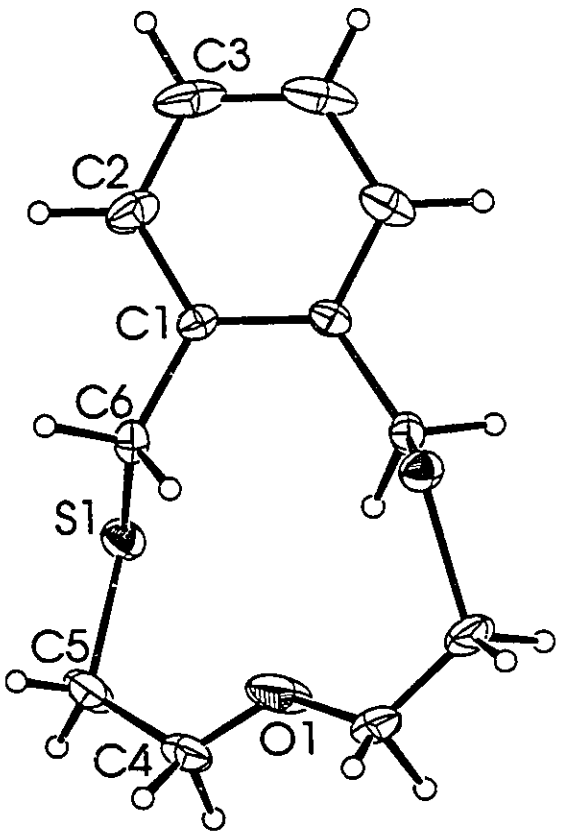

Figure 2.1 Perspective ORTEP drawings of the ligand ODT[9]OC, showing: a) the atom numbering scheme. Bond Distances: S1-C5 1.805(6), S1-C6 1.822(5), O1-C4 1.269(5)Å. Bond Angles: C5-S1-C6 101.0(3)°, C4-O1-C4' 134.1(7)°. Torsion angles C1-C6-S1-C5 161.6(3)°, C4'-O1-C4-C5 -180.0(7)°, S1-C5-C4-O1 20.9(8)°. b) the angle between the plane formed by the aromatic ring of ODT[9]OC and the plane formed by S1,C4,C5, and O1 is 38.10°.

b.

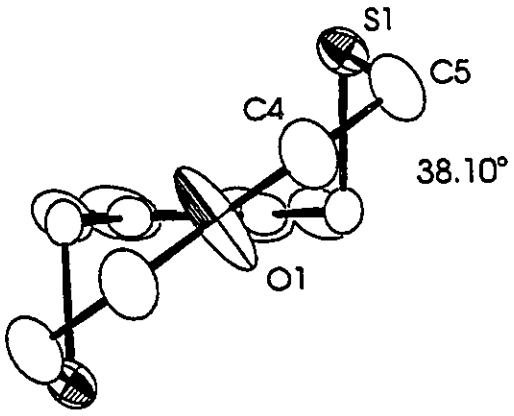

Table 2.1 Torsional Angles[a] of ODT[9]OC[b]

ODT[9]OC	angle
S1-C6-C1-C1'	-76.3(6)
C6-C1-C1'-C6'	-2.9(9)
C1-C6-S1-C5	161.6(3)
C4-C5-S1-C6	-71.2(5)
S1-C5-C4-O1	20.9(8)
C4'-O1-C4-C5	-180.0(7)
S1-C6-C1-C2	102.9(5)

[a] Sign is positive for a clockwise rotation of 1 to 4 viewed down the 2-3 bond.
[b] See Figure 2.1 for atom numbering scheme.

2.3.2 Synthesis and Solution Studies of Ag(I) Complexes

Silver(I) complexes of the formula $[Ag(TT[9]OC)_2][X]$, where X is one of the non-coordinating anions ClO_4^-, BF_4^-, BPh_4^-, or $CF_3SO_3^-$, were prepared by reacting two equivalents of TT[9]OC with one equivalent of AgX in CH_3CN at room temperature. The complex $[Ag(CDT[9]OC)_2][BF_4]$ is prepared in an analogous manner. The resulting colourless solids can be isolated in >90 % yield and are recrystallized by vapour diffusion of diethyl ether into CH_3CN solutions of the complexes. The crystalline materials are air stable and only $[Ag(TT[9]OC)_2][BPh_4]$ shows sensitivity to light, gradually becoming darker in colour with exposure.

The ^1H NMR spectra of $[AgL_2][X]$ complexes exhibit characteristics of a highly fluxional system. The only solvent in which all five complexes have comparable solubilities is CD_3CN, and at 300K averaged signals are observed for aromatic (δ 7.28-7.41 ppm; multiplet, 4H), benzylic (δ3.90 ppm; singlet, 4H), and SCH_2CH_2S (δ 2.83-2.93; multiplet,

8H) protons. When the samples were cooled to 235K in CD_3CN, broadening and loss of resolution occurred for all of these resonances. The complexes $[Ag(TT[9]OC)_2][CF_3SO_3]$ and $[Ag(TT[9]OC)_2][BPh_4]$ were soluble in acetone, and cooling $(CD_3)_2CO$ solutions of these complexes to 170K provided some further resolution of their ^1H NMR spectra. At this temperature the aromatic protons of the ligand are completely unresolved, resulting in a broad peak at δ 7.41 ppm (4H), but the benzylic protons are split into a very broad pair of doublets, δ 4.12 ppm (4H), and the methylenic protons of the SCH_2CH_2S chain are separated into a large, broad multiplet, centred at δ 3.69 ppm (4H), and a broad doublet, at δ 3.24 ppm (4H). The ^1H NMR spectrum of $[Ag(ODT[9]OC)_2][BF_4]$, **5** at 300K in CD_3CN is very similar to the ^1H NMR spectra of the TT[9]OC complexes, showing a multiplet at δ 7.27 (4H) ppm for aromatic protons, a singlet at δ 4.10 ppm (4H) for the benzylic protons, and broad multiplets at δ 3.73 ppm (4H) for OCH_2 and δ 2.94 ppm (4H) for SCH_2. On cooling to 235K, any observed resolution is lost as the resonances broaden at this limiting temperature. Complex **5** showed very limited solubility in acetone, and a low temperature (170K) spectrum of the complex in this solvent could not be obtained.

Even though the ^1H NMR spectra for the $[Ag(TT[9]OC)_2][X]$ complexes are broad and mostly unresolved, the gross features of the spectra are similar to the well resolved limiting ^1H NMR spectra for such complexes as $[Cu(TT[9]OC)(PPh_3)][ClO_4]$[54a] and $[Mo(TT[9]OC)(CO)_3]$[49], where TT[9]OC is coordinated in an endodentate conformation, *facially*, on the metal atom. Similarly, the ^1H NMR spectrum of $[Ag(ODT[9]OC)_2][BF_4]$ resembles the spectrum of the complex

$[Rh(COD)(ODT[9]OC)][BF_4]$[56], in which the oxygen atom is not coordinated to the metal atom.

The possibility of oxidizing of the Ag(I) cation to a Ag(II) species, which has been observed for $[Ag(9S3)_2]^+$, $[Ag(18S6)]^+$, and $[Ag(16S6)]^+$ [35,65-67], was investigated. Cyclic voltammetry of $[Ag(TT[9]OC)_2]^+$ in CH_3CN (0.1 M $[NBu_4][PF_6]$) at platinum electrodes showed an oxidation at E_{pa} = 0.70 V versus Fc/Fc^+ which is essentially irreversible; only a small return wave was observed, indicating that the oxidized product is unstable in CH_3CN at 298K. This is similar to the results observed for $[Ag(9S3)_2]^+$, $[Ag(18S6)]^+$, and $[Ag(16S6)]^+$. The S_6 homoleptic coordination sphere found in these crown thioether complexes results in relatively low oxidation potentials, E_{pa} = 0.79, 1.00 and 0.87 respectively, and are attributed to a higher electron density at the metal centre which promotes oxidation.

2.3.3 X-ray Structure of $[Ag(TT[9]OC)_2][ClO_4]$, (1)

The unit cell contains four $[Ag(TT[9]OC)_2]^+$ cations and four $[ClO_4]^-$ anions. A perspective view of the $[Ag(TT[9]OC)_2]^+$ cation for this complex is shown in Figure 2.2. The Ag atom is in an S_6 thioether environment with approximate octahedral geometry. Both the TT[9]OC ligands are in endodentate conformations and these two tridentate ligands sandwich the metal ion. Figure 2.7 shows that the relative orientation of the TT[9]OC ligands is such that the cation has a molecular centre of symmetry, although this is not imposed crystallographically. The Ag-S distances are 2.771(6), 2.725(5), 2.712(6) and 2.709(5) Å for S1, S3, S4 and S6 attached to the xylyl fragment, and 2.752(6) and

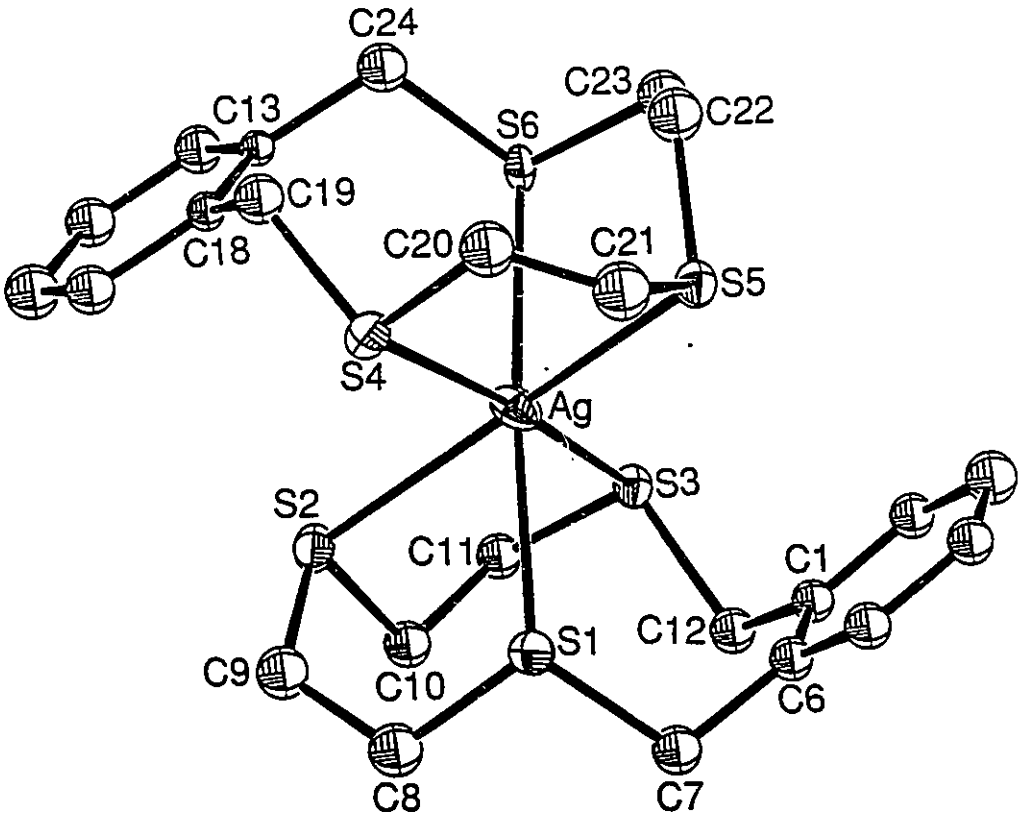

Figure 2.2 Perspective ORTEP drawing of the $[Ag(TT[9]OC)_2]^+$ cation for complex 1, [X] = ClO_4^-, showing the atom numbering scheme. Bond distances: Ag-S1 2.771(6), Ag-S2 2.752(6), Ag-S3 2.725(5), Ag-S4 2.788(6), Ag-S5 2.712(6), Ag-S6 2.709(5) A. Bond angles: S1-Ag-S2 77.3(2)°, S1-Ag-S3 96.3(2)°, S1-Ag-S4 83.6(2)°, S2-Ag-S5 96.4(2)°, S2-Ag-S6 175.8(2)°, S2-Ag-S3 79.5(2)°, S2-Ag-S4 94.6(2)°, S2-Ag-S5 171.2(2)°, S2-Ag-S6 105.9(2)°, S3-Ag-S4 173.9(2)°, S3-Ag-S5 107.7(2)°, S3-Ag-S6 81.8(2)°, S4-Ag-S5 78.3(2)°, S4-Ag-S6 98.7(2)°, S5-Ag-S6 80.6(2)°

2.788(6) Å for the central S2 and S4 atoms. The S-Ag-S angles for the five-membered chelate rings are 77.3(2), 79.5(2), 78.3(2) and 80.6(2)°, and the S-Ag-S angles for the seven-membered chelate rings involving the *o*-xylyl fragment are 96.3(2) and 98.7(2)°. The S-C and C-C bond distances are all within expected limits. The ClO_4^- anion has expected tetrahedral geometry and the Cl-O bond distances and O-Cl-O angles are normal.

2.3.4 X-ray Structure of $[Ag(TT[9]OC)_2][BPh_4]$, (3)

The unit cell contains four $[Ag(TT[9]OC)_2]^+$ cations and four $[BPh_4]^-$ anions, each of which has crystallographic two-fold site symmetry. A perspective view of the $[Ag(TT[9]OC)_2]^+$ cation for this complex is shown in Figure 2.3. The Ag atom is in a severely distorted tetahedral coordination sphere defined by two S atoms from each TT[9]OC ligand with the central S atom of each ligand oriented away from the metal centre. Figure 2.7 shows the relative orientation of the TT[9]OC ligands and emphasizes the crystallographic 2-fold axis relating the halves of the cation. The Ag-S distances are 2.688(4) and 2.548(2) Å for S1 and S3 and 3.183(5) and 3.94(5) Å for the two sites of the disordered, non-bonded central S2 atom. The S1-Ag-S3 angle for the seven-membered chelate ring is 103.7(1)° and the inter-ligand angles are 90.1(2), 104.3(1) and 140.0(2)° for S1-Ag-S1', S1-Ag-S3' and S3-Ag-S3'. The S-C and C-C bond distances are all within expected limits. The BPh_4^- anion has expected tetrahedral geometry and the B-C bond distances and C-B-C angles are normal.

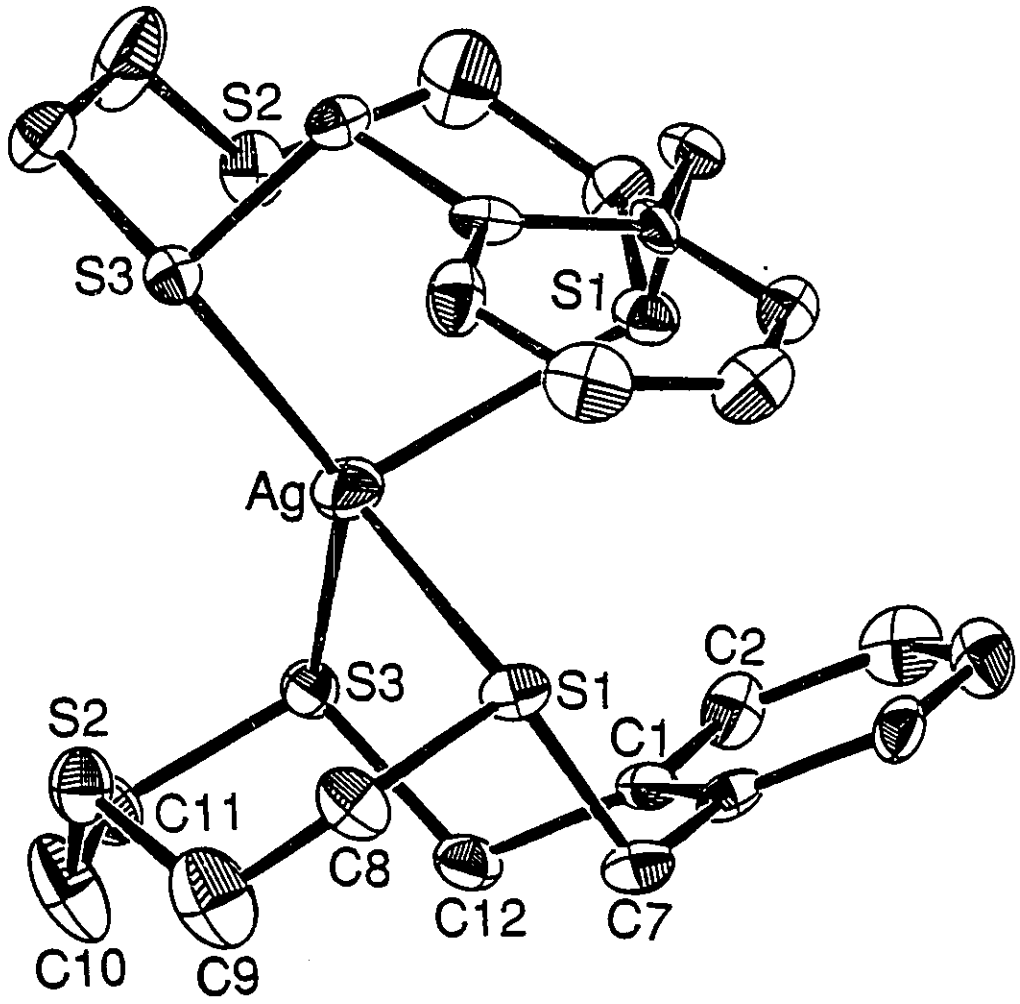

Figure 2.3 Perspective ORTEP drawing of the $[Ag(TT[9]OC)_2]^+$ cation for complex 3, [X] = BPh_4^-, showing the atom numbering scheme. Bond distances: Ag-S1 2.688(4) Ag-S3 2.548(3)Å, Ag...S2 3.183(5) and 3.94(2)Å for site occupancy of 72 and 28% respectively. Bond angles: S1-Ag-S3 103.7(1)°, S1-Ag-S1' 90.1(2)°, S1-Ag-S3' 104.3(1)°, S3-Ag-S3' 140.0(2)°.

2.3.5 X-ray Structure of $[Ag(TT[9]OC)_2][CF_3SO_3]$, (4)

The unit cell contains two $[Ag(TT[9]OC)_2]^+$ cations and two $[CF_3SO_3]^-$ anions. A perspective view of the $[Ag(TT[9]OC)_2]^+$ cation for this complex is shown in Figure 2.4. The Ag atom is in a tetrahedral coordination sphere. Three of the coordination sites are occupied by the sulphur atoms of one TT[9]OC ligand, which is in an endodentate conformation and coordinates in a *facial* manner to the metal atom, and the fourth site is occupied by a sulphur atom of another TT[9]OC ligand, which is in an exodentate conformation.

The Ag-S distances to the endodentate ligand are 2.600(4), 2.590(3), and 2.570(3) Å for S1, S2, and S3 respectively, and 2.476(2) Å to the S4 atom of the exodentate ligand. The S-Ag-S angles for the five-membered chelate rings are 84.6(1)° and 85.2(1)°, and the S-Ag-S angle for the seven-membered chelate ring is 107.3(1)°. The S-Ag-S angles between the exodentate and endodentate ligands are 106.0(1)°, 133.8(1)°, and 130.4(1)° to S1, S2, and S3 respectively. The S-C and C-C bond distances are all within expected limits. The only refined distance in the $CF_3SO_3^-$ anion was the S-C distance, which was disordered over two sites with distances of 1.74(2) and 1.75(2) Å.

2.3.6 X-ray Structure of $[Ag(ODT[9]OC)_2][BF_4]$, (5)

The unit cell contains four $[Ag(ODT[9]OC)_2]^+$ cations and four $[BF_4]^-$ anions each of which has crystallographic two-fold site symmetry. A perspective view of the $[Ag(ODT[9]OC)_2]^+$ cation of the complex is shown in Figure 2.5. The Ag atom is in a tetrahedral coordination sphere defined by the two sulphur atoms from each ODT[9]OC

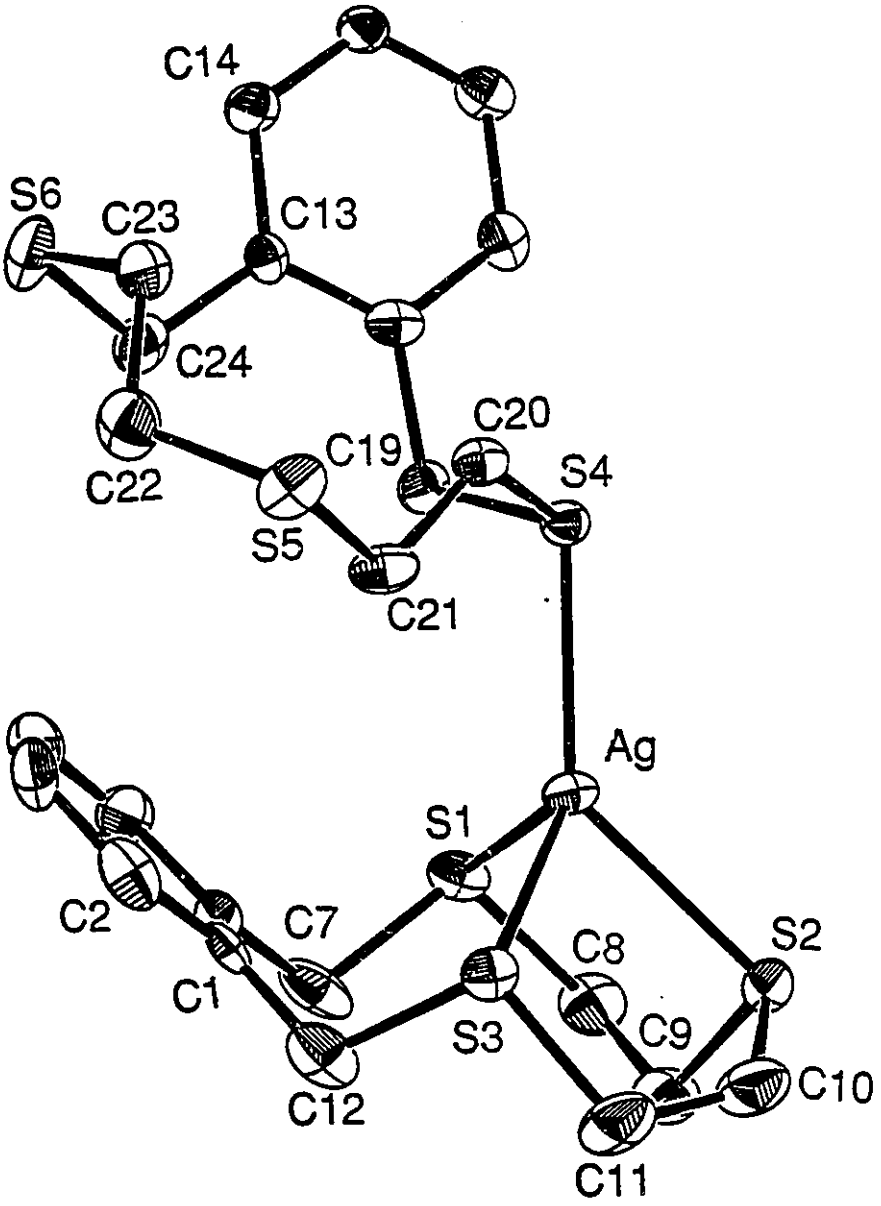

Figure 2.4 Perspective ORTEP drawing of the $[Ag(TT[9]OC)_2]^+$ cation for complex 4, [X] = $CF_3SO_3^-$, showing the atom numbering scheme. Bond Distances: Ag-S1 2.600(4), Ag-S2 2.590(3), Ag-S3 2.570(3), Ag-S4 2.476(3) Å.Non-bonded distances: Ag...S5 5.251(4), Ag...S6 7.115(5)Å. Bond Angles: S1-Ag-S2 84.6(1)°, S1-Ag-S3 107.3(1)°, S1-Ag-S4 106.0(1)°, S2-Ag-S3 85.2(1)°, S2-Ag-S4 133.8(1)°, S3-Ag-S4 130.4(1).

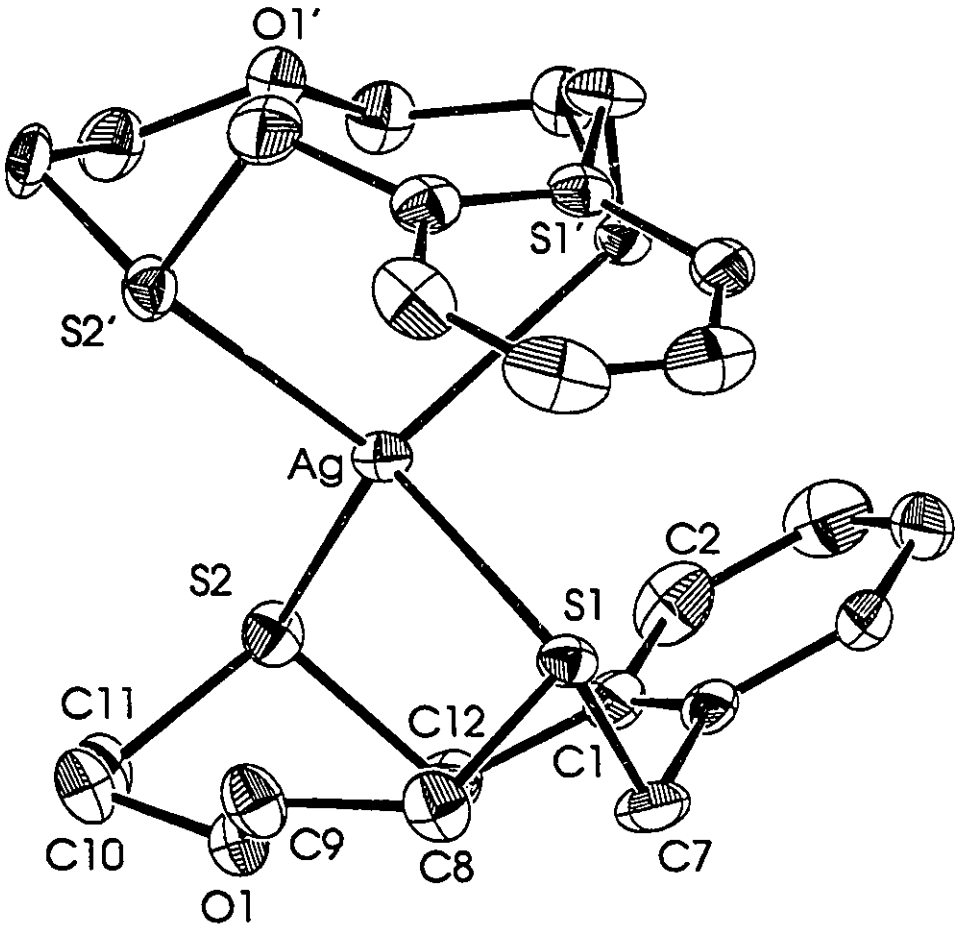

Figure 2.5 Perspective ORTEP drawing of the $[Ag(ODT[9]OC)_2]^+$ cation for complex 5, [X] = BF_4^-, showing the atom numbering scheme. Bond Distances: Ag-S1 2.630(2), Ag-S2 2.571(2)Å; Ag...O1 nonbonded distance is 3.294(4)Å. Bond Angles: S1-Ag-S2 107.02(5)°, S1-Ag-S1' 96.59(7)°, S1-Ag-S2' 115.62(5)°, S2-Ag-S2' 113.96(8)°.

ligand; the central oxygen atoms are oriented away from the metal centre. The Ag-S distances are 2.630(2), and 2.571(2) Å for S1 and S2 respectively; the Ag-O non-bonding distance is 3.294(4) Å. The S1-Ag-S2 angle for the seven-membered chelate ring is 107.02(5)° , and the interligand angles are as follows: S1-Ag-S1' 96.59(7)°, S1-Ag-S2' 115.62(5)°, S2-Ag-S2' 113.96(8)°. The S-C, O-C, and C-C distances are all within expected limits. The BF_4^- anion has expected tetrahedral geometry and the B-F bond distances and F-B-F angles are normal.

2.4 Discussion

2.4.1 Ligand Conformations

The previously determined X-ray structure of TT[9]OC shows that this molecule is essentially an *o*-xylyl fragment fused to a $SCH_2CH_2SCH_2CH_2S$ chain such that the ligand adopts an exodentate conformation with the sulphur donors oriented away from the centre of the macrocyclic cavity[49]. In general, the overall structures of thiacyclophane molecules are best described in terms of the torsional angles associated with the $S(CH_2)_nS(CH_2)_nS$ linkage, and the orientation of the xylyl fragment with respect to the aliphatic chain. An interesting structural feature of TT[9]OC is that the $SCH_2CH_2SCH_2CH_2S$ linkage shows SCCS torsional angles averaging 162(4)°, compared to 180° for the ideal "bracket" conformation usually observed in thioethers[15,64a], as discussed in the introductory chapter of this thesis. The effect of this distortion is to introduce strain into the $SCH_2CH_2SCH_2CH_2S$ unit, and therefore the overall energy difference between exodentate and endodentate conformations of the ligand is small. Molecular mechanics calculations

show that the energy difference is significantly less than between exodentate and endodentate conformations of the isomeric 2,5,8-trithia[9]-*m*-cyclophane (TT[9]MC), in which the exodentate conformation has a low energy minimum, compared to the endodentate conformation which is significantly higher. Similarly for TT[11]OC (Figure 2.6), the propyl linkages provide a longer, more flexible aliphatic chain, which is less strained, and the difference in the energy minima between endodentate and exodentate conformations is small. Therefore, although the introduction of an *ortho*-xylyl fragment does not result in preorganization of the sulphur donor sites as in 9S3, it does perturb the conformation to favour an exodentate to endodentate transformation.

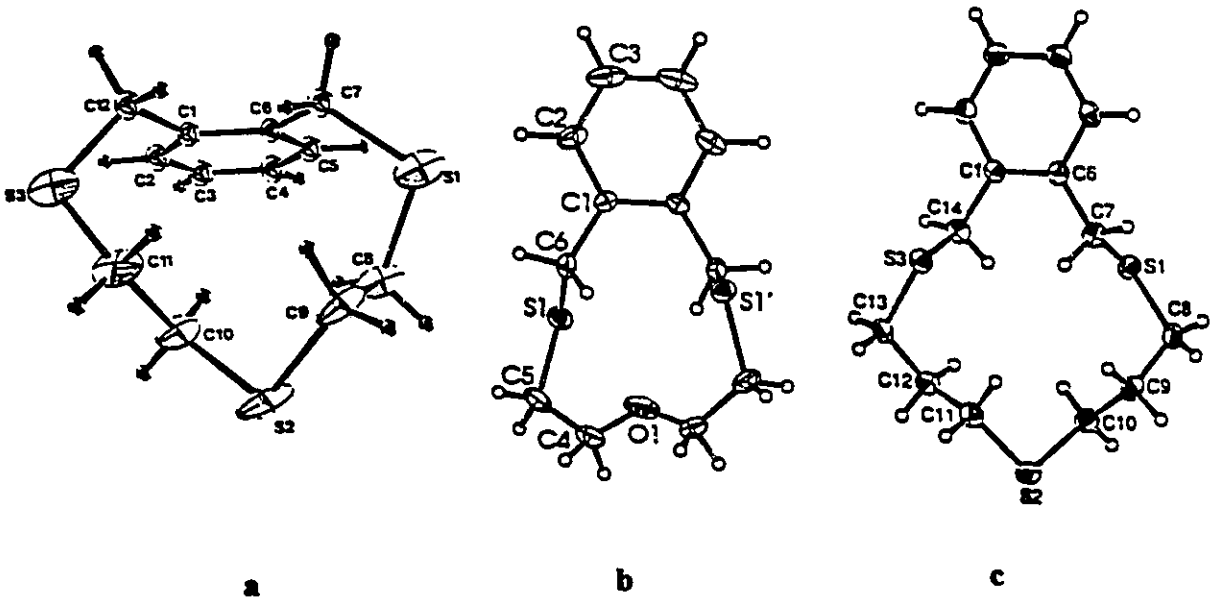

a b c

Figure 2.6 Perspective ORTEP drawings of a) TT[9]OC, b) ODT[9]OC, and c) TT[11]OC, showing the atom numbering schemes.

ODT[9]OC however, contains two sulphur donors, which are exodentate as expected, and an endodentate oxygen donor. Similar to TT[11]OC[11], the C(benzylic)-S

bonds are positioned on opposite sides of the aromatic ring, and the $SCH_2CH_2OCH_2CH_2S$ chain "loops" around from one face of the aromatic ring to the other. The major difference between ODT[9]OC and TT[11]OC is the orientation of the oxygen atom compared to that of the central sulphur atom. The central sulphur atom of TT[11]OC, similar to that in TT[9]OC, is exodentate, while in ODT[9]OC the oxygen atom is endodentate.The SCCO torsional angle is 20.9(8)°, and CCSC torsional angle is constrained to 161.6(3)°, but the COCC torsional angle is in an ideal *anti* conformation at -180.0(7)°. This factor, coupled with the inherent ring strain that results from a short alphatic chain connecting at *ortho* positions on the xylyl fragment, provides a macrocycle that can easily convert to a *facial* geometry.

2.4.2 Coordination of Ag(I) to TT[9]OC, Solution Studies

Silver(I) is an ideal metal centre for investigating the coordination chemistry of thioether ligands[15,35,43,67] and mixed-donor macrocyclic ligands[59,69,71]. The metal shows a strong affinity for thioether donors[71], and Ag(I) has weak stereochemical demands, often yielding complex geometries dictated by the conformational preferences of the ligand, rather than the bonding demands of the metal ion[54a,67]. Since there appear to be relatively small energy differences between the possible ligand conformations for TT[9]OC, it might be expected that in solution the structure of $[Ag(TT[9]OC)_2]^+$ would be fluxional due to metal-promoted interconversions between conformations. This is exactly what is observed, and is reminiscent of several $[Ag(15S5)_n]^+$ (n = 1, 2, n) complexes prepared by Schröder[69], where each of the three complexes showed only a single peak in their $^{13}C\{^1H\}$ NMR

spectra. For the silver complexes of TT[9]OC and ODT[9]OC, the ^{1}H NMR spectra at 300K are consistent with a highly fluxional system independent of the anion in the complex. Low temperature spectra were not reported by Schröder, but in the system presented in this chapter these spectra are consistent with a symmetrical coordination mode. Since electrochemical measurements show oxidation potentials similar to those of other complexes with an S_6 coordination sphere, octahedral geometry is assumed to be favoured for the $[Ag(TT[9]OC)_2]^+$ cations in solution.

2.4.3 Coordination of Ag(I) to TT[9]OC, Solid State Studies

Overall, the unexpected result from this study is that the solid state structures observed for the $[Ag(TT[9]OC)_2]^+$ cations are dependent upon the noncoordinating anions. Since there are no significant cation-anion interactions in the solid state, the effect of X^- on the structure of $[Ag(TT[9]OC)_2]^+$ must be the crystal packing compatability of $[Ag(TT[9]OC)_2]^+$ and X^-. It appears that each differently shaped and sized anion "directs" crystallization of a different form of $[Ag(TT[9]OC)_2]^+$. If it is assumed that there is rapid interchange of the cationic structures in solution, as borne out by the ^{1}H NMR evidence, it may be that the species that crystallizes is simply the least soluble one due to a favourable cation-anion match.

For the "spherical" anions ClO_4^- and BF_4^- (complexes **1** and **2**), both TT[9]OC ligands are in an endodentate conformation, resulting in pseudooctahedral geometry about the silver atom. The same coordination geometry occurs for $[Ag(9S3)_2]^+$ and is attributed to the preorganized, endodentate conformation of 9S3[35]. However, as mentioned in

Section 2.4.1, the ability to enforce facial coordination at a metal centre appears to be possible with TT[9]OC, in spite of the lack of preorganization to an endodentate conformation. For the larger spherical anion X = BPh_4^- in complex **3**, both TT[9]OC ligands adopt an unusual conformation in which the sulphur atoms adjacent to the xylyl ring are endodentate and coordinated to the metal centre, while the two central sulphur atoms remain exodentate. Figure 2.7a and b show the relative orientations of the ligands for complexes **1** and **3**, and demonstrate the difference between the coordination geometries of the cations. Figure 2.7c serves as a further comparison to the structure of cation **5**, $[Ag(ODT[9]OC)_2]^+$, in which the central oxygen atoms do not coordinate to the silver atom but are endodentate to the macrocyclic ring. The relationship between the structures of **1** and **3** (Figure 2.7a and b) can be thought of as a 90° rotation about the vector along which the drawings in Figure 2.7 are projected. This would occur with a concomitant breaking of the Ag-S2 bonds and a conformational change to make S2 exodentate. This is similar to the rhombic, or Ray-Dutt, twist used to describe racemization in octahedral, tris chelate complexes[72]. The interconversion of octathedral complexes through this type of distorted tetrahedral intermediate may represent a feasible pathway for the observed fluxionality of complexes **1 - 4** in solution.

The structure of cation **4**, in which the counterion is $CF_3SO_3^-$, is the most significant of the series. $[Ag(TT[9]OC)_2][CF_3SO_3]$ is the first example of a crown thioether complex in which both the exodentate and endodentate conformations of a macrocycle are bonded to the same metal ion. The conformation observed for the terminally bound, exodentate ligand is essentially the same as that found in the X-ray

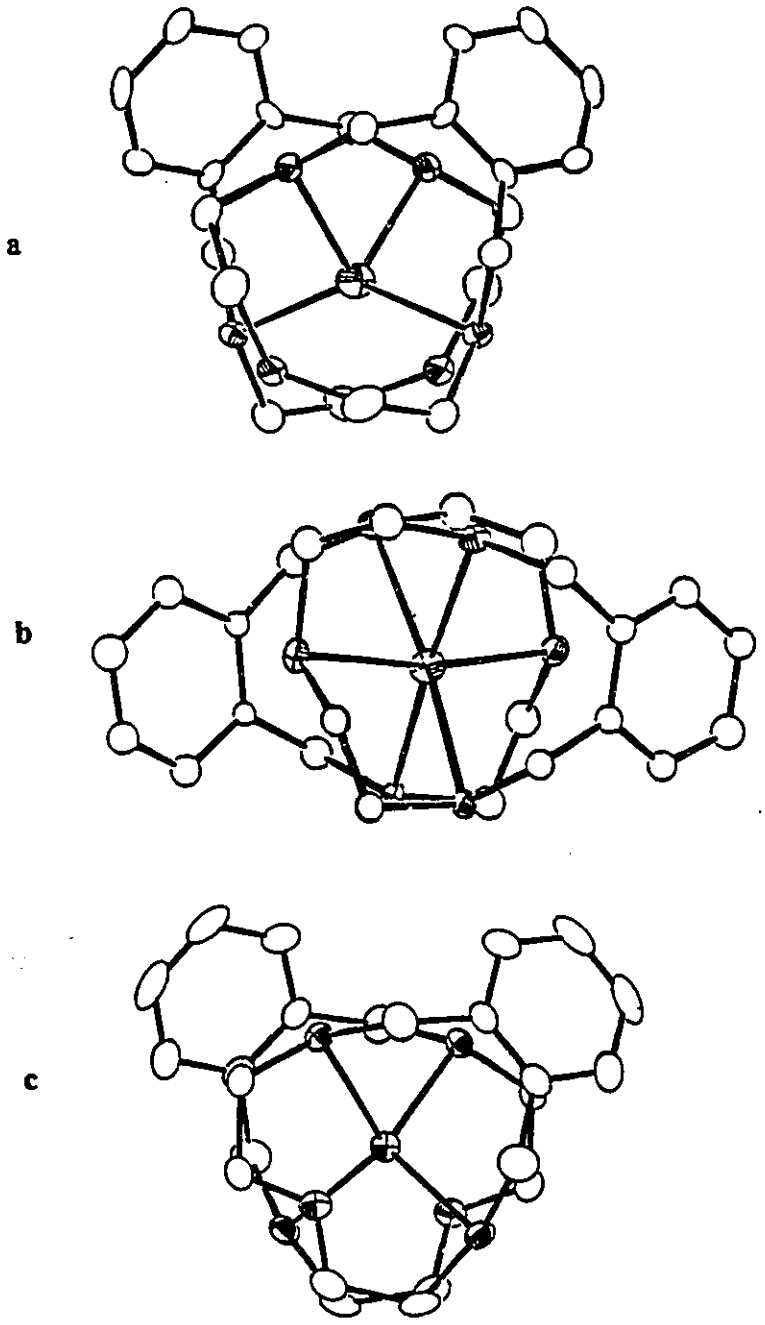

Figure 2.7 Perspective ORTEP drawing of a) $[Ag(TT[9]OC)_2]^+$ cation for complex 1, b) $[Ag(TT[9]OC)_2]^+$ cation for complex 2, $[Ag(TT[9]OC)_2]^+$ cation for complex 3, and c) $[Ag(ODT[9]OC)_2]^+$ cation for complex 5, showing the relative orientations of the ligands.

structure of the free ligand[49]. The corresponding structural parameters for the endodentate ligand compare very closely to those found for the pseudotetrahedral complex $[Ag(PPh_3)(TT[9]OC)][ClO_4]$, in which PPh_3 occupies the fourth coordination site, rather than an exodentate TT[9]OC molecule[54a]. Table 2.2 is a partial list of the torsional angles in TT[9]OC for the different $[AgL_2]^+$ cations as well as the torsional angles in ODT[9]OC for complex **5**. Although there are some differences in the chelate ring conformations (δ and λ), three basic ligand conformations can be distinguished for TT[9]OC: S_3 *exo* or exodentate, as observed in the free ligand; S_3 *endo* or endodentate, as observed in *facial* coordination of the ligand; and S_2 *endo*/S *exo*, the conformation which results in bidentate coordination.

Table 2.2 Comparison of Torsional Angles for TT[9]OC in Complexes 1, 3, and 4, and for ODT[9]OC for Complex 5[a]

	torsional angles (deg)				
sequence	**1**	**3**	**4[b]**	**4[c]**	**5**
C1-C6-C7-S1	-87(2)	-86.9(11	-104(1)	-115(1)	-101.9(6)
S1-C8-C9-E[d]	56(2)	-56(2)	-62(2)	-173.0(6)	57.9(7)
C8-C9-E-C10	51(2)	128.6(13)	148(1)	92(1)	-160.0(6)
C9-E-C10-C11	-152(1)	-126.8(14)	-59(2)	-90(1)	158.4(6)
E-C10-C11-S3	68(2)	49(2)	-49(2)	150.6(8)	-55.6(7)
S3-C12-C1-C6	111(2)	111.4(11	95(2)	146(1)	95.8(7)

[a]Sign is positive for a clockwise rotation of 1 to 4 viewed down the 2-3 bond. Values for **3** include only the major (78%) disorder model. [b]TT[9]OC *endo*. [c]TT[9]OC *exo*. [d]E = S for **1**, **3**, and **4**; O for **5**. S3 = S2 for **5**.

2.4.4 Solution and Solid State Studies of $[Ag(ODT[9]OC)_2][BF_4]$, (5).

Similar to complexes **1** - **4**, complex **5** is fluxional in solution; there is no resolution of the benzylic region of the ^1H NMR spectrum if the temperature is lowered. It is possible that this fluxionality is due to an S_4 - S_4O_2 coordination interconversion, however, this is unlikely since hard oxygen donor atoms are not prone to coordination to late transition metal atoms[57]. More likely, the fluxionality observed in solution is due to flexibility of the ligand itself.

The structure of the cation of complex **5** is markedly similar to that of **3**, $[Ag(TT[9]OC)_2][BPh_4]$, in that the Ag(I) atom is in a tetrahedral environment, coordinated to four sulphur atoms. The difference between these two structures lies in the orientation of the central donor atoms. In complex **3**, the central sulphur atoms are exodentate to the macrocyclic ring, oriented away from the silver atom. However, as expected for complex **5**, the oxygen donors are endodentate with respect to the macrocyclic ring, and do not coordinate to the silver atom. In order to compare complexes **3** and **5** more closely, they are shown in Figure 2.7a and c, respectively.

Although the structures of complexes of the formula $[Ag(TT[9]OC)_2][X]$ varied depending on the cation X^-, it was found that there was no such variation in the basic Ag-S_4 tetrahedral coordination sphere for complexes of the type $[Ag(ODT[9]OC)_2][X]$. Comparison of Figures 2.3 and 2.5 establishes that S_2 in complex **3** has the potential to coordinate to the metal atom, since it is in the correct orientation to do so. However, in complex **5**, the oxygen donor is well away from the Ag(I) atom, pointing into the macrocycle.

2.5 Summary and Conclusions

Solution behaviour and solid state structures of the complexes $[Ag(TT[9]OC)_2][X]$ demonstrate that TT[9]OC is capable of easily converting from an exodentate to an endodentate conformation. This property can be attributed to the strain introduced into the free ligand as a result of the incorporation of a rigid *o*-xylyl group resulting in a number of significant observations. Firstly, similarly to 9S3, TT[9]OC is capable of enforcing octahedral coordination geometry at Ag(I) by sandwiching the ion between two capping ligands. This occurs even though the sulphur donors are not preorganized as in 9S3. Secondly, TT[9]OC can adopt three different coordination modes and act as a two-, four-, or six-electron donor ligand, bonding through one, two, or three sulphur atoms. This combination of apparently strong metal-ligand interaction and conformational flexibility makes TT[9]OC unique in crown thioether chemistry.

Both TT[9]OC and ODT[9]OC have the potential to stabilize intermediate states in reaction chemistry when either is coordinated to a late transition element. TT[9]OC can coordinate to a transition metal atom through one, two, or three donors, and in solution Ag(I) complexes of the ligand show a great deal of fluxionality. ODT[9]OC on the other hand, seems to prefer coordination through only the sulphur donors, since hard oxygen donors are not usually compatible with late transition elements, and this factor introduces a higher likelihood of coordinative unsaturation at a late transition metal centre.

Chapter 3

3.1 Introduction

The coordination chemistry of crown thioethers has been the subject of intense investigations, and thorough reviews[14-16] have appeared recently. Results on Ag(I) complexes of crown thioethers indicate that, in addition to conventional binding modes, the sulphur donors of the macrocyclic ligands can readily bridge two metal centres. Examples of dimeric species include the asymmetric complex $[Ag(15S5)]_2^{2+}$, in which the silver atoms are bound to two sulphur donors of one crown thioether and one sulphur donor of another, and in which one long range Ag...S interaction completes a distorted tetrahedral environment about the silver atoms[73]. As well, the symmetrical complex $[AgL]_2^{2+}$ (L=2,5,7,10-tetrathia[12](2,5)thiophenophane)[74] in which the silver atoms are in an unusual trigonal bipyramidal environment composed of three sulphur atoms from one crown thioether, one bridging sulphur donor from a second ligand, and one non-bridging

sulphur donor from the second ligand is the result of a 1:1 reaction of a silver (I) salt with the ligand. The unique trinuclear complex $[Ag(9S3)]_3^{3+}$ co-crystallizes with $[Ag(9S3)_2]^+$ along with four ClO_4^- anions[43], and shows how this potentially tridentate ligand forms a bridge between silver atoms to complete the tetrahedral coordination sphere of the metal.

It was shown by Cooper[44], that although the ligand 9S3 is endodentate, and although complexation to a metal centre requires little if any conformational change for *facial* binding, the ligand can also show an unexpected conformational flexibility, as shown in the complex $[Cu_2(9S3)_3]^{2+}$, in which one ligand is coordinated to the metal in a *facial* manner, and a second ligand adopts an exodentate conformation, in which two sulphur donors coordinate to the metals, and the third remains free. This type of exodentate binding is also observed in the 1:5 reaction of $AgPF_6$ with $15S_2O_3$, which results in $[Ag_2(15S_2O_3)_3]^{2+}$; the Ag(I) atoms are in a distorted trigonal planar environment, bound to two sulphur atoms from a terminally bound bidentate macrocycle, and one sulphur donor from the exodentate sulphur atom of the bridging macrocycle[70]. The 1:1 reaction of $AgPF_6$ with $15S_2O_3$ results in a polymeric chain, where all the donor atoms of one ligand coordinate to Ag(I), and additionally, one of the sulphur donors bridges to another $[Ag(15S_2O_3)]^+$ fragment. The introduction of a ketone group to 9S3 provides for some structural rigidity, so that the 1:1 reaction of 9S3-one (3,6,9-trithiacyclodecanone) with $AgCF_3SO_3$ results in a complex consisting of polymeric helical strings with bridging thiocrown ethers between the individual Ag(I) ions[75].

In Chapter 2 it was shown that the crown thioether macrocycle TT[9]OC can bind to Ag(I) through one, two, or all three sulphur donor atoms, adopting endo- or exodentate

coordination geometries[58] depending on the counter ion. The ligand ODT[9]OC also coordinates to Ag(I), although only one type of binding mode was observed, through the two sulphur donors but not the oxygen donor of the ligand. In this chapter, 1:1 reactions of three different crown thioether ligands with Ag(I) are investigated: TT[9]OC, Me_2TT[9]OC, (2,5,8-triathia[9]-4, 5-dimethyl-*o*-cyclophane), and TT[9]MC, (2,5,8-triathia[9]-*m*-cyclophane), shown below. The complexes $(AgL)_4^{4+}$ (L = TT[9]OC or Me_2TT[9]OC) are the largest silver-crown thioether aggregates reported thus far, and they show a unique cation-anion interaction in the solid state. The complex $[Ag(TT[9]MC)]_x^{x+}$ is an example of a polymeric complex where the ligand TT[9]MC remains in an exodentate conformation, binding to three unique silver atoms, which then show further interactions with the counter ions.

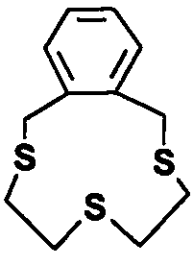

TT[9]OC

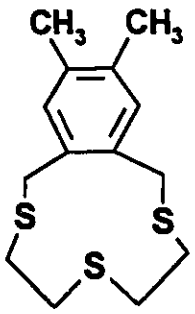

Me_2TT[9]OC

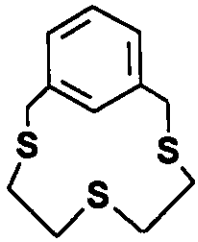

TT[9]MC

3.2 Experimental

TT[9]OC[54], Me_2TT[9]OC[54], and TT[9]MC[50] were prepared by literature methods. $AgBF_4$, $AgCF_3SO_3$, and all solvents were purchased from Aldrich and used as received. All reactions were conducted under an atmosphere of N_2 using standard Schlenk techniques, and all solvents were degassed prior to use. ^1H and $^{13}C\{^1H\}$ NMR spectra were recorded

at 300.1 and 75.4 MHz respectively, on a Bruker AC300 spectrometer locked to the deuterated solvent. Elemental analyses were performed by Microanalytical Services, Delta, British Columbia.

3.2.1 Preparation of $\{[Ag(TT[9]OC)][BF_4]\}_4 \cdot 2CH_3CN$, (6)

TT[9]OC (100 mg, 0.390 mmol) and $AgBF_4$ (76 mg, 0.390 mmol) were dissolved in CH_3CN (25 mL) and stirred for 1 h in the dark. The volume of the solution was reduced to *ca.* 10 mL under reduced pressure, and colourless crystals of the product were obtained by vapour diffusion of diethyl ether into this solution. Yield 148 mg, 84%. ^1H NMR (CD_3CN) (235K): δ 7.43 (br m, 16H, aromatic), 4.10 (br, 8H, benzylic), 3.79 (br s, 8H, benzylic), 3.43 (br s, 16H, SCH_2), 2.94 (br s, 16H, SCH_2). $^{13}C\{^1H\}$ NMR (CD^3CN): δ 134.58, 131.35, 128.83 (aromatic), 33.53 (benzylic), 33.40, 31.42(SCH_2). Anal. Calc'd for $C_{56}H_{76}N_4S_{12}Ag_4B_4F_{16}$: C: 34.16; H: 3.90. Found: C: 34.08; H: 3.85.

3.2.2 Preparation of $\{[Ag(TT[9]OC)][CF_3SO_3]\}_4$, (7)

TT[9]OC (100 mg, 0.390 mmol) and $AgCF_3SO_3$ (100 mg, 0.390 mmol) were mixed together in CH_3CN (25 mL) for 1 h in the dark. The volume of the solution was reduced to *ca.* half under reduced pressure, and colourless crystals of the product were obtained by vapour diffusion of diethyl ether into this solution. Yield 185 mg, 92%. NMR spectral data were identical to that of **6**, above. Anal. Calc'd for $C_{52}H_{64}O_{12}S_{24}Ag_4F_{12}$: C: 27.03; H: 2.80. Found: C: 26.96; H: 2.76.

3.2.3 Preparation of $\{[Ag(Me_2TT[9]OC)][BF_4]\}_4 2CH_3CN$, (8)

$Me_2TT[9]OC$ (100 mg, 0.390 mmol) and $AgBF_4$ (68 mg, 0.349 mmol) were mixed together in CH_3CN (5 mL) and the clear, colourless solution was stirred for 1 h in the dark. Acetone (5mL) was added to this solution and colourless crystals of the product were obtained by vapour diffusion of diethyl ether into this solution. Yield 134 mg, 80%. ^1H NMR (CD_3NO_2, 235K): δ 7.17 (s, 16H, aromatic), 4.14 (d, 8H, benzylic, J=11.4 Hz), 3.80 (d, 8H, benzylic), 3.53 (t, 16H, SCH_2), 2.98 (dt, 16H, SCH_2), 2.24 (s, 24H, CH_3). $^{13}C\{^1H\}$ NMR (CD_3NO_2): δ 134.14, 131.90, 128.22 (aromatic), 32.67 (benzylic), 30.87, 30.42 (SCH_2), 18.91 (CH_3). Anal. Calc'd for $C_{64}H_{100}N_4S_{12}Ag_4F_{16}$: C: 36.81; H: 4.79. Found: C: 36.74; H: 4.74.

3.2.4 Preparation of $\{[Ag(TT[9]MC)][CF_3SO_3]\cdot CH_3CN\}_x$, (9)

TT[9]MC (100 mg, 0.390 mmol) and $AgCF_3SO_3$ (100 mg, 0.390 mmol) were mixed together in CH_3CN (25 mL) and the clear colourless solution was stirred for 1 h in the dark. The volume of the solution was reduced to *ca.* 10 mL under reduced pressure, and clear colourless crystals of the product were obtained by vapour diffusion of diethyl ether into this solution. Yield 180 mg, 90%. ^1H NMR (CD_3CN): δ 8.02 (s, 4H, aromatic), 7.37 (m, 12H, aromatic), 3.99 (s, 16H, benzylic), 2.72 (t, 16H, SCH_2), 2.29 (t, 16H, SCH_2), $^{13}C\{^1H\}$ NMR(CD_3CN): δ 139.61, 128.00, 128.50 (aromatic), 36.17 (benzylic), 31.03, 29.20 (SCH_2). Anal. Calc'd for $C_{15}H_{19}NO_3S_4AgF_3$: C: 32.49; H: 3.46. Found: C: 32.40; H: 3.42.

3.2.5 X-ray Structure Determination of {[Ag(TT[9]OC)][BF_4]}2CH_3CN, (6)

General data collection information is given in Section 2.2.4 of this thesis. Colourless crystals of complex **6** were grown by vapour diffusion of diethyl ether into a CH_3CN solution of the complex. A statistical analysis of intensity distributions and a determination of systematic absences were consistent with the space group $P2_1/c$, and this was confirmed by successful solution refinement. A total of 6511 reflections were collected and 2706 reflections with $F_o^2>3\sigma(F_o^2)$ were used in the refinement. The positions of the silver and sulphur atoms were determined by direct methods, and the remaining non-hydrogen atoms were located from difference Fourier calculations. In the final cycles of refinement, all non-hydrogen atoms were assigned anisotropic thermal parameters, resulting in $R = 3.30\%$ and $R_w = 5.10\%$. A goodness of fit calculation resulted in a value of 1.88, and a final difference Fourier map calculation showed no peaks of chemical significance. A summary of machine and data collection parameters and crystal data is shown in Table A.3.1, positional parameters are listed in A.3.2 and bonding parameters are listed in Table A.3.3.

3.2.6 X-ray Structure Determination of {[Ag(TT[9]OC)][CF_3SO_3]}$_4$, (7)

Colourless crystals of complex **7** were grown by vapour diffusion of diethyl ether into an acetonitrile solution of the complex. A statistical analysis of intensity distributions and determination of systematic absences were consistent with the space group $P2_1/c$, and this was confirmed by successful solution refinement. A total of 6732 reflections were collected and 3295 reflections with $F_o^2>3\sigma(F_o^2)$ were used in the refinement. The positions

of the silver and sulphur atoms were determined by direct methods, and the remaining non-hydrogen atoms were located by difference Fourier calculations. In the final cycles of refinement, all non-hydrogen atoms were assigned anisotropic thermal parameters, resulting in $R = 5.10\%$ and $R_w = 5.80\%$. A goodness of fit calculation resulted in a value of 2.37, and a total difference Fourier calculation resulted in no peaks of chemical significance. A summary of machine and data collection parameters and crystal data is shown in Table A.3.4, positional parameters are listed in Table A.3.5 and bonding parameters are listed in Table A.3.6.

3.2.7 X-ray Structure Determination of $\{[Ag(Me_2TT[9]OC)][BF_4]\}_4 \cdot 2CH_3CN$, (8)

Colourless crystals of complex **8** were grown by vapour diffusion of diethyl ether into a 1:1 acetone:acetonitrile solution of the complex. A statistical analysis of intensity distributions and determination of systematic absences were consistent with the space group $P2_1/c$, and this was confirmed by successful solution refinement. A total of 7183 reflections were collected and 2907 reflections with $F_o^2 > 3\sigma(F_o^2)$ were used in the refinement. The positions of the silver and sulphur atoms were determined by direct methods, and the remaining non-hydrogen atoms were located by difference Fourier calculations. In the final cycles of refinement, all non-hydrogen atoms were assigned anisotropic thermal parameters except the disordered fluorine atoms, which were assigned isotropic thermal parameters, resulting in $R = 3.64\%$ and $R_w = 5.22\%$. A goodness of fit calculation resulted in a value of 1.55. A summary of machine and data collection

parameters and crystal data is shown in Table A.3.7, positional parameters are listed in A.3.8 and bond parameters are listed in Table A.3.9.

3.2.8 X-ray Structure Determination of {[Ag(TT[9]MC)][CF_3SO_3]·CH_3CN}$_x$, (9)

Colourless crystals of complex **9** were grown by vapour diffusion of diethyl ether into an acetonitrile solution of the complex. A statistical analysis of intensity distributions and determination of systematic absences were consistent with the space group $P2_1/c$, and this was confirmed by successful structure refinement. A total of 3906 reflections were collected and 1261 reflections with $F_o^2 > 3\sigma(F_o^2)$ were used in the refinement. The positions of the silver and sulphur atoms were determined by direct methods, and the remaining non-hydrogen atoms were located by difference Fourier calculations. In the final cycles of refinement, all non-hydrogen atoms were assigned anisotropic thermal parameters, resulting in $R = 4.11\%$ and $R_w = 5.69\%$. A goodness of fit calculation resulted in a value of 1.68. A summary of machine and data collection parameters and crystal data is shown in Table A.3.10, positional parameters are listed in A.3.11 and bond parameters are listed in Table A.3.12.

3.3 Results

3.3.1 Synthesis and Solution Studies

Complexes **6-9** are prepared by the reaction of one equivalent of ligand with one equivalent of the appropriate silver salt. The colourless complexes are obtained in yields of greater than 90% and are recrystallized by vapour diffusion of diethyl ether into an

acetonitrile solution or, in the case of complex **8**, $\{[Ag(Me_2TT[9]OC)][BF_4]\}_4$, into a 1:1 mixture of acetone and acetonitrile solution. The crystalline solids are all air stable and none show sensitivity to light.

The ^1H NMR spectra of complexes $\{[Ag(TT[9]OC)][BF_4]\}_4$, **6**, and $\{[Ag(TT[9]OC)][CF_3SO_3]\}_4$, **7**, are identical at room temperature, showing a multiplet due to aromatic protons at δ 7.44 ppm, a single peak at δ 4.00 ppm due to benzylic protons, and a broad single peak at δ 3.19 due to all of the SCH_2 protons. These broadened resonances can be resolved somewhat by recording ^1H NMR spectra at 235K, the limiting temperature for CD_3CN. At reduced temperatures the multiplet due to the aromatic protons is broadened, and the single peak due to the benzylic protons is split into two broad peaks at δ 4.10 and δ 3.79 ppm. Similarly, the single peak due to the SCH_2 protons is split into two broad peaks at δ 3.43 and δ 2.94 ppm. The $^{13}C\{^1H\}$ NMR spectra for both complexes are also identical, with expected resonances due to ligand carbon atoms.

The alteration of the crown thioether ligand TT[9]OC by the incorporation of methyl groups on the aromatic ring to form $Me_2TT[9]OC$, increases the solubility of its Ag(I) complex markedly. Complex **8** is quite soluble in acetonitrile, and therefore in order to successfully recrystallize the product, acetone, in which **8** is less soluble, was added to the reaction solution. Accordingly, the limiting ^1H NMR spectrum of complex **8** in CD_3NO_2, a non-coordinating solvent, was recorded. The aromatic proton resonances occur at δ 7.17 ppm as a singlet, and the benzylic proton resonances are somewhat more resolved than for **6** or **7**, occurring as broad doublets at δ 4.14 and δ 3.18 ppm.

Resonances due to SCH_2 protons are observed as broad triplets at δ 3.53 and δ 2.98 ppm, and a single resonance due to methyl protons is observed at δ 2.24 ppm. As for **6** and 7, the $^{13}C\{^1H\}$ NMR spectrum is well resolved and is similar to that of the free ligand.

Finally, the ^1H NMR spectrum of $\{[Ag(TT[9]MC)][CF_3SO_3]\}_x$, **9**, is quite well resolved, similar to the spectrum of the free ligand. A single peak occurs at δ 8.02 ppm due to the proton at the two position of the aromatic ring, a multiplet at δ 7.37 ppm due to the remaining aromatic protons, a singlet at δ 3.99 ppm due to benzylic protons, and two triplets at δ 2.72 and δ 2.29 ppm due to SCH_2 protons are observed.

3.3.2 X-Ray Structures of $\{[Ag(TT[9]OC)][BF_4]\}_4 \cdot 2CH_3CN$, (6), and $\{[Ag(TT[9]OC)][CF_3SO_3]\}_4$, (7)

The unit cells contain two $[Ag(TT[9]OC)]_4^{4+}$ cations, eight anions, and in the case of **6**, four molecules of CH_3CN. A perspective view of the $[Ag(TT[9]OC)]_4^{4+}$ cation of complex **6** is shown in Figure 3.1; it is a tetrameric aggregate with a crystallographically imposed centre of symmetry. In each of the two independent $[Ag(TT[9]OC)]^+$ fragments, the macrocyclic thioether is bonded *facially* to a Ag(I) ion: Ag1-S1 2.576(3), Ag1-S2 2.593(3), Ag1-S3 2.598(3), Ag2-S4 2.566(3), Ag2-S5 2.609(3), and Ag2-S6 2.570(3)Å for complex **6**, and Ag1-S1 2.602(3), Ag1-S2 2.611(3), Ag1-S3 2.564(4), Ag2-S4 2.556(3), Ag2-S5 2.609(3), and Ag2-S6 2.635(3) Å for complex 7. These $[Ag(TT[9]OC)]^+$ fragments are linked through bridging of the central sulphur donor of each macrocycle to the silver centre of the next fragment: Ag1-S5 2.456(3) and Ag2-S2' 2.454(3) Å for **6**, and Ag1-S5 2.468(3) and Ag2-S2' 2.485(3) Å for 7. This results in a

slightly distorted tetrahedral geometry at the Ag(I) centres. The bond distances and angles associated with the coordination of TT[9]OC to Ag(I) are very similar to those observed for the mononuclear complexes $[Ag(TT[9]OC)_2][X]$[58] and $[Ag(TT[9]OC)(PPh_3)][ClO_4]$[54] which contain *facially* coordinated TT[9]OC. The metal to metal distances are Ag1...Ag2 4.536(4) and Ag1...Ag2' 4.629(4) Å for adjacent ions, and Ag2-Ag2' 6.344(4) Å for symmetry related centres across the cavity of **6**. The Ag_4S_4 ring of **6** is very close to being a planar octagon with the average length of a side measuring 2.53(7) Å and an average internal angle of 134(5)° compared to 135° for an ideal planar octagon. A least squares plane calculation for Ag_4S_4 of **6** shows that the largest deviation from planarity is 0.269(3) Å for S5. The overall shape of the cation of **7** is very similar to that of **6**: Ag1...Ag2 4.663(4)Å, Ag1...Ag2' 6.916(4)Å, Ag2...Ag2' 6.194(4)Å; the average length of a side of the octagon is 2.55(7)Å, and the average internal angle is 134(5)°. A least squares plane calculation for Ag_4S_4 of **7** shows that the largest deviation from planarity 0.220(3)Å for S5.

The three dimensional shape of the $[Ag(TT[9]OC)]_4^{4+}$ cation is similar to that of a cylindrical disc. The disc radius is defined as the average distance from the inversion centre to the outer aromatic H atoms (H4 and H16), the thickness is the average distance between equatorial ethylene H atoms on TT[9]OC, and the hole radius as the average distance from the inversion centre to the Ag_4S_4 ring atoms. This results in a disc-shaped cation 16.3Å in diameter, 4.8Å thick, containing a hole of diameter 6.6 Å (for both **6** and **7**).

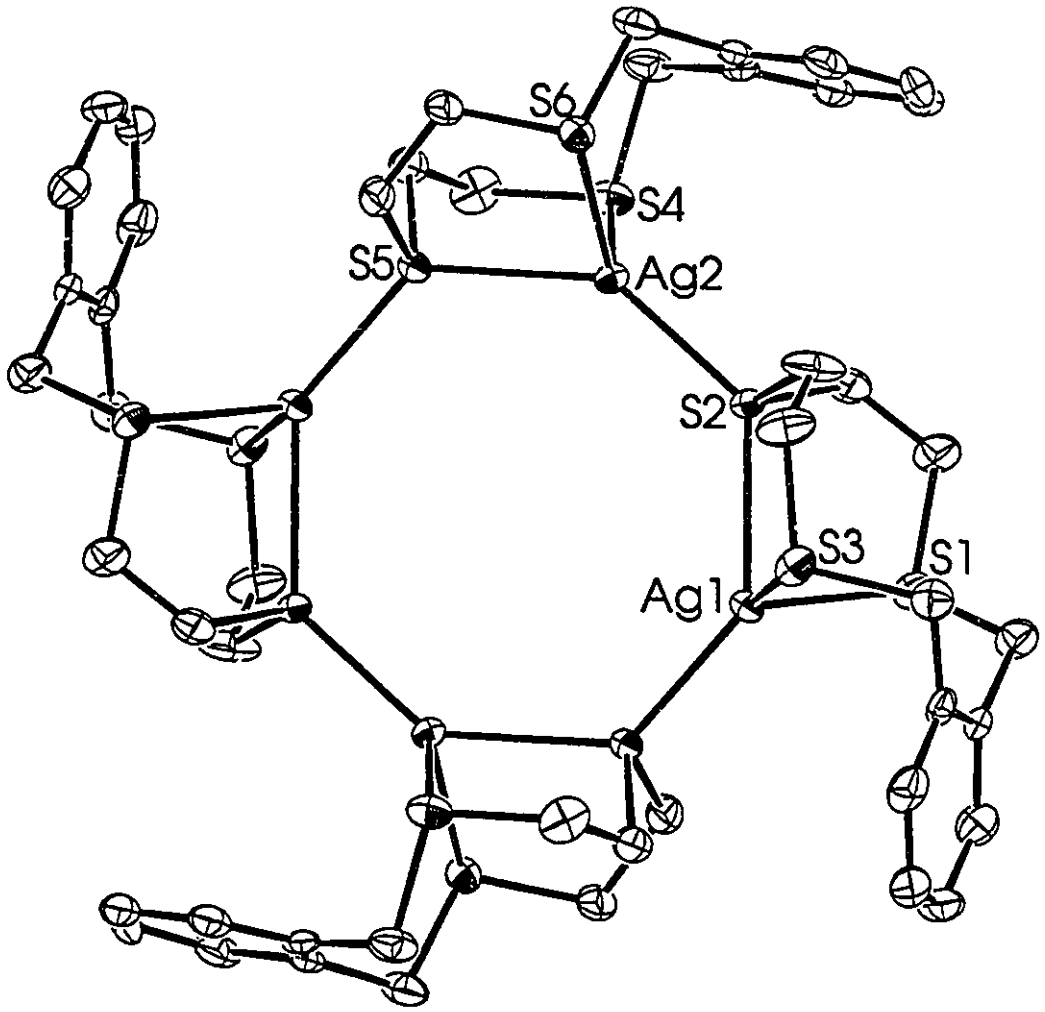

Figure 3.1: Perspective view of the cation of complex 6, $[Ag(TT[9]OC)]^{4+}$, showing the atom-numbering scheme; carbon atoms of the ligand are numbered as shown in Chapter 2. Thermal elipsoids of 30% probability are shown. Nonbonded distances: Ag1...Ag2 4.536(4), Ag1...Ag2' 4.629(4); and Ag2...Ag2' 6.344(4) Å. Bond distances: Ag1-S1 2.576(3), Ag1-S2 2.593(3), Ag1-S3 2.598(3), Ag1-S5 2.456(3), Ag2-S4 2.566(3), Ag2-S5 2.609(3), Ag2-S6 2.570(3), and Ag2-S2' 2.454(3)Å. Bond angles: S2-Ag1-S5 135.8(1)°, Ag1-S5-Ag2 127.8(1)°, S5-Ag2-S2' 140.6(1)°, Ag2'-S2-Ag1 132.0(1)°.

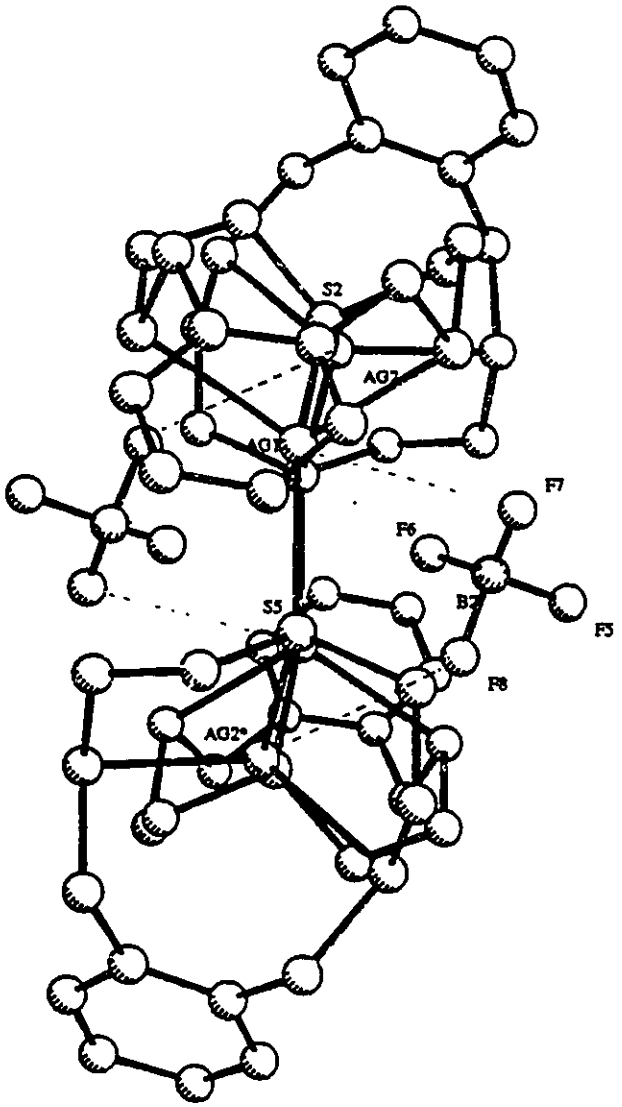

Figure 3.2 A side view of the $[Ag(TT[9]OC)]_4^{4+}$ cation of 6, showing the placement of two symmetry related BF_4^- anions inside the disc-shaped tetraction. Nonbonded distances are Ag1...F7 3.15(1), Ag2...F8 3.22(1) Å.

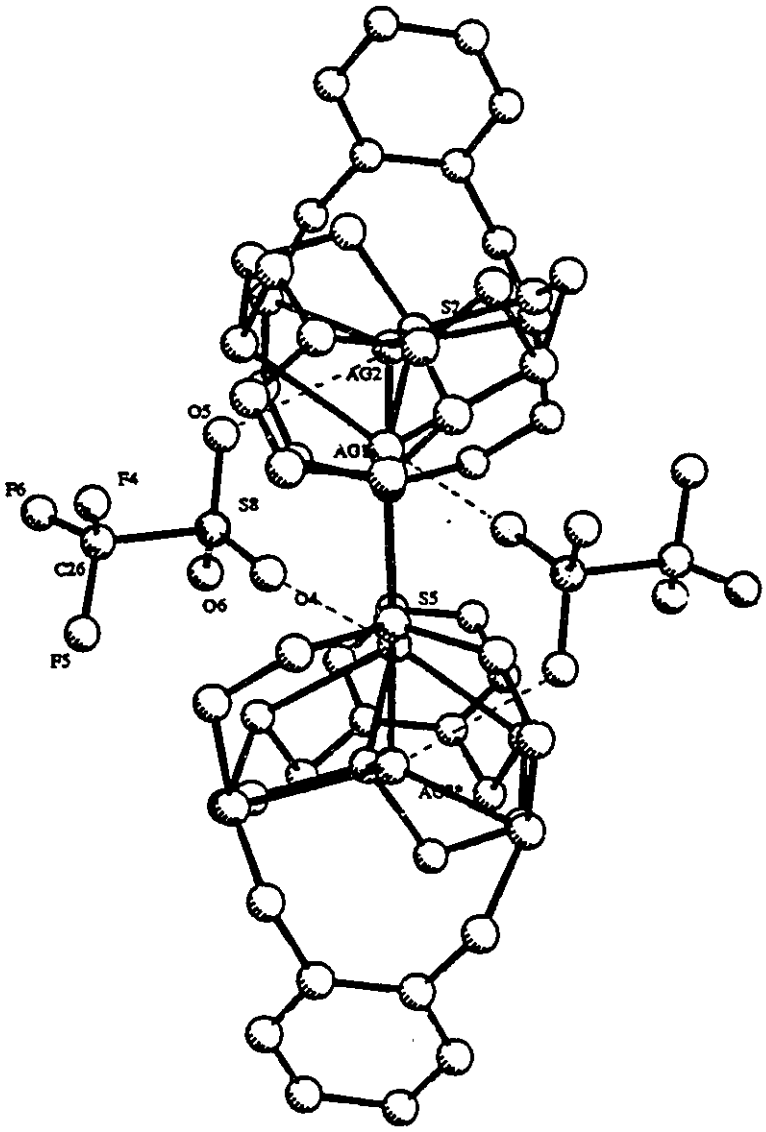

Figure 3.3 A side view of the $[Ag(TT[9]OC)]_4^{4+}$ cation of 7, showing the placement of two symmetry related $CF_3SO_3^-$ anions. Nonbonded distances are Ag1...O4 3.17(1), Ag2...O5 3.11(1) Å.

The BF_4^- anions of **6** were refined anisotropically and had normal tetrahedral geometry, and similarly, the $CF_3SO_3^-$ anions of 7 were refined anisotropically and geometries about both the carbon and sulphur atoms were tetrahedral. Two of the BF_4^- anions of **6**, and two of the $CF_3SO_3^-$ anions of 7 are included in the central cavities of the discs. Shown in Figures 3.2 and 3.3, Ag...F7 and Ag2...F8 distances are 3.15(1) and 3.22(1)Å in complex **6**, and Ag1...O4 and Ag2...O5 distances are 3.17(1) and 3.11(1) Å in complex 7. Both sets of distances are smaller than the sums of the van der Waals' radii for the atoms: Ag(1.72), F(1.47), and O(1.52)Å[76].

3.3.3 X-Ray Structure of $\{[Ag(Me_2TT[9]OC)][BF_4]\}_4 \cdot 2CH_3CN$, (8)

The unit cells contain two $[AgMe_2(TT[9]OC)]_4^{4+}$ cations, eight BF_4^- anions, and four molecules of CH_3CN. Complex **8** is a tetrameric aggregate similar to complexes **6** and 7, with a crystallographically imposed centre of symmetry. Figure 3.4 shows a perspective view of **8**, including two of the four BF_4^- anions. Significant bond distances are as follows: Ag1-S1 2.588(3), Ag1-S2 2.629(3), Ag1-S3 2.619(3), Ag2-S4 2.616(3), Ag2-S5 2.620(3), and Ag2-S6 2.559(3) Å . The $[Ag(TT[9]OC)]^+$ fragments are linked by the central sulphur donor of each macrocycle to the silver centre of the next fragment: Ag1-S5 2.477(3) and Ag2-S2 2.461(3) Å. The geometries about Ag1 and Ag2 are those of distorted tetrahedra, with S1-Ag1-S2 82.3(1)°, S1-Ag1-S3 111.1(1)°, S1-Ag-S5 118.8(1)°, S2-Ag1-S5 141.4(1)°, and S4-Ag2-S5 82.1(1)°, S4-Ag2-S6 109.4(1)°, S5-Ag2-S6 83.1(1)°, and S2-Ag2-S5 135.0(1)°. Again, these distances and angles are similar to those in $[Ag(TT[9]OC)_2][X]$[58] and $[Ag(TT[9]OC)(PPh_3)][ClO_4]$[54] complexes.

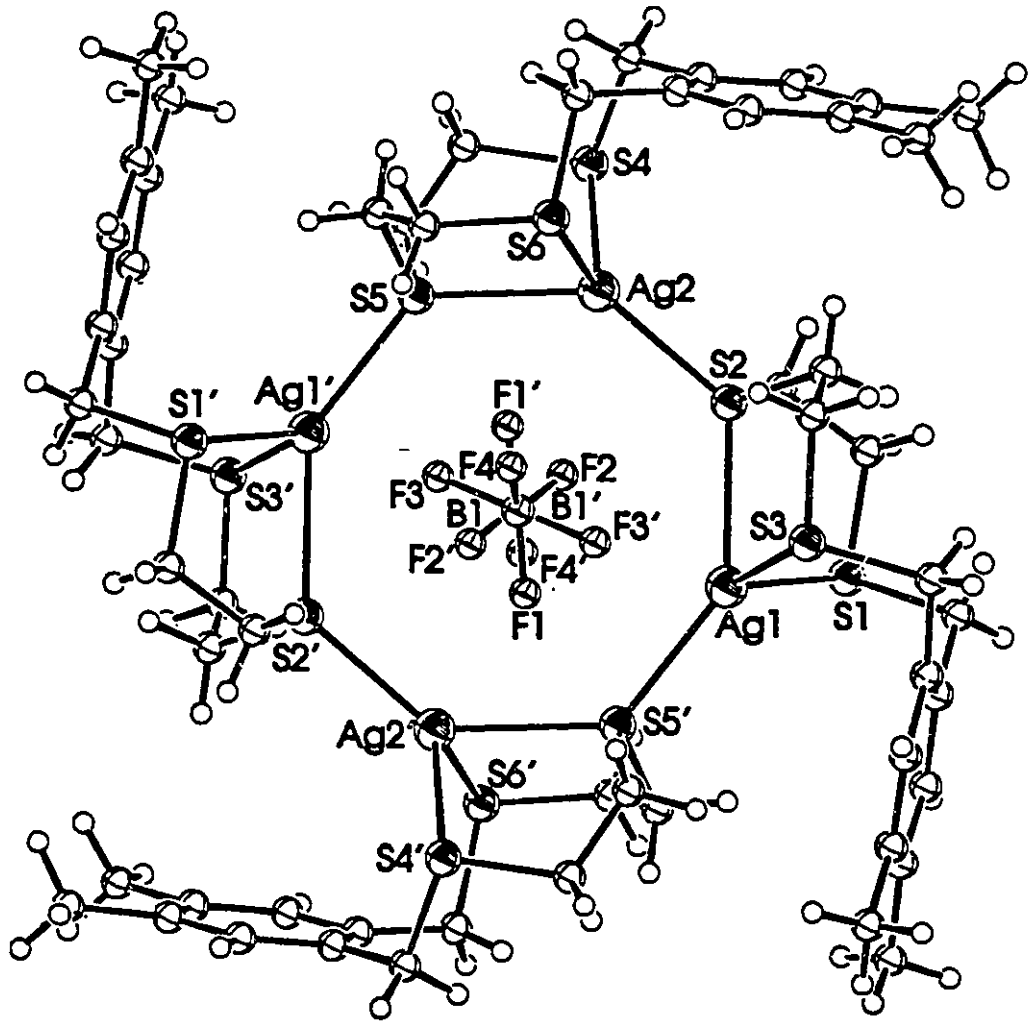

Figure 3.4 Perspective ORTEP view of the $[Ag(Me_2TT[9]OC)]_4^{4+}$ cation showing the placement of two symmetry related BF_4^- anions inside the central cavity. The view shown is down the B1...B1' vector, and all atoms are shown as ideal spheres. Carbon atoms are shown as boundary ellipses and their numbering is the same as that used in Chapter 2. Hydrogen atoms are shown as small, open spheres. Bond distances: Ag1...Ag1' 6.352(3), Ag2...Ag2' 6.627(5), Ag1...Ag2 4.564(3), Ag1...Ag2' 4.615(3), Ag1-S1 2.620(4), Ag1-S2 2.628(4), Ag1-S3 2.589(4), and Ag2-S4 2.618(4), Ag2-S5 2.619(3), Ag2-S6 2.562(4), Ag1-S5' 2.477(4), Ag2-S2' 2.460(3) Å.

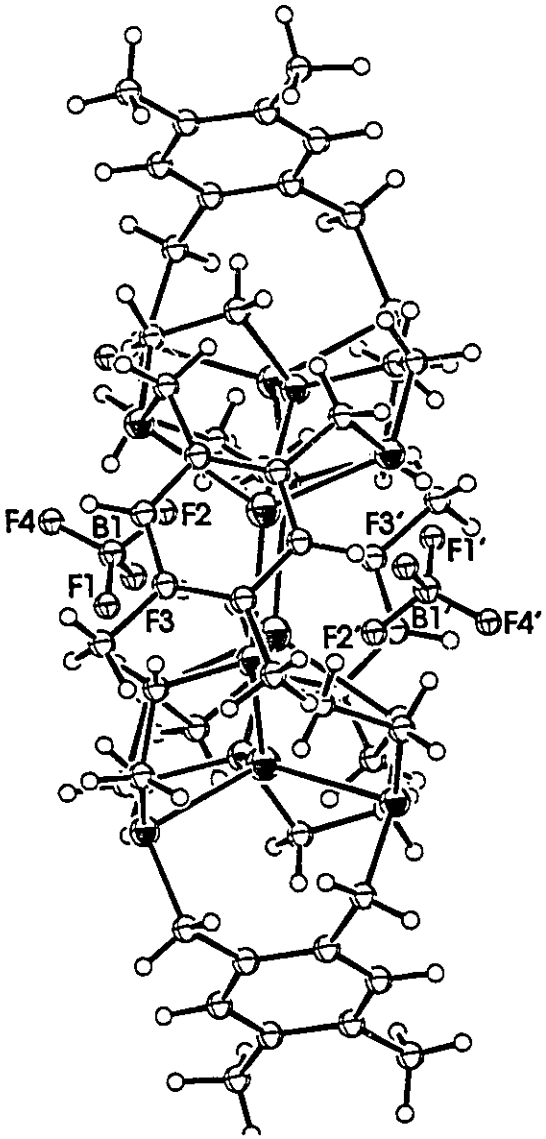

Figure 3.5 A side view of the $[Ag(Me_2TT[9]OC)]_4^{4+}$ cation of 8, showing the placement of two symmetry related BF_4^- anions inside the disc-shaped tetracation. The representation of each atom type is the same as in Figure 3.4. Significant distances are Ag1...F3 3.15(2) and Ag2...F2 3.11(2) Å.

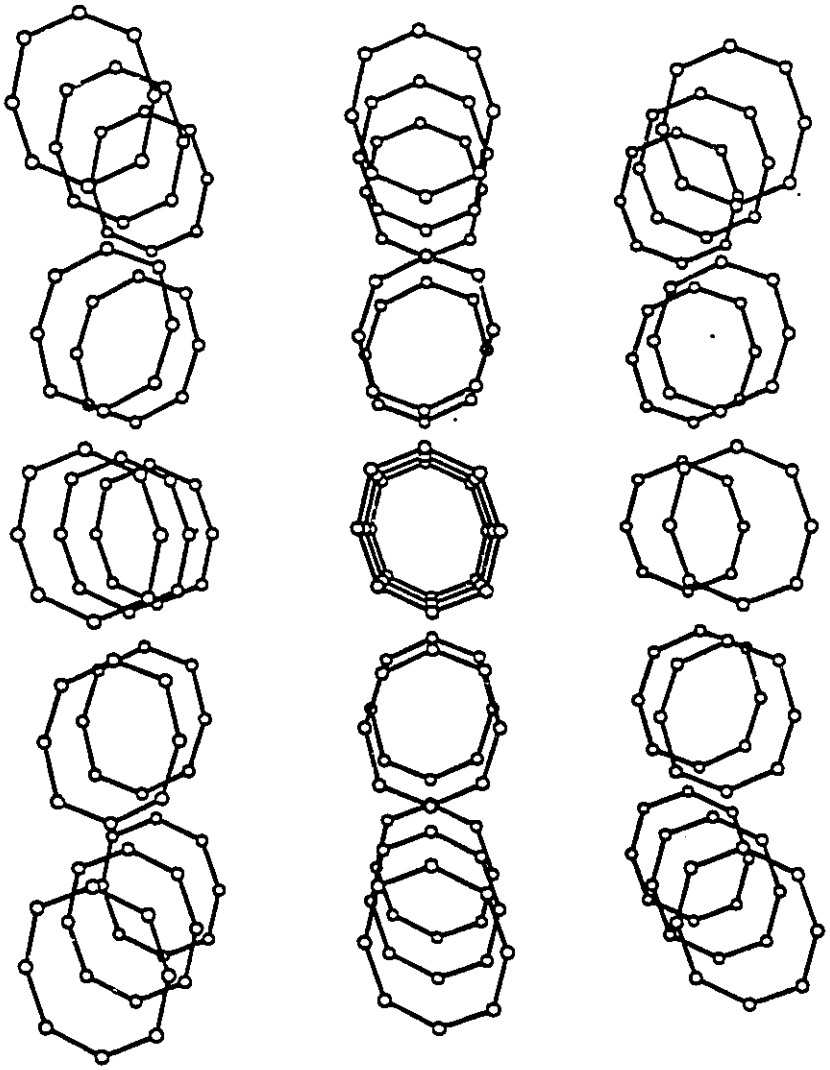

Figure 3.6 Packing diagram as viewed along the z axis for the $[Ag(Me_2TT[9]OC)]_4^{4+}$ cation showing the tubular array of the actagonal Ag_4S_4 rings in the solid state.

The Ag_4S_4 ring closely resembles a planar octagon with the average length of a side measuring 2.55(8) Å and an average internal angle of 133(5)°; a least squares plane calculation for the Ag_4S_4 core shows the mean deviation from planarity to be 0.151(3) Å, in which the largest deviation for S2 is 0.234(3) Å. The hole diameter of the cylindrical disc formed in the three dimensional shape of the $[Ag(Me_2TT[9]OC)]_4^{4+}$ cation is 6.5 Å. Ag1-Ag1' 6.352(3) and Ag2-Ag2' 6.627(5) Å. A side view of the molecule is shown in Figure 3.5. The closest contacts between the fluorine atoms of the BF_4^- anion and the Ag atoms are Ag1...F3 3.15(2) and Ag2...F2 3.11(2) Å, slightly shorter than the sum of the van der Waals' radii for Ag (1.72 Å) and F (1.47 Å)[13].

Figure 3.6 is a packing diagram as viewed along the z-axis, for the $[Ag(Me_2TT[9]OC)]_4^{4+}$ cation, showing the tubular orientation of the octagonal Ag_4S_4 rings in the solid state. The packing diagrams of **6** and **7** are essentially identical to that shown in Figure 3.6.

3.3.4 X-Ray Structure of $\{[Ag(TT[9]MC)][CF_3SO_3]\cdot CH_3CN\}_x$, (9)

The unit cell contains four $[Ag(TT[9]MC)]^+$ cations, four $CF_3SO_3^-$ anions, and four molecules of CH_3CN. A perspective view of the complex is shown Figure 3.7. The silver atom is in a distorted trigonal planar environment composed of three sulphur atoms from three different ligands, forming an infinite sheet-like lattice. The Ag-S distances are 2.545(5), 2.530(5), and 2.556(4) Å for S1, S2, and S3 respectively, and bond angles are S1-Ag-S2 135.9(1)°, S1-Ag-S3 106.3(2)°, and S2-Ag-S3 117.0(2)°. The triflate anion has

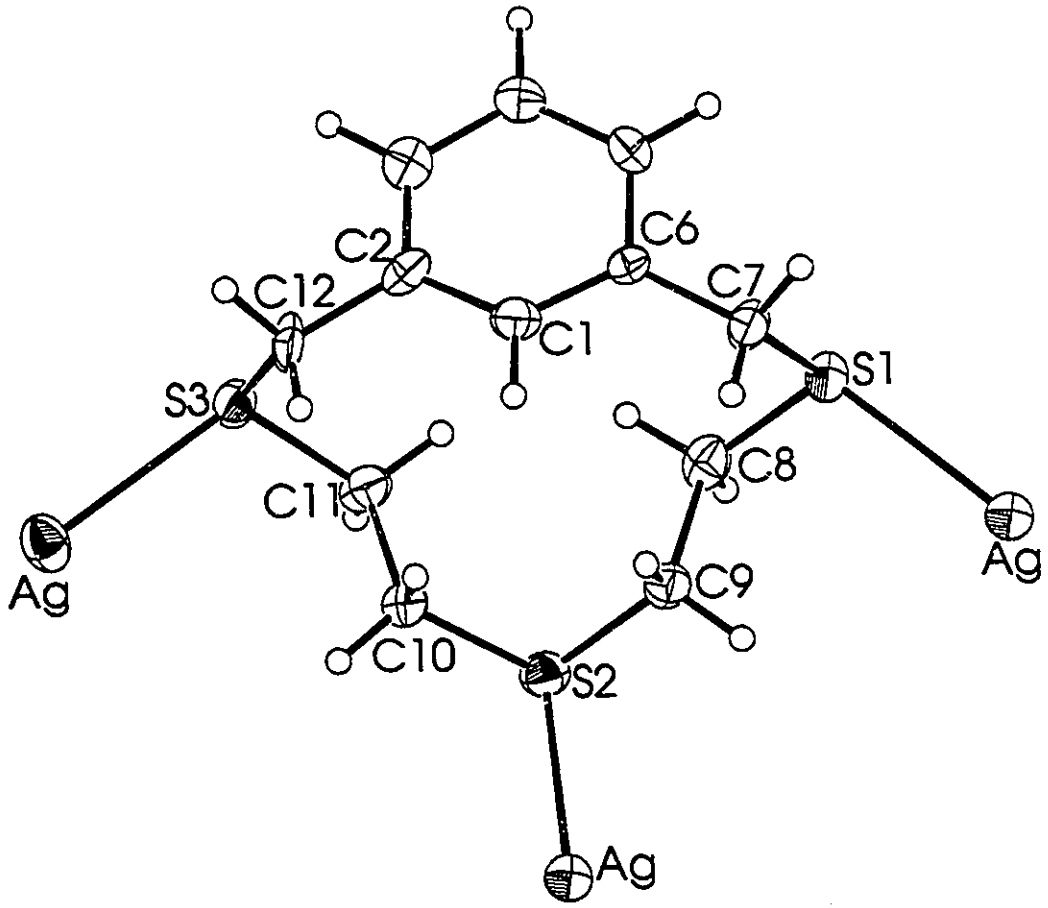

Figure 3.7 Perspective ORTEP view of the cation of complex 9, $[Ag(TT[9]MC)]^+$, showing the atom numbering scheme. Thermal ellipsoids are shown at 30% probability. Bond distances: Ag-S1 2.545(5), Ag'-S2 2.530(5), Ag"-S3 2.556(4) Å, Ag...Ag' 6.700(2), Ag...Ag" 6.113(4), Ag'...Ag" 10.061(3) Å. Bond Angles: S1-Ag-S3 135.9(1)°, S1-Ag-S3 106.3(2)°, S2-Ag-S3 117.0(2)°. Torsional angles: S1-C8-C9-S2 178.6(8)°, S2-C10-C11-S3 -175.5(7)°.

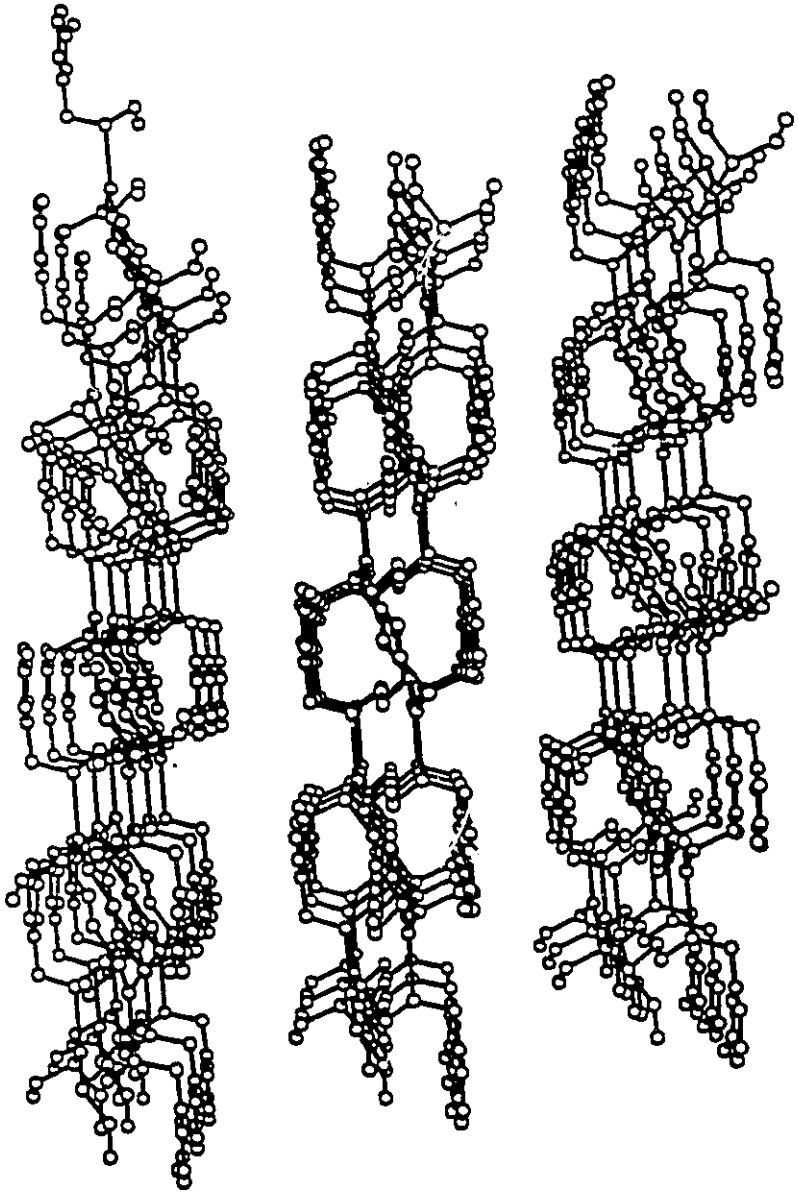

Figure 3.8 A packing diagram as viewed down the z axis of the polymer $[Ag(TT[9]MC)]_x^{x+}$, showing the layered formation of this complex in the solid state.

normal tetrahedral geometries about the carbon and sulphur atoms, and there is a Ag...O1 intramolecular contact of 2.66(1) Å.

An extended three dimensional view of the lattice structure is shown in Figure 3.8, as viewed down the z axis. Each silver atom is bonded to S1, S2, and S3 from three different TT[9]MC ligands, so that within the lattice the ligands are staggered to accomodate the trigonal planar geomtry about the Ag(I) atom. In each "sheet" there are two layers of TT[9]OC ligands, and the sheets run parallel to each other, in a series of infinite lattices. Distances between silver atoms are as follows: Ag...Ag' 6.700(2), Ag...Ag" 6.113(4), and Ag'...Ag" 10.061(3) Å. The triflate anions (not shown) are in close association with each Ag(I) atom, and may be seen as completing a distorted tetrahedral geometry at Ag(I).

3.4 Discussion

The 1:1 reaction of silver salts with TT[9]OC or Me_2TT[9]OC results in tetrameric Ag_4S_4 aggregates. Similar to other $Ag_xL_x^{x+}$ (x = 2 or 3) complexes[43,73,74], the solution NMR spectra of complexes **6-8** do not confirm their aggregate solid state structures. ^{1}H NMR spectra of $[AgL]_4^{4+}$ (L = TT[9]OC or Me_2TT[9]OC) in CD_3CN show only broad resonances for the aromatic, benzylic, and SCH_2CH_2S protons, suggesting a fluxionality in solution. It is possible, as observed for $[AgL_2]^+$ (L = TT[9]OC, ODT[9]OC) complexes in Chapter 2, that in the donor solvent the tetracation exists in equilibrium with solvated monomers or smaller solvated aggregates of $[AgL]^+$. A limiting (235K) ^{1}H NMR spectrum of $[Ag(Me_2TT[9]OC)]_4^{4+}$, **8**, in CD_3NO_2 was obtained, and although it is unlikely

that this solvent is competitive with Ag-S bond formation, this is not completely unambiguous evidence for the solution integrity of complexes **6**, **7**, or **8**.

Anion binding, and the synthesis of complexes capable of acting as anion receptors, are interesting for two reasons: 1) anions are known to play essential roles in chemical and biochemical processes, and 2) this field of coordination chemistry is relatively new[77]. In particular, neutral anion receptors[77] and complexes which include anions without hydrogen bonding[77b, 78] are of interest to the coordination chemist. Complexes **6-8** show a unique cation-anion interaction, not observed previously in other aggregate complexes of metals and crown thioethers. The three dimensional structures of **6-8** show a tubular array, with two anions interacting with each Ag_4S_4 cation. For $[Ag(TT[9]OC)]_4^{4+}$, **6** and **7**, the BF_4^- and $CF_3SO_3^-$ anions have Ag...F and Ag...O distances respectively, which are within the limits or slightly longer than their Van der Waals' interactions[77]. Similarly, for $[Ag(Me_2TT[9]OC)]_4^{4+}$, complex **8**, the BF_4^- anions appear to be almost enclosed by the peripheral structure of the $Me_2TT[9]OC$ ligand.

It has been shown previously[49,50] that the ligand TT[9]MC does not convert from an exodentate form to an endodentate one to allow for *facial* coordination to a metal centre. The 1:1 reaction of $AgCF_3SO_3$ with TT[9]MC therefore, reults in a polymeric lattice structure, with each silver atom serving to connect three TT[9]MC ligands through binding to three different sulphur donors. The ligand conformation in complex **9** is essentially identical to the free ligand conformation; torsional angles about the SCCS brackets are 178.6(8)° and -175.5(7)° for **9**, compared to 173.0° and -176.5° for the free ligand[79]. Similar to complexes **6-8**, cation-anion interaction is observed, although in the

case of complex **9** the Ag...O1 interaction may possibly serve to to fulfill a pseudotetrahedral coordination sphere about the silver atom. This is extremely similar to the complex $[Ag(12S3)(CF_3SO_3)]_x$ prepared by Cooper[44], where the exodentate comformation of 12S3 precludes tridentate coordination to one metal centre. In this case the $CF_3SO_3^-$ anion shows a definite bond to silver, and the Ag-O1 distance is 2.483(6) Å. The only other previously reported polymeric silver-crown thioether complex is that of $[Ag(15S_2O_3)(CF_3SO_3)]_x$, which exists as a chain of encapsulated silver atoms connected by one ditopic sulphur atom of the next metal-ligand complex[70].

3.5 Summary and Conclusions

The reaction of silver salts with various crown thioether ligands in a 1:1 ratio leads to various aggregate and polymeric structures. The complexes $[AgL]_4^{4+}$ (L = TT[9]OC or Me_2TT[9]OC) are the largest aggregate complexes containing bridging crown thioether ligands to be reported, and they show a unique interaction with their respective counterions. The further derivatization of the aromatic ring, for example, replacing the methyl groups of Me_2TT[9]OC by another crown thioether[80] or crown ether[81], is currently under investigation. Complexes of this type could show concurrent cation/anion binding, and increased solubility in non-competitive solvents should allow for complexation studies in solution. A polymeric complex of the type $[AgL]_x^{x+}$ (L = TT[9]MC) which also shows anionic interactions, may prove to be useful as a precursor to organometallic polymers if the aromatic ring of the ligand is derivatized. Derivatives of TT[9]MC are also being prepared, and a complete study of their complexation behaviour may prove interesting[28,83].

Chapter 4

4.1 Introduction

The impressive reactivity of Rh and Ir complexes containing six-electron capping ligands, such as tripodal phosphines, pyrazolylborates and cyclopentadienyl ligands[84-86], has prompted initial investigations into the possibility of employing tridentate thioether macrocycles, such as 1,4,7-trithiacyclononane, 9S3, as alternatives to these ancillary ligands[14-16]. For the most part, studies of transition metal complexes of crown thioethers have been restricted to structural and electrochemical/redox investigations. More recently however, reactivity studies have been undertaken. Schröder prepared and structurally characterized $[Rh(R)(9S3)]^+$ and $[Ir(R)(9S3)]^+$ (R = $(ethylene)_2$, 1,5-COD)[87] . The reaction chemistry of these compounds has yet to be investigated in any detail, but like some other Rh complexes of crown thioethers, they have been found to be good nucleophiles[87,88]. For

example, Schröder[87] found that dissolution of $[Rh(C_2H_4)_2(9S3)]^+$ or $[Rh(C_2H_4)(PR_3)(9S3)]^+$ (R = Cy, Ph) in CH_2Cl_2 afforded $[Rh(C_2H_4)(CH_2Cl)Cl(9S3)]^+$ and $[Rh(C_2H_4)(PR_3)(CH_2Cl)Cl(9S3)]^+$ respectively, in low yields. The final product in both cases was the Rh(III) complex $[Rh(9S3)Cl_3]$, which was found to be highly insoluble. Yoshida[88] observed that oxidative addition of CH_2Cl_2 readily occurred with 16 electron $[Rh(14S4)]^+$ and $[Rh(Me_4 14S4)]^+$ complexes, yielding coordinatively saturated $[RhCl(CH_2Cl)L]^+$, and proposed that the high nucleophilicity of the S_4-macrocyclic complexes was probably due to the low π-acidity of thioether ligands compared to PR_3; $RhCl(PPh_3)_3$ does not react with CH_2Cl_2.

The reaction of $[M(9S3)_2]^{3+}$ (M = Co, Rh, Ir) with base leads to deprotonation at a methylene carbon and subsequent rearrangement of the carbanion to yield a vinyl thioether complex via C-S bond cleavage[89]. In fact, it has been generally observed that C-H activation of thioether crowns occurs in basic solution when the ligands are coordinated to electropositive metal centres, where the first step in this process involves deprotonation at an α-methylene carbon. If these thioether complexes are synthesized under acidic conditions which prevent deprotonation, the high valent complexes are stable. In related work, we[51-53,82] and others[90] have shown that C-H activation of a macrocyclic thioether can lead to anionic, metalated ligands containing thioether donor atoms.

In Chapter 2 of this dissertation and in other work, it was shown that the ligand 2,5,8-trithia[9]-*o*-cyclophane (TT[9]OC) prefers to adopt a *facial* S_3-coordination mode[49,50,54a], but can also form stable metal complexes involving only one or two of the S donor atoms[58]. The related ligand, 5-oxa-2,8-dithia[9]-*o*-cyclophane (ODT[9]OC) also

has the potential for *facial* coordination, although the much poorer donor ability of the ether oxygen atom has thus far resulted in only the two S-atoms participating in coordination: bidentate coordination to Ag(I) was shown in Chapter 2. The small macrocyclic ring in these two ligands makes them ideal capping ligands, analogous to 9S3. However, the increased flexibility of thiacyclophanes may allow for a wider variety of attainable structures in solution, resulting in the generation of unsaturated species and an enhanced reaction chemistry. Reported herein are the synthesis, structures, and basic reaction chemistry of the complexes $[M(COD)(L)]^+$, where M = Rh, Ir; COD = 1,5-cyclooctadiene, and L = (TT[9]OC) or (ODT[9]OC).

4.2 Experimental

$[RhCl(COD)]_2$[91], $[IrCl(COD)]_2$[92], $[IrCl(COE)_2]_2$[93], TT[9]OC[54a], and ODT[9]OC[56] were prepared by literature methods. $AgBF_4$, $NOBF_4$, $[RhCl(CO)_2]_2$, organic reagents, and all deuterated solvents were purchased from Aldrich and used as received. All reactions were carried out under an atmosphere of N_2 unless otherwise specified, using standard Schlenk techniques, and all solvents were degassed prior to use. ^1H and $^{13}C\{^1H\}$ NMR spectra (300-220 K) were recorded at 300.1 and 75.4 MHz respectively on a Bruker AC300 spectrometer locked to the deuterated solvent. $^{31}P\{^1H\}$ NMR spectra were recorded at 81.0 MHz on a Bruker AM200 spectrometer with an external H_3PO_4 reference. Infrared spectra were recorded on a Nicolet 5DX FTIR spectrometer. Elemental analyses were performed by Microanalytical Services, Delta, British Columbia, Canada.

4.2.1 General Preparation of [M(COD)(L)][BF_4] Complexes

$AgBF_4$ (2 mmolex) was weighed into a 50 mL Schlenk flask in a drybox and then this flask was attached to a Schlenk line. $[MCl(COD)]_2$ (M = Rh, Ir) (1 mmole) was added against the flow of N_2, followed by acetone. The resulting coloured solution (orange or yellow) and white precipitate of AgCl(s) were stirred for 2 h, after which the precipitate was allowed to settle. This solution was then filtered into a solution of thioether ligand (2 equiv.) in acetone and stirred overnight. The volume of the resulting solution was reduced by *ca.* half and the desired product crystallized by diffusion of diethyl ether into the mother liquor.

[Rh(COD)(TT[9]OC)][BF_4], (10): Yield: 380 mg (76 %), orange microcrystals. Anal. Calcd for $C_{20}H_{28}RhS_3BF_4$: C, 43.33; H, 5.10. Found: C, 43.16; H, 5.03.

[Ir(COD)(TT[9]OC)][BF_4], (11): Yield: 385 mg (77 %), yellow microcrystals. Anal. Calcd for $C_{20}H_{28}IrS_3BF_4$: C, 37.32; H, 4.39. Found: C, 37.22; H, 4.33.

[Rh(COD)(ODT[9]OC)][BF_4], (12): Yield: 340 mg (68 %), orange microcrystals. Anal. Calcd for $C_{20}H_{28}RhOS_2BF_4$: C, 44.62; H, 5.25. Found: C, 44.95; H, 5.26.

[Ir(COD)(ODT[9]OC)][BF_4], (13): Yield: 325 mg (65 %), orange microcrystals. Anal. Calcd for $C_{20}H_{28}IrOS_2BF_4$: C, 38.27; H, 4.51. Found: C, 38.62; H, 4.48.

4.2.2 Reaction of Complexes 10 - 13 with Phenylacetylene

The complex (100 mg) was dissolved in acetone (5 mL) and phenyl acetylene (2.0 molar equivalent) was added to the solution. The solution was stirred for 3 h, solvent was removed *in vacuo*, and the remaining orange (complexes **10**, **12**, **13**) or yellow (**11**) solid was washed with diethyl ether (3 x 3 mL). ^{1}H NMR (acetone-d_6) indicated that no reaction had occurred.

4.2.3 Reactions of Complexes 10 - 13 with H_2

The complex (100 mg) was dissolved in acetone (5 mL) and refluxed under an atmosphere of H_2 for 10 h. After removal of solvent under reduced pressure, ^{1}H NMR indicated that no reaction had occurred.

4.2.4 Reactions of Complexes 10 - 13 with PPh_3

The complex (100 mg) was dissolved in acetone, and PPh_3 (1.0 equivalent) was added. The solution was stirred for 3 h, and then solvent was removed *in vacuo*, leaving orange (complexes **10**, **12**, **13**) or yellow (**11**) solid. After washing with diethyl ether (3 x 3 mL), ^{1}H NMR indicated that no reaction had occurred. If excess phosphine is used in this reaction, then ^{1}H NMR spectroscopy indicates that free TT[9]OC or ODT[9]OC is present in solution.

4.2.5 Preparation of $[Rh(CO)_2(TT[9]OC)][BF_4]$, (14) and $[(TT[9]OC)Rh(\mu\text{-}CO)_3Rh\text{-}(TT[9]OC)][BF_4]_2$, (15)

Method I: **10** (20 mg, 0.0361 mmol) was dissolved in acetone (0.5 mL) under an atmosphere of CO and stirred for 2 h, during which time the solution changed colour from orange to orange-red. Stirring was stopped, and the solution was cooled to -20°C for 48 h under CO to precipitate an orange solid found to be a mixture of **14** and **15**. Recrystalliziation of this solid under CO yields a very small amount of **14**; under N_2 **15** is obtained in 30% yield. **14**: IR: ν(CO): 2059, 1933. cm^{-1}. A satisfactory elemental analysis could not be obtained as samples were consistently contaminated with **15**. **15**: IR: ν(CO): 1862, 1841 cm^{-1}. Anal. Calcd for $C_{27}H_{32}S_6O_3Rh_2B_2F_8$: C, 33.21; H, 3.31. Found: C, 33.17; H, 3.28.

Method II: $AgBF_4$, (100 mg, 0.514 mmol) was weighed into a Schlenk flask in a drybox and then this flask was attached to a Schenk line. $[RhCl(CO)_2]_2$ (100 mg, 0.217 mmol) was added against the flow of N_2, followed by acetone (10 mL). The resultant yellow mixture was stirred for 10 min and then TT[9]OC (132 mg, 0.514 mmol) was added as a solid against the flow of N_2. The mixture was stirred overnight, and then the volume of the solution was reduced by *ca.* half. The products **14** and **15** were co-crystallized by diffusion of diethyl ether into the mother liquor under N_2. Yield 150 mg, of a 2:1 mixture of **15** to **14**. 50 mg **14**, 10%; 100 mg **15**, 47%. **15** was recrystallized by diffusion of diethyl ether into an acetone solution of the complex. **14** was not stable in solution long enough to be recrystallized, deomposing within 12 h.

4.2.6 Preparation of [Rh(CO)(PPh_3)(TT[9]OC)][BF_4], (16)

15 (100 mg, 0.102 mmol) was dissolved in acetone (10 ml), and a solution of PPh_3 (53 mg, 0.205 mmol) in acetone (3 mL) was added. The resultant orange solution was stirred for 1 h, the volume was reduced, and the product recrystallized by cooling the solution to -20°C for 24 h. IR: ν(CO): 1959 cm^{-1}, $^{31}P\{^1H\}$ NMR: δ 41.23 ppm, J_{Rh-P} = 133 Hz. Yield orange microcrystals 123 mg, 93 %. Anal. Calcd for $C_{31}H_{31}ORhS_3BF_4$: C: 52.77; H: 4.43. Found: C: 52.71; H: 4.40.

4.2.7 Reaction of 15 with MeI

15 (20 mg, 0.020 mmol) was placed in an NMR tube under N_2 and acetone-d_6 (0.5 mL) was added. MeI (10 μL, 0.020 mmol) was added to the NMR tube, which was shaken for 10 minutes. The orange solution darkened slightly, but the ^1H NMR spectrum of the reaction mixture indicated that no reaction had occurred.

4.2.8 Preparation of [Ir(CO)(COE)(TT[9]OC)][BF_4], (17)

$AgBF_4$ (43 mg, 0.223 mmol) was weighed into a 50 mL Schlenk flask in a drybox and then this flask was attached to a Schlenk line. $[IrCl(COE)_2]_2$ (100 mg, 0.112 mmol) was added as a solid, followed by acetone (25 mL). The resultant brown mixture was stirred for 1 h, and then a solution of TT[9]OC (57 mg, 0.223 mmol) in acetone (5 mL) was added. The resulting yellow mixture was stirred for 2 h and then the N_2 atmosphere was replaced by CO. Stirring was continued for 10 h, and then the mixture was filtered to yield a yellow solution. Yellow microcrystals of [Ir(CO)(COE)(TT[9]OC)][BF_4] were

obtained by diffusion of diethyl ether into the mother liquor under an atmosphere of CO. Yield 45 mg (61 %). IR: ν(CO) 2073 cm^{-1}. Anal. Calcd for $C_{21}H_{30}OIrS_3BF_4$: C, 38.35; H, 4.61. Found: C, 38.27; H, 4.66.

4.2.9 Preparation of $[Ir(CO)_2(TT[9]OC)][BF_4]$, (18)

$AgBF_4$ (43 mg, 0.22 mmol) was weighed into a Schlenk flask in a drybox and then this flask was transferred to a Schlenk line. $[IrCl(COE)_2]_2$ (100 mg, 0.112 mmol) was added as a solid against the flow of N_2. The atmosphere was changed to CO and the solid $[IrCl(COE)_2]_2$ began to darken. CH_3CN (10 mL) was added, resulting in an intense blue-green precipitate and a pale yellow solution. This mixture was stirred for 30 min and then TT[9]OC (57 mg, 0.22 mmol) was added as a solid against the flow of CO. The mixture gradually lightened in colour, resulting in a yellow-orange solution and grey AgCl precipitate. After stirring for 10 h under CO the mixture was filtered to yield a yellow solution. The product was precipitated by diffusion of diethyl ether into the mother liquor. Yield of pale yellow microcrystals, 30 mg (46 %). IR: ν(CO) 2095, 2045 cm^{-1}. Anal. Calcd for $C_{14}H_{16}IrS_3O_2BF_4$: C, 28.42; H, 2.73. Found: C, 28.33; H, 2.67.

4.2.10 Reaction of $[Ir(CO)_2(TT[9]OC)][BF_4]$ with PPh_3

18 (100 mg, 0.169 mmol) was dissolved in acetone (5 mL) and a solution of PPh_3 (44 mg, 0.169 mmol) in acetone (5 mL) was added. The resultant orange solution was stirred for 3 h, with no observed change. The solvent was removed *in vacuo*, and the orange solid dissolved in acetone-d_6; ^1H NMR indicated that no reaction had occurred.

4.2.11 Reaction of $[Ir(CO_2)(TT[9]OC)][BF_4]$ with Me_3NO

18 (100 mg, 0.169 mmol) was dissolved in acetone (5 mL) and Me_3NO (8 mg, 0.169 mmol) was added as a solid. The resultant orange solution was stirred for 3 h, with no observed change. The solvent was removed *in vacuo*, and the orange solid dissolved in acetone-d_6; ^1H NMR and infrared spectroscopies indicated that no reaction had occurred.

4.2.12 Preparation of $[Rh(CO)_3(ODT[9]OC)][BF_4]$, (19)

Method I: 12 (20 mg, 0.0372 mmol) was dissolved in acetone (1 mL) under an atmosphere of CO and stirred for 2 h, during which time the solution did not change colour. The solution was cooled to -20 °C for 48 h, and a yellow-orange powder precipitated. After removing the mother liquor by syringe, the precipitate was washed with diethyl ether to remove COD and then dried *in vacuo*. Yield 8 mg, 42%. IR: ν(CO) 2103, 2044, 2015 cm^{-1}. Anal. Calcd for $C_{15}H_{16}O_4S_2RhBF_4$: C, 35.04; H, 3.14. Found: C, 34.93; H, 3.11.

Method II: $AgBF_4$ (100 mg, 0.514 mmol) was weighed out in a drybox into a Schlenk flask and then this flask was transferred to a Schlenk line. $[RhCl(CO)_2]_2$ (100 mg, 0.217 mmol) was added against the flow of N_2, followed by acetone (10 mL). The resultant yellow mixture was stirred for 10 min and then a solution of ODT[9]OC (124 mg, 0.514 mmol) in acetone (10 mL) was added and the mixture was stirred overnight. The solution was filtered, and the volume reduced by *ca.* half, and **19** was recrystallized by diffusion of diethyl ether into the mother liquor. Yield: 150 mg, 56%.

4.2.13 Preparation of $[Ir(CO)_3(ODT[9]OC)][BF_4]$, (20)

13 (20 mg, 0.0319 mmol) was dissolved in acetone (0.5 mL) and stirred under an atmosphere of CO for 30 min. The solution changed colour from orange to red to dark orange and a yellow powder precipitated from solution after about 10 minutes. The product was filtered, washed with diethyl ether to remove free COD, and dried *in vacuo*. Yield 12 mg, 62%. IR: ν(CO), 2024 cm^{-1} (br). Anal. Calcd for $C_{15}H_{16}O_4S_2IrBF_4$: C, 29.85; H, 2.68. Found: C, 29.76; H, 2.58.

4.2.14 Preparation of $[Rh(COD)(NO)(TT[9]OC)][BF_4]_2$, (21)

10 (20 mg, 0.0372 mmol) was weighed into an NMR tube and $NOBF_4$ (5 mg, 0.0423 mmol) added as a solid. The tube was capped and placed under an atmosphere of N_2. Acetone-d_6 (0.5 mL) was added and the ^1H NMR and infrared spectra of the resultant brown solution were recorded immediately. IR (CH_3CN): ν(NO) 1686 cm^{-1}. This compound was completely decomposed within 15 min of mixing with apparent loss of cyclooctadiene, detected by ^1H NMR spectroscopy. No pure solid product could be isolated before this decomposition occurred.

4.2.15 Preparation of $[Ir(COD)(NO)(TT[9]OC)][BF_4]_2$, (22)

11 (20 mg, 0.032 mmol) was weighed into an NMR tube and $NOBF_4$ (4 mg, 0.04 mmol) was added as a solid. The tube was capped and placed under an N_2 atmosphere. Acetone-d_6 (0.5 mL) was added and the NMR and infrared spectra of the resultant bright yellow solution were recorded immediately. NMR spectra (acetone-d_6) clearly showed 2

products in a 1:1 ratio. IR (CH_3CN): ν(NO) 1678, 1639 cm^{-1}. This mixture was completely decomposed within 30 min of mixing with apparent loss of cyclooctadiene, as detected by ^1H NMR spectroscopy. No pure solid product could be isolated before this decomposition occurred.

4.2.16 Preparation of $[Rh(COD)(NO)(ODT[9]OC)][BF_4]_2$, (23)

12 (20 mg, 0.0372 mmol) was weighed into an NMR tube and $NOBF_4$ (4 mg, 0.04 mmol) was added as a solid. The tube was capped and placed under an N_2 atmosphere. Acetone-d_6 was added and the NMR and infrared spectra of the resultant dark green solution were recorded immediately, clearly showing that two products were present in a 1:3 ratio. IR (CH_3CN): ν(NO) 1712, 1671 cm^{-1}. This mixture was completely decomposed within 30 min of mixing with apparent loss of cyclooctadiene, as detected by ^1H NMR spectroscopy. No pure solid product could be isolated before this decomposition occurred.

4.2.17 Preparation of $[Ir(COD)(NO)(ODT[9]OC)][BF_4]_2$, (24)

13 (100 mg, 0.159 mmol) and $NOBF_4$ (19 mg, 0.160 mmol) were weighed out and placed in a flask under N_2. Acetone (5 mL) was added and the resultant dark green solution stirred for 5 min. Diethyl ether was added until a small amount of precipitate formed. The mixture was cooled to -20 °C for 10 h to give **24** as well formed dark green crystals suitable for single crystal X-ray analysis. Yield: 50 mg, 43%. After this initial crystallization, further product could not be isolated due to decomposition. Dissolution of

the green crystals from the sample used for diffraction study showed two products in solution in a 1:2 ratio. IR (KBr pellet): ν(NO) 1708 cm^{-1}. IR (CH_3CN): ν(NO) 1695, 1655 cm^{-1}. Anal. Calcd for $C_{20}H_{28}IrO_2NS_2B_2F_8$: C, 32.27; H, 3.80. Found: C, 32.12; H, 3.89.

4.2.18 X-ray Structure Determination of [Rh(COD)(TT[9]OC)][BF_4], (10)

General data collection information is given in Section 2.2.4 of this work. Orange crystals of complex **10** were grown by vapour diffusion of diethyl ether into an acetonitrile solution of the complex. A statistical analysis of intensity distributions and a determination of systematic absences were consistent with the space group $Pca2_1$, and this was confirmed by successful solution refinement. A total of 2277 reflections were collected and 1192 reflections with $F_o > 3\sigma(F_o)$ were used in the refinement. The position of the rhodium atom was determined by the conventional heavy atom method, and the remaining non-hydrogen atoms were located from difference Fourier calculations. In the final cycles of refinement, the rhodium, sulphur, boron, and fluorine atoms were assigned anisotropic thermal parameters, and carbon atoms were assigned isotropic thermal parameters, resulting in $R = 5.26\%$ and $R_w = 5.70\%$. A goodness of fit calculation resulted in a value of 1.72, and a final difference Fourier map calculation showed no peaks of chemical significance. A summary of crystal data, intensity collection, and structure refinement is listed in Table A.4.1, positional parameters are listed in Table A.4.2, and bonding parameters are listed in Table A.4.3.

4.2.19 X-ray Structure Determination of [Ir(COD)(TT[9]OC)][BF_4], (11)

Yellow crystals suitable for diffraction studies were grown by cooling an acetonitrile solution of the complex to -20°C for three days. A statistical analysis of intensity distributions was consistent with $P\bar{1}$, and this was confirmed by successful structure refinement. A total of 3823 reflections were collected and 2935 reflections with $F_o > 3\sigma(F_o)$ were used in the refinement. The position of the iridium atom was determined by the conventional heavy atom method, and the remaining non-hydrogen atoms were located from successive difference Fourier calculations. In the final cycles of refinement, the iridium, sulphur, boron, and fluorine atoms were assigned anisotropic thermal parameters, and the carbon atoms were assigned isotropic thermal parameters, resulting in $R = 4.06\%$ and $R_w = 4.41\%$. A goodness of fit calculation resulted in a value of 1.49, and a final difference Fourier map calculation showed no peaks of chemical significance. A summary of collection data, intensity collection, and structure refinement is shown in Table A.4.4, positional parameters are listed in Table A.4.5, and bonding parameters are listed in Table A.4.6.

4.2.20 X-ray Structure Determination of [Rh(COD)(ODT[9]OC)][BF_4], (12)

Orange crystals of [Rh(COD)(ODT[9]OC)][BF_4] suitable for X-ray diffraction studies were grown by diffusion of diethyl ether into an acetone solution of the complex. A statistical analysis of intensity distributions and a determination of systematic absences were consistent with the space group $P2_1/c$, and this was confirmed by successful structure refinement. A total of 4233 reflections were collected and 2312 reflections with $F_o >$

$3\sigma(F_o)$ were used in the refinement. The position of the rhodium atom was determined by the conventional heavy atom method, and the remaining non-hydrogen atoms were located by successive difference Fourier calculations. In the final cycles of refinement, the rhodium, sulphur, oxygen, boron, and fluorine atoms were assigned anisotropic thermal parameters, and the carbon atoms were assigned isotropic thermal parameters, resulting in $R = 5.84\%$ and $R_w = 6.87\%$. A goodness of fit calculation resulted in a value of 1.85, and a final difference Fourier map calculation showed no peaks of chemical significance. A summary of crystal data, intensity collection, and structure refinement is shown in Table A.4.7, positional parameters are listed in Table A.4.8, and bonding parameters are listed in Table A.4.9.

4.2.21 X-ray Structure Determination of [Ir(COD)(ODT[9]OC)][BF_4], (13)

Orange crystals of **13** suitable for X-ray diffraction study were grown by cooling an acetone solution of the complex to -20°C for 24 h. A statistical analysis of intensity distributions was consistent with $P\bar{1}$, and this was confirmed by successful structure refinement. A total of 4047 reflections were collected and 3802 reflections with $F_o > 3\sigma(F_o)$ were used in the refinement. The position of the iridium atom was determined by the conventional heavy atom method, and the remaining non-hydrogen atoms were located from successive difference Fourier calculations. In the final cycles of refinement, the iridium, sulphur, oxygen, boron, and fluorine atoms were assigned anisotropic thermal parameters, and the carbon atoms were assigned isotropic thermal parameters, resulting in $R = 6.59\%$ and $R_w = 7.38\%$. A goodness of fit calculation resulted in a value of 2.95, and

a final difference Fourier map calculation showed no peaks of chemical significance. A summary of collection data, intensity collection, and structure refinement is shown in Table A.4.10 positional parameters are listed in Table A.4.11, and bonding parameters are listed in Table A.4.12.

4.2.22 X-ray Structure Determination of [Ir(CO)(COE)(TT[9]OC)][BPh_4], (17)

Yellow crystals of [Ir(CO)(COE)(TT[9]OC)][BPh_4] were grown by diffusion of diethyl ether into an acetonitrile solution of the complex under an atmosphere of CO. A statistical analysis of intensity distributions and a determination of systematic absences were consistent with the space group *Pbca*, and this was confirmed by successful structure refinement. A total of 6726 reflections were collected, and 1493 reflections with $F_o > 3\sigma(F_o)$ were used in the refinement. The position of the iridium atom was determined by the conventional heavy atom method, and the remaining non-hydrogen atoms were located by successive difference Fourier calculations. In the final cycles of refinement, the iridium, sulphur, boron, and oxygen atoms were assigned anisotropic thermal parameters, and the carbon atoms were assigned isotropic thermal parameters, except for the carbon atoms of the BPh_4^- anion, which were input as rigid phenyl groups and assigned isotropic thermal parameters. This resulted in $R = 7.68\%$, and $R_w = 7.98\%$. A goodness of fit calculation resulted in a value of 1.73, and a final difference Fourier map calculation showed no peaks of chemical significance. A summary of crystal data, intensity collection, and structure refinement is shown in Table A.4.13, positional parameters are listed in Table A.4.14, and bonding parameters are listed in Table A.4.15.

4.2.23 X-ray Structure Determination of [Ir(NO)(COD)(ODT[9]OC)][BF_4]$_2$, (24)

Emerald green crystals of [Ir(NO)(COD)(ODT[9]OC)][BF_4]$_2$ suitable for X-ray diffraction studies were grown by cooling an acetone/diethyl ether solution of the complex to -20°C for 24 h. A statistical analysis of intensity distributions and a determination of systematic absences were consistent with the space group *Pnma*, and this was confirmed by successful structural refinement. A total of 2603 reflections were collected and 1180 reflections with $F_o > 3\sigma(F_o)$ were used in the refinement. The position of the iridium atom was determined by conventional heavy atom methods, and the remaining non-hydrogen atoms were located by successive difference Fourier calculations. In the final cycles of refinement, the iridium, sulphur, oxygen, nitrogen, carbon, boron, and fluorine atoms were assigned anisotropic thermal parameters, resulting in $R = 4.83\%$, and $R_w = 5.11\%$. A goodness of fit calculation resulted in a value of 1.79, and a final difference Fourier map calculation showed no peaks of chemical significance. A summary of crystal data, intensity collection, and structure refinement is shown in Table A.4.16, positional parameters are listed in Table A.4.17, and bonding parameters are listed in Table A.4.18.

4.3 Results

4.3.1 Synthesis of [M(COD)(L)][BF_4] Complexes

Rh(I) and Ir(I) complexes of TT[9]OC and ODT[9]OC were prepared by displacing solvent from [M(COD)(acetone)$_2$][BF_4] which was prepared *in situ* from the reaction of [MCl(COD)]$_2$ with two equivalents of $AgBF_4$ in acetone, as summarized in Equation 4.1.

$$[MCl(COD)]_2 + 2AgBF_4 + 2L \xrightarrow{\text{acetone}} 2[M(COD)L][BF_4] + 2AgCl \qquad (4.1)$$

Yields of these complexes range from 65 - 77 %, and the yellow or orange materials are soluble in polar organic solvents such as acetone and acetonitrile. ^{1}H NMR resonances for coordinated TT[9]OC or ODT[9]OC are consistent with a symmetrical coordination mode in which both benzylic sulphur atoms are coordinated to the metal. The most notable ^{1}H NMR spectral feature is the splitting of the benzylic proton resonances from a singlet, as observed in the free ligand, to a pair of doublets upon complexation. The ^{1}H NMR spectrum of [Ir(COD)(ODT[9]OC)][BF_4], **13**, in acetone-d_6 is shown in Figure 4.1, where the benzylic splitting is readily apparent at δ 4.84 ppm, with geminal coupling of 11.88 Hz. This splitting is the result of coordination of the benzylic sulphur atoms in a symmetrical fashion and formation of a seven membered chelate ring, placing the benzylic protons in axial and equatorial positions[78]. These benzylic resonances are readily apparent in the ^{1}H NMR spectra of all four $[M(COD)(L)]^+$ complexes and are a useful spectroscopic tool for monitoring the extent of a reaction in these systems. ^{1}H and $^{13}C\{^1H\}$ NMR data for complexes **10 - 13** are listed in Table 4.1.

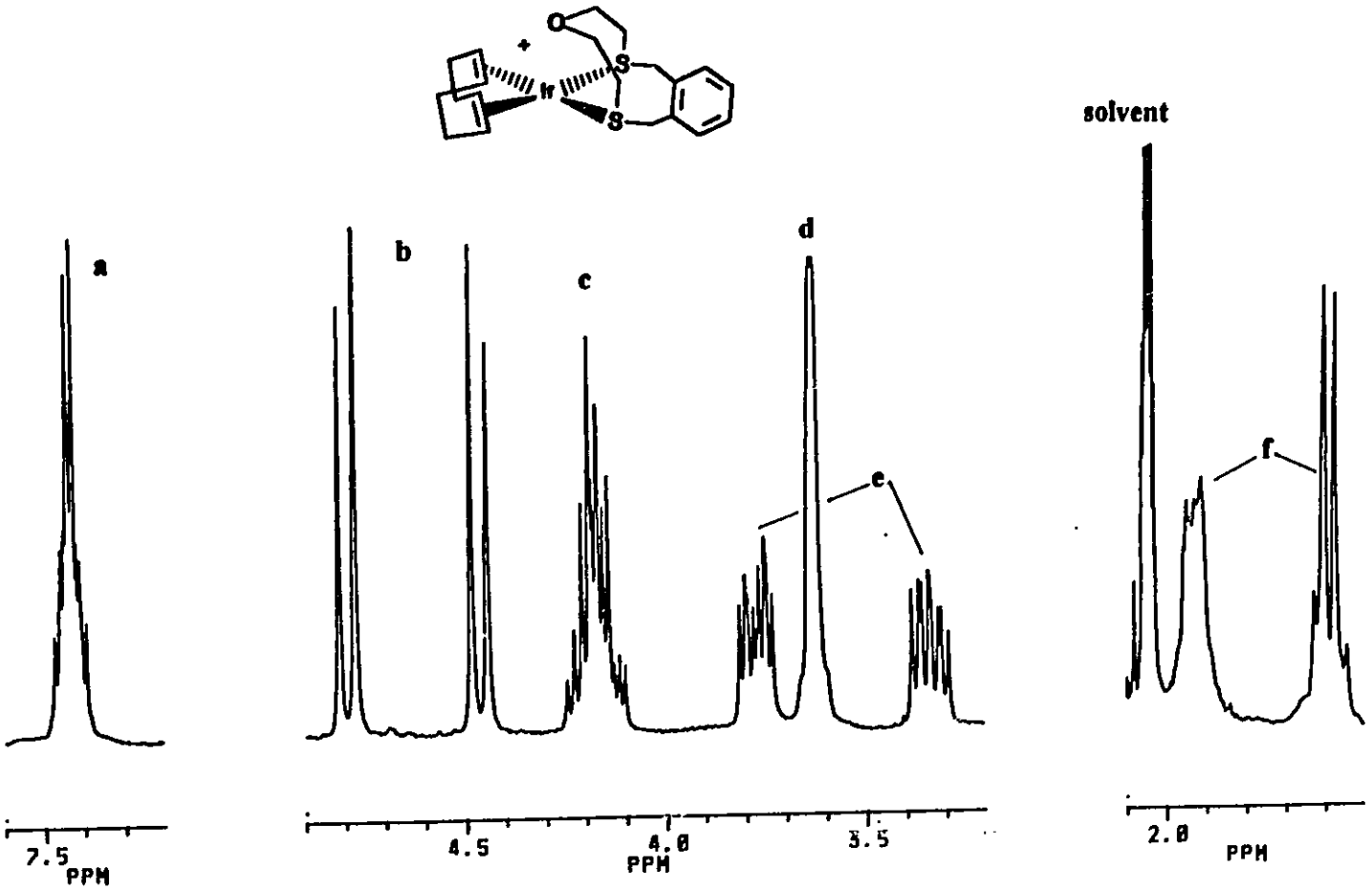

Figure 4.1 ^{1}H NMR spectrum of [Ir(COD)(ODT[9]OC)][BF_4], 13, in acetone-d_6. The peaks are labelled as follows: a) aromatic, b) benzylic, c) OCH_2, d) COD olefin, e) SCH_2, f) COD aliphatic.

Table 4.1 ^{1}H, $^{13}C\{^{1}H\}$ NMR Spectral Data for Complexes 10 - 13

^{1}H NMR, acetone-d_6

Complex	Aromatic	Benzylic	ECH_2[a]	Olefin	CH_2S	COD CH_2
10	7.44-7.34 (m,4H)	4.61 (m,4H) J=12.41 Hz	4.37 (m,4H)	3.47 (s,4H)	3.31-3.19 (m,4H)	2.28 (br,4H) 1.81 (q,4H)
11	7.47-7.38 (m,4H)	4.64 (d,2H) J=11.47 Hz 4.24 (d,2H)	3.48 (m,4H)	3.17 (br,4H)	3.26 (m,4H)	2.11 (br,4H) 1.81 (q,4H)
12	7.48 (s,4H)	4.31 (dd,2H) J=11.85 Hz J_{Rh-H}=2.00Hz 4.27 (d,2H)	4.17 (m,4H)	4.10 (s,4H)	3.51-3.28 (m,4H)	2.13 (br,4H) 1.90 (d,4H)
13	7.47 (m,4H)	4.84 (d,2H) J=11.88 Hz 4.49 (d,2H)	4.21 (m,4H)	3.69 (br,4H)	3.81-3.40 (m,4H)	1.98 (br,4H) 1.65 (q,4H)

$^{13}C\{^{1}H\}$ NMR, acetone-d_6

10	134.14, 131.09, 128.81	38.80	36.57	79.66 (d, J_{Rh-C}=10.5 Hz)	35.79	30.85
11	133.64, 131.13, 128.93	40.52	38.31	64.48	38.03	32.34
12	134.14, 130.91, 129.33	37.75	64.79	85.19 (d, J_{Rh-C}=12.0 Hz)	35.85	31.15
13	134.49, 131.74, 130.02	40.31	67.13	69.59	36.52	32.36

[a]E = S2 for complexes 10 and 11, O for complexes 12 and 13.

4.3.2 X-ray Structure of [Rh(COD)(TT[9]OC)][BF_4], (10)

The unit cell contains four [Rh(COD)(TT[9]OC)]$^+$ cations, and four BF_4^- anions. A perspective ORTEP drawing of the cation of complex **10** is shown in Figure 4.2. [Rh(COD)(TT[9]OC)]$^+$ is five-coordinate with an overall geometry best described as a distorted trigonal bipyramid. TT[9]OC is coordinated in a *facial* manner to two equatorial sites with Rh-S distances of Rh-S1 2.422(4) and Rh-S3 2.494(5) Å and one axial site with a shorter Rh-S distance of Rh-S2 2.316(5) Å. The larger seven-membered chelate ring involving the xylyl group spans the two equatorial coordination sites with an angle of 102.0(2)° for S1-Rh-S3, while the angles at Rh for the two five-membered chelate rings are 86.2(2) and 84.5(5)° for S1-Rh-S2 and S2-Rh-S3 respectively. The COD ligand occupies the remaining equatorial and axial sites in the trigonal bipyramid; the Rh-C distances of Rh-C13 2.23(2) and Rh-C14 2.18(2) Å for the olefinic bond in the axial position are slightly longer than those in the equatorial position: Rh-C17 2.12(2) and Rh-C18 2.10(2) Å.

4.3.3 X-ray Structure of [Ir(COD)(TT[9]OC)][BF_4], (11)

The unit cell contains two [Ir(COD)(TT[9]OC)]$^+$ cations, and four BF_4^- anions. A perspective ORTEP drawing of the complex cation of **11** is shown in Figure 4.3. The solid state structure of [Ir(COD)(TT[9]OC)]$^+$ is similar to that of complex **10**, showing the same distorted trigonal bipyramidal geometry. TT[9]OC is coordinated in a *facial* manner to two equatorial sites and one axial site but the variation in bond distances between these two sites is not as pronounced as for **10**; Ir-S1 2.444(3), Ir-S3 2.375(2) and Ir-S2 2.317(3) Å.

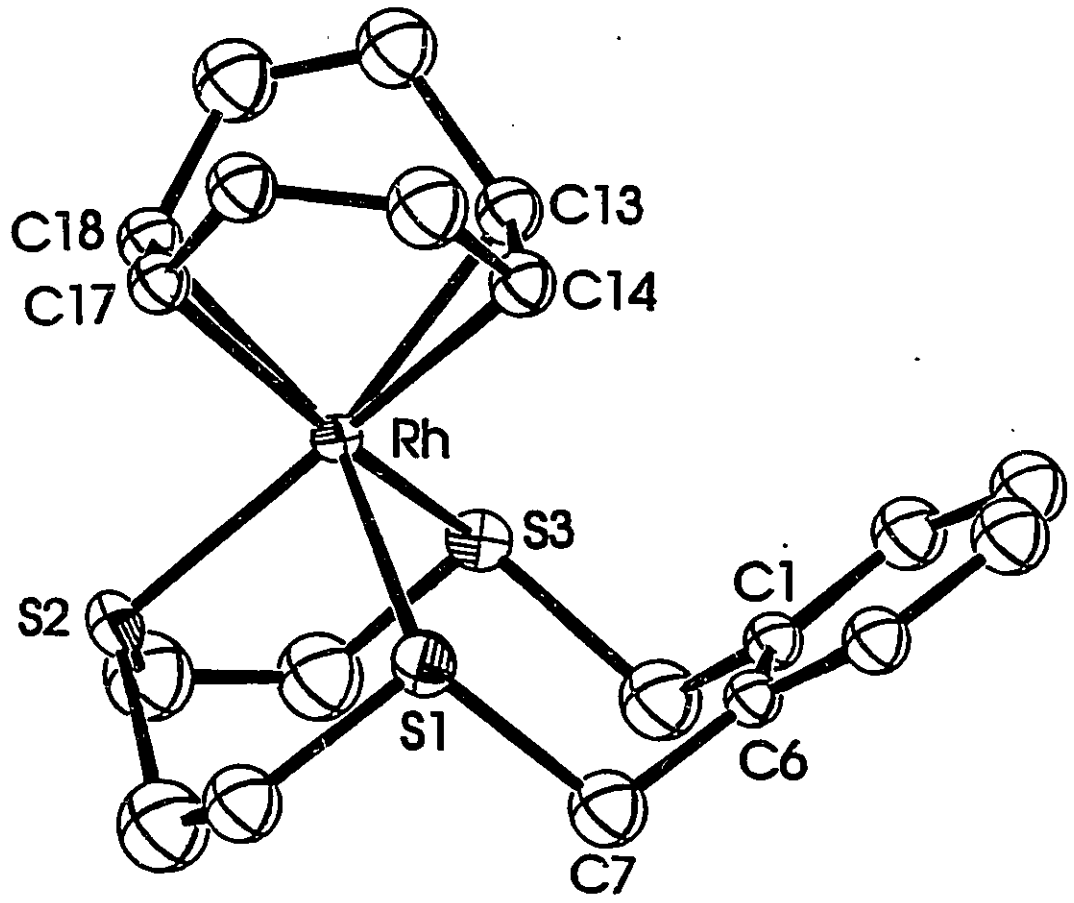

Figure 4.2 ORTEP drawing of the $[(Rh(COD)(TT[9]OC)]^+$ cation of 10, showing the atom-numbering scheme. Thermal ellipsoids of 30% probability are shown. Bond distances: Rh-S 2.422(4), Rh-S2 2.316(5), Rh-S3 2.494(5), Rh-C13 2.23(2), Rh-C14 2.18(2), Rh-C17 2.12(2), Rh-C18 2.10(2)Å. Bond angles: S1-Rh-S2 86.2(2)°, S1-Rh-S3 102.0(2)°, S2-Rh-S3 85.5(2)°, S1-Rh-C13 84.5(5)°, S1-Rh-C17 154.4(5)°, S2-Rh-C13 157.3(5)°, S2-Rh-C17 89.9(5)°, S3-Rh-C13 116.7(5)°, S3-Rh-C17 1029(5)°.

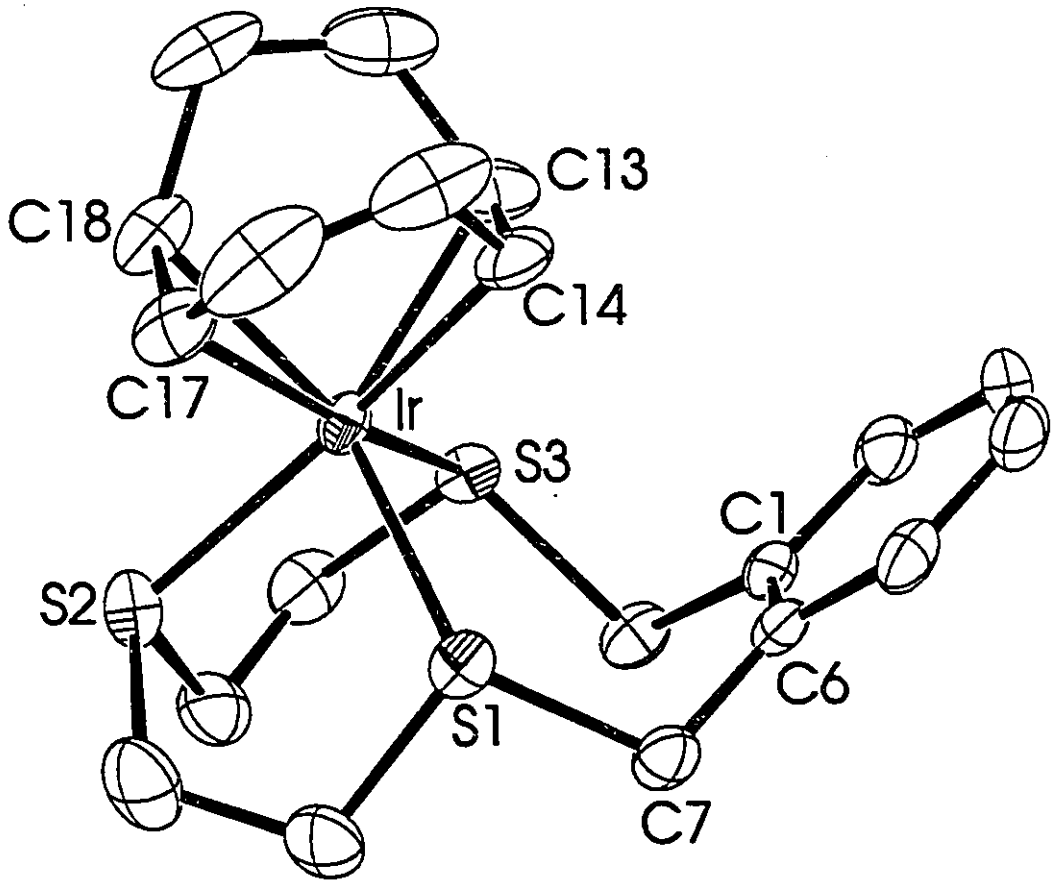

Figure 4.3 ORTEP drawing of the $[(Ir(COD)(TT[9]OC)]^+$ cation of 11, showing the atom-numbering scheme. Thermal ellipsoids of 30% probability are shown. Bond distances: Ir-S1 2.444(3), Ir-S2 2.317(3), Ir-S3 2.375(2), Ir-C13 2.17(1), Ir-C14 2.20(1), Ir-C17 2.12(1), Ir-C18 2.12(1) Å. Bond angles: S1-Ir-S2 86.7(1)°, S1-Ir-S3 100.33(8)°, S2-Ir-S3 85.8(1)°, S1-Ir-C13 117.6(5)°, S1-Ir-C17 98.7(3)°, S2-Ir-C13 154.9(5)°, S2-Ir-C17 88.6(4)°, S3-Ir-C13 83.6(4)°, S3-Ir-C17 159.8(4)°.

Also, as in **10**, the seven-membered chelate ring spans the two equatorial coordination sites with a larger angle of 100.33(8)° for S1-Ir-S3 while the angles for the two five-membered chelate rings are 86.7(1) and 85.8(1)° for S1-Ir-S2 and S2-Ir-S3 respectively. The COD ligand occupies the remaining equatorial and axial sites in the trigonal bipyramid with Ir-C13 2.17(1), Ir-C14 2.20(1), Ir-C17 2.12(1) and Ir-C18 2.12(1) Å.

4.3.4 X-ray Structure of [Rh(COD)(ODT[9]OC)][BF_4], (12)

The unit cell contains four [Rh(COD)(ODT[9]OC)]$^+$ cations, and four BF_4^- anions. A perspective ORTEP drawing of the complex cation of **12** is shown in Figure 4.4. [Rh(COD)(ODT[9]OC)]$^+$ is four-coordinate with a square planar geometry. The mixed S,O-donor ligand ODT[9]OC is coordinated to the Rh centre employing only the two benzylic sulphur atoms with Rh-S distances of Rh-S1 2.373(3) and Rh-S2 2.431(3) Å. Although the oxygen donor atom of ODT[9]OC is in an endodentate position required for chelation to the metal, there is no Rh-O bond as the Rh...O1 distance is 2.717(8) Å. The angle subtended at rhodium involving the xylyl group is slightly larger than the ideal angle of 90°, S1-Rh-S2 100.9(1)°, but this is presumably required to accommodate the large and relatively rigid seven-membered ring. The COD ligand chelates to the remaining coordination sites of the square plane with Rh-C distances of Rh-C13 2.15(1), Rh-C14 2.19(1), Rh-C17 2.12(1) and Rh-C18 2.12(1) Å.

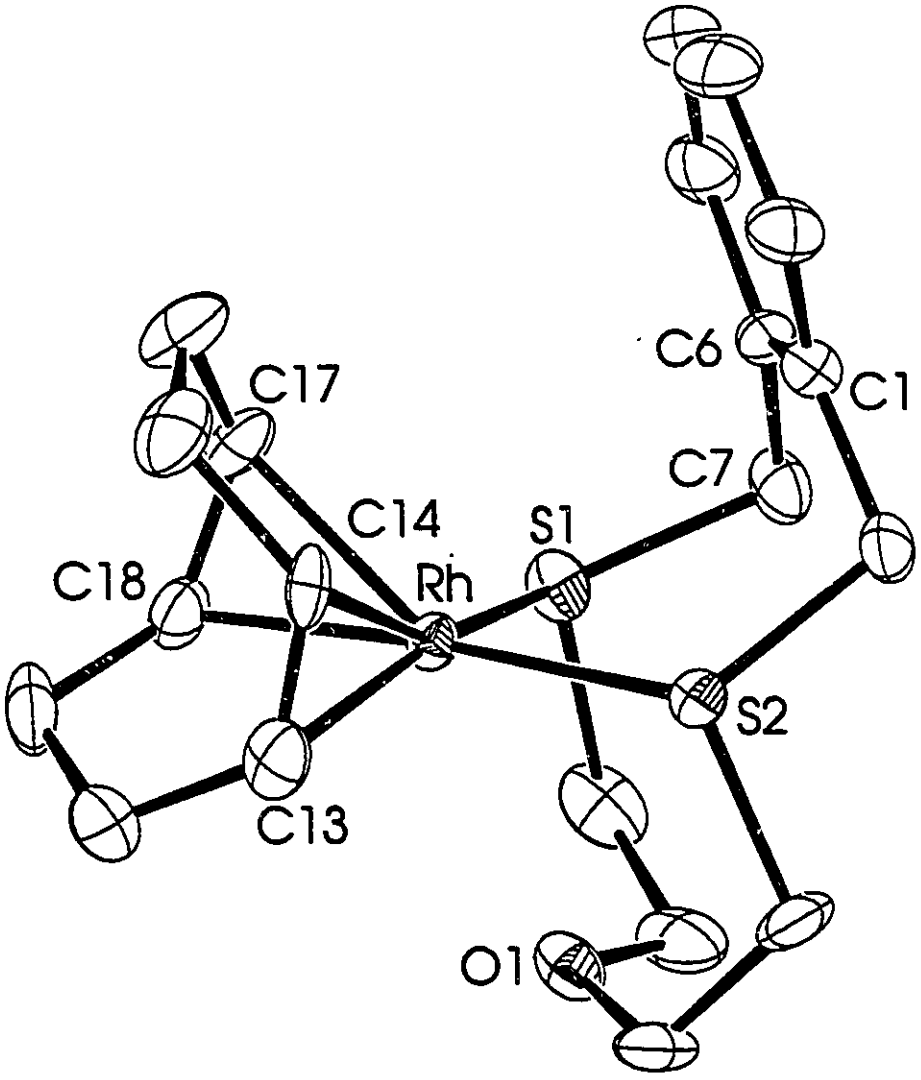

Figure 4.4 ORTEP drawing of the [(Rh(COD)(ODT[9]OC)]$^+$ cation of 12, showing the atom-numbering scheme. Thermal ellipsoids of 30% probability are shown. Bond distances: Rh-S1 2.373(3), Rh-S2 2.431(3), Rh-C13 2.15(1), Rh-C14 2.19(1), Rh-C17 2.12(1), Rh-C18 2.12(1) Å. Nonbonded distance: Rh...O1 2.717(8) Å. Bond angles: S1-Rh-S2 100.9(1)°, S1-Rh-C13 161.7(4)°, S1-Rh-C14 159.5(3)°, S1-Rh-C17 84.8(3)°, S1-Rh-C18 87.7(3)°, S2-Rh-C13 88.8(3)°, S2-Rh-C14 84.1(3)°, S2-Rh-C17 145.1(4)°, S2-Rh-C18 170.9(3)°.

4.3.5 X-ray Structure of [Ir(COD)(ODT[9]OC)][BF_4], (13)

As with the solid state structures of **10** and **11**, the structures of the Rh(I) and Ir(I) complexes containing ODT[9]OC are also similar. The unit cell contains two [Ir(COD)(ODT[9]OC)]$^+$ cations, and two BF_4^- anions. A perspective ORTEP drawing of the cation of complex **13** is shown in Figure 4.5. [Ir(COD)(ODT[9]OC)]$^+$ is four-coordinate with square planar geometry; the mixed S,O-donor ligand ODT[9]OC is coordinated to Ir(I) employing only the two benzylic sulphur atoms. The Ir-S distances are Ir-S1 2.407(6) and Ir-S2 2.348(5) Å with a non-bonding Ir...O1 distance of 2.59(1) Å and chelate angle of 100.8(2)° for S1-Ir-S2. The COD ligand chelates to the remaining coordination sites of the square plane with Ir-C distances of Ir-C13 2.08(2), Ir-C14 2.02(3), Ir-C17 2.14(2) and Ir-C18 2.20(2) Å.

4.3.6 Reactions of [M(COD)(L)][BF_4] with CO

The reaction chemistry of **10** - **13** with CO is summarized in Schemes 4.1 - 4.3. [Rh(COD)(TT[9]OC)][BF_4], **10** and [Ir(COD)(TT[9]OC)] [BF_4], **11**, are coordinatively saturated, 18-electron species, and as such, are relatively unreactive. Substitution reactions to replace COD with phosphine or acetylenes, and reactions with H_2, did not result in the formation of isolable products containing the thioether ligand. However, stirring a concentrated solution of **10** under an atmosphere of CO for five minutes results in a colour change from orange to brick red. $^{13}C\{^1H\}$ and ^1H NMR spectroscopy (data is shown in Table 4.2) show the formation of two products: the dicarbonyl complex [$Rh(CO)_2$(TT[9]OC)][BF_4], **14**, and the binuclear carbonyl complex

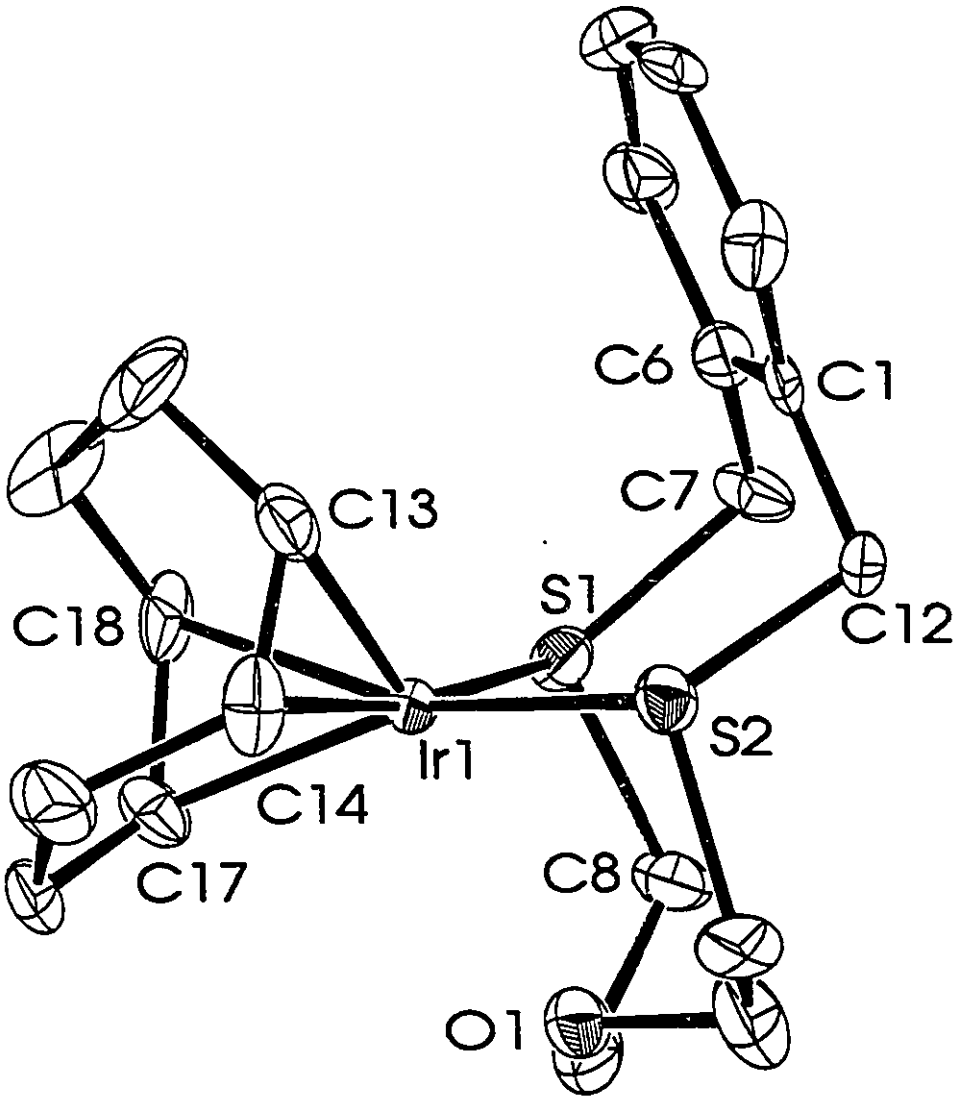

Figure 4.5 ORTEP drawing of the [(Ir(COD)(ODT[9]OC)]$^+$ cation of 13, showing the atom-numbering scheme. Thermal ellipsoids of 30% probability are shown. Bond distances: Ir-S1 2.407(6), Ir-S2 2.348(5), Ir-C13 2.08(2), Ir-C14 2.02(3), Ir-C17 2.14(2), Ir-C18 2.20(2) Å. Nonbonding Ir...O1 distance: 2.59(1) Å. Bond angles: S1-Ir-S2 100.8(2)°, S1-Ir-C13 133.1(7)°, S1-Ir-C14 169.3(7)°, S1-Ir-C17 96.2(6)°, S1-Ir-C18 81.4(7)°, S2-Ir-C13 85.0(6)°, S2-Ir-C14 85.7)6)°, S2-Ir-C17 156.0(6)°.

Table 4.2 ^{1}H, $^{13}C\{^{1}H\}$ NMR data for Complexes 14 - 20

^{1}H, NMR, Acetone-d_6, 300K

Complex	Aromatic	Benzylic	E[b]CH_2	CH_2S
14	7.66 (s,4H)	4.60 (d,2H) J=12.40 Hz 4.47 (d,2H)	3.63-3.20 (m, 8H)	
15	7.51-7.41 (m,4H)	4.63 (dd,2H) J=11.63 Hz; J_{Rh-H}=2.13 Hz 4.40 (d,2H)	3.61 (m,4H)	3.79 (m,2H) 3.33 (m,2H)
16	7.71-7.43 (m,4H)	4.59 (dd) J=11.82 Hz; J_{Rh-H}=2.70 Hz	3.23-2.96 (m, 8H)	
17[a]	7.45 (s,4H)	4.72 (d,2H) J=11.34 Hz 4.44 (d,2H)	3.57 (m,4H)	3.38 (m,4H)
18	7.75 (m,4H)	4.86 (d,2H) J=11.76 Hz 4.35 (d,2H)	3.67 (m,4H)	3.90 (m,2H) 3.48 (m,2H)
19	7.48 (s,4H)	4.58 (d,2H) J=11.70 Hz 4.26 (d,2H)	4.12 (m,4H)	3.82 (m,4H)
20	7.62-7.46 (m,4H)	5.06 (d,1H) J=11.96 Hz 4.88 (d,1H) J=11.75 Hz 4.27 (m,2H) J=11.70 Hz	4.74 (ddd,1H) 4.44 (m,1H) 3.98 (dt,1H) 3.49 (m,1H)	3.39 (q,1H) 3.34 (q,1H) 3.23 (ddd,1H) 3.02 (dq,1H)

[a]COE (olefin): δ 3.85 (m,2H); COE (CH_2): δ 2.15 (m,4H), 1.60 (m,4H), 1.50 (s,4H).

[b]As previously, E = S for **14 - 18**, E = O for **19** and **20**.

Table 4.2 Continued

$^{13}C\{^1H\}$ NMR Data

Complex	Solvent	T(K)	CO	Aromatic	ECH_2	Benzylic	$CH_2\delta$
15	ace	180	185.75, 184.86	132.16, 131.74, 129.78	37.69	37.44	37.11
16	ace	190	192.04 (dd) J_{Rh-C}=64.1 Hz J_{P-C}=13 Mz	136.55, 131.72, 129.86 ligand 135.07, 132.22, 129.31, PPh_3 11.33, 11.93, 9.53 Hz	39.24	36.47	36.16
17[c]	CD_3CN	235	184.34	135.53, 131.62, 130.04	41.19	39.60.	34.66
18	ace	300	166.68	134.27, 131.99, 131.08	41.11	39.67	36.60
19	ace	210	179.97, 179.03	132.51, 130.79, 130.12	39.27	64.22	38.29
20	CD_3CN	300	169.65, 168.37, 157.68	133.42, 132.45, 130.04	44.29, 37.38	80.52, 77.17	37.18, 34.38

[c]COE (olefin): δ 65.95 ppm; COE(CH_2): δ 33.20, 31.80, 31.68 ppm

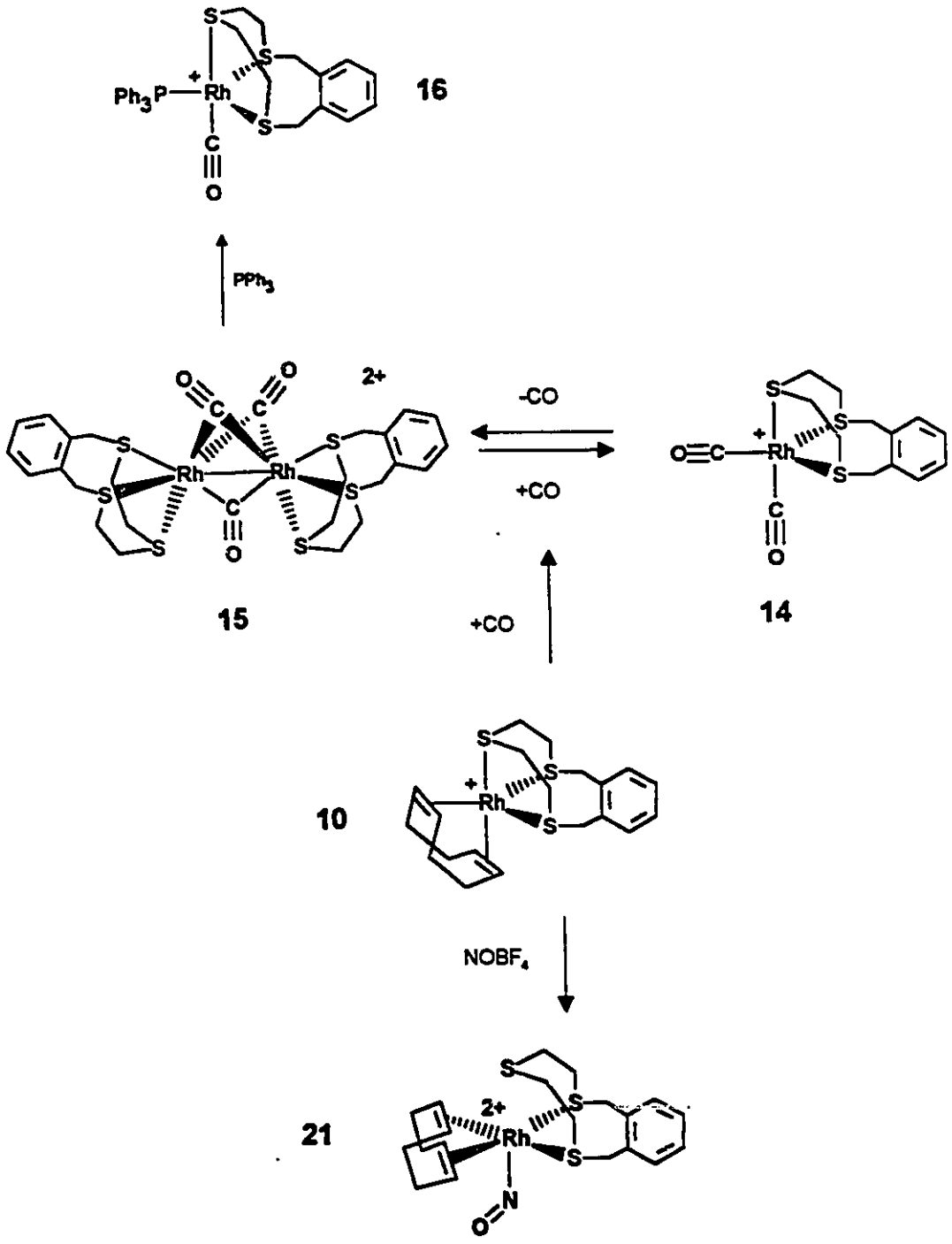

Scheme 4.1. Reactions of [Rh(COD)(TT[9]OC)][BF_4], (10)

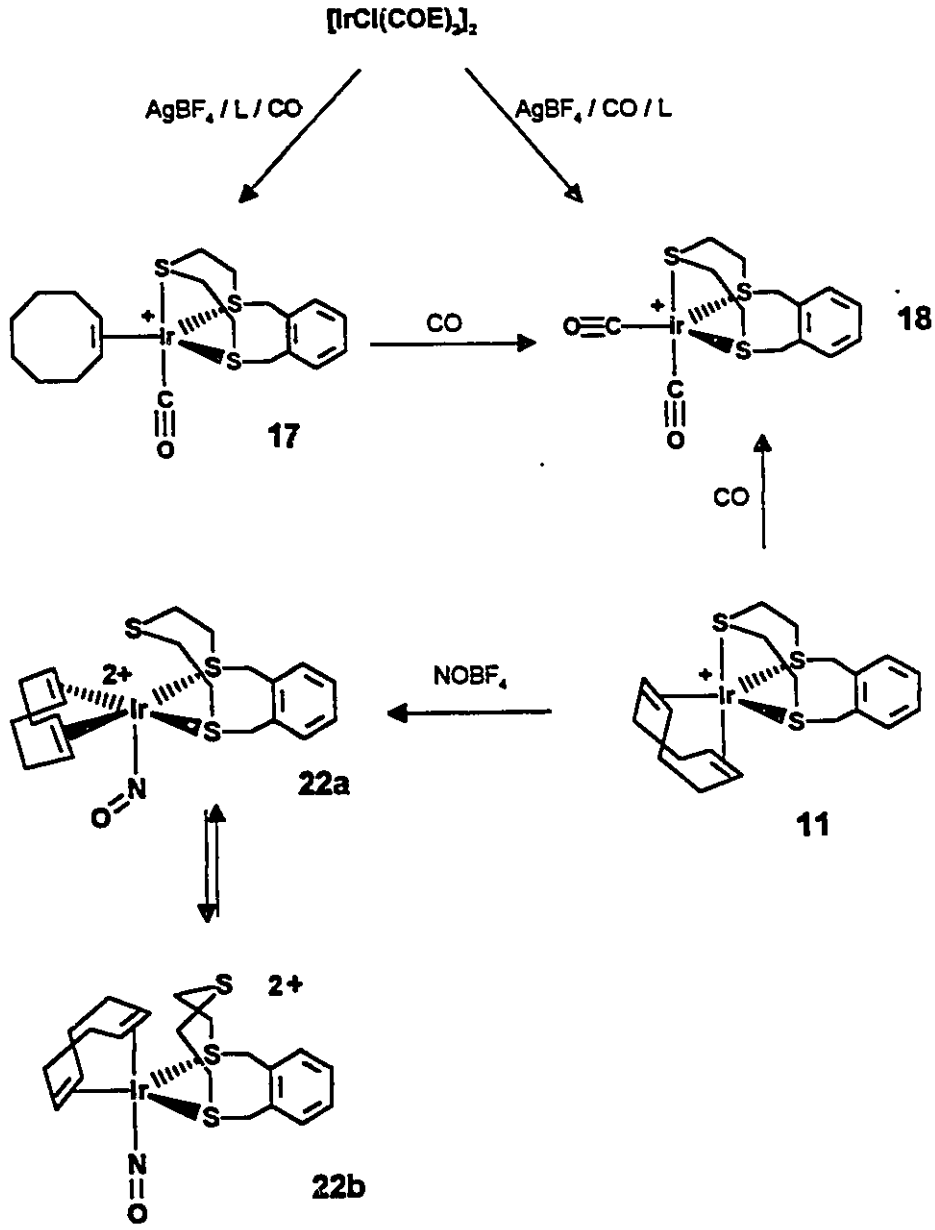

Scheme 4.2. Reactions of [Ir(COD)(TT[9]OC)][BF_4], (11)

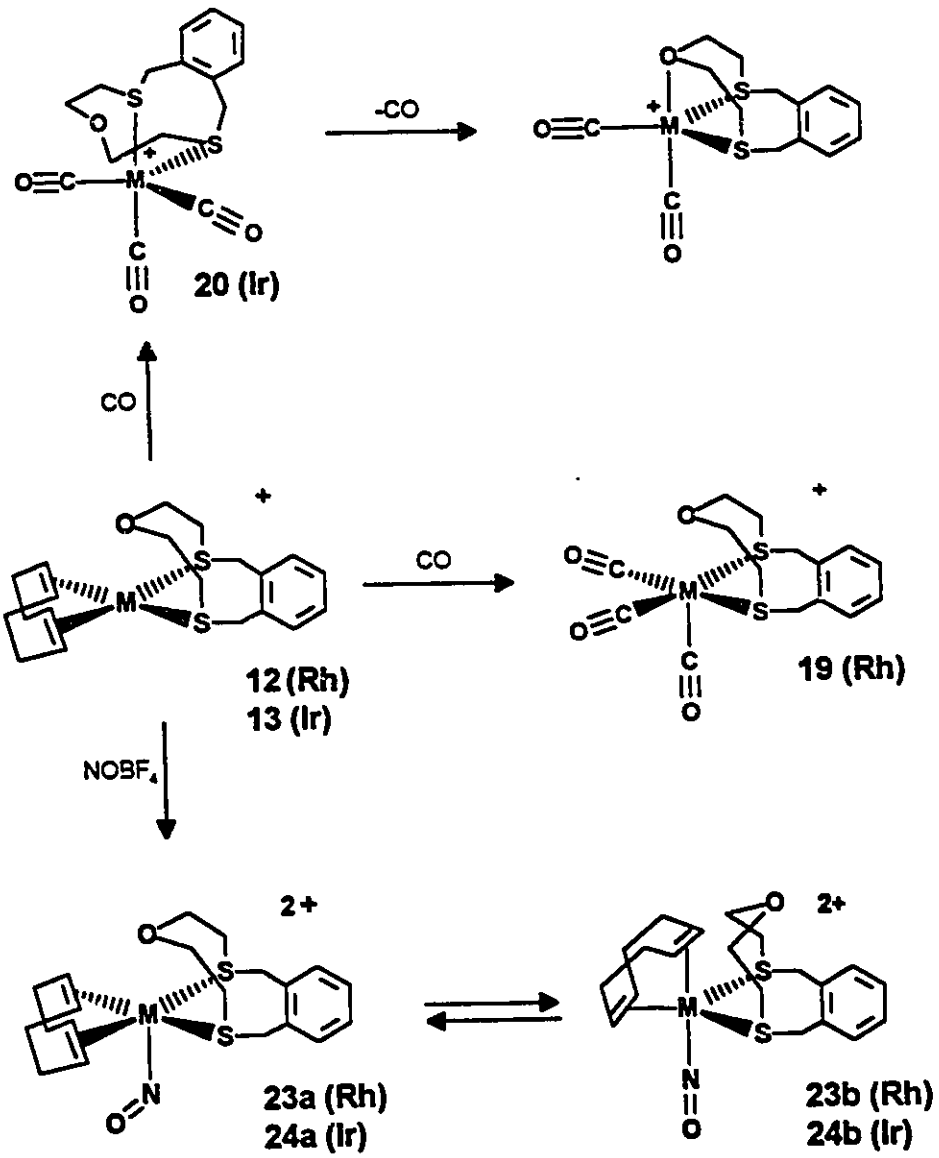

Scheme 4.3 Reactions of [M(COD)(ODT[9]OC)][BF_4], (12, M = Rh; 13, M = Ir)

$[(TT[9]OC)Rh(\mu\text{-}CO)_3Rh(TT[9]OC)][BF_4]_2$, **15**, which contains a Rh-Rh bond. Replacing the CO atmosphere with N_2 results in complete conversion to **15**; orange-red microcrystals of **15** could be isolated by removing the solvent from the reaction mixture, washing the residue with diethyl ether to remove COD, and recrystallizing a saturated solution at -20°C. Figure 4.6 shows the benzylic portion of the ^1H NMR spectrum of complexes **14** and **15**; as the CO atmosphere is replaced by a N_2 atmosphere, **14** is converted completely to **15**. The infrared spectrum of the mixture shows two ν(CO) absorptions at 2059 and 1933 cm^{-1}, attributable to the terminal carbonyls in complex **14**, and two ν(CO) absorptions at 1862 and 1841 cm^{-1}, due to the bridging carbonyl groups in complex **15**[94].

Complexes **14** and **15** can alternatively be synthesized from $[RhCl(CO)_2]_2$ in an analogous manner to complexes **10 - 13**, in higher yields than when starting from **10** and displacing COD with CO. Although the yield of **14** was greater using this method, carbonyl resonances were not visible in the $^{13}C\{^1H\}$ NMR spectrum, even at 170K. As well, it was not possible to obtain satisfactory elemental analysis.

The metal-metal bonded complex is reactive; PPh_3 is easily added across the bond with concomitant loss of CO to produce the monomer $[Rh(CO)(PPh_3)(TT[9]OC)][BF_4]$, **16**, in quantitative yield. The infrared spectrum of this complex shows one absorption at 1959 cm^{-1}, indicative of a terminal carbonyl. The PPh_3 resonance occurs at δ 41.23 ppm in the $^{31}P\{^1H\}$ NMR spectrum, with $J_{Rh\text{-}P}$ = 133 Hz. In the $^{13}C\{^1H\}$ NMR spectrum the carbonyl resonance is observed as a doublet of doublets at δ 192.04 ppm, $J_{Rh\text{-}C}$ = 64.1 Hz, and $J_{P\text{-}C}$ = 13 Hz.

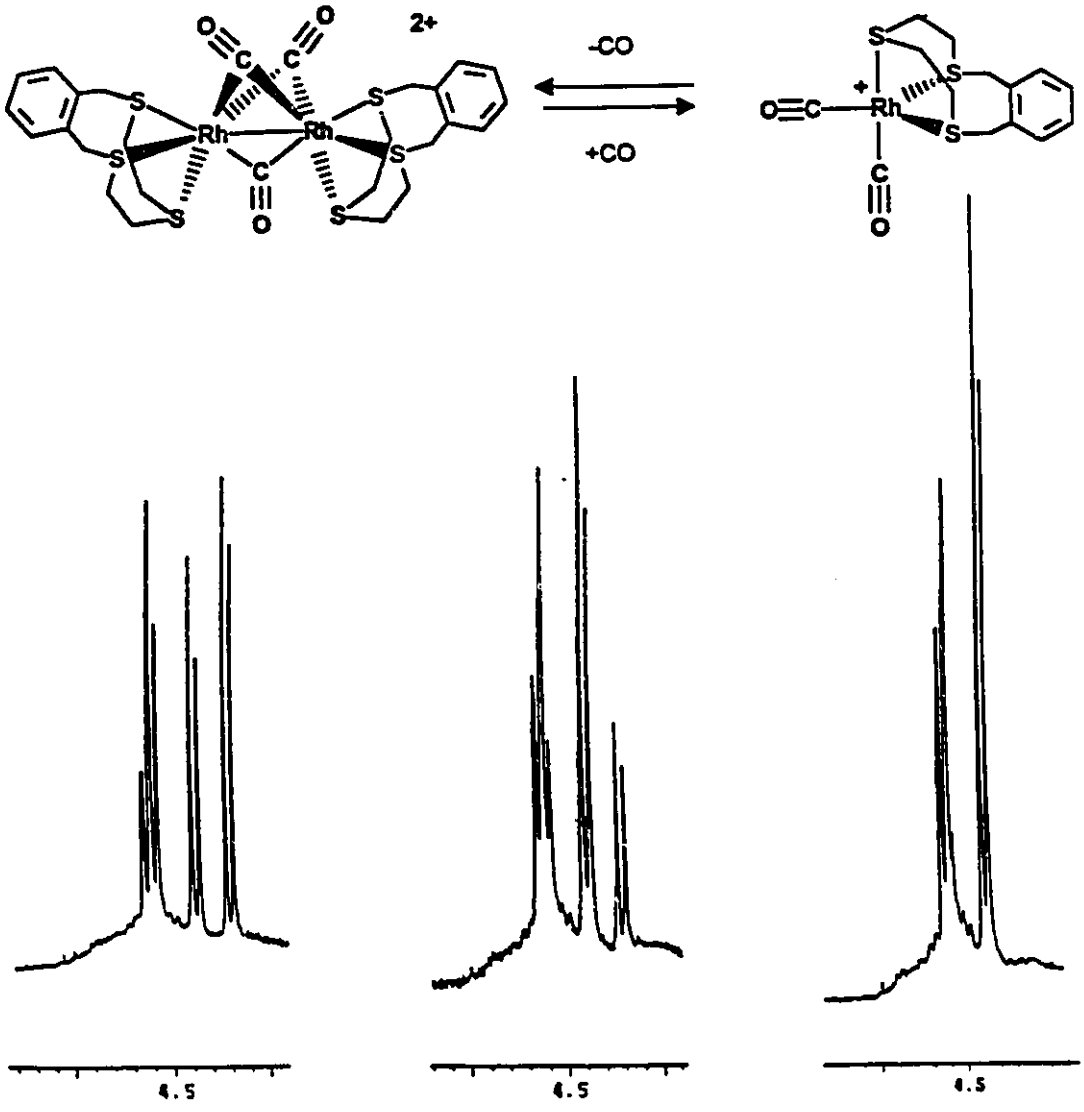

Figure 4.6 Benzylic portion of the ^{1}H NMR spectrum of a mixture of $[Rh(CO)_2(TT[9]OC)][BF_4]$, 14, and $[(TT[9]OC)Rh(\mu\text{-}CO)_2Rh(TT[9]OC)][BF_4]_2$, 15 under a CO atmosphere. As the NMR tube is evacuated and the CO atmosphere is replaced by an N_2 atmosphere, the mixture of the two compounds converts completely to complex 15, as Figures 4.6a - 4.6c demonstrate.

In contrast to **10**, the analogous Ir complex [Ir(COD)(TT[9]OC)][BF_4], **11**, was quite inert to substitution by CO. When a solution of **11** was refluxed for an extended period of time under an atmosphere of CO, a single product was detected by NMR spectroscopy (*ca* 5 %) which could not be isolated. In order to increase the likelihood of CO substitution, [IrCl(COE)$_2$]$_2$ and $AgBF_4$ were mixed in a donor solvent under N_2 in the presence of TT[9]OC (presumably forming [Ir(COE)$_2$(TT[9]OC)][BF_4], which could not be isolated due to decomposition in solution), followed by the introduction of an atmosphere of CO. The major product from this reaction was isolated and identified as [Ir(CO)(COE)(TT[9]OC)][BF_4], **17**. The ^{1}H NMR spectrum of **17** shows that COE is still present in the complex while the $^{13}C\{^1H\}$ NMR spectrum at 235K shows only one resonance at δ 184 ppm due to the carbonyl ligand, as well as peaks attributable to TT[9]OC and COE. A single sharp ν(CO) absorption was observed at 2073 cm^{-1} in the infrared spectrum. Another minor product from this reaction was shown to be identical to that produced from the reaction of **11** with CO, but again this complex could not be isolated in sufficient quantity for full characterization.

It was found that by changing the conditions for the substitution reaction employing [IrCl(COE)$_2$]$_2$, the minor component from the previous reactions of **11** with CO, and [IrCl(COE)$_2$]$_2$ with TT[9]OC and CO, could be prepared as the major product. [IrCl(COE)$_2$]$_2$ was added to solid $AgBF_4$ under an atmosphere of CO to yield an intense blue-green solid that was insoluble in CH_3CN. Solid TT[9]OC was added to this mixture, and after 20 minutes, the solution became yellow in colour, with grey AgCl precipitate. After filtering the solution to remove precipitated AgCl, and removal of solvent,

$[Ir(CO)_2(TT[9]OC)][BF_4]$, **18**, was isolated in 46% yield. The ^1H NMR spectrum shows only resonances for coordinated ligand while the low temperature $^{13}C\{^1H\}$ NMR spectrum shows CO resonances at δ 175 and 168 ppm as well as the expected resonances for coordinated TT[9]OC. The infrared spectrum shows two terminal ν(CO) absorptions at 2095 and 2045 cm^{-1}.

The coordinatively unsaturated complexes **12** and **13**, containing ODT[9]OC, were expected to be much more reactive than **10** and **11**. $[Rh(COD)(ODT[9]OC)][BF_4]$, **12**, reacts immediately with CO to form a yellow product, $[Rh(CO)_3(ODT[9]OC)][BF_4]$, **19**, which is soluble in acetone and acetonitrile. The infrared spectrum of **19** shows three ν(CO) absorptions at 2103, 2044, and 2015 cm^{-1}, consistent with the assignment of **19** as the coordinatively saturated tricarbonyl species. The ^1H NMR spectrum of this complex at 210K shows the expected resonances for a product in which only the sulphur atoms are bound to Rh, similar to **12**. In the reaction of $[Ir(COD)(ODT[9]OC)][BF_4]$, **13**, with CO in acetone, definitive colour changes are observed from, orange to red-purple to pale orange, followed by the precipitation of an orange solid, formulated as $[Ir(CO)_3(ODT[9]OC)][BF_4]$, **20**, which is soluble in acetonitrile. The ^1H NMR spectrum of **20** (shown in Figure 4.7) is unusual since it clearly shows two sets of benzylic resonances, indicating that ODT[9]OC is asymmetrically bound to the Ir centre. The $^{13}C\{^1H\}$ NMR spectrum of **20** is consistent with this structural assignment since three CO resonances, and separate peaks for all ligand carbon atoms are observed. The IR spectrum shows only one broad, strong terminal ν(CO) absorption at 2042 cm^{-1}. In an attempt to recrystallize **20**, a solution of the complex was cooled to -20 °C, resulting in the precipitation of a

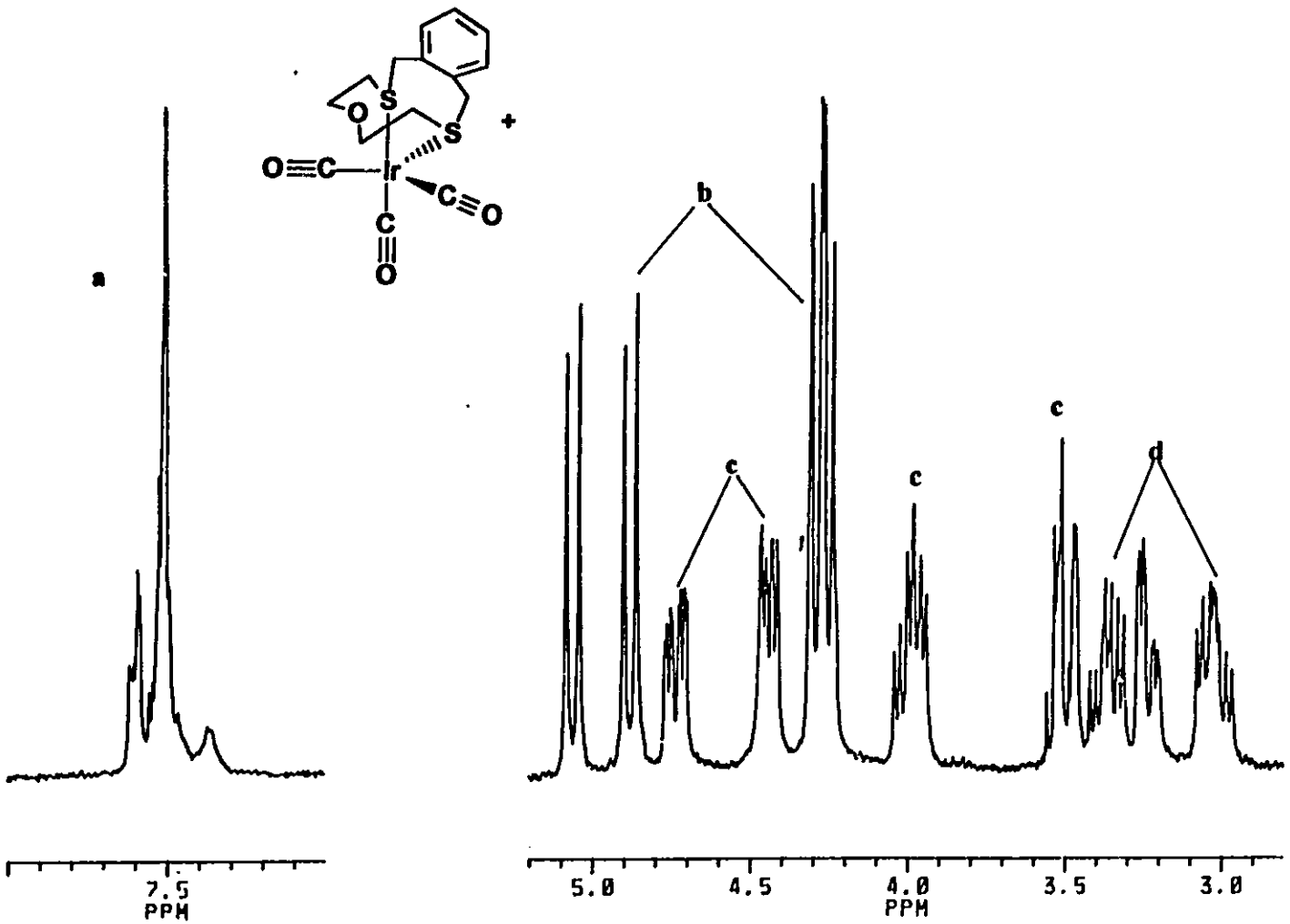

Figure 4.7 ^{1}H NMR spectrum of [Ir(CO)$_3$(ODT[9]OC)][BF$_4$], 20, in CD$_3$CN. The peaks are labelled as follows: a) aromatic, b) benzylic, c) OCH$_2$, d) SCH$_2$.

purple product, which could be isolated if the solution was kept cold. If allowed to warm to room temperature, the solution becomes yellow again and the product redissolves. The IR spectrum of this purple solid exhibits two terminal ν(CO) absorptions at 2052 and 1968 cm^{-1}, but the ^1H NMR spectrum showed only broad resonances at low temperatures required for generation of this complex in solution. A possible structural assignment is the dicarbonyl complex $[Ir(CO)_2(ODT[9]OC)][BF_4]$, formed by coordination of the oxygen atom of the ligand and loss of CO at low temperature.

4.3.7 X-ray Structure of $[Ir(COE)(CO)(TT[9]OC)][BPh_4]$, (17)

The unit cell contains eight $[Ir(COE)(CO)(TT[9]OC)]^+$ cations and eight BF_4^- anions. A perspective ORTEP drawing of the complex cation of 17 is shown in Figure 4.8. $[Ir(COE)(CO)(TT[9]OC)]^+$ is a five coordinate complex with a distorted trigonal bipyramidal geometry about the Ir(I) atom. TT[9]OC is coordinated in a *facial* manner to two equatorial sites with Ir-S distances of Ir-S1 2.39(2) and Ir-S3 2.41(1) Å, and one axial site with a Ir-S distance of Ir-S2 2.35(1) Å The seven-membered chelate ring involving the xylyl group spans the two equatorial coordination sites with an angle of 106.8(4)° for S1-Ir-S3 while the angles at iridium for the two five-membered chelate rings are 87.5(5)° and 85.9(5)° for S1-Ir-S2 and S2-Ir-S3 respectively. The COE and CO ligands occupy the remaining equatorial and axial sites respectively with an Ir-C distance of 1.70(4) Å for the carbonyl group and distances of Ir-C14 2.17(5) and Ir-C15 2.18(4) Å for the olefinic bond.

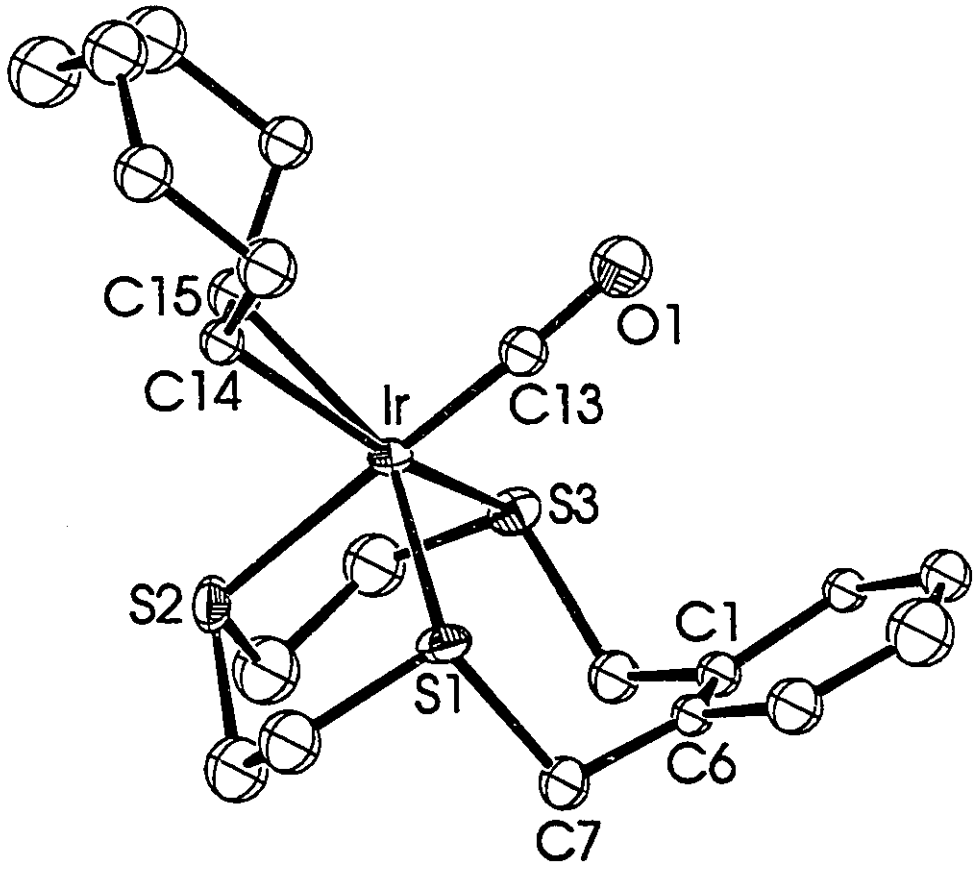

Figure 4.8 ORTEP drawing of the [(Ir(COE)(CO)(TT[9]OC)]$^+$ cation of 17, showing the atom-numbering scheme. Thermal ellipsoids of 30% probability are shown. Bond distances: Ir-S1 2.39(1), Ir-S2 2.35(1), Ir-S3 2.41(1), Ir-C13 1.70(4), Ir-C14 2.17(5), Ir-C15 2.18(4) Å. Bond angles: S1-Ir-S2 87.5(5)°, S1-Ir-S3 106.8(4)°, S2-Ir-S3 85.9(4)°, S1-Ir-C13 91(2)°, S1-Ir-C14 108(1)°, S1-Ir-C15 149(1)°, S2-Ir-C13 178(2)°, S2-Ir-C14 81(1)°, S2-Ir-C15 85(1)°, S3-Ir-C13 94(1)°, S3-Ir-C14 142(1)°, S3-Ir-C15 102(1)°, C13-Ir-C14 100(2)°, C13-Ir-C15 97(2)°.

4.3.8 Reactions of [M(COD)(L)][BF_4] with $NOBF_4$

The reaction chemistry of **10** - **13** with NO^+ is summarized in Schemes 4.1 - 4.3; ^1H and $^{13}C\{^1H\}$ NMR data are listed in Table 4.3. In general, the reactions of **10** - **13** with one equivalent of $NOBF_4$ are identical, differing only in the apparent thermal stability of the adducts **21** - **24** formed. In each case, the ^1H NMR spectrum was recorded immediately upon mixing the two reagents. Only the adduct **24** derived from **13** was stable enough to allow isolation of a solid product.

Complex **21**, $[Rh(NO)(COD)(TT[9]OC)][BF_4]_2$, is the least stable product; even when the reaction of **10** with $NOBF_4$ is carried out at -78 °C, the reaction mixture immediately turns dark brown and precipitates a brown solid which is unisolable. For complex **21**, ^1H NMR and IR spectroscopy showed evidence for only one product in solution, as well as free COD. If the solvent for this reaction is changed to acetonitrile from acetone, the same single product is formed without immediate decomposition, however, this only results in an improved ^1H NMR spectrum, since the compound still decomposes before an adequate $^{13}C\{^1H\}$ NMR spectrum can be recorded. Similar reactions with **11**, **12**, and **13** (in either acetone or acetonitrile) produced adducts **22**, **23**, and **24** which showed increasing stability on going from TT[9]OC to ODT[9]OC and from Rh(I) to Ir(I). ^1H and $^{13}C\{^1H\}$ NMR spectra and solution IR spectra of these three NO complexes showed the presence of two products in solution while the solid state infrared spectrum for **24** exhibited a single ν(NO) stretching frequency[94] at 1708 cm^{-1}.

The observation of two species in solution for **21** - **24** is significant since this occurred even when X-ray quality crystals of **24** were used for the NMR sample;

Table 4.3 ^{1}H, $^{13}C\{^{1}H\}$ NMR Data for Complexes 21 - 24

^{1}H NMR (acetone d_6)

Compund	Aromatic	COD olefin	Benzylic	E^{a}-CH_2	CH_2-S	COD Aliphatic
21	7.67, m, 4H	6.37 (m, 2H), 5.88 (m, 2H)	5.41 (d, 2H) J=14.69 Hz 4.54 (dd,2Hz) $J_{(Rh-H)}$=1.6Hz	4.83 (m,4H)	3.96 (m,4H)	3.62 (m,4H) 3.08 (m,2H) 2.78 (m,2H)
22a	7.81 (m, 2H) 7.61 (m,2H)	5.23 (m, 4H)	5.11 (d, 2H) 4.57 (d, 2H) J=12.42 Hz	4.06 (m, 4H)	3.74 (m, 2H) 3.60 (m, 2H)	2.55 (m, 4H), 2.33 (m, 4H)
22b	7.42 (s, 4H)	5.68 (m, 2H), 5.55 (m, 2H)	4.71 (d, 2H) 4.19 (d, 2H) J=14.67 Hz	4.16(m,4H)	3.41 (m, 2H) 3.21 (m, 2H)	2.10 (m, 4H), 1.86 (m, 4H)
23a	7.81 (m, 2H) 7.63 (m, 4H)	6.08 (m, 2H), 5.94 (m, 2H)	4.94 (dd, 2H) J=12.47 Hz J_{Rh-H}=2.74 Hz 4.81 (d,2H)	4.33 (m, 4H)	3.54-3.21 (m, 4H)	2.53 (m, 4H), 2.25 (m, 4H)
23b	7.43 (s, 4H)	6.49 (m, 2H), 6.23 (m, 2H)	4.70 (dd, 2H) J=14.63 Hz J_{Rh-H}=2.30 Hz 4.33(d, 2H)	4.56 (t, 4H)	4.12 (t, 4H)	2.81 (m, 4H), 2.61 (m, 4H)
24a	7.85 (m, 2H) 7.66 (m, 2H)	5.98 (m, 2H), 5.92 (br s,2H)	5.11 (d, 2H) 4.39 (d, 2H) J=14.39 Hz	3.77 (m, 4H)	3.73 (m, 2H) 3.30 (m, 2H)	2.76 (m, 4H), 2.14 (m, 4H)
24b	7.43 (s, 4H)	6.36 (m, 2H), 5.98 (m, 2H)	5.25 (d, 2H) 5.10 (d, 2H) J=12.44 Hz	4.75-4.63 (m, 4H)	4.32 (m, 4H)	2.59 (m, 4H), 2.45 (m, 4H)

Table 4.3 cont.

$^{13}C\{^1H\}NMR$, (acetone - d_6)

Compund	Aromatic	COD olefin	Benzylic	E*-CH_2	CH_2-S	COD Aliphatic
22a	140.49, 137.67, 136.01	114.43, 95.02	44.29	43.44	39.75	38.88
22b	137.06, 135.87, 134.54	115.94, 94.18	45.96	43.56	43.49	40.95
23a	140.94, 136.99, 136.61	126.16 122.50	41.87	74.16	41.07	38.73
23b	137.55, 136.11, 135.28	128.29 120.93	44.51	71.29	42.95	40.67
24a	136.19, 131.43, 133.11	109.82, 104.40	37.61	71.50	37.44	29.35
24b	133.09, 131.61, 130.63	110.92, 103.33	40.85	68.28	39.66	29.49

*As previously, E =S for 21 and 22, and E = O for 23and 24.

the ^{1}H NMR spectra of complexes **24a** and **24b** is shown in Figure 4.9. Both complexes are symmetrical in solution, and in order to determine which resonances in the ^{1}H NMR spectra were related to each other, nuclei were sucessively decoupled . The ^{1}H NMR decoupling experiments, and solution IR measurements, suggest that the observation of two compounds is the result of an equilibrium between a square pyramidal M(III) product containing a bent NO^- ligand , and a trigonal bipyramidal M(I) product containing a linear NO^+ ligand (Figure 4.9).

4.3.9 X-ray Structure of [Ir(NO)(COD)(ODT[9]OC)][BF4]$_2$ (24)

The unit cell contains four $[Ir(NO)(COD)(ODT[9]OC)]^+$ cations, eight BF_4^- anions, and four molecules of water. A perspective ORTEP drawing of the complex cation of **24** is shown in Figure 4.10. The cation is situated on a crystallographic mirror plane which bisects both chelating ligands and results in a 50:50 disorder of the NO oxygen atom on each side of the mirror. Both BF_4^- anions (one displaying a 3-fold rotational disorder; 50:50) also sit on the mirror as does a water molecule which is H-bonded between the two anions. $[Ir(COD)(NO)(ODT[9]OC)]^{2+}$ exhibits distorted square pyramidal geometry with the mixed S,O-donor ligand ODT[9]OC coordinated to Ir(I) employing the two benzylic sulphur atoms. The NO group is bent, Ir-N1-O1 137(2)°, and occupies the apical position such that the O1-N1-O1' angle is 67(4)°. The Ir-S distances are Ir-S1 2.378(5) and Ir-S2 2.348(5) Å with a non-bonding Ir...O1 distance of 2.87(3) Å and a chelate angle of 101.8(3)° for S1-Ir-S2. The COD ligand chelates to the remaining

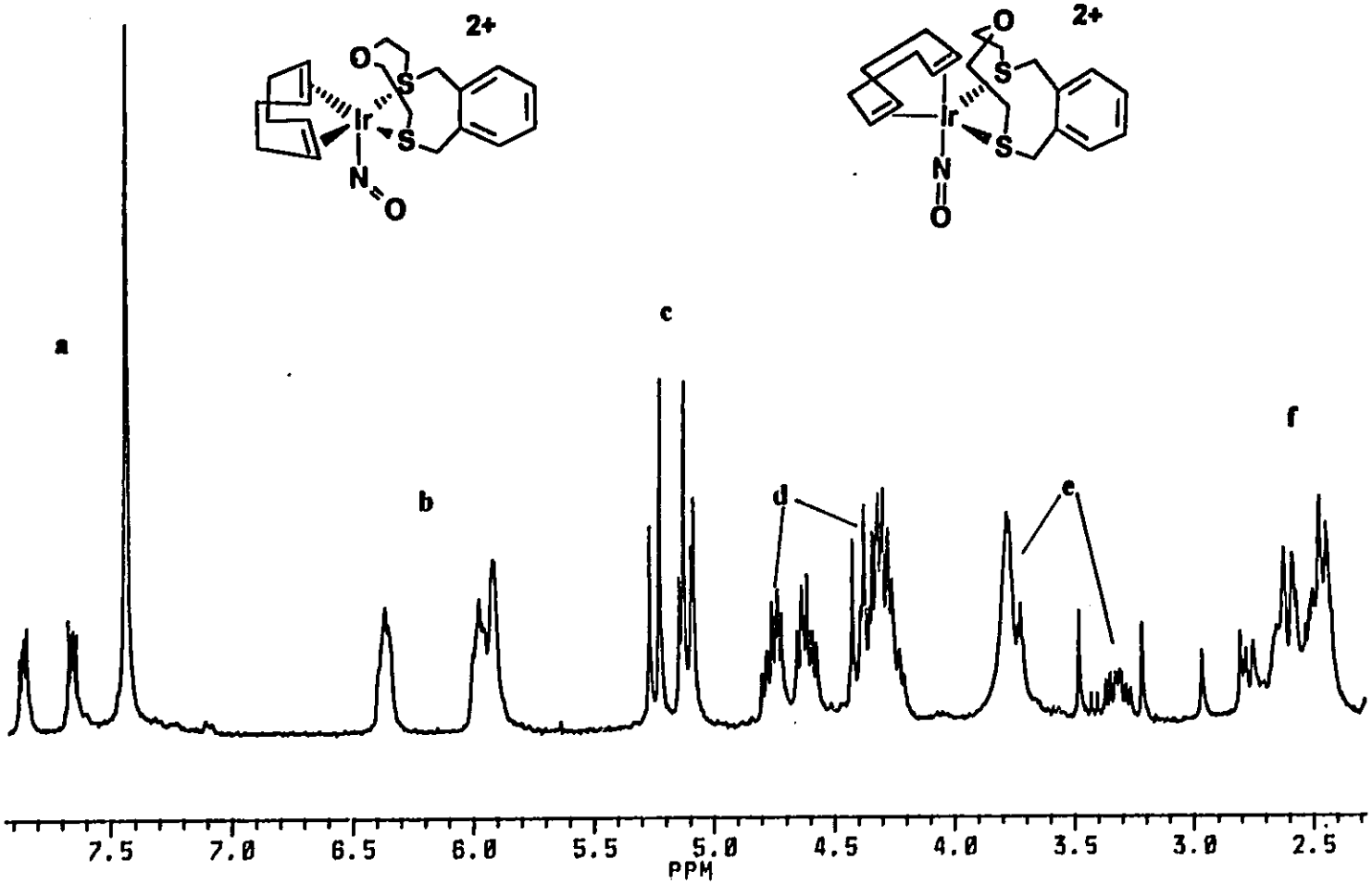

Figure 4.9 ^{1}H NMR spectrum of [Ir(COD)(NO)(ODT[9]OC)][BF_4]$_2$, 24a and 24b, in acetone-d_6. The peaks are labelled as follows: a) aromatic, b) COD olefin, c) benzylic, d) OCH_2, e) SCH_2, f) COD aliphatic.

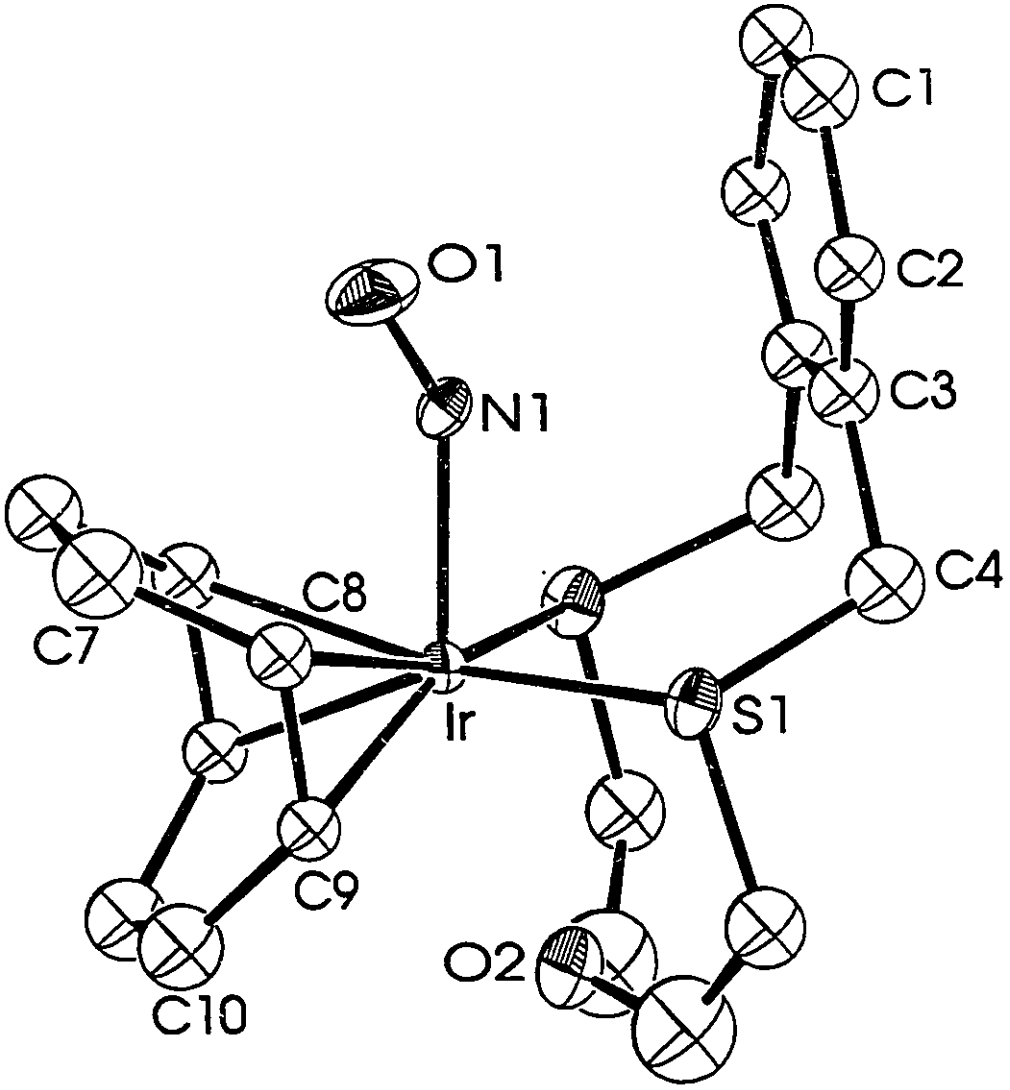

Figure 4.10 ORTEP drawing of the [(Ir(COD)(NO)(ODT[9]OC)]$^+$ cation of 24, showing the atom-numbering scheme. Thermal ellipsoids of 30% probability are shown. Bond distances: Ir-S1 2.378(5), Ir-N1 1.99(3), Ir-C8 2.20(2), Ir-C9 2.25(2) Å, N1-O1 1.07(3) Å, and Ir...O2 nonbonded distance is 2.87(3) Å. Bond angles: S1-Ir-S1' 101.8(3)°, S1-Ir-N1 88.8(5)°, S1-Ir-C8 85.1(5)°, S1-Ir-C8' 156.6(5)°, S1-Ir-C9 88.1(5)°, S1-Ir-C9' 163.8(5)°, N1-Ir-C8 113.8(7)°, N1-Ir-C9 78.4(7)°, Ir-N1-O1 137(2)°, O1-Ir-O1' 67(4)°.

coordination sites of the square plane with Ir-C distances of Ir-C8 2.20(2), Ir-C9 2.25(2),Ir-C13 2.08(2), Ir-C14 2.02(3), Ir-C17 2.14(2) and Ir-C18 2.20(2) Å.

4.4 Discussion

4.4.1 Preparation of Complexes 10 - 13

Rh(I) and Ir(I) complexes of TT[9]OC are structurally quite similar, as are those of ODT[9]OC. However, the ligands themselves seem to impose the coordination sphere at the metal; all three of the sulphur donors of TT[9]OC coordinate to the metal in a *facial* mode, and the COD ligand completes the coordination sphere, making **10** and **11** trigonal bipyramidal complexes. However, because the harder oxygen donor of ODT[9]OC does not coordinate to the metal, (Rh...O 2.717(8) Å, and Ir...O 2.59(1)Å) **12** and **13** are coordinatively unsaturated square planar complexes; the oxygen atom does not occupy the apical position of a square pyramid.

For all complexes **10 - 13**, weak metal-alkene π back-bonding is expected due to the cationic charge on the complexes[87]. This is indicated by the upfield shifts of the alkene resonances in the ^{1}H NMR spectra, to values ranging from δ 3.17 for **11** to 4.10 for **12**, as opposed to δ 5.54 ppm for the free COD ligand.

Schröder[87] has prepared $[M(olefin)(9S3)]^+$ (M = Rh, Ir; olefin = COD, C_2H_4) complexes, in 70% (Rh(I)) and 30% (Ir(I)) yields. 9S3 coordinates to the metal in a *facial* manner, similar to TT[9]OC, where one of the Rh-S distances is slightly shorter than the other two. This is analogous to the M-S2 (apical sulphur) distances in **10** and **11**. Schröder was also able to isolate crystals of $[Rh(C_2H_4)_2(9S3)]^+$, but this complex, as well as

$[Rh(COD)(9S3)]^+$, proved to be unreactive, remaining inert to substitution by PR_3 or CO, even when the complex was heated in the presence of either of these reagents. However, as described in the introduction to this chapter, $[Rh(COD)(9S3)]^+$ does oxidatively add CH_2Cl_2. Complexes **10** - **13** do not undergo oxidative addition with either CH_2Cl_2 or MeI.

4.4.2 Reactions of 10 - 13 with CO

As shown in Scheme 4.1, reaction of **10** with CO results in two complexes, a terminal carbonyl complex $[Rh(CO)_2(TT[9]OC)]^+$, **14**, and a bridged carbonyl complex $[(TT[9]OC)Rh(\mu\text{-}CO)_3Rh(TT[9]OC)]^{2+}$, **15**. Complex **14** gradually loses CO in solution under N_2 to convert to **15**, but under an atmosphere of CO **15** does not completely convert to **14**, and the two complexes exist in a 1:1 equilibrium. If **14** and **15** are prepared by reaction of $[RhCl(CO)_2]_2$ with $AgBF_4$ and TT[9]OC, they are obtained in much higher yields than when COD is displaced by CO. In fact, unless the reaction solution is extremely concentrated there is consistent contamination by **10**.

Dinuclear carbonyl-bridged rhodium species with either capping[95] or macrocyclic ligands[96] have been reported previously. Shown below in Figure 4.10, the most similar complex to **15** is the dinuclear capped complex $[(MeGa(N_2C_3H_3)_3]_2Rh_2(\mu\text{-}CO)_3$. Only complexes **a** and **b** have been structurally characterized by X-ray crystallography, and in both cases the short Rh-Rh distances (2.581 and 2.58 A, respectively) indicate that a metal-metal bond exists, completing the coordination sphere of each metal atom. Following this logic then, complex **c** was also proposed to contain a Rh-Rh bond[96b], and similarly, complex **15**.

Following this logic then, complex **c** was also proposed to contain a Rh-Rh bond[96b], and similarly, complex **15**.

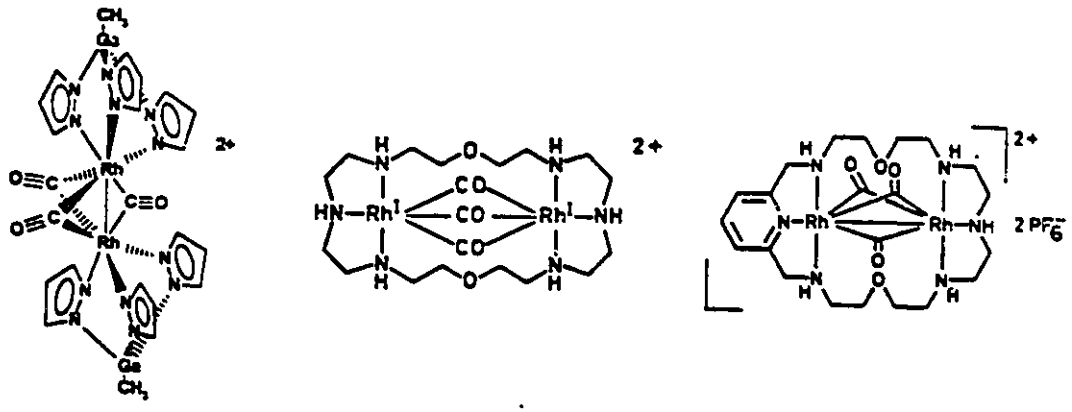

a **b** **c**

Figure 4.11 Dinuclear Rhodium Carbonyl Complexes

Complex **15** is slightly more reactive than the structurally similar complex $[(MeGa(N_2C_3H_3)_3]_2Rh_2(\mu\text{-}CO)_3$, which, when heated with PPh_3 yields the dimer $[Rh(\mu\text{-}N_2C_3H_3)(CO)(PPh_3)]_2$, and when mixed with I_2 yields a complex that does not contain any carbonyl groups[95]. Complex **15** however, reacts with PPh_3 at room temperature to yield $[Rh(CO)(PPh_3)(TT[9]OC)][BF_4]$, **16**, in quantitative yield. The $\nu(CO)$ band in the infrared spectrum of complex **16** occurs at 1959 cm^{-1}, versus 2059 and 1933 cm^{-1} for $[Rh(CO)_2(TT[9]OC)][BF_4]$, **14.** Other macrocyclic dimeric Rh(I) complexes are more unreactive[96-98], but most of these are complexes of ditopic ligands in which the two metals are held in proximity by one ligand.

the preparation of **18** was attempted by using a starting material with more labile olefin ligands, $[Ir(COE)_2Cl]_2$. Complex **17**, $[Ir(COE)(CO)(TT[9]OC)[BF_4]$, is prepared by the reaction of $[Ir(COE)_2Cl]_2$ with $AgBF_4$ under N_2, followed by the addition of TT[9]OC, then CO, presumably forming $[Ir(COE)_2(TT[9]OC)[BF_4]$ as an intermediate. Attempts to isolate this complex proved futile; even in the presence of a slight excess of COE the product decomposed, and the ^1H NMR spectrum indicated the presence of free TT[9]OC and COE. Complex **17** is quite unreactive to excess CO and heat, decomposing with time. However, the elusive complex **18** can be prepared if the order of addition of reactants is altered in the reaction to prepare complex **17**; if $[Ir(COE)_2Cl]_2$ and $AgBF_4$ are placed together in an atmosphere of CO, a blue-black insoluble complex forms. Addition of TT[9]OC to this mixture yields $[Ir(CO)_2(TT[9]OC)[BF_4]$, **18**, as the only product. However, **18**, like **11**, is extremely unreactive, resisting displacement of CO with other ligands (PR_3, acetylenes) even when refluxed in DMF, and when **18** is mixed with Me_3NO in an attempt to remove a carbonyl ligand, no reaction occurs.

The carbonyl complexes **19** and **20**, $[M(CO)_3(ODT[9]OC)][BF_4]$, are easily prepared by stirring a solution of either **12** or **13** under CO to displace the COD ligand. If $[Rh(COD)(ODT[9]OC)][BF_4]$, **12** is stirred under an atmosphere of CO for extended periods of time, free ODT[9]OC ligand is observed in the ^1H NMR, indicating that a homoleptic carbonyl complex may have been formed. Like **14** and **15**, **19** can be prepared from $[RhCl(CO)_2]_2$, and again, this approach results in higher yields than when starting from **12**, with no contamination by COD, and without proceeding to the homoleptic carbonyl complex. However, **19** is not stable in solution under N_2 for any length of time.

Finally, complex **20**, $[Ir(CO)_3(ODT[9]OC)][BF_4]$, is relatively unreactive also, similar to **18**. Unlike the other complexes prepared thus far, the ^1H NMR spectrum of **20** is not symmetrical, as shown in Scheme 4.3 and Figure 4.7. This asymmetry is similar to that identified in the structure of a related complex $[PdCl_2(TT[9]MC)]$[50], in which TT[9]MC acts as a bidentate ligand, coordinating through only one benzylic sulphur atom and the central aliphatic sulphur atom to form a five-membered chelate ring. It is possible that **20** is a stable intermediate which, when cooled, loses a labile CO ligand so that ODT[9]OC binds symmetrically, employing all three donor atoms. However, if this is the case, then a complex in which the oxygen atom of ODT[9]OC is bound to Ir(I) must exist. The purple product isolated when **20** is cooled could possibly be that type of compound, a five-coordinate trigonal bipyramidal complex shown in Scheme 4.3. This would be the only example so far of a complex in which ODT[9]OC coordinates to a metal centre through all three donor atoms, which may explain its instability; the oxygen donor is not likely to stabilize the Ir(I) complex.

4.4.3 Reactions of 10 - 13 with $NOBF_4$

The chemistry of transition metal nitrosyl complexes has been reviewed extensively[99], and for purposes of clarity a brief discussion of the bonding modes of this ligand is given here. The nitrosonium ion, NO^+, is isoelectronic with CO. However, the coordination chemistry of NO is markedly different in that it can adopt two bonding modes: linear, formally NO^+, and bent, formally NO^- [94, 100], shown in Figure 4.12 below. Complexes **21 - 24** exhibit two "hybridization isomers" containing bent and linear NO.

coordination chemistry of NO is markedly different in that it can adopt two bonding modes: linear, formally NO^+, and bent, formally NO^- [94, 100], shown in Figure 4.12 below. Complexes **21 - 24** exhibit two "hybridization isomers" containing bent and linear NO. This is strongly reminiscent of the complexes $[Co(Cl_2)(NO)(PR_3)_2]$ studied by Collman and Ibers[100], among the first complexes to be thoroughly examined to determine the nature of the bent and linear nitrosyl ligand.

M^{z+2} d^{n-3} NO^- M^z d^n NO^+

Figure 4.12 Bent and Linear NO

The bonding situation for bent nitrosyl complexes arises when the π^* acceptor orbital on the linear NO^+ ligand becomes energetically more stable than the metal d-electrons. By bending the linear MNO group, a d-electron pair is transferred to an sp^2 nonbonding orbital on the (now) bent NO ligand. Although this is a simplified viewpoint, it illustrates that the conversion of linear NO^+ to bent NO^- is equivalent to an intramolecular electron transfer of an electron pair from the metal to the ligand. As a result of this electron transfer, the coordination geometry about the metal atom changes to

metals' coordination spheres. The trends in stability then, differ for NO^+ complexes as compared to carbonyl complexes of **10** - **13**. While complex **10** reacts with $NOBF_4$ to yield only one relatively unstable product, **11** - **13** each yield two products, one the M(I) NO^+ compound, and the other the M(III) NO^- compound. Two ν(NO) stretching frequencies are observed in the solution IR spectra for **22** - **24** (the IR spectrum of complex **21** only indicates that one compound is present in solution), and although it is not a hard and fast rule, it is generally accepted that linear ν(NO) frequencies are often higher than bent ν(NO) frequencies. This rule is especially not applicable when comparing dissimilar compounds, and since both linear and bent ν(NO) frequencies overlap, it is difficult to comment on the IR spectra, except to say that they reiterate the fact that two complexes are present in solution, and that they are probably the linear and bent forms of the nitrosyl ligand.

The complexes **12** and **13** containing ODT[9]OC have square planar geometry and can therefore easily accommodate the addition of NO to form square pyramidal M(III) products. This can occur without rearrangement of the macrocycle, which translates into an increased stability for **23** and **24**. Analogous reactions of NO with **10** and **11** to form **21** and **22** require the axial S2 atom of TT[9]OC to be displaced in order to accommodate the NO group. Although it has been previously demonstrated that this ligand conformation is possible[58], it is very likely that this perturbation destabilizes complexes of TT[9]OC relative to those of ODT[9]OC. Alternatively, the linear nitrosyl (NO^+) ligand tends to be more stable in a position in the coordination sphere of the metal which favours π-backbonding. This would mean the rearrangement of the COD ligand so that NO^+ can

occupy a position in the trigonal plane of the M(I) complex[94]. In complexes **21** and **22**, $[M(COD)(NO)(TT[9]OC)]^{2+}$, then, two scenarios are possible: 1) NO^+ occupies an unfavourable axial position in the M(I) tbp complexes, or 2) the COD ligand is rearranged in order that NO^+ can occupy a trigonal planar position. Either or both of these situations, along with the displacement of the apical sulphur atom in the M(III) complexes, can act to destabilize the complexes, leading to loss of COD and subsequent decomposition. All of the compounds **21** - **24** eventually decompose in solution, yielding free COD.

4.5 Summary and Conclusions

The trithiacyclophane ligand TT[9]OC is capable of acting as a capping ligand for the $[M(COD)]^+$ fragments (M = Rh(I) and Ir(I)). Analogous to the Rh(I) and Ir(I) complexes $[M(9S3)(COD)]^+$ and $[M(9S3)(C_2H_4)_2]^+$ reported by Schröder[87], these complexes have trigonal bipyramidal geometry about the metal atoms and are coordinatively saturated. However, unlike the complexes of 9S3, the complexes of TT[9]OC undergo substitution of the olefinic ligand by CO, albeit slowly, to yield the carbonyl complexes $[Rh(CO)_2(TT[9]OC)][BF_4]_2$, **14**, $[(TT[9]OC)Rh(\mu\text{-}CO)_3Rh(TT[9]OC)][BF_4]_2$, **15**, and $[Ir(CO)_2(TT[9]OC)][BF_4]$, **18**. This is a result of the greater flexibility of TT[9]OC and reflects this ligand's previously demonstrated ability to undergo slippage to a bidentate coordination mode[96] (Chapter 2). Complex **15** is unique in that it is one of the few dimeric carbonyl complexes reported which contain capping macrocyclic ligands. It is also unique in its facile reaction with PPh_3 to form a monomeric complex, $[Rh(CO)(PPh_3)(TT[9]OC)][BF_4]$, **16**.

The accessibility of a 16-electron intermediate facilitates the observed substitution reactions; this was successfully modelled by replacing the central S-atom in TT[9]OC by an ether O-atom. The ligand ODT[9]OC acts as a bidentate S_2-chelate and yields coordinatively unsaturated, square planar complexes which undergo facile substitution of the olefin groups by CO to yield carbonyl complexes of the type $[M(CO)_3(ODT[9]OC)][BF_4]$. The flexibility and slippage of TT[9]OC from a tridentate to a bidentate mode was also demonstrated by the addition of NO^+ to the four complexes $[M(COD)(L)][BF_4]$; formation of the five-coordinate NO^+ adducts $[M(NO)(COD)(L)]^{2+}$ requires a bidentate coordination mode for the thiacyclophane. This is demonstrated by the X-ray structure of $[Ir(NO)(COD)(ODT[9]OC)]^{2+}$ and reflected in the relative stability of the four adducts.

The synthetic, spectroscopic and structural data described in this chapter provide a solid background for future evaluation of complexes containing thiacyclophanes as capping, ancillary ligands. The availability of rhodium(I) and iridium(I) carbonyl complexes of these thioether macrocyles will allow for future comparison to similar complexes containing cyclopentadienyl, tripodal phosphine and pyrazolylborate ligands.

Chapter 5

5.1 Introduction

It was shown in Chapter 4 that the ligands TT[9]OC and ODT[9]OC have the potential to bind to metal centres as tridentate capping ligands, similar to tripodal phosphine, pyrazolylborate, cyclopentadienyl, or η^6-arene ligands. Ru(II) complexes containing phosphine ligands, such as $RuCl_2(PPh_3)_3$ and $RuHCl(PPh_3)_3$, are well known hydrogenation catalysts[101], and to this end, Ru(II) complexes of crown thioethers have the potential to undergo similar reaction chemistry. Up until quite recently, most of the crown thioether complexes that have been synthesized have been used in coordination and electrochemical studies[14-16], however, investigations by Schröder[87], Hill[102], and our group[56] have shown that thioether ligands are able to support systems containing other organic ligands such as olefins, σ-vinyl, and thiocarbonyl groups.

The reaction chemistry of $[M(COD)L]^+$ (M=Rh(I) and Ir(I), (L = TT[9]OC, ODT[9]OC, 9S3) was discussed in the previous chapter. Hill[102] has concentrated on Ru(II) complexes of 9S3, with the hope of comparing this ligand to other capping ligands. It is known[101] that phosphine ligands can be easily displaced by other ligands at Ru(II), and the reaction of $[Ru(CH=CHR)Cl(CO)(PPh_3)_2]$ with 9S3 gives $[Ru(CH=CHR)(CO)(PPh_3)(9S3)]Cl$, in quantitative yield[102a]. The synthesis of crown thioether complexes with mixed ligand sets is an area open to study, since there is limited knowledge of the ligand reactions that this coordination sphere might support. Bennett[103] has shown that intramolecular deprotonation, ring opening, and subsequent C-C bond formation occurs when $[Ru(\eta^6\text{-}C_6Me_6)(9S3)][PF_6]$ reacts with KO^tBu to yield $[Ru(SCH=CH_2)(\eta^6\text{-}C_6Me_6CH_2CH_2CH_2SCH_2CH_2S)]$. This base-induced bond cleavage was found to be irreversible (reprotonation did not occur) and the study suggested that if this was the case, the extent to which crown thioethers can be attached to electron-rich transition metal centres, and the reaction chemistry they promote or undergo, may be limited. Finally, an alternative approach to the study of Ru(II) crown thioether complexes is to compare their reaction and coordination chemistry to that of the active sites of the oxidoreductases, as Sellmann[25,104] has done. The influences of the sulphur ligands are important, in that they can stabilize unusual structures and oxidation states, or can stabilize species containing CO, NO, and N_2H_4.

In this chapter, the complexes $RuCl_2(PPh_3)(L)$ (L = TT[9]OC, ODT[9]OC) are prepared, and their reactions with CO, NO, and alkylating reagents are explored. As well, the complex $RuHCl(PPh_3)_2(TT[9]OC)$ is prepared and discussed. Our approach is to

prepare crown thioether complexes of Ru(II) and then to subject these complexes to a variety of reagents, in order to obtain a complete overview of their reactivities.

5.2 Experimental

$RuCl_2(PPh_3)_3$[105], $RuHCl(PPh_3)_3$[106], TT[9]OC[54a], and ODT[9]OC[56] were prepared by literature methods. $NOBF_4$, LiPh, LiMe, EtMgBr, PhMgBr, $AlMe_3$, $AgBF_4$, $AgClO_4$, and all deuterated solvents were purchased from Aldrich and used as received. All reactions were carried out under an atmosphere of N_2 using standard Schlenk techniques, and all solvents were dried and degassed prior to use. ^1H and $^{13}C\{^1H\}$ NMR spectra were recorded at 300.1 and 75.4 MHz respectively, on a Bruker AM300 spectrometer locked to the deuterated solvent. $^{31}P\{^1H\}$ NMR spectra were recorded at 81.0 MHz on a Bruker AM200 spectrometer with an external H_3PO_4 reference. Infrared spectra were recorded on a Nicolet 5DX FTIR spectrometer.

5.2.1 Synthesis of $RuCl_2(PPh_3)$(ODT[9]OC), (25)

Method I:

To a brown solution of $RuCl_2(PPh_3)_3$ (1.00g., 1.04 mmol) in CH_2Cl_2 (50 mL) was added a solution of ODT[9]OC (250 mg, 1.04 mmol) in CH_2Cl_2 (10 mL). The mixture was stirred for three days, during which time the solution turned orange and an orange precipitate formed. Solvent was removed *in vacuo*, and the orange residue was washed with toluene (3x15mL) and dried under vacuum. The product was recrystallized by cooling a CH_2Cl_2 solution to -20°C for 24 h. Yield 548 mg, 78%. $^{13}C\{^1H\}$NMR: ($CDCl_3$):

δ 135.25, 133.40, 129.38 (aromatic, ODT[9]OC), 134.27, 132.20, 127.74, 132.00, 128.65, 128.50 (aromatic, PPh_3), 70.13 (OCH_2), 39.08, 31.53(SCH_2). ^1H NMR ($CDCl_3$): δ 8.09-6.94 (m, 19H, aromatic), 4.45 (m, 2H, OCH_2), 3.34 (d, 2H, benzylic, J = 13.87 Hz), 2.96 (d, 2H, benzylic), 2.92 (m, 2H, SCH_2), 2.80 (m, 2H, SCH_2), 2.51 (m, 2H, OCH_2). $^{31}P\{^1H\}$ NMR (CH_2Cl_2): δ 56.21 (s, PPh_3). Anal. Calcd for $C_{30}H_{31}Cl_2S_2OPRu$: C: 53.40; H: 4.64. Found: C: 53.32; H: 4.63.

Method II:

$RuCl_2(PPh_3)_3$ (1.00g, 1.04 mmol) and ODT[9]OC (250 mg, 1.04 mmol) were stirred together in toluene (50 mL) for two days, forming a yellow slurry. The mixture was filtered in air on a Buchner funnel, and washed with toluene (2 x 10mL). The crude product was then recrystallized by cooling a CH_2Cl_2 solution to -20°C. Yield 510 mg, 73%. Using this method however, ^1H NMR showed the presence of two isomers. Data for **25a** is given above. Data for **25b** is as follows: $^{13}C\{^1H\}$NMR ($CDCl_3$): δ 134.7-125.3 (aromatic, ODT[9]OC, and PPh_3), 74.04 (OCH_2), 35.65, 27.61 (SCH_2). ^1H NMR ($CDCl_3$): δ 7.76-7.11 (m, 19H, aromatic), 5.02 (d, 2H, benzylic, J = 13.52 Hz), 4.71 (d, 2H, benzylic), 4.28 (m, 4H, OCH_2), 4.10-3.67 (m, 4H, SCH_2). $^{31}P\{^1H\}$ NMR (CH_2Cl_2): δ 41.73 (s, PPh_3).

5.2.2 Reaction of $RuCl_2(PPh_3)$(ODT[9]OC) with CO

Complex **25** (50 mg, 0.074 mmol) was suspended in CH_2Cl_2 (10mL), and stirred under an atmosphere of CO for 4 h. Solvent was removed *in vacuo*, and the yellow solid

was washed with diethyl ether (2 x 5 mL) to remove PPh_3. The resultant yellow solid was insoluble in most organic solvents, and solution spectra could not be obtained. IR: ν(CO): 1994 cm^{-1}. Yield 30 mg, 92% crude product.

5.2.3 Reaction of $RuCl_2(PPh_3)$(ODT[9]OC) with $NOBF_4$

Complex **25** (50 mg, 0.074 mmol) was suspended in CH_2Cl_2 (5 mL) and $NOBF_4$ (9 mg, 0.075 mmol) was added. The orange solid immediately dissolved, resulting in an intense purple solution. The ^1H NMR spectrum was extremely fluxional and did not resolve even when the temperature was reduced to 180K. The solvent was removed *in vacuo* to leave a black-purple oil, but attempts to recrystallize the product resulted in its decomposition. $^{31}P\{^1H\}$ NMR (acetone): δ 44.0 ppm. IR: (KBr pellet): ν(NO) 1876 cm^{-1}, crude product.

5.2.4 Reaction of $RuCl_2(PPh_3)$(ODT[9]OC) with Alkylating Agents

a) Lithium Reagents

Complex **25** (20 mg, 0.029 mmol) was suspended in THF (5 mL), and two equivalents of the appropriate reagent (1.0 M solution in THF) were added *via* syringe. The mixtures were stirred for 2 h, during which time no change was observed. ^1H NMR spectroscopy ($CDCl_3$) indicated that no reaction had occurred. The mixtures were refluxed in THF for 2 - 4 h, with no observed changes, and as before ^1H NMR spectroscopy indicated that no reaction had occurred.

b) $AlMe_3$

Complex **25** (20 mg, 0.029 mmol) was suspended in THF (5 mL), and $AlMe_3$ (40 μL, 0.040 mmol of a 1.0 M solution in toluene) was added. The mixture was stirred for 2 h, and then the solvent was removed *in vacuo*. ^1H NMR ($CDCl_3$) indicated that starting material was still present, as well as other products that were unidentifiable.

c) Phenylacetylene

Complex **25** (20 mg, 0.029 mmol) was dissolved in CH_3CN (10 mL) and phenyl acetylene (21 μL, 0.145 mmol) was added. The solution was refluxed for 4 h with no observed change in the yellow solution. Solvent was removed *in vacuo*, leaving a yellow oily solid, which was washed with diethyl ether (2 x 3 mL), resulting in a yellow powder. ^1H NMR spectroscopy ($CDCl_3$) indicated that no reaction had occurred.

5.2.5 Reaction of $RuCl_2(PPh_3)$(ODT[9]OC) with Silver Salts

Complex **25** (100 mg, 0.148 mmol) was suspended in CH_3CN (10 mL) under N_2 and two equivalents of the appropriate silver salt ($AgBF_4$ or $AgClO_4$) were added as solids against the flow of N_2. The mixture was refluxed for 2 h in the dark, resulting in a yellow solution and dark coloured precipitate. The mixture was filtered, and the solvent removed *in vacuo* to leave a yellow solid. ^1H NMR spectroscopy (CDCN or $CDCl_3$) indicated that no reaction had occurred.

5.2.6 Reaction of $RuCl_2(PPh_3)(ODT[9]OC)$ with $NaBH_4$

Complex **25** (100 mg, 0.148 mmol) was suspended in toluene (10 mL) under an atmosphere of H_2. $NaBH_4$ (28 mg, 0.740 mmol) was added as a solution in H_2O (0.1 mL), and the mixture was refluxed for 5 h under a stream of H_2, with no change in the yellow slurry. The mixture was filtered through a Schlenk filter, and the yellow solid was dried *in vacuo*. ^1H NMR ($CDCl_3$) indicated that no hydride species was present, and that no reaction had occurred. The toluene solution also did not contain a hydride species.

5.2.7 Synthesis of $RuCl_2(PPh_3)(TT[9]OC)$, (26)

To a brown solution of $RuCl_2(PPh_3)_3$ (1.00 g, 1.04 mmol) in CH_2Cl_2 (30 mL) was added a solution of TT[9]OC (267 mg, 1.04 mmol) in CH_2Cl_2 (10 mL). The brown solution was stirred for 12 h, becoming orange. Solvent was removed *in vacuo*, and the orange oil washed with diethyl ether (4 x 10 mL) to remove PPh_3. The product was dried under vacuum, and recrystallized by cooling a concentrated CH_2Cl_2 solution to -20°C for 24 h. Yield 585 mg, 81%. $^{13}C\{^1H\}$NMR ($CDCl_3$) Isomer **26a**: δ 135.44-132.03 (aromatic TT[9]OC and PPh_3), 39.61 (benzylic), 35.50, 35.22 (SCH_2). Isomer **26b**: δ 129.46-127.16 (aromatic TT[9]OC and PPh_3) 38.25 (benzylic), 33.79, 29.95 (SCH_2). ^1H NMR ($CDCl_3$) Isomer **26a**: δ 8.09 (m, 4H, TT[9]OC aromatic), 7.68-6.96 (m, 15H, PPh_3), 3.74 (d, 2H, benzylic, J = 13.63 Hz), 3.30 (d, 2H, benzylic), 1.83-1.23 (m, 8H, SCH_2). Isomer **26b**: δ 7.90 (m, 4H, TT[9]OC aromatic), 7.33-7.04 (m, 15H, PPh_3), 5.34 (d, 2H, benzylic, J = 13.57 Hz), 5.20 (d, 2H, benzylic), 3.02- 2.49 (m, 8H, SCH_2). $^{31}P\{^1H\}$ NMR (CH_2Cl_2):

Isomer **26a**: δ 36.61 (s, PPh_3); Isomer **26b**: δ 32.06 (s, PPh_3). Anal. Calcd for $C_{30}H_{31}Cl_2S_2PRu$: C: 52.16; H: 4.53. Found: C: 52.01; H: 4.50.

5.2.8 Reaction of $RuCl_2(PPh_3)$(TT[9]OC) with CO

Complex **26** (50 mg, 0.072 mmol) was dissolved in CH_2Cl_2 (8 mL) and stirred under an atmosphere of CO for 4 h. The solvent was removed *in vacuo*, to leave a yellow oil which was washed with diethyl ether (2 x 5 mL) to remove PPh_3. The resultant yellow solid was insoluble in most organic solvents, and solution spectra could not be obtained. IR: ν(CO) 1975 and 2020 cm^{-1}. Yield 30 mg, 90% crude product.

5.2.9 Reaction of $RuCl_2(PPh_3)$(TT[9]OC) with $NOBF_4$

Complex **26** (50 mg, 0.072 mmol) was dissolved in CH_2Cl_2 (8 mL) and $NOBF_4$ (8 mg, 0.072 mmol) was added. The orange solution immediately changed colour to burgundy. The ^1H NMR spectrum of the complex was extremely fluxional and did not resolve even when the temperature was reduced to 180 K. Solvent was removed *in vacuo* to leave a red oil, but attempts to recrystallize the product resulted in its decomposition. $^{31}P\{^1H\}$NMR: δ 45.13 ppm. IR: (KBr pellet): (νNO): 1905 cm^{-1} , crude product.

5.2.10 Reaction of $RuCl_2(PPh_3)$(TT[9]OC) with Alkylating Agents

a) Lithium Reagents

Complex **26** (20 mg, 0.030 mmol) was suspended in THF (5 mL), and two equivalents of the appropriate reagent (1.0 M solution in THF) were added *via* syringe.

The mixtures were stirred for 2 h, during which time no change in the yellow slurry was observed. ^{1}H NMR spectroscopy ($CDCl_3$) indicated that no reaction had occurred. The mixtures were refluxed in THF for 2 - 4 h, with no observed changes, and as before ^{1}H NMR spectroscopy indicated that no reactions had occurred.

b) $AlMe_3$

Complex **26** (20 mg, 0.030 mmol) was suspended in THF (5 mL), and Al Me_3(40 μL, 0.040 mmol of a 1.0 M solution in toluene) was added. The yellow solid dissolved within 30 min, resulting in an orange solution which was stirred for 2 h. The THF was removed *in vacuo* and the resultant orange oil dissolved in $CDCl_3$ (0.5 mL). However, ^{1}H NMR spectroscopy indicated that starting materials were still present, as well as intractable products.

c) Phenylacetylene

Complex **26** (20 mg, 0.030 mmol) was dissolved in CH_3CN (10 mL), and phenyl acetylene (21 μL, 0.145 mmol) was added. The yellow solution was refluxed for 4 h with no observed change. Solvent was removed *in vacuo*, leaving a yellow oily solid, which was washed with diethyl ether (2 x 3 mL), resulting in a yellow powder. ^{1}H NMR spectroscopy ($CDCl_3$) indicated that no reaction had occurred.

5.2.11 Reaction of $RuCl_2(PPh_3)$(TT[9]OC) with Silver Salts

Complex **26** (100 mg, 0.144 mmol) was suspended in CH_3CN (10 mL) under N_2 and two equivalents of the appropriate silver salt ($AgBF_4$ or $AgClO_4$) were added as a solid against the flow of N_2. The mixture was refluxed for 2 h in the dark, resulting in a yellow solution and dark coloured precipitate. The mixture was filtered, and the solvent removed *in vacuo* to leave a yellow solid. ^{1}H NMR spectroscopy (CDCN or $CDCl_3$) indicated that no reaction had occurred.

5.2.12 Reaction of $RuCl_2(PPh_3)$(TT[9]OC) with $NaBH_4$

Complex **26** (100 mg, 0.144 mmol) was suspended in toluene (10 mL) under an atmosphere of H_2. $NaBH_4$ (28 mg, 0.740 mmol) was added as a solution in H_2O (0.1 mL), and the mixture was refluxed for 5 h under a stream of H_2 with no change in the yellow slurry. The mixture was filtered through a Schlenk filter, and the yellow solid was dried *in vacuo*. ^{1}H NMR spectroscopy ($CDCl_3$) indicated that a very small amount of complex **27** was present, from the observation of a pair of doublets at δ -11.5 ppm. However, the minute amount of product precluded its isolation. Further refluxing (up to three days) did not yield more of complex **27** or any other hydride species.

5.2.13 Preparation of $RuHCl(PPh_3)_2$(TT[9]OC), (27)

$RuHCl(PPh_3)_3$ (200 mg, 0.216 mmol) was suspended in benzene (10 mL) under N_2, and a solution of TT[9]OC (55 mg, 0.216 mmol) in benzene (10 mL) was added *via* syringe. The $RuHCl(PPh_3)_3$ dissolved, the solution became brown, and an off-white

precipitate formed after 15 minutes. After stirring for 2 h the solid was filtered on a Schlenk filter, washed with benzene (2 x 3 mL), and dried *in vacuo*. Yield pale yellow microcrystals: 85 mg, 43%. $^{13}C\{^1H\}$NMR (acetone-d_6): δ 137.14-128.71 (aromatic), 39.11, 38.11 (benzylic), 38.01, 35.85, 33.31, 32.90 (SCH_2). ^1H NMR (acetone-d_6): δ 7.83 (m, 4H, TT[9]OC aromatic), 7.61-7.14 (m, 15H, PPh_3), 4.00 (s, 2H, benzylic), 3.96 (d, 1H, benzylic, J = 13.21Hz), 3.85 (d, 1H, benzylic), 3.24 (m, 2H, SCH_2), 3.02 (m, 2H, SCH_2), 2.88 (m, 2H, SCH_2), -0.01 (td, 1H, SCH_2), -0.39 (td, 1H, SCH_2), -11.69 (dd, 1H, Ru-H, J_{P-H} = 20.15 Hz). $^{31}P\{^1H\}$NMR (acetone): δ 53.84 (d, PPh_3, J_{P-P} = 32.7 Hz), 50.37 (d, PPh_3). IR: ν(Ru-H) 1939 cm^{-1}. Anal. Calc'd for $C_{48}H_{47}ClS_3P_2Ru$: C: 52.30; H: 5.17. Found: C: 52.23; H: 5.15.

5.2.14 Reaction of $RuHCl(PPh_3)_2(TT[9]OC)$ with $AgBF_4$

Complex **27** (20 mg, 0.022 mmol) was dissolved in acetone (5 mL), and $AgBF_4$ (5 mg, 0.025 mmol) was added as a solid against the flow of N_2. The mixture was stirred for 12 h in the dark, during which time a dark precipitate formed. The mixture was filtered, and the solvent removed in *vacuo* to leave an off-white solid. The ^1H NMR spectrum of this solid in acetone-d_6 indicated that no reaction had occurred.

5.2.15 Attempt to Displace PPh_3 from $RuHCl(PPh_3)_2(TT[9]OC)$

Complex **27** (20 mg, 0.022 mmol) was dissolved in a mixture of acetone/toluene (5 mL:2 mL) and refluxed under N_2 for 10 h with no observed change in solution. The

solvent was removed *in vacuo*, and ^{1}H NMR spectroscopy (acetone-d_6) indicated that no reaction had occurred.

5.2.16 Reaction of $RuHCl(PPh_3)_3$ with ODT[9]OC

$RuHCl(PPh_3)_3$ (200 mg, 0.216 mmol) was suspended in toluene (10 mL) under H_2 at -78°C, and a solution of ODT[9]OC (55 mg, 0.216 mmol) in toluene (10 mL) was added *via* syringe. The $RuHCl(PPh_3)_3$ dissolved, and the solution gradually changed from purple to brown. The brown solution was allowed to warm to room temperature, and after stirring for 2 h, solvent was removed in *vacuo*. ^{1}H NMR spectroscopy (acetone-d_6) indicated that uncoordinated ODT[9]OC was present in solution, and that no metal hydride species was present in solution.

5.2.17 X-ray Structure Determination of $RuCl_2(PPh_3)$(ODT[9]OC), (26)

Orange crystals of $RuCl_2(PPh_3)$(ODT[9]OC) suitable for X-ray diffraction were grown by cooling a dichloroethane solution of the complex to -20°C for three days. A statistical analysis of intensity distributions and determination of systematic absences were consistent with the space group $P2_1/c$, and this was confirmed by successful structure refinements. A total of 3459 reflections were collected and 1809 reflections with $F_o^2 > 3\sigma(F_o^2)$ were used in the refinement. The intensities of the standard reflections showed significant decay (18.4%) after $2\theta = 40°$ due to loss of solvent from the crystal lattice; data collection was stopped at this point, and a linear decay correction was applied to the data. The position of the ruthenium atom was determined using direct methods and the E map

with highest figure of merit, and the remaining non-hydrogen atoms were located from successive Fourier calculations. In the final cycles of refinement, the ruthenium, sulphur, oxygen, phosphorous, and chlorine atoms were assigned anisotropic thermal parameters, resulting in R = 5.52% and R_w = 5.63%. A goodness fit calculation resulted in a value of 2.18, and a final difference Fourier map calculation showed no peaks of chemical significance. A summary of crystal data, intensity collection, and structure refinement is shown in Table A.5.1, positional parameters are listed in Table A.5.2, and bonding parameters are listed in Table A.5.3.

5.3 Results and Discussion

5.3.1 Syntheses of $RuCl_2(PPh_3)(L)$ Complexes

The ligands ODT[9]OC and TT[9]OC react slowly with $RuCl_2(PPh_3)_3$ at room temperature, displacing two PPh_3 ligands to yield the coordinatively saturated complexes $RuCl_2(PPh_3)$(ODT[9]OC), **25**, and $RuCl_2(PPh_3)$(TT[9]OC), **26**. Complex **25** is a yellow powder which is air stable, and is obtained in moderate yield by cooling a concentrated CH_2Cl_2 solution. It is soluble in chlorinated solvents, likely due to hydrogen bonding which occurs between the chlorinated solvent, the chloride ligands, and the macrocycle ethylene protons, as observed for the complex $RuCl_2(PPh_3)$(9S3)[102b]. Complex **25** is not soluble in polar organic solvents such as acetone or acetonitrile, but is soluble in DMSO. The ^1H NMR spectrum of **25** indicates only one product when the complex is prepared in CH_2Cl_2. The benzylic resonances for this complex are shifted upfield from other ODT[9]OC complexes[56], at δ 3.34 and 2.96 ppm as shown in Figure 5.1. The $^{31}P\{^1H\}$ NMR spectrum

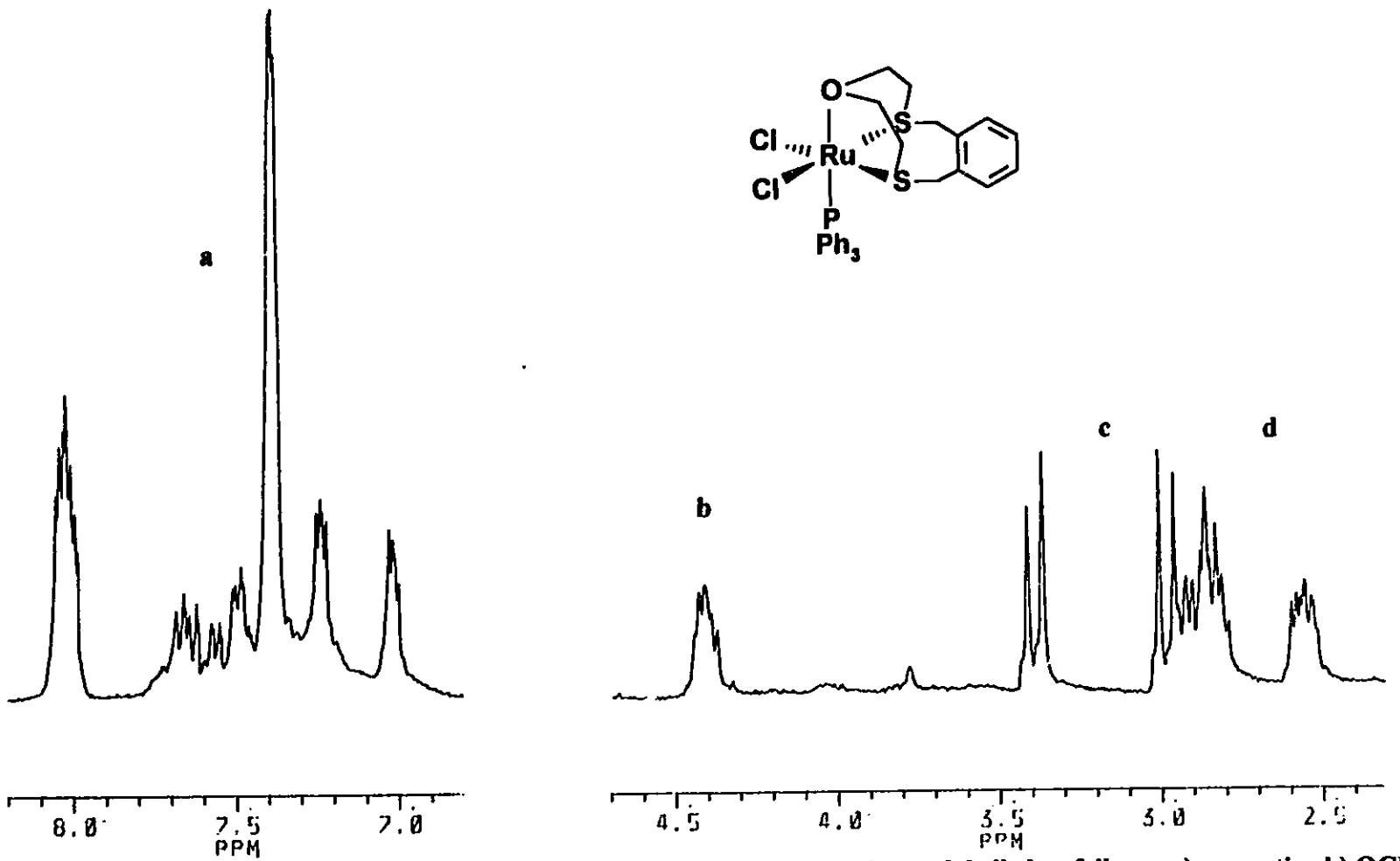

Figure 5.1 ^{1}H NMR spectrum of $RuCl_2(PPh_3)(ODT[9]OC)$, 25, in $CDCl_3$. Peaks are labelled as follows: a) aromatic, b) OCH_2, c) benzylic, d) SCH_2.

of **25** shows one resonance at δ 56.21 ppm; the downfield shift compared to **26** indicates that PPh_3 is *trans* to the oxygen donor of the crown thioether, and this is borne out in the X-ray diffraction study (vide infra). The $^{13}C\{^1H\}$ NMR spectrum of **25** shows well-resolved peaks in the aromatic region due to PPh_3 and ODT[9]OC, and the expected resonances for OCH_2 at δ 70.13 ppm and SCH_2 at δ 39.08 and 31.53 ppm are clearly resolved.

The synthesis of **25** from a toluene solution of the reactants was thought to be more straightforward, since unreacted starting materials and free PPh_3 would remain in solution, while **25** would form as a precipitate, owing to its insolubility in non-polar solvents. However, if complex **25** is prepared in toluene, two isomers are formed, **25a**, in which PPh_3 is *trans* to oxygen, and **25b**, in which PPh_3 is *cis* to the oxygen donor of ODT[9]OC, as shown below in Figure 5.2. The ^1H NMR spectrum now shows two sets of resonances for the two isomers, which are clearly resolved, and the $^{31}P\{^1H\}$ NMR spectrum now shows a second peak at δ 41.73 ppm for isomer **25b**. The mixture of

a **b**

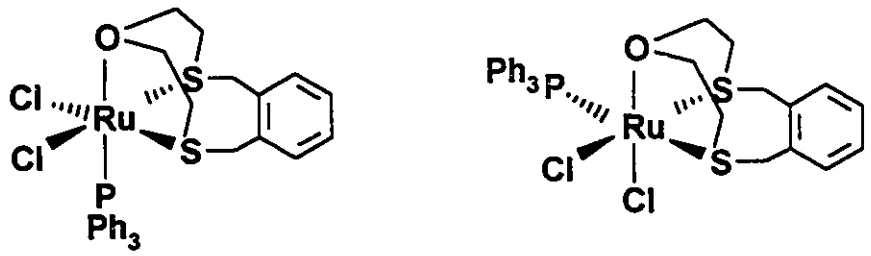

Figure 5.2 Isomers a and b of $RuCl_2(PPh_3)$(ODT[9]OC), (25)

products entirely isomerizes to the *trans* product **25a**, after being stirred in chlorinated solvent for 12 h.

Complex **26**, $RuCl_2(PPh_3)$(TT[9]OC) is prepared by stirring a CH_2Cl_2 solution of $RuCl_2(PPh_3)_3$ with TT[9]OC overnight, resulting in an orange microcrystalline solid after recrystallization from CH_2Cl_2. Complex **26** is obtained in moderate yield (70%), but unlike complex **25** two isomers are formed from the CH_2Cl_2 reaction mixture. The ^1H NMR spectrum of this mixture, shown in Figure 5.3, is quite similar to that of complex **25** from toluene, showing **a** and **b** isomers, which do not isomerize after being stirred in CH_2Cl_2. There was no change in the ^1H NMR spectrum of the mixture up to 355 K, and due to insolubility in non-chlorinated solvents it was not possible to record ^1H NMR spectra at higher temperatures.

The benzylic protons of isomers **26a** and **26b** are again well separated owing to their different ligand environments; resonances for **26a** are shifted upfield, to δ 3.74 and 3.30 ppm, and for **26b** are shifted downfield, to δ 5.34 and 5.20 ppm. The $^{31}P\{^1H\}$ NMR spectrum of the mixture shows two resonances at δ 36.61 and 32.06 ppm; since the PPh_3 ligand is *trans* to sulphur in both isomers, it is not expected that these resonances would be significantly different, as they were for **a** and **b** isomers of complex **25**, $RuCl_2(PPh_3)$(ODT[9]OC).

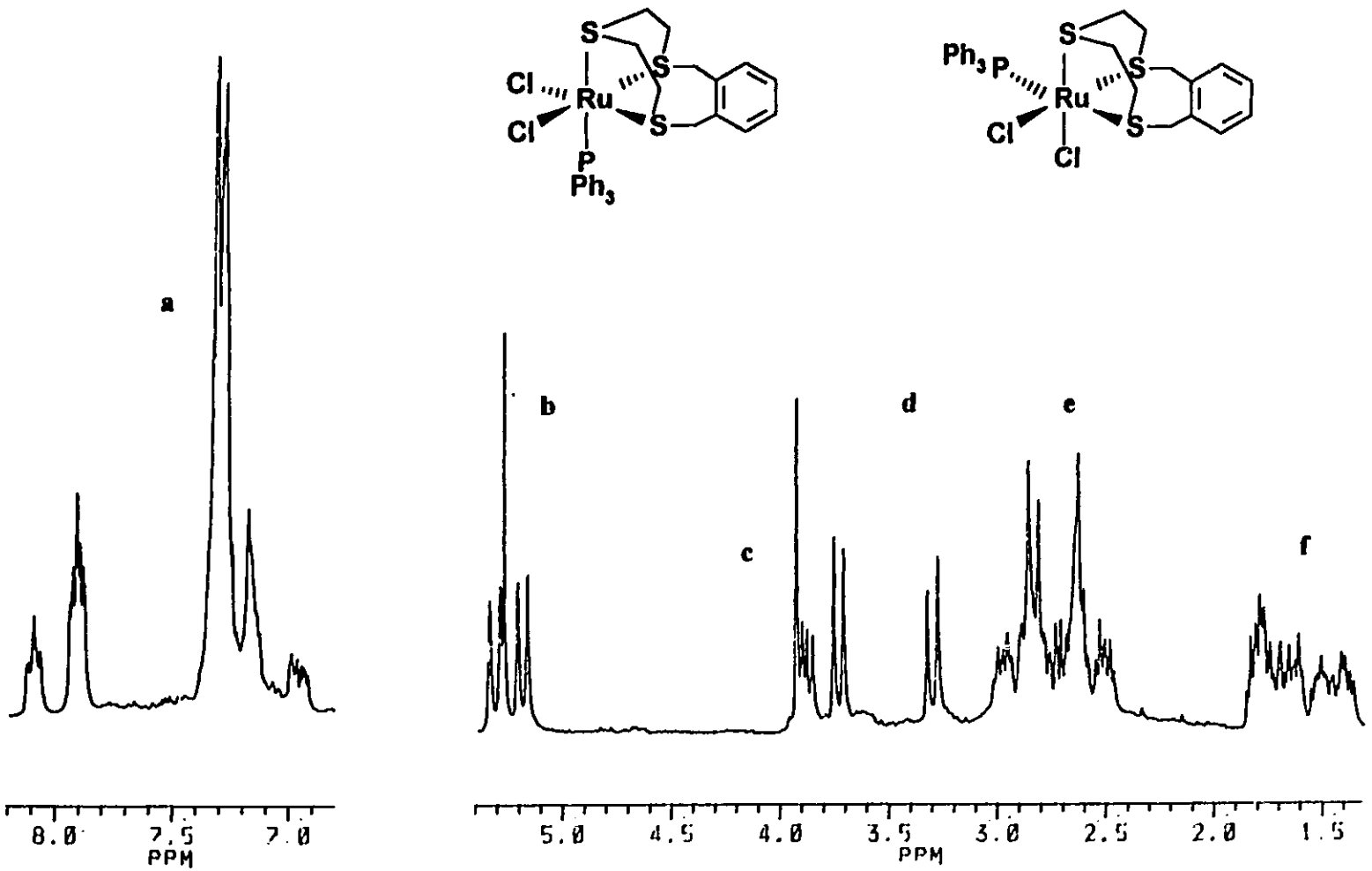

Figure 5.3 ^{1}H NMR spectrum of $RuCl_2(PPh_3)(TT[9]OC)$, 26, in $CDCl_3$. Two isomers are clearly visible, and peaks are labelled as follows: a) aromatic, b) benzylic (26b), c) SCH_2 (26a), d) benzylic (26a), e) SCH_2 (26b), f) SCH_2 (26a).

5.3.2 X-Ray Structure of $RuCl_2(PPh_3)$(ODT[9]OC), (25)

The unit cell contains four $RuCl_2(PPh_3)$(ODT[9]OC) molecules, and four molecules of $Cl(CH_2)_2Cl$. A perspective ORTEP drawing of complex **25** is shown in Figure 5.4. $RuCl_2(PPh_3)$(ODT[9]OC) is six-coordinate with an overall geometry best described as distorted octahedral. ODT[9]OC is coordinated *facially* at Ru(II), with two equatorial Ru-S distances of Ru-S1 2.310(4) Å and Ru-S2 2.290(4) Å and one axial Ru-O distance of 2.232(9) Å. The seven-membered xylyl chelate ring spans the equatorial sites with an angle of S1-Ru-S2 of 102.6(2)°, and the angles at Ru for the five-membered chelate rings are S1-Ru-O1 81.8(3)° and S3-Ru-O1 83.9(3)°. The Ru-P distance is 2.262(4) Å, *trans* to the axial oxygen atom; the angle at O1-Ru-P1 is 179.4(3)°. The two chlorine atoms fill the rest of the coordination sphere: Ru-Cl1 2.429(4) Å and Ru-Cl2 2.428(4) Å. The PPh_3 ligand is bent away slightly from the equatorial sulphur atoms; S1-Ru-P1 93.4(2)° and S2-Ru-P1 95.5(1)°. All bond distances and angles compare well to other ruthenium thioether complexes, where Ru-S distances range from 2.377 Å for $[Ru(9S3)_2][BPh_4]_2$ [107] to 2.356 Å for $RuCl_2(PPh_3)(9S3)$[102c].

An unusual feature of the structure of complex **25** is the aromatic portion of ODT[9]OC, which is bent downward, away from PPh_3 to minimize interactions between the two ligands. The benzylic carbon atoms are oriented toward PPh_3, and this explains the upfield shift of the benzylic protons in the ^1H NMR spectrum, which is due to shielding by the phenyl rings of the phosphine ligand. It can also be inferred then, that in isomer **25b** of this complex, ODT[9]OC is in a conformation similar to that of other thiacyclophane ligands, according to results with Rh(I) and Ir(I) complexes[56] studied in Chapter 4, and

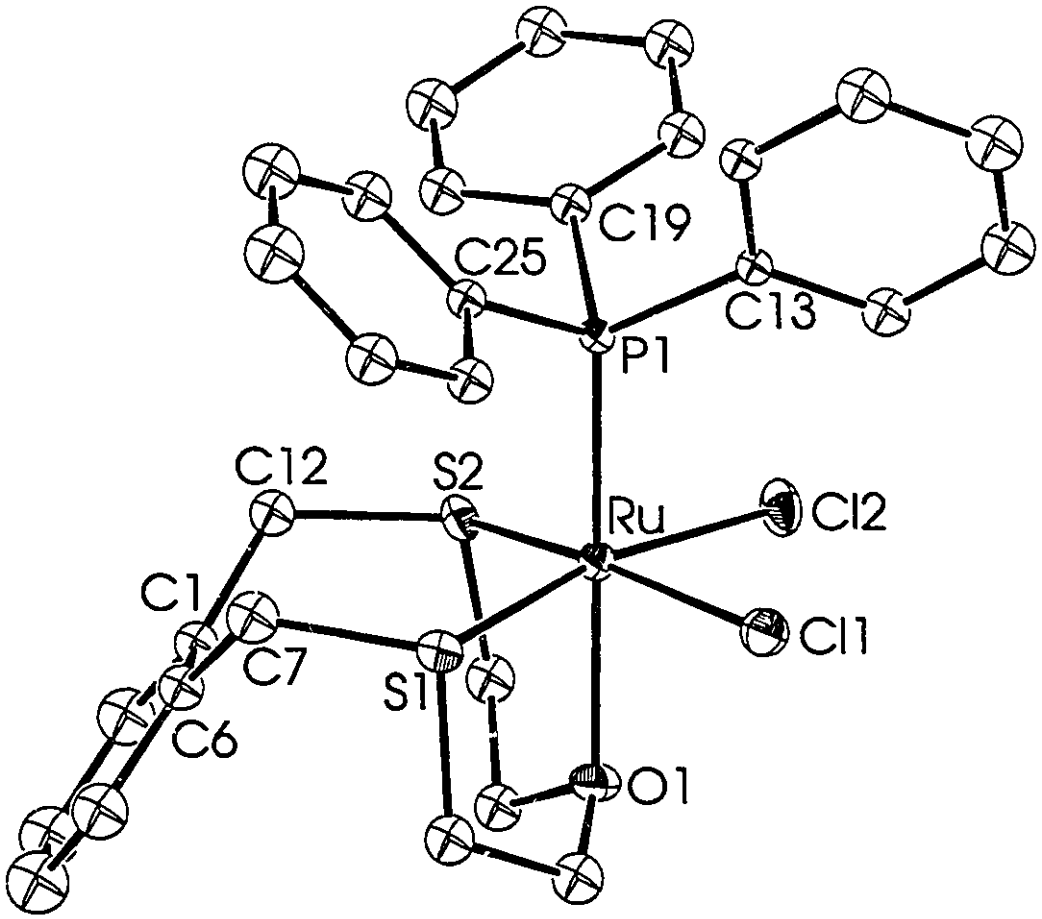

Figure 5.4 ORTEP drawing of $RuCl_2(PPh_3)$(ODT[9]OC), 25, showing the atom-numbering scheme. Thermal ellipsoids of 30% probability are shown. Bond distances: Ru-S1 2.309(4), Ru-S2 2.290(4), Ru-O1 2.232(9), Ru-P1 2.262(4), Ru-Cl1 2.429(4), Ru-Cl2 2.428(4)Å. Bond angles: S1-Ru-S2 102.6(2)°,S1-Ru-P1 98.4(1)°,S1-Ru-O1 81.8(3)°, S1-Ru-Cl1 82.6(1)°, S1-Ru-Cl2 169.6(2)°, S2-Ru-P1 95.5(2)°,S2-Ru-O1 83.9(3)°, S2-Ru-Cl2 81.9(1)°, S2-Ru-O1°, 83.9(3) S2-Ru-Cl2 81.9(1)°, S2-Ru-Cl1 170.2(1)°, O1-Ru-Cl1 88.7(3)°, O1-RuCl2 89.4(3)°, O1-Ru-P1 179.4(3)°, Cl1-Ru-P1 91.9(1)°, Cl1-Ru-Cl2 91.7(1)°, Cl2-Ru-P1 90.4(1)°.

similar to the structure shown in Figure 5.5 of $RuCl_2(DMSO)(TT[9]OC)$[108]; crystallographic data for this complex are given in Tables A.5.4 (data collection parameters), A.5.5 (positional parameters), and A.5.6 (bonding parameters).

$RuCl_2(DMSO)(TT[9]OC)$ provides an interesting contrast to complex **25**, the most obvious difference lying in the conformation of the thioether ligand. The dihedral angles between the planes through the equatorial sulphur atoms, the ruthenium atom, and the chlorine atoms and the planes through C1,C6, C7, and C12 of the aromatic/benzylic portion of the thioether ligands are 142.33° for **25** and 112.90° for $RuCl_2(DMSO)(TT[9]OC)$. Other bond distances and angles are not significantly different, except for the central sulphur atom S2 of $RuCl_2(DMSO)(TT[9]OC)$, where Ru-S2 2.342(2)Å compared to the Ru-O1 distance in **25** of 2.232(9)Å. However, the Ru-S2 distance is very close to Ru-S1 in $RuCl_2(PPh_3)(9S3)$[102c], 2.356(2) Å, even though in one case the central sulphur atom is *trans* to sulphur of DMSO, and in the other case the sulphur atom is *trans* to phosphorus of PPh_3. In both cases, this distance is slightly longer than Ru-S distances in the same plane as the chlorine atoms. While there is a possibility that the longer Ru-S distance is due to a σ-trans effect, an alternative explanation is that competitive π-acceptance plays a role in the destabilization of the Ru-S interaction[102c].

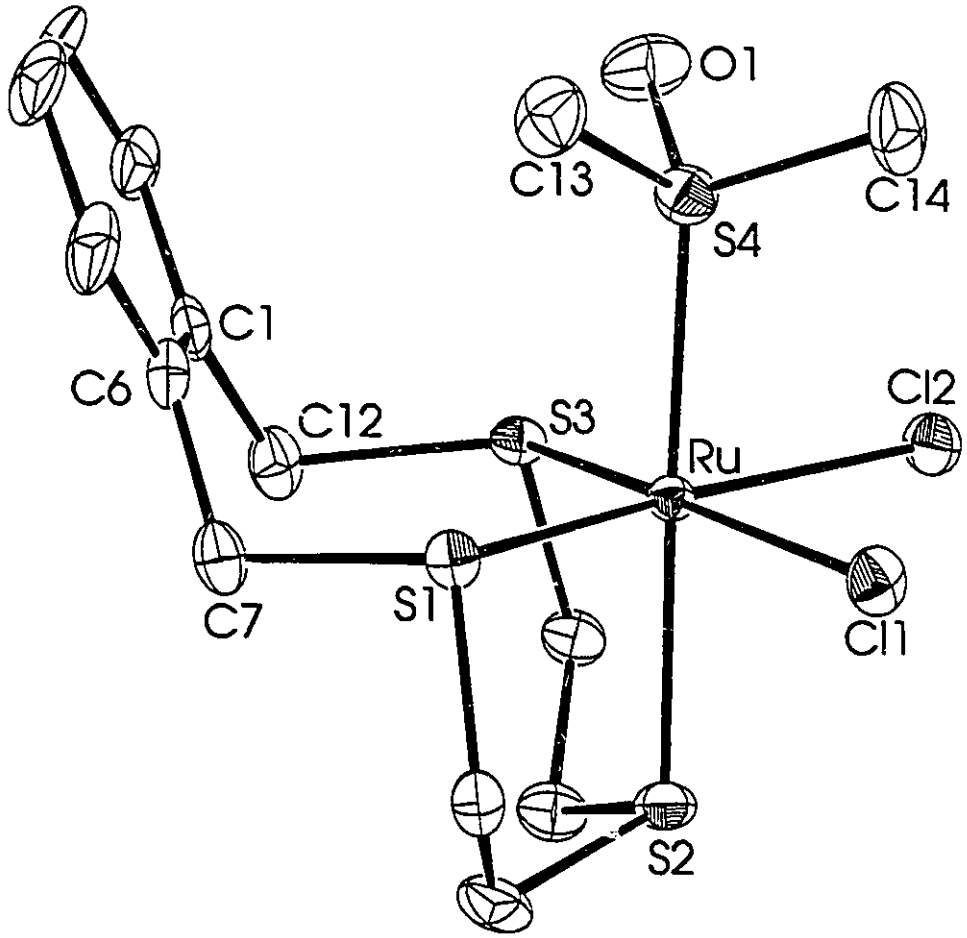

Figure 5.5 ORTEP drawing of $RuCl_2$(DMSO)(TT[9]OC), showing the atom-numbering scheme. Thermal ellipsoids of 30% probability are shown. Bond distances: Ru-S(1) 2.292(2), Ru-S(2) 2.342(2), Ru-S(3) 2.294(2), Ru-S(4) 2.296(2), Ru-Cl1 2.452(2), RuCl2 2.458(2)Å. Bond Angles: Cl(1)-Ru-Cl(2) 89.81(7)°, Cl(1)-Ru-S(1) 83.98(8)°, Cl(1)-Ru-S(2) 87.58(8)°, Cl(1)-Ru-S(3) 170.28(8)°, Cl(1)-Ru-S(4) 93.14(8)°, Cl(2)-Ru-S(1) 173.78(8)°, Cl(2)-Ru-S(2) 92.03(8)°, Cl(2)-Ru-S(3) 81.88(7)°, Cl(2)-Ru-S(4) 85.02(8)°, S(1)-Ru-S(2) 87.33(8)°, S(1)-Ru-S(3) 104.27(8)°, S(1)-Ru-S(4) 95.69(8)°, S(2)-Ru-S(3) 87.68(8)°, S(2)-Ru-S(4) 176.96(9)°, S(3)-Ru-S(4) 91.16(8)°.

5.3.3 Reactions of Complexes $RuCl_2(PPh_3)(ODT[9]OC)$, and $RuCl_2(PPh_3)(TT[9]OC)$

Complexes **25** and **26**, $RuCl_2(PPh_3)(ODT[9]OC)$, and $RuCl_2(PPh_3)(TT[9]OC)$ respectively, are in many respects similar to $[M(COD)L]^+$ complexes in terms of reactivity[56]. Attempts to separate the two isomers of each compound (particularly **26**) were unsuccessful, due to their insolubility in most solvents.

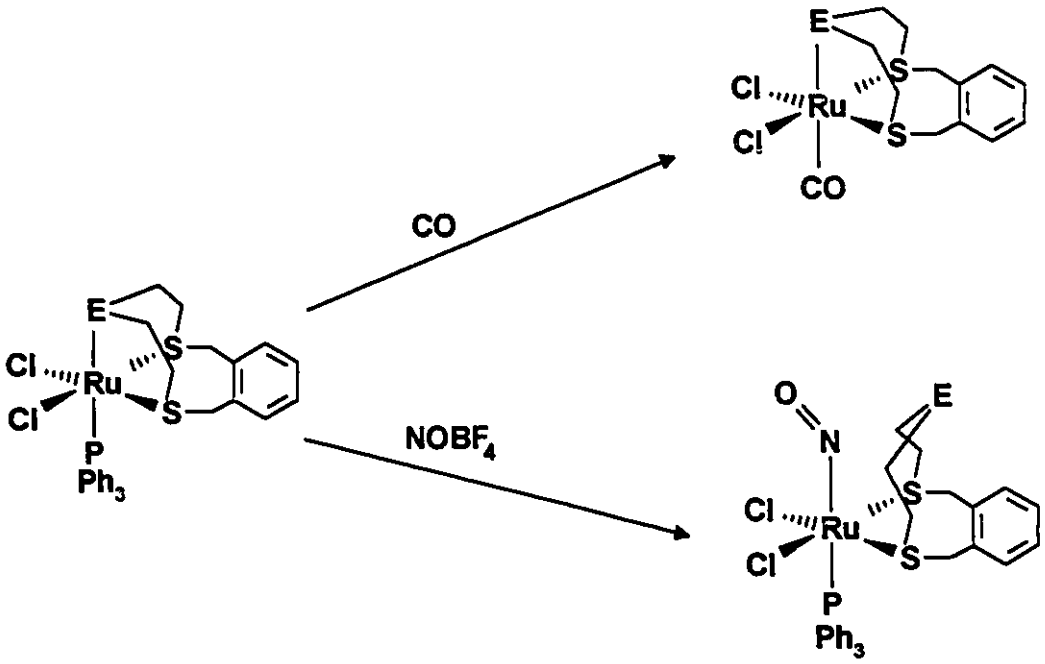

Scheme 5.1 Reactions of $RuCl_2(PPh_3)L$ with CO and $NOBF_4$.

As observed in Chapter 4 for $[M(COD)L]^+$, reactions with isoelectronic CO and NO^+ results in quite different products for both **25** and **26**, as shown in Scheme 5.1. $RuCl_2(PPh_3)L$ reacts with CO, displacing PPh_3, to yield an insoluble yellow powder; the solid state infrared spectra of the carbonyl derivatives show ν(CO) bands at 1994 (complex **25**) and 1975 and 2020 (complex **26**) cm^{-1}, indicating that for complex **26**, two carbonyl derivatives are synthesized. The $^{31}P\{^1H\}$NMR spectrum of the reaction solvent indicates the presence of free PPh_3, with a single resonance at δ -5.0 ppm. The CO complexes are soluble in DMSO, but the ^1H NMR spectrum in this solvent is quite fluxional, perhaps due to exchange between DMSO and CO. Similar insolubilities have been observed for Rh(III) complexes of crown thioethers such as $RhCl_3(9S3)$[87] and $RhCl_3(14S3)$[88]

Reactions of **25** and **26** with $NOBF_4$ results in intensely coloured solutions, and ^1H NMR spectra did not resolve, even when temperatures were lowered to 180K. If the mother liquor is removed *in vacuo*, the infrared spectra of the resulting oily solids show bands at 1876 cm^{-1} for purple **25**, and 1905 cm^{-1} for red **26**, consistent with ν(NO) stretching frequencies. The $^{31}P\{^1H\}$ NMR spectra of both complexes are virtually identical, with resonances at δ 44.00 ppm for **25** and δ 45.13 ppm for **26**. This would indicate that in both cases only one NO compound exists (rather than two isomers), and that NO is trans to PPh_3, since the chemical shift of the phosphine ligand is so similar for both products. The complexes are also similar in stability, decomposing to form brown solutions within 36 h. Similar to $[M(COD)L]^+$ complexes, the displacement of the apical

donor atom of the ligand may cause destabilization of the product, resulting in decomposition.

It is likely that the NO ligands in these derivatives are linear (NO^+), due to the shift to higher wave numbers of the ν(NO) frequencies[109]. High values for ν(NO) are normal for six-coordinate 18-electron species, and especially for ruthenium nitrosyl compounds.

$RuCl_2(PPh_3)$(ODT[9]OC), **25**, and $RuCl_2(PPh_3)$(TT[9]OC), **26**, are remarkably robust complexes which do not react with terminal acetylenes, Grignard reagents, or metal alkyls. In all cases, THF solutions of **25** or **26** were unaffected by the reagent, even after stirring for extended periods of time or after refluxing the THF reaction mixture. Complexes **25** and **26** do react with two molar equivalents of $AlMe_3$ to yield intractable products, and according to their ^1H NMR spectra, starting materials are still present in solution.

5.3.4 Synthesis of $RuHCl(PPh_3)_2$(TT[9]OC), (27)

Complex **27**, $RuHCl(PPh_3)_2$(TT[9]OC), was prepared by displacing PPh_3 from $RuHCl(PPh_3)_3$; the product precipitates as pale yellow microcrystals from a toluene solution in 40% yield. Synthesis of complex **27** at reduced temperature or under an atmosphere of H_2 does not improve yields. Complex **27** is soluble in acetone and chlorinated solvents, and slowly decomposes in the latter. Overall, the ^1H NMR spectrum of **27** indicates that the structure is as shown in Figure 5.6. The presence of two sets of benzylic resonances, a pair of doublets due to axial and equatorial benzylic protons at δ 3.96 and 3.85 ppm, and a singlet at δ 4.00 ppm indicate that the complex is bound

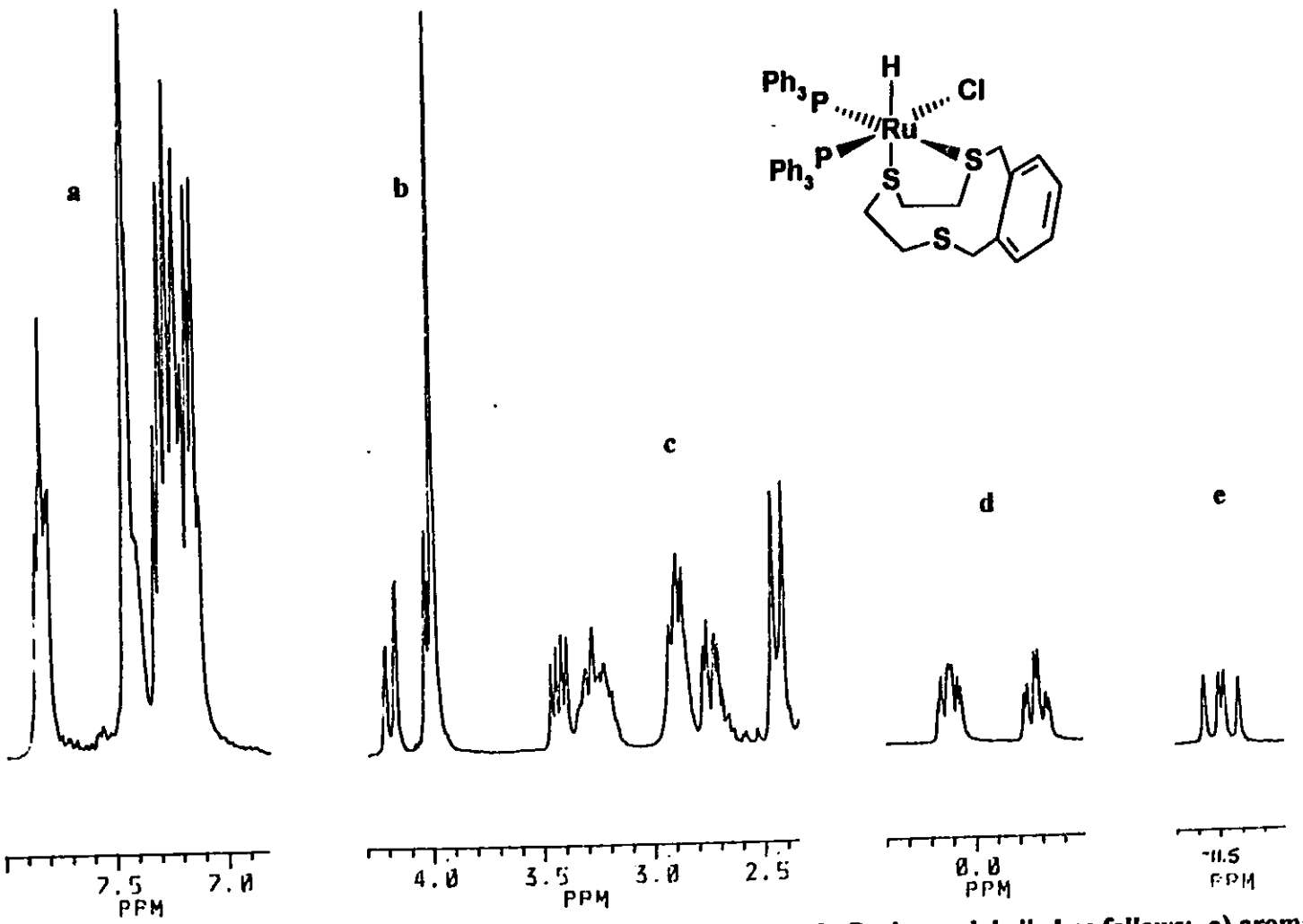

Figure 5.6 ^{1}H NMR spectrum of RuHCl(PPh$_3$)$_2$(TT[9]OC), 27, in acetone-d$_6$. Peaks are labelled as follows: a) aromatic, b) benzylic, c) SCH$_2$, d) SCH$_2$ (ethylene), e) Ru hydride.

asymmetrically to Ru(II), through S1 and S2. Two triplets of doublets at approximately 0 ppm are due to the ethylene protons of TT[9]OC, which are shielded by the PPh_3 phenyl rings. The ruthenium hydride is observed at δ -11.69 ppm, coupled to two phosphorus atoms, resulting in two doublets with coupling constants of approximately 20 Hz. The $^{31}P\{^1H\}$ NMR spectrum of this complex indicates that two PPh_3 ligands are present, and P-P coupling of 32.7 Hz is in the range for *cis* phosphorus atoms[110].

Heating complex **27** in an attempt to displace PPh_3 and form the complex $RuHCl(PPh_3)(TT[9]OC)$ in which all three sulphur donors coordinate to the metal centre, was not successful, even when **27** was refluxed in a mixture of toluene and acetone at 70°C for three hours. Similarly, attempts to form the salt $[RuH(PPh_3)_2(TT[9]OC)][BF_4]$ were not successful; in both cases the starting material was unaffected by heat and by silver salts, although it is expected that the chloride ligand would be labile[1]. $RuHCl(PPh_3)_3$ does not react with ODT[9]OC, presumably because the ligand does not have enough π-acceptor capability due to the oxygen donor, and cannot stabilize the ruthenium centre.

The overt stability of complex **27** may be due to the fact that in solution $RuHCl(PPh_3)_3$ does not dissociate[111] to form $RuHCl(PPh_3)_2$. In comparison, the facile reaction of $RuCl_2(PPh_3)_3$ with crown thioethers or with a wide variety of ligands[101] that substitute for PPh_3 is due to the fact that PPh_3 ligands are quite labile in this complex, and that in solution $RuCl_2(PPh_3)_3$ dissociates to $RuCl_2(PPh_3)_2$. This type of dissociation is not observed for any of complexes **25** - **27**; there is no evidence of free PPh_3 in the $^{31}P\{^1H\}$ NMR spectra of the complexes.

5.4 Summary and Conclusions

Previously, tridentate coordination of ODT[9]OC had not been observed in Ag(I)[58] or Rh(I), Ir(I)[56] complexes containing this ligand. However, the increased basicity of ruthenium and its ability to stabilize hard donor atoms permit tridentate *facial* coordination to occur. $RuCl_2(PPh_3)$(ODT[9]OC), **25** provides an interesting structural comparison to $RuCl_2$(DMSO)(TT[9]OC)[111], in that steric interactions with PPh_3 are minimized by the ODT[9]OC ligand folding away from the phosphine, and of the 30 or more complexes involving TT[9]OC or ODT[9]OC, this is unique.

The complexes $RuCl_2(PPh_3)L$ (L = ODT[9]OC or TT[9]OC) are robust, relatively unreactive compounds which are resistant to reaction at the anionic ligands but which undergo substitution for PPh_3 by CO. They also react with $NOBF_4$ to displace the central donor atom of the crown thioether. As reported in Chapter 4 for $[M(COD)L]^+$ complexes, slippage to a bidentate coordination mode is demonstrated in reactions of $RuCl_2(PPh_3)L$ with $NOBF_4$, although in the case of Ru(II), both complexes have approximately the same stability in solution due to similar perturbations of the central donor atoms of the ligands.

Complex **27**, $RuHCl(PPh_3)_2$(TT[9]OC), is also very stable in the solid state and in solution, but may show potential in the isolation of intermediates in reaction chemistry. The preliminary reactions of $RuCl_2(PPh_3)L$ (L = ODT[9]OC, **25** and L = TT[9]OC, **26**) indicate that they may be useful in enzyme modelling studies because of the stabilizing influence of the ligand, and further work along these lines is proceeding.

Appendix A

Table A. 2.1
Summary of Crystal Data, Intensity Collection, and Structure Refinement for ODT[9]OC

formula	$C_{12}H_{16}OS_2$
fw	240.40
a, Å	11.076(1)
b, Å	11.196(9)
c, Å	99.913(6)
α, deg	
β, deg	101.45(6)
γ, deg	
cryst syst	monoclinic
space group	*C2/c* (No. 15)
V, Å^3	1204(2)
ρ (calcd), g/cm^{-3}	1.326
Z	4
μ, cm^{-1}	4.13 (empirical)
avg trans factor	0.9814
diffractometer	Rigaku AFC6S
λ, Å	0.71069
T, °C	24
take-off angle	6.0
detect aper, mm	6.0 hor; 6.0 vert
cryst to detect, cm	40
scan type	ω-2θ
scan speed, deg/min	32.0 omega
scan width, deg	1.05 + 0.3 tanθ
data collected	1221
data $F_o^2 > 3\sigma(F_o^2)$	625
variables	70
goodness of fit	1.91
$R(F_o)^a$, %	5.60
$R_w(F_o)^a$, %	4.11

[a] $R = \Sigma||F_o|-|F_c||/\Sigma|F_o||$, $R_w = (\Sigma w(|F_o|-|F_c|)^2/\Sigma wF_o2)^{1/2}$ and $w = 1/\sigma^2(F)$

Table A.2.2
Positional parameters and B(eq) for ODT[9]OC

atom	x	y	z	B(eq)
S(1)	0.7935(1)	0.4706(1)	0.1885(1)	3.92(6)
O(1)	1.0000	0.6527(5)	1/4	11.1(4)
C(1)	0.7949(5)	0.6227(5)	0.1285(6)	5.7(3)
C(2)	0.9163(4)	0.4051(4)	0.1146(4)	3.4(2)
C(3)	0.9609(4)	0.2922(4)	0.1843(4)	3.2(2)
C(4)	0.8980(5)	0.6969(4)	0.1896(6)	5.8(3)
C(5)	0.9258(4)	0.1823(5)	0.1228(6)	5.1(3)
C(6)	0.9633(5)	0.0761(4)	0.1844(7)	6.8(4)

Table A.2.3
Summary of Bond Distances and Angles for ODT[9]OC

Distances (Å)

S(1)-C(5)	1.805(6)	C(3)-C(3)	1.39(1)
S(1)-C(6)	1.822(5)	O(1)-C(4)	1.269(5)
C(4)-C(5)	1.445(7)	O(1)-C(4)	1.269(5)
C(1)-C(1)	1.414(8)	C(1)-C(2)	1.393(6)
C(1)-C(6)	1.478(6)	C(2)-C(3)	1.363(7)

Angles(°)

C(5)-S(1)-C(6)	101.0(2)	C(4)-O(1)-C(4')	134.1(7)
C(1')-C(1)-C(2)	18.0(3)	S(1)-C(5)-C(4)	117.6(4)
C(1')-C(1)-C(6)	21.2(2)	C(2)-C(1)-C(6)	120.8(4)
C(1)-C(2)-C(3)	122.7(5)	C(2)- C(3)-C(3')	119.2(3)
S(1)-C(6)-C(1)	111.3(3)	O(1)-C(4)-C(5)	121.9(5)

Table A.2.4
Summary of Crystal Data, Intensity Collection, and Structure Refinement for $[Ag(TT[9]OC)_2][ClO_4]$, (1)

formula	$C_{24}H_{32}AgClO_4S_6$
fw	720.28
a, Å	8.317(2)
b, Å	26.178(11)
c, Å	13.361(5)
α, deg	
β, deg	101.14(2)
γ, deg	
cryst syst	monoclinic
space group	$P2_1/n$ (No. 14)
V, Å^3	2854(3)
ρ (calcd), g/cm^{-3}	1.676
Z	4
μ, cm^{-1}	12.45 (empirical)
avg trans factor	0.89-1.00
diffractometer	Rigaku AFC6S
λ, Å	0.71069
T, °C	24
take-off angle	6.0
detect aper, mm	6.0 hor; 6.0 vert
cryst to detect, cm	40
scan type	ω-2θ
scan speed, deg/min	32.0 omega
scan width, deg	1.05 + 0.30 tanθ
data collected	5139
data $F_o^2 > 3\sigma(F_o^2)$	1577
variables	206
goodness of fit	1.74
$R(F_o)^a$, %	7.06
$R_w(F_o)^a$, %	7.58

[a] $R = \Sigma||F_o|-|F_c||/\Sigma|F_o||$, $R_w = (\Sigma w(|F_o|-|F_c|)^2/\Sigma wF_o2)^{1/2}$ and $w = 1/\sigma^2(F)$

Table A.2.5
Positional parameters and B(eq) for $[Ag(TT[9]OC)_2][ClO_4]$, (1)

Atom	x	y	z	B(eq)
Ag	.7522(2)	.37439(8)	.24848(13)	4.76(7)
S(1)	1.0336(6)	.3637(2)	.1682(4)	4.1(3)
S(2)	.6780(7)	.2925(2)	.1187(4)	4.1(3)
S(3)	.5698(6)	.4214(2)	.0827(4)	3.2(2)
S(4)	.9270(6)	.3166(2)	.4084(5)	4.1(3)
S(5)	.8702(6)	.4479(2)	.3862(4)	4.0(3)
S(6)	.4799(6)	.3924(2)	.3261(4)	3.5(2)
C(1)	.842(2)	.4795(7)	.088(1)	3.3(4)
C(2)	.795(2)	.5224(7)	.128(1)	3.8(4)
C(3)	.898(3)	.5531(9)	.198(2)	5.3(5)
C(4)	1.060(2)	.5385(7)	.222(2)	4.2(5)
C(5)	1.110(2)	.4932(8)	.185(1)	4.1(4)
C(6)	1.006(2)	.4649(7)	.117(2)	3.6(4)
C(7)	1.064(2)	.4156(8)	.082(2)	4.5(5)
C(8)	.999(2)	.3072(8)	.086(2)	5.4(5)
C(9)	.885(2)	.2701(8)	.112(2)	5.2(5)
C(10)	.617(2)	.3249(7)	.003(1)	4.0(4)
C(11)	.494(2)	.3668(7)	.0047(13)	3.8(4)
C(12)	.717(2)	.4500(7)	.015(2)	3.9(4)
C(13)	.489(2)	.2918(7)	.3789(13)	2.3(4)
C(14)	.349(2)	.2717(8)	.320(2)	4.3(4)
C(15)	.362(2)	.2268(8)	.277(2)	4.4(5)
C(16)	.498(3)	.1985(9)	.288(2)	5.6(5)
C(17)	.643(2)	.2177(8)	.350(2)	4.5(5)
C(18)	.636(2)	.2659(7)	.3997(14)	2.8(4)
C(19)	.783(2)	.2840(8)	.472(2)	4.7(5)
C(20)	1.009(3)	.3640(9)	.506(2)	5.9(5)
C(21)	1.033(3)	.4152(9)	.466(2)	6.6(6)
C(22)	.709(3)	.4509(9)	.458(2)	5.5(5)
C(23)	.542(2)	.4504(8)	.399(2)	4.7(5)
C(24)	.472(2)	.3434(8)	.424(2)	4.6(5)
Cl)	.4940(6)	.3907(2)	.6974(4)	4.0(2)
O(1)	.632(2)	.3730(7)	.6631(10)	7.1(8)
O(2	.394(2)	.4164(7)	.6180(13)	9(1)
O(3)	.541(2)	.4229(7)	.7802(12)	8(1)
O(4)	.407(3)	.3516(7)	.727(2)	12(1)

Table A.2.6
Summary of Bond Distances and Angles for $[Ag(TT[9]OC)_2][ClO_4]$, (1)

Distances (Å)

Ag-S(1)	2.771(6)	S(4)-C(20)	1.84(2)
Ag-S(2)	2.752(6)	S(5)-C(21)	1.77(2)
Ag-S(3)	2.725(5)	S(5)-C(22)	1.79(2)
Ag-S(4)	2.788(6)	S(6)-C(23)	1.83(2)
Ag-S(5)	2.712(6)	S(6)-C(24)	1.84(2)
Ag-S(6)	2.709(5)	C(1)-C(12)	1.50(2)
S(1)-C(7)	1.83(2)	C(6)-C(7)	1.48(3)
S(1)-C(8)	1.83(1)	C(8)-C(9)	1.45(3)
S(2)-C(9)	1.84(2)	C(10)-C(11)	1.51(2)
S(2)-C(10)	1.82(2)	C(13)-C(24)	1.50(2)
S(3)-C(11)	1.81(2)	C(18)-C(19)	1.48(2)
S(3)-C(12)	1.82(2)	C(20)-C(21)	1.47(2)
S(4)-C(19)	1.81(2)	C(22)-C(23)	1.46(3)
C(1)-C(2)	1.33(2)	C(13)-C(14)	1.37(2)
C(1)-C(6)	1.40(2)	C(13)-C(18)	1.38(2)
C(2)-C(3)	1.40(2)	C(14)-C(15)	1.32(2)
C(3)-C(4)	1.38(2)	C(15)-C(16)	1.34(2)
C(4)-C(5)	1.38(2)	C(16)-C(17)	1.41(3)
C(5)-C(6)	1.35(2)	C(17)-C(18)	1.43(2)
Cl-O(1)	1.40(1)	Cl-O(3)	1.39(1)
Cl-O(2)	1.39(2)	Cl-O(4)	1.36(2)

Angles (°)

S(1)-Ag-S(2)	77.3(2)	C(11)-S(3)-C(12)	103.3(9)
S(1)-Ag-S(3)	96.3(2)	C(19)-S(4)-C(20)	100.0(10)
S(1)-Ag-S(4)	83.6(2)	C(21)-S(5)-C(22)	105.5(11)
S(2)-Ag-S(5)	96.4(2)	C(23)-S(6)-C(24)	104.1(10)
S(2)-Ag-S(6)	175.8(2)	S(1)-C(7)-C(6)	111(1)
S(2)-Ag-S(3)	79.5(2)	S(1)-C(8)-C(9)	115(2)
S(2)-Ag-S(4)	94.6(2)	S(2)-C(9)-C(8)	118(2)
S(2)-Ag-S(5)	171.2(2)	S(2)-C(10)-C(11)	111(1)
S(2)-Ag-S(6)	105.9(2)	S(3)-C(11)-C(10)	117(1)
S(3)-Ag-S(4)	173.9(2)	S(3)-C(12)-C(1)	110(1)
S(3)-Ag-S(5)	107.7(2)	S(4)-C(19)-C(18)	112(1)
S(3)-Ag-S(6)	81.8(2)	S(4)-C(20)-C(21)	114(2)
S(4)-Ag-S(5)	78.3(2)	S(4)-Ag-S(6)	98.7(2)
S(5)-C(22)-C(23)	116(2)	S(5)-Ag-S(6)	80.6(2)
S(6)-C(23)-C(22)	116(2)	C(7)-S(1)-C(8)	104.3(10)

S(6)-C(24)-C(13)	109(1)	C(9)-S(2)-C(10)	102.2(10)
C(2)-C(1)-C(6)	118(2)	C(14)-C(13)-C(18)	123(2)
C(2)-C(1)-C(12)	118(2)	C(14)-C(13)-C(24)	116(2)
C(6)-C(1)-C(12)	124(2)	C(18)-C(13)-C(24)	121(2)
C(1)-C(2)-C(3)	124(2)	C(13)-C(14)-C(15)	117(2)
C(2)-C(3)-C(4)	116(2)	C(14)-C(15)-C(16)	126(2)
C(3)-C(4)-C(5)	120(2)	C(15)-C(16)-C(17)	118(2)
C(4)-C(5)-C(6)	121(2)	C(16)-C(17)-C(18)	119(2)
C(5)-C(6)-C(1)	120(2)	C(17)-C(18)-C(13)	117(2)
C(1)-C(6)-C(7)	121(2)	C(13)-C(18)-C(19)	124(2)
C(5)-C(6)-C(7)	119(2)	C(17)-C(18)-C(19)	119(2)
O(1)-C(l)-O(2)	109(1)	O(2)-C(l)-O(3)	111(1)
O(1)-C(l)-O(3)	110(1)	O(2)-C(l)-O(4)	108(1)
O(1)-C(l)-O(4)	111(1)	O(3)-C(l)-O(4)	108(1)

Table A.2.7
Summary of Crystal Data, Intensity Collection, and Structure Refinement for [Ag(TT[9]OC)$_2$][BPh$_4$] , (3)

formula	**$C_{48}H_{52}AgBS_6$**
fw	940.08
a, Å	16.257(5)
b, Å	16.031(6)
c, Å	16.962(5)
α, deg	
β, deg	93.25(3)
γ, deg	
cryst syst	monoclinic
space group	*C*2/*c* (No. 15)
V, Å^3	4413(4)
ρ (calcd),g/cm^{-3}	1.270
Z	4
μ, cm^{-1}	6.17 (empirical)
avg trans factor	0.92 to 1.00
diffractometer	Rigaku AFC6S
λ, Å	0.71069
T, °C	24
take-off angle	6.0
detect aper, mm	6.0 hor; 6.0 vert
cryst to detect, cm	40
scan type	ω-2θ
scan speed, deg/min	32.0 omega
scan width, deg	1.05 + 0.30 tanθ
data collected	4058
data $F_o^2 > 3\sigma(F_o^2)$	1495
variables	166
goodness of fit	1.86
$R(F_o)^a$, %	6.79
$R_w(F_o)^a$, %	6.90

[a] $R = \Sigma||F_o|-|F_c||/\Sigma|F_o||$, $R_w = (\Sigma w(|F_o|-|F_c|)^2/\Sigma wF_o2)^{1/2}$ and $w = 1/\sigma^2(F)$

Table A.2.8
Positional parameters and B(eq) for $[Ag(TT[9]OC)_2][BPh_4]$, (3)

Atom	x	y	z	B(eq)
Ag	.0000	.3153(1)	.2500	5.9(1)
S(1)	.1076(2)	.4337(2)	.2113(2)	4.2(2)
S(2)	.1492(3)	.2230(3)	.1732(3)	5.1(2)
S(2A)	.161(1)	.262(1)	.093(1)	8(1)
S(3)	.0576(2)	.2610(2)	.1169(2)	3.9(2)
C(1)	.0613(7)	.4264(8)	.0770(6)	3.5(6)
C(2)	.145(1)	.4407(9)	.0725(7)	5.1(8)
C(3)	.1773(8)	.517(1)	.0927(8)	6.0(9)
C(4)	.124(1)	.5787(9)	.1178(7)	5.8(8)
C(5)	.0404(9)	.5666(8)	.1246(7)	4.3(7)
C(6)	.0078(8)	.4899(8)	.1038(6)	3.5(6)
C(7)	.0829(7)	.4759(8)	.1139(6)	4.3(7)
C(8)	.2090(7)	.3853(8)	.2045(8)	5.2(7)
C(9)	.212(1)	.309(1)	.155(1)	9(1)
C(10)	.094(1)	.189(1)	.091(1)	9(1)
C(11)	.0050(9)	.1768(8)	.0850(7)	5.2(7)
C(12)	.0326(8)	.3435(7)	.0486(6)	4.5(7)
C(13)	.0637(4)	.0532(4)	.3083(4)	4.4(1)
C(14)	.0884(4)	.0794(4)	.3844(4)	4.4(1)
C(15)	.1787(4)	.0400(4)	.3993(4)	4.4(1)
C(16)	.0964(4)	.0196(5)	.2777(3)	4.4(1)
C(17)	.1539(4)	.0662(4)	.3232(4)	4.4(1)
C(18)	.1459(4)	.0328(5)	.4299(3)	4.4(1)
C(19)	.0652(4)	.1684(4)	.3012(4)	4.2(1)
C(20)	.0931(4)	.2543(4)	.2719(3)	4.2(1)
C(21)	.1519(4)	.2900(3)	.3113(4)	4.2(1)
C(22)	.1828(4)	.2578(4)	.3800(4)	4.2(1)
C(23)	.1550(4)	.1809(4)	.4094(3)	4.2(1)
C(24)	.0962(4)	.1362(3)	.3700(45	4.2(1)
B	.0000	.111(1)	.2500	2.3(3)

Table A2.9
Summary of Bond Distances and Angles for $[Ag(TT[9]OC)_2][BPh_4]$, (3)

Distances (Å)

Ag-S(1)	2.688(4)	S(3)-C(11)	1.79(1)
Ag-S(3)	2.548(3)	S(3)-C(12)	1.82(1)
S(1)-C(7)	1.81(1)	C(1)-C(12)	1.50(2)
S(1)-C(8)	1.83(1)	C(6)-C(7)	1.49(2)
S(2)-C(9)	1.76(2)	C(8)-C(9)	1.49(2)
S(2)-C(10)	1.70(2)	C(10)-C(11)	1.46(2)
C(1)-C(2)	1.37(2)	C(5)-C(6)	1.39(2)
C(1)-C(6)	1.40(2)	S(2B)-C(13)	1.67(1)
C(2)-C(3)	1.38(2)	S(2B)-C(19)	1.69(1)
C(3)-C(4)	1.37(2)	S(2A)-C(9)	1.51(2)
C(4)-C(5)	1.37(2)	S(2A)-C(10)	1.61(2)

Nonbonded Distances (Å)

Ag...S(2)	3.183(5)	Ag...S(2A)	3.94(2)

Angles (°)

S(1)-Ag-S(3)	103.7(1)	S(1)-C(7)-C(6)	109.1(8)
S(1)-Ag-S(1)'	90.1(2)	S(1)-C(8)-C(9)	116.5(9)
S(1)-Ag-S(3)'	104.3(1)	S(2)-C(9)-C(8)	120.0(12)
S(3)-Ag-S(3)'	140.0(2)	S(2)-C(10)-C(11)	125.5(13)
C(7)-S(1)-C(8)	104.8(6)	S(3)-C(11)-C(10)	117.1(10)
C(9)-S(2)-C(10)	113.2(9)	S(3)-C(12)-C(1)	110.9(8)
C(11)-S(3)-C(12)	101.8(6)		
C(2)-C(1)-C(6)	119(1)	C(1)-C(6)-C(5)	119(1)
C(2)-C(1)-C(12)	117(1)	C(1)-C(6)-C(7)	121(1)
C(6)-C(1)-C(12)	123(1)	C(5)-C(6)-C(7)	120(1)
C(1)-C(2)-C(3)	122(2)	C(13)-B-C(19)	112.6(3)
C(2)-C(3)-C(4)	118(2)	C(13)-B-C(13)'	112.9(10)
C(3)-C(4)-C(5)	122(2)	C(13)-B-C(19)'	102.8(3)
C(4)-C(5)-C(6)	120(2)	C(19)-B-C(19)'	113.5(13)

Since the BPh_4 anion phenyls are input as rigid groups CC = 1.40 Å, CCC = 120°. The designation A represents the minor component of a 72/28 disorder for S2.

Table A.2.10.
Summary of Crystal Data, Intensity Collection, and Structure Refinement for $[Ag(TT[9]OC)_2][CF_3SO_3]$, (4)

formula	$C_{25}H_{32}AgF_3O_3S_7$
fw	769.93
a, Å	12.390(2)
b, Å	14.158(4)
c, Å	9.290(3)
α, deg	91.04(3)
β, deg	109.64(2)
γ, deg	83.37(2)
cryst syst	triclinic
space group	$P\bar{1}$ (No. 2)
V, Å^3	1524.9(9)
ρ (calcd),g/cm^{-3}	1.657
Z	2
μ, cm^{-1}	11.59 (empirical)
avg trans factor	0.87 to 1.00
diffractometer	Rigaku AFC6S
λ, Å	0.71069
T, °C	24
take-off angle	6.0
detect aper, mm	6.0 horz; 6.0 vert
cryst to detect, cm	40
scan type	ω-2θ
scan speed, deg/min	32.0 omega
scan width, deg	1.05 + 0.30 tanθ
data collected	5622
data $F_o^2 > 3\sigma(F_o^2)$	2815
variables	309
goodness of fit	2.02
$R(F_o)^a$, %	6.76
$R_w(F_o)^a$, %	7.28

$^a R = \Sigma||F_o|-|F_c||/\Sigma|F_o||$, $R_w = (\Sigma w(|F_o|-|F_c|)^2/\Sigma wF_o2)^{1/2}$ and $w = 1/\sigma^2(F)$

Table A.2.11
Positional parameters and B(eq) for $[Ag(TT[9]OC)_2][CF_3SO_3]$, (4)

Atom	x	y	z	B(eq)
Ag	.56321(8)	.17496(7)	.5476(1)	4.04(5)
S(1)	.7075(3)	.0944(2)	.4240(4)	4.7(2)
S(2)	.4095(3)	.0967(2)	.3295(4)	4.9(2)
S(3)	.4717(3)	.3314(2)	.3994(4)	4.5(2)
S(4)	.6517(2)	.1429(2)	.8260(3)	3.7(1)
S(5)	.6616(3)	.4484(3)	.9449(5)	6.2(2)
S(6)	1.0274(3)	.3446(3)	1.1429(5)	6.9(2)
S(7A)	.2752(8)	.2252(7)	.769(1)	7.1(2)
S(7B)	.287(1)	.2228(8)	.748(1)	10.0(3)
F(1A)	.331(1)	.338(1)	.609(2)	10.7(4)
F(2A)	.178(1)	.391(2)	.657(2)	10.7(4)
F(3A)	.342(2)	.380(2)	.836(2)	10.7(4)
F(1B)	.345(1)	.394(1)	.734(2)	13.2(5)
F(2B)	.179(2)	.362(2)	.589(2)	13.2(5)
F(3B)	.214(2)	.374(2)	.830(2)	13.2(5)
O(1A)	.3897(8)	.181(2)	.845(2)	7.1(2)
O(2A)	.209(1)	.224(1)	.869(2)	7.1(2)
O(3A)	.222(1)	.174(1)	.634(1)	7.1(2)
O(1B)	.188(1)	.174(2)	.727(2)	10.0(3)
O(2B)	.334(2)	.197(2)	.630(2)	10.0(3)
O(3B)	.372(1)	.197(2)	.893(1)	10.0(3)
C(1)	.691(1)	.355(1)	.415(1)	4.7(7)
C(2)	.736(2)	.431(1)	.515(2)	7(1)
C(3)	.851(2)	.419(2)	.619(2)	9(1)
C(4)	.918(2)	.340(2)	.618(3)	9(1)
C(5)	.879(1)	.272(1)	.524(2)	6.4(9)
C(6)	.766(1)	.275(1)	.421(1)	4.4(6)
C(7)	.733(1)	.192(1)	.321(1)	5.7(7)
C(8)	.611(1)	.031(1)	.274(2)	6.5(8)
C(9)	.492(1)	.076(1)	.198(2)	6.9(9)
C(10)	.313(1)	.203(1)	.254(2)	8(1)
C(11)	.358(1)	.293(1)	.236(2)	8(1)
C(12)	.571(1)	.367(1)	.308(2)	7.0(8)
C(13)	.962(1	.1578(8)	1.093(1)	3.7(6)
C(14)	1.027(1)	.133(1)	1.244(1)	4.5(6)
C(15)	1.014(1)	.051(1)	1.311(1)	4.7(6)
C(16)	.936(1)	.007(8)	1.232(2)	4.8(7)
C(17)	.866(1)	.0175(9)	1.082(7)	4.2(6)
C(18)	.880(1)	.0996(9)	1.013(1)	3.7(6)

C(19)	.805(1)	.1179(6)	.845(1)	4.3(6)
C(20)	.650(1)	.2547(9)	.923(1)	4.1(6)
C(21)	.646(1)	.342(1)	.830(1)	5.0(6)
C(22)	.821(1)	.448(1)	1.003(2)	7.1(9)
C(23)	.886(1)	.393(1)	1.150(2)	6.2(8)
C(24)	.987(1)	.245(1)	1.023(25	5.5(7)
C(25A)	.279(1)	.341(1)	.712(2)	10.7(4)
C(25B)	.258(1)	.347(1)	.724(2)	13.2(5)

Table A.2.12
Summary of Bond Distances and Angles for $[Ag(TT[9]OC)_2][CF_3SO_3]$, (4)

Distances (Å)

Ag-S(1)	2.600(4)	S(5)-C(21)	1.81(1)
Ag-S(2)	2.590(3)	S(5)-C(22)	1.86(2)
Ag-S(3)	2.570(3)	S(6)-C(23)	1.83(2)
Ag-S(4)	2.476(3)	S(6)-C(24)	1.79(1)
S(1)-C(7)	1.81(2)	C(1)-C(12)	1.48(2)
S(1)-C(8)	1.80(1)	C(6)-C(7)	1.49(2)
S(2)-C(9)	1.84(2)	C(8)-C(9)	1.49(2)
S(2)-C(10)	1.81(2)	C(10)-C(11)	1.47(2)
S(3)-C(11)	1.82(2)	C(13)-C(24)	1.51(2)
S(3)-C(12)	1.83(2)	C(18)-C(19)	1.54(2)
S(4)-C(19)	1.84(1)	C(20)-C(21)	1.51(2)
S(4)-C(20)	1.81(1)	C(22)-C(23)	1.51(2)
C(1)-C(2)	1.44(2)	C(1)-C(6)	1.38(2)
C(1)-C(12)	1.48(2)	C(2)-C(3)	1.42(3)
C(3)-C(4)	1.32(4)	C(4)-C(5)	1.31(3)
C(5)-C(6)	1.40(2)	C(13)-C(14)	1.39(2)
C(13)C(18)	1.38(2)	C(14)-C(15)	1.39(2)
C(15)C(16)	1.36(2)	C(16)-C(17)	1.39(2)
S(7A)-C(25A)	1.74(2)	C(17)-C(18)	1.39(2)
S(7B)-C(25B)	1.75(2)		

Nonbonded distances (Å)

Ag...S5	5.251(4)	Ag...S6	7.115(5)

Angles (°)

S(1)-Ag-S(2)	84.6(1)	S(1)-C(7)-C(6)	112(1)
S(1)-Ag-S(3)	107.3(1)	S(1)-C(8)-C(9)	118(1)
S(1)-Ag-S(4)	106.0(1)	S(2)-C(9)-C(8)	113(1)
S(2)-Ag-S(3)	85.2(1)	S(2)-C(10)-C(11)	121(1)
S(2)-Ag-S(4)	133.8(1)	S(3)-C(11)-C(10)	117(1)
S(3)-Ag-S(4)	130.4(1)	S(3)-C(12)-C(1)	110(1)
C(7)-S(1)-C(8)	102.7(7)	S(4)-C(19)-C(18)	111(1)
C(9)-S(2)-C(10)	104.3(8)	S(4)-C(20)-C(21)	116(1)
C(11)-S(3)-C(12)	101.2(8)	S(5)-C(21)-C(20)	120(1)
C(19)-S(4)-C(20)	102.1(6)	S(5)-C(22)-C(23)	114(1)
C(21)-S(5)-C(22)	98.6(7)	S(6)-C(23)-C(22)	109(1)
C(23)-S(6)-C(24)	99.8(6)	S(6)-C(24)-C(13)	118(1)
C(14)-C(13)-C(18)	119(1)	C(14)-C(13)-C(24)	118(1)

C(18)-C(13)-C(24)	124(1)	C(13)-C(14)-C(15)	121(1)
C(14)-C(15)-C(16)	121(1)	C(15)-C(16)-C(17)	119(1)
C(2)-C(1)-C(6)	116(1)	C(16)-C(17)-C(18)	120(1)
C(2)-C(1)-C(12)	120(1)	C(13)-C(18)-C(17)	121(1)
C(6)-C(1)-C(12)	124(1)	C(13)-C(18)-C(19)	123(1)
C(1)-C(2)-C(3)	121(2)	C(17)-C(18)-C(19)	116(1)
C(2)-C(3)-C(4)	119(2)	C(3)-C(4)-C(5)	121(2)
C(4)-C(5)-C(6)	124(2)	C(1)-C(6)-C(5)	119(1)
C(1)-C(6)-C(7)	122(1)	C(5)-C(6)-C(7)	119(1)

Since the CF_3SO_3 anion is input as rigid CF_3 and SO_3 groups CF =1.33 Å, FCF = 109°, SO = 1.43 Å, OSO = 109°. The designations A and B represent pairs of 50/50 disordered atoms.[1]

Table A.2.13
Summary of Crystal Data, Intensity Collection, and Structure Refinement for [Ag(ODT[9]OC)$_2$][BF$_4$], (5)

formula	**$C_{24}H_{32}AgF_4BS_4O_2$**
fw	675.43
a, Å	16.354(5)
b, Å	13.056(5)
c, Å	13.345(4)
α, deg	
β, deg	101.88(2)
γ, deg	
cryst syst	monoclinic
space group	*Cc* (No. 15)
V, Å^3	2788(1)
ρ (calcd),g/cm^{-3}	1.610
Z	4
μ, cm^{-1}	4.13 (empirical)
avg trans factor	0.9207
diffractometer	Rigaku AFC6S
λ, Å	0.71069
T, °C	24
take-off angle	6.0
detect aper, mm	6.0 horz; 6.0 vert
cryst to detect, cm	40
scan type	ω-2θ
scan speed, deg/min	32.0 omega
scan width, deg	1.05 + 0.30 tanθ
data collected	2583
data $F_o^2 > 3\sigma(F_o^2)$	1501
variables	165
goodness of fit	1.75
$R(F_o)^a$, %	3.05
$R_w(F_o)^a$, %	3.88

$^a R = \Sigma||F_o|-|F_c||/\Sigma|F_o||$, $R_w = (\Sigma w(|F_o|-|F_c|)^2/\Sigma wF_o2)^{1/2}$ and $w = 1/\sigma^2(F)$

Table A.2.14
Positional parameters and B(eq) for $[Ag(ODT[9]OC)_2][BF_4]$, (5)

atom	x	y	z	B(eq)
Ag	1/2	0.19027(6)	3/4	3.18(3)
S(1)	0.5731(1)	0.3243(1)	0.3867(1)	3.15(8)
S(2)	0.6165(1)	0.0829(1)	0.6983(1)	3.71(8)
F(1)	0.4350(5)	0.3014(6)	0.2518(6)	20.5(7)
F(2)	0.4887(4)	0.1887(4)	0.1668(4)	10.7(4)
O(1)	0.6533(3)	0.1122(3)	0.9346(3)	4.0(2)
C(1)	0.6706(4)	0.2769(5)	0.6664(6)	4.0(3)
C(2)	0.6527(5)	0.2919(6)	0.5608(6)	5.7(4)
C(3)	0.6206(6)	0.3841(8)	0.5201(6)	6.8(5)
C(4)	0.6057(5)	0.4611(7)	0.5813(7)	5.9(5)
C(5)	0.6226(4)	0.4472(5)	0.6859(6)	4.3(4)
C(6)	0.6550(4)	0.3553(5)	0.7282(5)	3.3(3)
C(7)	0.6703(4)	0.3456(5)	0.8454(5)	4.5(3)
C(8)	0.6108(4)	0.2643(5)	1.0101(5)	4.1(3)
C(9)	0.6063(5)	0.1498(5)	1.0054(5)	4.4(4)
C(10)	0.6310(5)	0.0119(5)	0.8996(6)	4.9(4)
C(11)	0.6569(4)	-0.0079(5)	0.7990(6)	4.8(4)
C(12)	0.7024(4)	0.1733(6)	0.7055(6)	5.8(4)
B(1)	1/2	0.247(1)	1/4	7(1)

Table A.2.15
Summary of Bond Distances and Angles for $[Ag(ODT[9]OC)_2][BF_4]$, (5)

Distances (Å)

Ag-S(1)	2.630(2)	C(4)-C(5)	1.38(1)
Ag-S(1)	2.630(2)	Ag-S(2)	2.571(2)
C(5)-C(6)	1.384(8)	Ag-S(2)	2.571(2)
S(1)-C(7)	1.807(6)	C(6)-C(7)	1.538(8)
S(1)-C(8)	1.814(6)	S(2)-C(11)	1.812(7)
S(2)-C(12)	1.822(7)	C(8)-C(9)	1.497(9)
F(1)-B(1)	1.28(1)	F(2)-B(1)	1.33(1)
O(1)-C(9)	1.422(8)	O(1)-C(10)	1.412(8)
C(1)-C(2)	1.393(9)	C(10)-C(11)	1.511(9)
C(1)-C(6)	1.371(9)	C(1)-C(12)	1.503(9)
C(2)-C(3)	1.38(1)	C(3)-C(4)	1.35(1)

Nonbonded Distances

Ag...O1	3.294(4)Å

Angles (°)

S(1)-Ag-S(1)	96.59(7)	S(1)-Ag-S(2)	107.02(5)
S(1)-Ag-S(2)	115.62(5)	C(1)-C(6)-C(5)	120.3(7)
S(1)-Ag-S(2)	115.62(5)	C(1)-C(6)-C(7)	122.6(7)
S(1)-Ag-S(2)	107.02(5)	C(5)-C(6)-C(7)	117.1(7)
S(2)-Ag-S(2)	113.96(8)	S(1)-C(7)-C(6)	110.7(4)
Ag-S(1)-C(7)	101.2(2)	Ag-S(1)-C(8)	111.3(2)
C(7)-S(1)-C(8)	100.8(3)	Ag-S(2)-C(11)	109.6(2)
Ag-S(2)-C(12)	103.8(2)	C(11)-S(2)-C(12)	103.1(3)
S(1)-C(8)-C(9)	112.9(5)	C(9)-O(1)-C(10)	113.7(5)
C(2)-C(1)-C(6)	118.5(7)	C(2)-C(1)-C(12)	117.6(8)
C(6)-C(1)-C(12)	123.9(7)	C(1)-C(2)-C(3)	120.3(8)
O(1)-C(9)-C(8)	110.1(6)	C(2)-C(3)-C(4)	120.9(8)
C(3)-C(4)-C(5)	119.4(8)	O(1)-C(10)-C(11)	110.7(6)
C(4)-C(5)-C(6)	120.5(8)	S(2)-C(11)-C(10)	114.9(5)
S(2)-C(12)-C(1)	110.9(5)	F(1)-B(1)-F(1)	113(2)
F(1)-B(1)-F(2)	111.1(5)	F(1)-B(1)-F(2)	106.0(4)
F(1)-B(1)-F(2)	106.0(4)	F(1)-B(1)-F(2)	111.1(5)
F(2)-B(1)-F(2)	110(1)		

Table A.3.1
Summary of Crystal Data, Intensity Collection, and Structure Refinement for $\{[Ag(TT[9]OC)][BF_4]\}_4 \bullet 2CH_3CN$, (6)

formula	$C_{52}H_{70}S_{12}N_2Ag_4B_4F_{16}$
fw	1886.54
a, Å	14.525(7)
b, Å	16.703(11)
c, Å	16.250(6)
α, deg	
β, deg	115.54(3)
γ, deg	
cryst syst	monoclinic
space group	$P2_1/c$ (No. 14)
V, Å^3	3557(6)
ρ (calcd), g/cm^{-3}	1.761
Z	2
μ, cm^{-1}	15.12 (empirical)
avg trans factor	0.9416
diffractometer	Rigaku AFC6S
λ, Å	0.7107
T, °C	23.0
take off angle, deg	6.0
detect-aper, mm	6.0 horiz, 6.0 vert
cryst to detect, cm	40
scan type	ω-2θ
scan speed, deg/min	32.0 omega
scan width, deg	1.05 + 0.30 tanθ
data collected	6511
data, $F_o^2>3\sigma(F_o^2)$	2706
variables	407
goodness of fit	1.88
$R(F_o)^a$, %	3.30
$R_w(F_o)^a$, %	5.10

[a] $R = \Sigma||F_o|-|F_c||/\Sigma|F_o||$, $R_w = (\Sigma w(|F_o|-|F_c|)^2/\Sigma wF_o2)^{1/2}$ and $w = 1/\sigma^2(F)$

Table A.3.2
Positional Parameters for {[Ag(TT[9]OC)][BF_4]}$_\infty$ •2(CH3CN), (6)

Atom	x	y	z	B(eq)
Ag(1)	0.27891(6)	0.50352(6)	-0.16419(6)	4.69(4)
Ag(2)	0.49224(7)	0.69764(5)	0.01013(7)	5.03(4)
S(1)	0.2838(2)	0.5717(2)	-0.3044(2)	5.7(2)
S(2)	0.3242(2)	0.6460(2)	-0.0950(2)	4.5(1)
S(3)	0.1083(2)	0.5358(2)	-0.1556(2)	4.7(1)
S(4)	0.6137(3)	0.7642(2)	-0.0462(2)	5.5(2)
S(5)	0.6618(2)	0.6355(2)	0.1302(2)	4.3(1)
S(6)	0.5000(2)	0.7774(2)	0.1482(2)	4.9(2)
C(1)	0.0463(9)	0.4818(8)	-0.3335(8)	4.8(7)
C(2)	0.0092(9)	0.4033(10)	-0.3345(10)	6.5(8)
C(3)	0.029(1)	0.3465(11)	-0.386(1)	9(1)
C(4)	0.081(1)	0.364(1)	-0.4359(12)	10(1)
C(5)	0.1155(10)	0.4401(11)	-0.4313(10)	7.2(8)
C(6)	0.1018(9)	0.4983(9)	-0.3815(8)	5.0(6)
C(7)	0.1494(9)	0.5790(8)	-0.3812(8)	6.9(7)
C(8)	0.3199(10)	0.6723(8)	-0.2641(9)	7.0(8)
C(9)	0.2782(9)	0.7036(7)	-0.2003(8)	6.1(7)
C(10)	0.2256(9)	0.6636(7)	-0.0549(8)	5.8(7)
C(11)	0.1207(8)	0.6366(7)	-0.1179(8)	5.7(6)
C(12)	0.0224(8)	0.5441(8)	-0.2782(8)	6.7(8)
C(13)	0.4607(10)	0.8960(7)	0.0217(8)	4.3(6)
C(14)	0.3579(12)	0.9161(8)	-0.0149(10)	6.4(8)
C(15)	0.3039(11)	0.9302(9)	-0.106(1)	7.7(9)
C(16)	0.352(1)	0.9285(9)	-0.1613(10)	8(1)
C(17)	0.452(1)	0.9076(8)	-0.1287(11)	6.9(8)
C(18)	0.5079(10)	0.8917(7)	-0.0384(10)	4.8(6)
C(19)	0.6166(9)	0.8653(8)	-0.0062(8)	6.2(7)
C(20)	0.7332(9)	0.7183(9)	0.0244(10)	8.2(9)
C(21)	0.7556(9)	0.6970(9)	0.1183(9)	8.7(8)
C(22)	0.6618(10)	0.6749(8)	0.2355(8)	7.4(8)
C(23)	0.6249(10)	0.7543(8)	0.2331(8)	7.1(8)
C(24)	0.5153(10)	0.8799(7)	0.1225(9)	6.2(7)
F(1)	1.0307(6)	0.3382(6)	0.9428(7)	16.8(8)
F(2)	0.8853(8)	0.2845(6)	0.9094(7)	12.9(7)
F(3)	0.9799(6)	0.2436(5)	0.8452(6)	10.4(5)
F(4)	0.9027(8)	0.3575(6)	0.8150(6)	14.3(7)
F(5)	0.3984(10)	0.4409(9)	0.1701(8)	18(1)
F(6)	0.454(1)	0.5474(9)	0.1660(10)	23(1)
F(7)	0.4847(9)	0.4541(9)	0.1036(9)	20(1)
F(8)	0.3427(7)	0.4932(8)	0.0468(6)	15.0(7)

B(1)	0.955(1)	0.3056(11)	0.881(1)	6(1)
B(2)	0.423(2)	0.494(2)	0.1184(11)	12(2)
N(1)	0.1781(11)	0.1169(9)	0.7384(10)	10(1)
C(25)	0.1585(11)	0.0800(9)	0.6766(11)	7(1)
C(26)	0.1329(9)	0.0318(8)	0.5984(9)	7.1(8)

Table A.3.3
Summary of Bond Distances and Angles for $\{[Ag(TT[9]OC)][BF_4]\}_4 \bullet 2(CH_3CN)$, (6)

Distances (Å)

Ag(1)-S(1)	2.576(3)	Ag(1)-S(2)	2.593(3)
Ag(1)-S(3)	2.598(3)	Ag(1)-S(5)	2.456(3)
Ag(2)-S(2)	2.454(3)	Ag(2)-S(4)	2.566(3)
Ag(2)-S(5)	2.609(3)	Ag(2)-S(6)	2.570(3)
S(1)-C(7)	1.81(1)	S(1)-C(8)	1.80(1)
S(2)-C(9)	1.82(1)	S(2)-C(10)	1.83(1)
S(3)-C(11)	1.77(1)	S(3)-C(12)	1.84(1)
S(4)-C(19)	1.80(1)	S(4)-C(20)	1.79(1)
S(5)-C(21)	1.78(1)	S(5)-C(22)	1.83(1)
S(6)-C(23)	1.78(1)	S(6)-C(24)	1.80(1)
C(1)-C(2)	1.42(2)	C(1)-C(6)	1.37(2)
C(2)-C(3)	1.38(2)	C(3)-C(4)	1.36(2)
C(4)-C(5)	1.36(2)	C(5)-C(6)	1.33(2)
C(1)-C(12)	1.51(1)	C(6)-C(7)	1.51(2)
C(8)-C(9)	1.50(1)	C(10)-C(11)	1.49(1)
C(13)-C(24)	1.50(1)	C(18)-C(19)	1.50(1)
C(20)-C(21)	1.46(2)	C(22)-C(23)	1.43(2)
C(13)-C(14)	1.39(1)	C(13)-C(18)	1.42(1)
C(14)-C(15)	1.36(2)	C(15)-C(16)	1.36(2)
C(16)-C(17)	1.35(2)	C(17)-C(18)	1.36(2)
F(1)-B(1)	1.24(2)	F(2)-B(1)	1.33(2)
F(3)-B(1)	1.31(2)	F(4)-B(1)	1.34(2)
F(5)-B(2)	1.37(3)	F(6)-B(2)	1.14(3)
F(7)-B(2)	1.22(2)	F(8)-B(2)	1.24(2)
N(1)-C(25)	1.11(2)	C(25)-C(26)	1.41(2)

Angles (°)

S(1)-Ag(1)-S(2)	83.1(1)	S(1)-Ag(1)-S(3)	110.3(1)
S(1)-Ag(1)-S(5)	118.5(1)	S(2)-Ag(1)-S(3)	81.7(1)
S(2)-Ag(1)-S(5)	140.51(9)	S(3)-Ag(1)-S(5)	115.7(1)

S(2)-Ag(2)-S(4)	122.3(1)	S(2)-Ag(2)-S(5)	135.7(1)
S(2)-Ag(2)-S(6)	116.5(1)	S(4)-Ag(2)-S(5)	82.3(1)
S(4)-Ag(2)-S(6)	108.0(1)	S(5)-Ag(2)-S(6)	83.2(1)
C(7)-S(1)-C(8)	104.3(6)	Ag(1)-S(2)-Ag(2)	127.9(1)
C(9)-S(2)-C(10)	102.8(6)	C(11)-S(3)-C(12)	102.9(6)
C(19)-S(4)-C(20)	107.7(7)	Ag(1)-S(5)-Ag(2)	132.1(1)
C(21)-S(5)-C(22)	101.7(7)	C(23)-S(6)-C(24)	101.4(6)
S(1)-C(7)-C(6)	107.3(8)	S(1)-C(8)-C(9)	115.8(9)
S(2)-C(9)-C(8)	111.8(9)	S(2)-C(10)-C(11)	115.5(8)
S(3)-C(11)-C(10)	116.5(8)	S(3)-C(12)-C(1)	111.6(9)
S(4)-C(19)-C(18)	107.0(9)	S(4)-C(20)-C(21)	119.5(9)
S(5)-C(21)-C(20)	115(1)	S(5)-C(22)-C(23)	117.3(9)
S(6)-C(23)-C(22)	118(1)	S(6)-C(24)-C(13)	111.3(9)
Ag(1)-S(1)-C(7)	101.9(4)	Ag(1)-S(1)-C(8)	101.9(4)
Ag(1)-S(2)-C(9)	99.0(4)	Ag(1)-S(2)-C(10)	102.1(4)
Ag(2)-S(2)-C(9)	108.7(4)	Ag(2)-S(2)-C(10)	113.0(4)
Ag(1)-S(3)-C(11)	105.0(4)	Ag(1)-S(3)-C(12)	100.1(4)
Ag(2)-S(4)-C(19)	101.0(4)	Ag(2)-S(4)-C(20)	102.2(4)
Ag(1)-S(5)-C(21)	111.1(5)	Ag(1)-S(5)-C(22)	105.7(4)
Ag(2)-S(5)-C(21)	102.1(4)	Ag(2)-S(5)-C(22)	100.1(4)
Ag(2)-S(6)-C(23)	102.1(4)	Ag(2)-S(6)-C(24)	104.7(4)
C(2)-C(1)-C(6)	120(1)	C(2)-C(1)-C(12)	117(1)
C(6)-C(1)-C(12)	123(1)	C(1)-C(2)-C(3)	118(1)
C(2)-C(3)-C(4)	122(2)	C(3)-C(4)-C(5)	117(2)
C(4)-C(5)-C(6)	125(2)	C(1)-C(6)-C(5)	118(2)
C(1)-C(6)-C(7)	124(1)	C(5)-C(6)-C(7)	118(1)
C(14)-C(13)-C(18)	118(1)	C(14)-C(13)-C(24)	118(1)
C(18)-C(13)-C(24)	124(1)	C(13)-C(14)-C(15)	121(1)
C(14)-C(15)-C(16)	120(2)	C(15)-C(16)-C(17)	121(2)
C(16)-C(17)-C(18)	121(2)	C(13)-C(18)-C(17)	119(1)
C(13)-C(18)-C(19)	122(1)	C(17)-C(18)-C(19)	119(1)
F(1)-B(1)-F(2)	112(2)	F(1)-B(1)-F(3)	113(2)
F(1)-B(1)-F(4)	111(2)	F(2)-B(1)-F(3)	110(2)
F(2)-B(1)-F(4)	101(2)	F(3)-B(1)-F(4)	109(2)
F(5)-B(2)-F(6)	103(2)	F(5)-B(2)-F(7)	100(3)
F(5)-B(2)-F(8)	100(3)	F(6)-B(2)-F(7)	117(3)
F(6)-B(2)-F(8)	126(3)	F(7)-B(2)-F(8)	106(2)
N(1)-C(25)-C(26)	179(2)		

Table A.3.4
Summary of Crystal Data, Intensity Collection, and Structure Refinement for $\{[Ag(TT[9]OC)][CF_3SO_3]\}_4$, (7)

formula	$C_{52}H_{64}S_{16}O_{12}Ag_4B_4F_{12}$
fw	2053.60
a, Å	12.308(2)
b, Å	23.381(4)
c, Å	14.018(2)
α, deg	
β, deg	113.30(1)
γ, deg	
cryst syst	monoclinic
space group	$P2_1/c$ (No. 14)
V, Å^3	3705(1)
ρ (calcd), g/cm^{-3}	1.841
Z	2
μ, cm^{-1}	15.47 (empirical)
avg trans factor	0.9228
diffractometer	Rigaku AFC6S
λ, Å	0.7107
T, °C	23.0
take off angle, deg	6.0
detect-aper, mm	6.0 horiz, 6.0 vert
cryst-detect, cm	40
scan type	ω-2θ
scan speed, deg/min	32.0 omega
scan width, deg	1.05 + 0.30 tanθ
data collected	6732
data, $F_o^2>3\sigma(F_o^2)$	3295
variables	433
goodness of fit	2.37
$R(F_o)^a$, %	5.10
$R_w(F_o)^a$, %	5.80

[a] $R = \Sigma||F_o|-|F_c||/\Sigma|F_o||$, $R_w = (\Sigma w(|F_o|-|F_c|)^2/\Sigma wF_o2)^{1/2}$ and $w = 1/\sigma^2(F)$

Table A.3.5
Positional Parameters for $\{[Ag(TT[9]OC)][CF_3SO_3]\}_4$, (7)

Atom	x	y	z	B(eq)
Ag(1)	0.37210(8)	-0.13372(4)	0.43821(8)	4.61(5)
Ag(2)	0.26165(9)	0.05706(4)	0.36550(8)	4.54(5)
S(1)	0.3152(3)	-0.1607(1)	0.2443(2)	4.3(2)
S(2)	0.2287(3)	-0.0480(1)	0.3588(3)	4.3(1)
S(3)	0.2066(3)	-0.1689(2)	0.4911(3)	5.6(2)
S(4)	0.2565(3)	0.1161(1)	0.2103(3)	4.8(2)
S(5)	0.4103(3)	0.1357(1)	0.4727(3)	4.3(1)
S(6)	0.1275(3)	0.1073(1)	0.4478(3)	4.6(2)
C(1)	0.227(1)	-0.2673(6)	0.392(1)	4.8(7)
C(2)	0.286(2)	-0.3076(8)	0.465(1)	7(1)
C(3)	0.370(2)	-0.3428(8)	0.455(2)	10(1)
C(4)	0.397(2)	-0.3360(8)	0.370(2)	11(1)
C(5)	0.338(2)	-0.2981(7)	0.296(1)	7.1(9)
C(6)	0.256(1)	-0.2609(6)	0.305(1)	4.5(6)
C(7)	0.204(1)	-0.2139(6)	0.225(1)	5.6(7)
C(8)	0.232(1)	-0.0980(7)	0.180(1)	7.1(9)
C(9)	0.159(1)	-0.0682(7)	0.226(1)	9(1)
C(10)	0.113(1)	-0.0650(7)	0.404(2)	9(1)
C(11)	0.098(2)	-0.112(1)	0.438(2)	18(2)
C(12)	0.137(1)	-0.2286(7)	0.408(1)	6.8(8)
C(13)	-0.023(1)	0.1086(5)	0.246(1)	4.3(6)
C(14)	-0.107(1)	0.0661(8)	0.233(1)	7(1)
C(15)	-0.145(1)	0.0298(8)	0.151(2)	8(1)
C(16)	-0.100(1)	0.0333(6)	0.078(1)	6.4(8)
C(17)	-0.018(1)	0.0745(6)	0.083(1)	5.1(7)
C(18)	0.022(1)	0.1120(5)	0.167(1)	4.0(6)
C(19)	0.116(1)	0.1541(6)	0.1716(9)	5.0(6)
C(20)	0.364(1)	0.1708(7)	0.273(1)	6.5(8)
C(21)	0.369(1)	0.1929(5)	0.376(1)	5.8(7)
C(22)	0.347(1)	0.1584(5)	0.564(1)	5.4(7)
C(23)	0.215(1)	0.1653(6)	0.525(1)	5.9(7)
C(24)	0.017(1)	0.1468(5)	0.339(1)	4.9(6)
S(7)	0.1583(3)	0.1775(2)	0.8901(4)	6.0(2)
S(8)	0.5677(4)	0.0109(2)	0.3434(3)	5.7(2)
F(1)	0.341(1)	0.1672(5)	0.846(1)	12.4(8)
F(2)	0.3166(8)	0.0995(4)	0.9346(9)	10.8(6)
F(3)	0.195(1)	0.1082(5)	0.7702(8)	12.5(7)
F(4)	0.610(1)	0.0187(5)	0.1782(9)	13.1(8)
F(5)	0.430(1)	0.0210(5)	0.1502(7)	10.9(7)
F(6)	0.5241(9)	-0.0568(5)	0.1878(8)	10.6(6)
O(1)	0.243(1)	0.2029(4)	0.9906(8)	9.6(6)

O(2)	0.1153(8)	0.2177(4)	0.8096(8)	7.7(5)
O(3)	0.0779(8)	0.1380(5)	0.8996(8)	9.2(6)
O(4)	0.573(1)	0.0712(4)	0.3518(8)	9.6(7)
O(5)	0.678(1)	-0.0161(5)	0.3917(9)	11.0(7)
O(6)	0.473(1)	-0.0162(5)	0.3560(8)	10.6(8)
C(25)	0.264(2)	0.1355(9)	0.861(2)	9(1)
C(26)	0.535(1)	0.0002(8)	0.207(1)	7(1)

Table A.3.6
Summary of Bond Distances and Angles for $\{[Ag(TT[9]OC)][CF_3SO_3]\}_4$, (7)

Distances (Å)

Ag(1)-S(3)	2.564(4)	Ag(1)-S(1)	2.602(3)
Ag(1)-S(2)	2.611(3)	Ag(1)-S(5)	2.468(3)
Ag(2)-S(2)	2.485(3)	Ag(2)-S(4)	2.556(3)
Ag(2)-S(5)	2.609(3)	Ag(2)-S(6)	2.635(3)
S(1)-C(7)	1.79(1)	S(1)-C(8)	1.81(1)
S(2)-C(9)	1.78(1)	S(2)-C(10)	1.81(1)
S(3)-C(11)	1.82(2)	S(3)-C(12)	1.81(1)
S(4)-C(19)	1.82(1)	S(4)-C(20)	1.80(2)
S(5)-C(21)	1.83(1)	S(5)-C(22)	1.83(1)
S(6)-C(23)	1.80(1)	S(6)-C(24)	1.84(1)
C(1)-C(12)	1.50(2)	C(6)-C(7)	1.51(2)
C(8)-C(9)	1.47(2)	C(10)-C(11)	1.24(2)
C(13)-C(24)	1.50(2)	C(18)-C(19)	1.51(2)
C(20)-C(21)	1.52(2)	C(22)-C(23)	1.50(2)
S(7)-O(1)	1.50(1)	S(7)-O(2)	1.402(9)
S(7)-O(3)	1.398(9)	S(7)-C(25)	1.80(2)
S(8)-O(4)	1.41(1)	S(8)-O(5)	1.40(1)
S(8)-O(6)	1.39(1)	S(8)-C(26)	1.81(2)
F(1)-C(25)	1.29(2)	F(2)-C(25)	1.29(2)
F(3)-C(25)	1.37(2)	F(4)-C(26)	1.23(2)
F(5)-C(26)	1.31(2)	F(6)-C(26)	1.36(2)
C(1)-C(2)	1.37(2)	C(1)-C(6)	1.42(2)
C(2)-C(3)	1.38(2)	C(3)-C(4)	1.37(2)
C(4)-C(5)	1.34(2)	C(5)-C(6)	1.37(2)
C(13)-C(14)	1.40(2)	C(13)-C(18)	1.41(2)
C(14)-C(15)	1.35(2)	C(15)-C(16)	1.36(2)
C(16)-C(17)	1.38(2)	C(17)-C(18)	1.39(2)

Angles (°)

S(1)-Ag(1)-S(2)	83.3(1)	S(1)-Ag(1)-S(5)	108.3(1)

S(1)-Ag(1)-S(3)	108.0(1)	S(2)-Ag(1)-S(3)	83.6(1)
S(2)-Ag(1)-S(5)	130.2(1)	S(3)-Ag(1)-S(5)	132.5(1)
S(2)-Ag(2)-S(4)	123.5(1)	S(2)-Ag(2)-S(5)	141.7(1)
S(2)-Ag(2)-S(6)	109.6(1)	S(3)-Ag(2)-S(5)	83.4(1)
S(4)-Ag(2)-S(6)	108.9(1)	S(5)-Ag(2)-S(6)	81.5(1)
C(7)-S(1)-C(8)	103.8(7)	C(9)-S(2)-C(10)	100.9(9)
C(11)-S(3)-C(12)	102(1)	C(19)-S(4)-C(20)	102.9(6)
C(21)-S(5)-C(22)	103.7(6)	C(23)-S(6)-C(24)	100.9(6)
S(1)-C(7)-C(6)	108.3(9)	S(1)-C(8)-C(9)	119(1)
S(2)-C(9)-C(8)	117(1)	S(2)-C(10)-C(11)	126(1)
S(3)-C(11)-C(10)	127(2)	S(3)-C(12)-C(1)	112.1(9)
S(3)-C(19)-C(18)	108.6(9)	S(5)-C(20)-C(21)	117(1)
S(5)-C(21)-C(20)	111(1)	S(5)-C(22)-C(23)	118.3(9)
S(5)-C(23)-C(22)	116.2(9)	S(6)-C(24)-C(13)	107.6(8)
Ag(1)-S(1)-C(7)	101.4(4)	Ag(1)-S(1)-C(8)	101.0(5)
Ag(1)-S(2)-C(9)	102.0(5)	Ag(1)-S(2)-C(10)	100.0(5)
Ag(2)-S(2)-C(10)	110.0(6)	Ag(2)-S(2)-C(9)	107.8(6)
Ag(1)-S(3)-C(11)	100.8(6)	Ag(1)-S(3)-C(12)	106.5(4)
Ag(2)-S(4)-C(19)	102.6(4)	Ag(2)-S(4)-C(20)	101.8(5)
Ag(1)-S(5)-C(21)	108.6(4)	Ag(1)-S(5)-C(22)	109.3(4)
Ag(2)-S(5)-C(21)	99.3(4)	Ag(2)-S(5)-C(22)	102.2(4)
Ag(2)-S(6)-C(23)	105.6(4)	Ag(2)-S(6)-C(24)	104.4(4)
O(1)-S(7)-O(2)	112.9(7)	O(1)-S(7)-O(3)	115.3(7)
O(1)-S(7)-C(25)	97.7(8)	O(2)-S(7)-O(3)	117.6(6)
O(2)-S(7)-C(25)	104.9(8)	O(3)-S(7)-C(25)	105.2(8)
O(4)-S(8)-O(5)	114.0(7)	O(4-)S(8)-O(6)	117.0(8)
O(4)-S(8)-C(26)	102.1(8)	O(5)-S(8)-O(6)	115.4(8)
O(5)-S(8)-C(26)	102.5(8)	O(6)-S(8)-C(26)	102.7(7)
C(2)-C(1)-C(6)	118(1)	C(2-)C(1)-C(12)	121(2)
C(6)-C(1)-C(12)	121(1)	C(1)-C(2)-C(3)	122(2)
C(2)-C(3)-C(4)	118(2)	C(3)-C(4)-C(5)	120(2)
C(4)-C(5)-C(6)	123(2)	C(1)-C(6)-C(5)	117(1)
C(1)-C(6)-C(7)	122(1)	C(5)-C(6)-C(7)	121(1)
C(14)-C(13)-C(18)	116(1)	C(14)-C(13)-C(24)	120(1)
C(18)-C(13)-C(24)	124(1)	C(13)-C(14)-C(15)	122(2)
C(14)-C(15)-C(16)	120(2)	C(15)-C(16)-C(17)	121(2)
C(16)-C(17)-C(18)	120(1)	C(13)-C(18)-C(17)	121(1)
C(13)-C(18)-C(19)	122(1)	C(17)-C(18)-C(19)	117(1)
S(7)-C(25)-F(1)	112(1)	S(7)-C(25)-F(2)	111(2)
S(7)-C(25)-F(3)	103(1)	F(1)-C(25)-F(2)	110(2)
F(1)-C(25)-F(3)	110(2)	F(2)-C(25)-F(3)	112(2)
S(8)-C(26)-F(4)	115(1)	S(8)-C(26)-F(5)	110(1)
S(8)-C(26)-F(6)	108(1)	F(4)-C(26)-F(5)	111(2)
F(4)-C(26)-F(6)	108(1)	F(5)-C(26)-F(6)	104(1)

Table A.3.7
Summary of Crystal Data, Intensity Collection, and Structure Refinement for {[Ag(Me$_2$TT[9]OC)][BF$_4$]}$_4$ •2(CH$_3$CN), (8)

formula	**$C_{60}H_{86}S_{12}N_2Ag_4B_4F_{16}$**
fw	1998.90
a, Å	14.878(8)
b, Å	17.356(7)
c, Å	16.804(12)
α, deg	
β, deg	114.95(4)
γ, deg	
cryst syst	monoclinic
space group	$P2_1/c$ (No.14)
V, Å^3	3934(4)
ρ (calcd), g/cm^{-3}	1.688
Z	2
μ, cm^{-1}	13.77 (empirical)
avg trans factor	0.9613
diffractometer	Rigaku AFC6S
λ, Å	0.7107
T, °C	23.0
take off angle, deg	6.0
detect-aper, mm	6.0 horiz, 6.0 vert
cryst to detect, cm	40
scan type	ω–2θ
speed, deg/min	32.0 omega
scan width, deg	1.05 + 0.30 tanθ
data collected	7183
data, $F_o^2>3\sigma(F_o^2)$	2907
variables	435
goodness of fit	1.55
$R(F_o)^a$, %	3.64
$R_w(F_o)^a$, %	5.22

$^a R = \Sigma||F_o|-|F_c||/\Sigma|F_o||$, $R_w = (\Sigma w(|F_o|-|F_c|)^2/\Sigma wF_o2)^{1/2}$ and $w = 1/\sigma^2(F)$

Table A.3.8.
Positional Parameters for $\{[Ag(Me_2TT[9]OC)][BF_4]\}_4 \bullet 2(CH_3CN)$, (8)

Atom	x	y	z	B(eq)
Ag(1)	-0.21144(7)	0.02094(5)	-0.15923(6)	4.33(4)
Ag(2)	0.00767(7)	0.18794(6)	0.03697(6)	4.27(4)
S(1)	-0.2071(2)	0.1084(2)	-0.2823(2)	4.5(2)
S(2)	-0.1596(2)	0.1495(2)	-0.0683(2)	3.9(1)
S(3)	-0.3728(2)	0.0445(2)	-0.1362(2)	4.3(1)
S(4)	0.0076(2)	0.2532(2)	0.1773(2)	4.6(2)
S(5)	0.1612(2)	0.1157(2)	0.1538(2)	3.8(1)
S(6)	0.1390(2)	0.2519(2)	-0.0018(2)	4.5(2)
C(1)	-0.4396(8)	0.0151(8)	-0.3138(7)	3.8(5)
C(2)	-0.4760(8)	-0.0590(9)	-0.3261(8)	4.8(7)
C(3)	-0.4582(9)	-0.1116(7)	-0.3809(8)	4.1(6)
C(4)	-0.4055(8)	-0.0869(8)	-0.4277(7)	4.0(6)
C(5)	-0.3732(8)	-0.0121(8)	-0.4169(7)	4.4(6)
C(6)	-0.3869(8)	0.0412(7)	-0.3601(8)	3.9(6)
C(7)	-0.498(1)	-0.1930(8)	-0.3891(8)	7.1(8)
C(8)	-0.3848(9)	-0.1395(8)	-0.4882(8)	6.4(7)
C(9)	-0.3405(9)	0.1197(7)	-0.3499(7)	4.7(6)
C(10)	-0.1696(8)	0.2009(7)	-0.2283(7)	4.9(6)
C(11)	-0.2052(8)	0.2186(6)	-0.1568(8)	4.7(6)
C(12)	-0.2484(8)	0.1572(7)	-0.0216(7)	5.0(6)
C(13)	-0.3555(8)	0.1380(7)	-0.0845(7)	4.9(6)
C(14)	-0.4602(7)	0.0662(7)	-0.2493(8)	5.2(6)
C(15)	0.0444(9)	0.3765(7)	0.0193(8)	4.3(6)
C(16)	-0.001(1)	0.3992(7)	-0.068(1)	5.1(7)
C(17)	-0.099(1)	0.4224(7)	-0.1076(8)	4.5(6)
C(18)	-0.156(1)	0.4214(7)	-0.060(1)	4.8(6)
C(19)	-0.1082(9)	0.4010(7)	0.0284(9)	4.6(6)
C(20)	-0.011(1)	0.3785(7)	0.0684(8)	4.1(6)
C(21)	-0.263(1)	0.4441(8)	-0.0990(8)	7.3(8)
C(22)	-0.147(1)	0.4448(8)	-0.2039(9)	7.2(8)
C(23)	0.0321(9)	0.3541(7)	0.1640(8)	5.2(6)
C(24)	0.124(1)	0.2203(8)	0.2646(8)	6.8(8)
C(25)	0.151(1)	0.1396(8)	0.2548(7)	5.6(7)
C(26)	0.2614(8)	0.1773(7)	0.1576(8)	5.7(7)
C(27)	0.2507(8)	0.2011(7)	0.0673(8)	5.3(7)
C(28)	0.1481(9)	0.3452(7)	0.0515(7)	4.9(6)
F(1a)a	0.577(3)	0.199(2)	0.083(2)	10.0(8)
F(2a)	0.517(2)	0.241(1)	0.172(2)	6.2(6)
F(3a)	0.486(2)	0.122(2)	0.131(2)	9.7(7)
F(4a)	0.628(2)	0.159(2)	0.218(2)	14(1)
F(1b)	0.488(1)	0.176(1)	0.067(1)	12.8(6)

F(2b)	0.568(2)	0.220(1)	0.208(1)	11.0(6)
F(3b)	0.570(1)	0.1007(8)	0.171(1)	8.4(4)
F(4b)	0.642(1)	0.191(1)	0.127(1)	9.8(5)
F(5a)	0.936(2)	0.045(1)	0.135(1)	9.7(6)
F(6a)	0.850(1)	-0.030(1)	0.026(1)	9.3(5)
F(7a)	0.863(1)	-0.075(1)	0.143(1)	8.1(4)
F(8a)	0.988(2)	-0.077(2)	0.108(2)	13.0(7)
F(5b)	0.952(2)	-0.033(1)	0.043(2)	11.7(7)
F(6b)	0.949(3)	-0.098(2)	0.144(2)	15(1)
F(7b)	0.985(2)	-0.005(1)	0.182(1)	10.7(7)
F(8b)	0.841(2)	-0.005(2)	0.086(2)	16(1)
B(1)	0.553(4)	0.180(2)	0.141(2)	21(3)
B(2)	0.925(3)	-0.022(3)	0.110(2)	21(3)
N(1)	0.319(1)	0.1396(8)	0.7830(8)	8.6(8)
C(29)	0.344(1)	0.099(1)	0.841(1)	6.2(9)
C(30)	0.372(1)	0.048(1)	0.913(1)	9(1)

[a] F atoms designated a and b indicate models for a two-fold disorder about the central boron atom in each BF_4^- anion. Site occupancy a:b is 62:38 for F1-F4 and 53:47 for F5-F8.

Table A.3.9
Summary of Bond Distances and Angles for $\{[Ag(Me_2TT[9]OC)][BF_4]\}_4 \cdot 2(CH_3CN)$, (8)

Distances (Å)

Ag(1)-S(1)	2.588(3)	Ag(1)-S(2)	2.629(3)
Ag(1)-S(3)	2.619(3)	Ag(1)-S(5)	2.477(3)
Ag(2)-S(2)	2.461(3)	Ag(2)-S(4)	2.616(3)
Ag(2)-S(5)	2.620(3)	Ag(2)-S(6)	2.559(3)
S(1)-C(9)	1.83(1)	S(1)-C(10)	1.81(1)
S(2)-C(11)	1.81(1)	S(2)-C(12)	1.80(1)
S(3)-C(13)	1.81(1)	S(3)-C(14)	1.83(1)
S(4)-C(23)	1.82(1)	S(4)-C(24)	1.82(1)
S(5)-C(25)	1.82(1)	S(5)-C(26)	1.81(1)
S(6)-C(27)	1.81(1)	S(6)-C(28)	1.83(1)
C(1)-C(14)	1.53(1)	C(3)-C(7)	1.52(2)
C(4)-C(8)	1.49(1)	C(6)-C(9)	1.50(1)
C(10)-C(11)	1.54(1)	C(12)-C(13)	1.53(1)
C(15)-C(20)	1.39(1)	C(15)-C(28)	1.51(1)
C(15)-C(16)	1.39(1)	C(16)-C(17)	1.38(1)
C(17)-C(18)	1.39(2)	C(17)-C(22)	1.52(2)
C(18)-C(19)	1.40(1)	C(18)-C(21)	1.50(1)
C(19)-C(20)	1.37(1)	C(20)-C(23)	1.52(1)
C(24)-C(25)	1.48(2)	C(26)-C(27)	1.51(1)
C(1)-C(2)	1.38(2)	C(1)-C(6)	1.39(1)
C(2)-C(3)	1.40(2)	C(3)-C(4)	1.39(2)
C(4)-C(5)	1.37(2)	C(5)-C(6)	1.40(2)
C(15)-C(16)	1.39(1)	C(15)-C(20)	1.39(1)
C(16)-C(17)	1.38(1)	C(17)-C(18)	1.39(2)
C(18)-C(19)	1.40(1)	C(19)-C(20)	1.37(1)
F(1a)-B(1)	1.22(3)	F(2a)-B(1)	1.38(5)
F(3a)-B(1)	1.36(3)	F(4a)-B(1)	1.35(5)
F(1b)-B(1)	1.21(4)	F(2b)-B(1)	1.26(3)
F(3b)-B(1)	1.45(4)	F(4b)-B(1)	1.45(4)
F(5a)-B(2)	1.22(5)	F(6a)-B(2)	1.39(4)
F(7a)-B(2)	1.56(5)	F(8a)-B(2)	1.34(4)
F(5b)-B(2)	1.37(3)	F(6b)-B(2)	1.41(5)
F(7b)-B(2)	1.19(4)	F(8b)-B(2)	1.18(4)
N(1)-C(29)	1.13(2)	C(29)-C(30)	1.42(2)

Angles (°)

S(1)-Ag(1)-S(2)	82.3(1)	S(1)-Ag(1)-S(3)	111.1(1)
S(1)-Ag(1)-S(5)	118.8(1)	S(2)-Ag(1)-S(3)	81.0(1)

S(2)-Ag(1)-S(5)	141.4(1)	S(3)-Ag(1)-S(5)	115.1(1)
S(2)-Ag(2)-S(4)	112.4(1)	S(2)-Ag(2)-S(5)	135.0(1)
S(2)-Ag(2)-S(6)	125.7(1)	S(4)-Ag(2)-S(5)	82.1(1)
S(4)-Ag(2)-S(6)	109.4(1)	S(5)-Ag(2)-S(6)	83.1(1)
C(9)-S(1)-C(10)	103.9(5)	Ag(1)-S(2)-Ag(2)	127.4(1)
C(11)-S(2)-C(12)	102.7(6)	C(13)-S(3)-C(14)	102.0(6)
C(23)-S(4)-C(24)	103.2(6)	Ag(1)-S(5)-Ag(2)	129.8(1)
C(25)-S(5)-C(26)	103.1(6)	C(27)-S(6)-C(28)	105.0(6)
S(1)-C(9)-C(6)	107.3(9)	S(1)-C(10)-C(11)	115.7(8)
S(2)-C(11)-C(10)	112.2(9)	S(2)-C(12)-C(13)	115.0(7)
S(3)-C(13)-C(12)	115.0(8)	S(3)-C(14)-C(1)	110.4(8)
S(4)-C(23)-C(20)	112.4(8)	S(4)-C(24)-C(25)	114(1)
S(5)-C(25)-C(24)	116.9(9)	S(5)-C(26)-C(27)	112.9(8)
S(6)-C(27)-C(26)	117.3(9)	S(6)-C(28)-C(15)	107.0(8)
Ag(1)-S(1)-C(9)	100.0(4)	Ag(1)-S(1)-C(10)	103.1(4)
Ag(1)-S(2)-C(11)	99.7(4)	Ag(1)-S(2)-C(12)	103.1(4)
Ag(2)-S(2)-C(11)	109.0(4)	Ag(2)-S(2)-C(12)	111.8(4)
Ag(1)-S(3)-C(13)	104.9(4)	Ag(1)-S(3)-C(14)	99.9(4)
Ag(2)-S(4)-C(23)	103.3(4)	Ag(2)-S(4)-C(24)	103.2(4)
Ag(1)-S(5)-C(25)	109.2(4)	Ag(1)-S(5)-C(26)	109.4(4)
Ag(2)-S(5)-C(25)	101.5(4)	Ag(2)-S(5)-C(26)	100.9(4)
Ag(2)-S(6)-C(27)	102.6(4)	Ag(2)-S(6)-C(28)	99.6(4)
C(2)-C(1)-C(6)	120(1)	C(2)-C(1)-C(14)	118(1)
C(6)-C(1)-C(14)	122(1)	C(1)-C(2)-C(3)	122(1)
C(2)-C(3)-C(4)	119(1)	C(2)-C(3)-C(7)	120(1)
C(4)-C(3)-C(7)	122(1)	C(3)-C(4)-C(5)	118(1)
C(3)-C(4)-C(8)	122(1)	C(5)-C(4)-C(8)	121(1)
C(4)-C(5)-C(6)	125(1)	C(1)-C(6)-C(5)	116(1)
C(1)-C(6)-C(9)	125(1)	C(5)-C(6)-C(9)	119(1)
C(16)-C(15)-C(20)	118(1)	C(16)-C(15)-C(28)	117(1)
C(20)-C(15)-C(28)	125(1)	C(15)-C(16)-C(17)	123(1)
C(16)-C(17)-C(18)	120(1)	C(16)-C(17)-C(22)	121(1)
C(18)-C(17)-C(22)	119(1)	C(17)-C(18)-C(19)	117(1)
C(17)-C(18)-C(21)	123(1)	C(19)-C(18)-C(21)	120(1)
C(18)-C(19)-C(20)	124(1)	C(15)-C(20)-C(19)	119(1)
C(15)-C(20)-C(23)	122(1)	C(19)-C(20)-C(23)	119(1)
N(19)-C(29)-C(30)	178(2)	F(1a)-B(1)-F(2a)	113(4)
F(1a)-B(1)-F(3a)	122(3)	F(1a)-B(1)-F(4a)	116(5)
F(2a)-B(1)-F(3a)	103(4)	F(2a)-B(1)-F(4a)	98(2)
F(3a)-B(1)-F(4a)	101(3)	F(1b)-B(1)-F(2b)	135(6)
F(1b)-B(1)-F(3b)	105(2)	F(1b)-B(1)-F(4b)	103(2)
F(2b)-B(1)-F(3b)	106(3)	F(2b)-B(1)-F(4b)	103(3)
F(3b)-B(1)-F(4b)	98(4)	F(5a)-B(2)-F(6a)	112(3)
F(5a)-B(2)-F(7a)	117(2)	F(5a)-B(2)-F(8a)	134(5)
F(6a)-B(2)-F(7a)	88(3)	F(6a)-B(2)-F(8a)	100(3)

F(7a)-B(2)-F(8a)	97(4)	F(5b)-B(2)-F(6b)	96(3)
F(5b)-B(2)-F(7b)	121(4)	F(5b)-B(2)-F(8b)	113(3
F(6b)-B(2)-F(7b)	82(2)	F(6b)-B(2)-F(8b)	115(5)
F(7b)-B(2)-F(8b)	121(4)		

Table A.3.10
Summary of Crystal Data, Intensity Collection, and Structure Refinement for $\{[Ag(TT[9]MC)][CF_3SO_3]\bullet CH_3CN\}_x$, (9)

formula	$C_{15}H_{19}S_4O_3NAgF_3$
fw	554.42
a, Å	11.218(2)
b, Å	11.317(3)
c, Å	17.035(7)
α, deg	
β, deg	104.17(2)
γ, deg	
cryst syst	monoclinic
space group	$P2_1/c$ (No.14)
V, Å^3	2097(2)
ρ (calcd), g/cm^{-3}	1.756
Z	4
μ, cm^{-1}	13.75 (empirical)
avg trans factor	0.9057
diffractometer	Rigaku AFC6S
λ, Å	0.7107
T, °C	23.0
take off angle, deg	6.0
detect-aper, mm	6.0 horiz, 6.0 vert
cryst to detect, cm	40
scan type	ω-2θ
scan speed, deg/min	32.0 omega
scan width, deg	1.05 + 0.30 tanθ
data collected	3906
data, $F_o^2>3\sigma(F_o^2)$	1261
variables	245
goodness of fit	1.68
$R(F_o)^a$, %	4.11
$R_w(F_o)^a$, %	5.69

$^a R = \Sigma||F_o|-|F_c||/\Sigma|F_o||$, $R_w = (\Sigma w(|F_o|-|F_c|)^2/\Sigma wF_o2)^{1/2}$ and $w = 1/\sigma^2(F)$

Table A.3.11.
Positional Parameters for {[Ag(TT[9]MC)][CF_3SO_3]•CH_3CN}$_x$, (9)

Atom	x	y	z	B(eq)
Ag(1)	0.1017(1)	0.0135(1)	0.18348(7)	4.52(7)
S(1)	0.1412(4)	-0.1998(4)	0.1499(3)	4.1(2)
S(2)	-0.0760(4)	-0.2084(4)	-0.1084(3)	3.8(2)
S(3)	0.1299(4)	-0.5221(4)	-0.1631(2)	3.8(2)
C(1)	0.302(1)	-0.337(1)	0.007(1)	3.8(9)
C(2)	0.303(2)	-0.445(2)	-0.028(1)	5(1)
C(3)	0.315(2)	-0.543(2)	0.019(1)	8(1)
C(4)	0.325(2)	-0.533(2)	0.104(1)	9(1)
C(5)	0.322(2)	-0.424(2)	0.139(1)	6(1)
C(6)	0.306(1)	-0.323(1)	0.089(1)	3.5(8)
C(7)	0.290(1)	-0.205(1)	0.1246(9)	3.9(8)
C(8)	0.038(1)	-0.250(1)	0.0593(9)	3.9(8)
C(9)	0.024(2)	-0.164(1)	-0.013(1)	3.9(9)
C(10)	0.020(1)	-0.298(1)	-0.1554(8)	3.0(7)
C(11)	0.028(1)	-0.426(1)	-0.1265(9)	4.0(8)
C(12)	0.280(1)	-0.458(1)	-0.1185(9)	4.1(8)
S(4)	0.2288(5)	0.0285(6)	0.8815(4)	6.1(3)
F(1)	0.323(1)	0.233(1)	0.875(1)	14(1)
F(2)	0.445(1)	0.114(1)	0.911(1)	13(1)
F(3)	0.362(2)	0.115(1)	0.7962(8)	15(1)
O(1)	0.126(1)	0.067(1)	0.833(1)	14(1)
O(2)	0.236(2)	0.049(2)	0.963(1)	16(2)
O(3)	0.270(2)	-0.081(1)	0.870(2)	16(2)
C(13)	0.340(2)	0.125(2)	0.860(2)	7(1)
N(1)	0.359(2)	0.061(2)	0.219(1)	9(1)
C(14)	0.401(2)	0.105(2)	0.179(1)	6(1)
C(15)	0.452(2)	0.168(2)	0.122(2)	11(2)

Table A.3.12
Summary of Bond Distances and Angles for
{[Ag(TT[9]MC)][CF_3SO_3]•CH_3CN}$_x$, (9)

Distances (Å)

Ag-S(1)	2.545(5)	Ag-S(2)	2.530(5)
Ag-S(3)	2.556(4)	S(1)-C(7)	1.82(1)
S(1)-C(8)	1.78(2)	S(2)-C(9)	1.81(2)
S(2)-C(10)	1.80(1)	S(3)-C(11)	1.80(1)
S(3)-C(12)	1.82(2)	C(2)-C(12)	1.51(2)
C(6)-C(7)	1.49(2)	C(8)-C(9)	1.55(2)
C(10)-C(11)	1.53(2)	C(1)-C(2)	1.37(2)
C(1)-C(6)	1.39(2)	C(2)-C(3)	1.35(2)
C(3)-C(4)	1.42(2)	C(4)-C(5)	1.38(2)
C(5)-C(6)	1.41(2)	S(4)-O((1)	1.32(1)
S(4)-O(2)	1.39(2)	S(4)-O(3)	1.35(2)
S(4)-C(13)	1.76(2)	F(1)-C(13)	1.27(2)
F(2)-C(13)	1.29(2)	F(3)-C(13)	1.18(3)
N(1)-C(14)	1.04(2)	C(14)-C(15)	1.43(3)

Angles (°)

S(1)-Ag-S(2)	135.9(1)	S(1)-Ag-S(3)	106.3(2)
S(2)-Ag-S(3)	117.0(2)	C(7)-S(1)-C(8)	102.9(7)
C(9)-S(2)-C(10)	104.5(7)	C(11)-S(3)-C(12)	102.5(7)
S(1)-C(7)-C(6)	110(1)	S(1)-C(8)-C(9)	114(1)
S(2)-C(9)-C(8)	117(1)	S(2)-C(10)-C(11)	113(1)
S(3)-C(11)-C(10)	117(1)	S(3)-C(12)-C(2)	112(1)
Ag-S(1)-C(7)	107.6(5)	Ag-S(1)-C(8)	112.8(5)
Ag-S(2)-C(9)	100.3(5)	Ag-S(2-)C(10)	105.7(5)
Ag-S(3)-C(11)	113.7(5)	Ag-S(3)-C(12)	106.4(5)
C(2)-C(1)-C(6)	123(2)	C(1)-C(2)-C(3)	119(2)
C(1)-C(2)-C(12)	121(2)	C(3)-C(2)-C(12)	120(2)
C(2)-C(3)-C(4)	121(2)	C(3)-C(4)-C(5)	120(2)
C(4)-C(5)-C(6)	119(2)	C(1)-C(6)-C(5)	118(2)
C(1)-C(6)-C(7)	122(2)	C(5)-C(6)-C(7)	119(2)
O(1)-S(4)-O(2)	114(1)	O(1)-S(4)-O(3)	119(1)
O(1)-S(4)-C(13)	103(1)	O(2)-S(4)-O(3)	111(1)
O(2)-S(4)-C(13)	103(1)	O(3)-S(4)-C(13)	104(1)
S94)-C(13)-F(1)	114(2)	S(4)-C(13)-F(2)	112(2)
S(4)-C(13)-F(3)	117(2)	F(1)-C(13)-F(2)	97(2)
F(1)-C(13)-F(3)	110(2)	F(2)-C(13)-F(3)	105(3)
N(1)-C(14)-C(15)	177(3)		

Table A.4.1
Summary of Crystal Data, Intensity Collection, and Structure Refinement for [Rh(COD)(TT[9]OC)][BF_4], (10)

formula	**$C_{20}H_{28}BF_4RhS_3$**
fw	554.30
a, Å	23.951(4)
b, Å	8.845(2)
c, Å	10.463(8)
α, deg	
β, deg	
γ, deg	
cryst syst	orthorhombic
space group	$Pca2_1$ (No. 29)
V, Å^3	2217(1)
ρ, g/cm^{-3}	1.661
Z	4
μ, cm^{-1}	10.669 (empirical)
avg trans factor	0.9533
diffractometer	Rigaku AFC6S
λ, Å	0.71069
T, °C	24
take-off angle, deg	6.0
detect aper, mm	6.0 hor; 6.0 vert
cryst to detect, cm	40
scan type	ω-2θ
scan speed, deg/min	32.0 omega
scan width, deg	1.05 + 0.30 tanθ
data collected	2277
data $F_o^2 > 3\sigma(F_o^2)$	1192
variables	161
goodness of fit	1.72
$R(F_o)^a$, %	5.26
$R_w(F_o)^a$, %	5.70

[a] $R = \Sigma||F_o|-|F_c||/\Sigma|F_o||$, $R_w = (\Sigma w(|F_o|-|F_c|)^2/\Sigma wF_o2)^{1/2}$ and $w = 1/\sigma^2(F)$

Table A.4.2
Positional parameters and B(eq) for [Rh(COD)(TT[9]OC)][BF_4], (10)

atom	x	y	z	B(eq)
Rh	0.09959(04)	0.2439(01)	0.0001	3.37(4)
S(1)	0.1974(02)	0.1746(05)	0.0024(08)	4.0(2)
S(2)	0.0816(02)	0.0121(06)	0.0216(06)	5.1(3)
S(3)	0.0797(02)	0.2588(07)	0.2337(05)	4.7(2)
F(1)	0.3335(09)	0.053(02)	0.166(02)	15(2)
F(2)	0.4153(07)	0.006(03)	0.069(02)	13(1)
F(3)	0.3816(10)	0.221(02)	0.088(04)	28(4)
F(4)	0.3456(11)	0.056(03)	0.022(03)	19(2)
C(1)	0.1800(07)	0.384(02)	0.291(02)	3.7(4)
C(2)	0.1722(08)	0.535(02)	0.338(02)	4.9(4)
C(3)	0.2055(09)	0.648(03)	0.296(02)	6.7(5)
C(4)	0.2448(10)	0.623(02)	0.212(02)	6.4(5)
C(5)	0.2518(10)	0.482(02)	0.160(02)	6.1(5)
C(6)	0.2216(06)	0.361(02)	0.199(02)	3.7(4)
C(7)	0.2346(09)	0.211(02)	0.151(02)	7.2(6)
C(8)	0.1950(09)	0.030(02)	0.004(03)	8.4(6)
C(9)	0.1437(11)	0.105(03)	0.024(03)	9.2(7)
C(10)	0.0725(12)	0.043(03)	0.196(03)	9.5(8)
C(11)	0.0497(09)	0.076(03)	0.265(02)	6.7(6)
C(12)	0.1434(09)	0.261(02)	0.337(02)	6.7(5)
C(13)	0.1289(08)	0.456(02)	0.094(02)	5.0(4)
C(14)	0.0961(07)	0.489(02)	0.014(03)	4.8(4)
C(15)	0.0339(09)	0.534(02)	0.005(03)	7.5(5)
C(16)	0.0046(09)	0.431(02)	0.057(02)	5.4(5)
C(17)	0.0198(07)	0.275(02)	0.083(02)	4.2(4)
C(18)	0.0556(08)	0.227(02)	0.173(02)	4.6(4)
C(19)	0.0824(11)	0.332(03)	0.271(03)	7.6(7)
C(20)	0.1063(10)	0.459(03)	0.235(03)	7.4(6)
B(1)	0.376(02)	0.108(04)	0.079(05)	12(3)

Table A.4.3
Summary of Bond Distances and Angles for [Rh(COD)(TT[9]OC)][BF_4], (10)

Distances(Å)

Rh-S(1)	2.422(4)	C(1)-C(6)	1.40(2)
Rh-S(2)	2.316(5)	C(1)-C(12)	1.47(2)
Rh-S(3)	2.494(5)	C(2)-C(3)	1.36(3)
Rh-C(13)	2.23(2)	C(3)-C(4)	1.30(3)
Rh-C(14)	2.18(2)	C(4)-C(5)	1.37(2)
Rh-C(17)	2.12(2)	C(5)-C(6)	1.36(2)
Rh-C(18)	2.10(2)	C(6)-C(7)	1.45(2)
S(1)-C(7)	1.86(2)	C(8)-C(9)	1.41(3)
S(1)-C(8)	1.81(2)	C(10)-C(11)	1.39(3)
S(2)-C(9)	1.76(2)	C(13)-C(14)	1.41(3)
S(2)-C(10)	1.86(3)	C(13)-C(20)	1.57(3)
S(3)-C(11)	1.80(2)	C(14)-C(15)	1.54(2)
S(3)-C(12)	1.87(2)	C(15)-C(16)	1.45(3)
F(1)-B(1)	1.44(5)	C(16)-C(17)	1.53(2)
F(2)-B(1)	1.32(4)	C(17)- C(18)	1.34(2)
F(3)-B(1)	1.01(3)	C(18)-C(19)	1.52(3)
F(4)-B(1)	1.36(5)	C(19)-C(20)	1.31(3)
C(1)-C(2)	1.43(2)		

Angles (°)

S(1)-Rh-S(2)	86.2(2)	C(9)-S(2)-C(10)	107(1)
S(1)-Rh-S(3)	102.0(2)	Rh-S(3)-C(11)	101.8(8)
S(1)-Rh-C(13)	84.5(5)	Rh-S(3)-C(12)	114.2(7)
S(1)-Rh-C(14)	106.9(4)	C(11) S(3)-C(12)	104(1)
S(1)-Rh-C(17)	154.4(5)	C(2)-C(1)-C(6)	118(2)
S(1)-Rh-C(18)	117.3(6)	C(2)-C(1)-C(12)	120(2)
S(2)-Rh-S(3)	85.5(2)	C(6)-C(1)-C(12)	123(2)
S(2)-Rh-C(13)	157.3(5)	C(1)-C(2)-C(3)	120(2)
S(2)-Rh-C(14)	164.0(6)	C(2)-C(3)-C(4)	121(2)
S(2)-Rh-C(17)	89.9(5)	C(3)-C(4)-C(5)	121(2)
S(2)-Rh-C(18)	85.5(5)	C(4)-C(5)-C(6)	122(2)
S(3)-Rh-C(13)	116.7(5)	C(1)-C(6)-C(5)	118(2)
S(3)-Rh-C(14)	82.8(7)	C(1)-C(6)-C(7)	122(2)
S(3)-Rh-C(17)	102.9(5)	C(5)-C(6)-C(7)	120(2)
S(3)-Rh-C(18)	138.9(6)	S(1)-C(7)-C(6)	111(1)
C(13)-Rh-C(14)	37.2(8)	S(1)-C(8)-C(9)	120(2)
C(13)-Rh-C(17)	89.6(7)	S(2)-C(9)-C(8)	118(2)
C(13)-Rh-C(18)	80.5(7)	S(2)-C(10)-C(11)	116(2)
C(14)-Rh-C(17)	82.1(7)	S(3)-C(11)-C(10)	116(2)

C(14)-Rh-C(18)	96.1(8)	S(3)-C(12)-C(1)	108(1)
C(17)-Rh-C(18)	37.1(6)	Rh-C(13)-C(14)	69(1)
Rh-S(1)-C(7)	114.2(7)	Rh-C(13)-C(20)	109(1)
Rh-S(1)-C(8)	102.8(7)	C(14)-C(13)-C(20)	124(2)
C(7)- S(1)-C(8)	101(1)	Rh-C(14)-C(13)	73(1)
Rh-S(2)-C(9)	105.7(8)	Rh-C(14)-C(15)	107(1)
Rh-S(2)-C(10)	105.1(9)	C(13)-C(14)-C(15)	123(2)
C(14)-C(15)-C(16)	118(2)	C(15)-C(16)-C(17)	114(2)
Rh-C(17)-C(16)	113(1)	Rh-C(17)-C(18)	71(1)
C(16)-C(17)-C(18)	131(2)	Rh-C(18)-C(17)	72(1)
Rh-C(18)-C(19)	109(1)	C(17)-C(18)-C(19)	123(2)
C(18)-C(19)-C(20)	121(3)	C(13)-C(20)-C(19)	114(2)
F(1)-B(1)-F(2)	109(4)	F(1)-B(1)-F(3)	112(4)
F(1)-B(1)-F(4)	90(3)	F(2)-B(1)-F(3)	126(4)
F(2)-B(1)-F(4)	95(2)	F(3)-B(1)-F(4)	119(7)

Table A.4.4 Summary of Crystal Data, Intensity Collection, and Structure Refinement for [Ir(COD)(TT[9]OC)][BF_4], (11)

formula	**$C_{20}H_{28}BF_4IrS_3$**
fw	643.61
a, Å	11.085(6)
b, Å	12.649(2)
c, Å	7.965(2)
α, deg	103.10(1)
β, deg	93.93(3)
γ, deg	89.45(2)
cryst syst	triclinic
space group	*P*$\bar{1}$ (No. 2)
V, Å^3	1085.2(5)
ρ, g/cm^{-3}	1.970
Z	2
μ, cm^{-1}	64.459 (empirical)
avg trans factor	0.8393
diffractometer	Rigaku AFC6S
λ, Å	0.71069
T, °C	24
take-off angle	6.0
detect aper, mm	6.0 horiz, 6.0 vert
cryst todetect, cm	40
scan type	w/2θ
speed, deg/min	32.0 omega
scan width, deg	1.05 + 0.30 tanθ
data collected	3823
data, $F_o^2>3\sigma(F_o^2)$	2935
variables	263
goodness of fit	1.49
$R(F_o)$, %	4.06
$R_w(F_o)$, %	4.41

[a] $R = \Sigma||F_o|-|F_c||/\Sigma|F_o||$, $R_w = (\Sigma w(|F_o|-|F_c|)^2/\Sigma wF_o2)^{1/2}$ and $w = 1/\sigma^2(F)$

Table A.4.5
Positional parameters and B(eq) for [Ir(COD)(TT[9]OC)][BF_4], (11)

atom	x	y	z	B(eq)
Ir	0.21548(4)	0.36124(3)	0.20559(5)	3.16(2)
S(1)	0.3260(3)	0.2750(2)	0.4143(3)	4.1(1)
S(2)	0.0405(3)	0.3059(2)	0.3050(4)	5.1(1)
S(3)	0.1831(2)	0.2096(2)	0.0309(3)	3.4(1)
C(1)	0.404(1)	0.1245(7)	0.011(1)	3.8(4)
C(2)	0.459(1)	0.1246(9)	0.142(1)	5.2(5)
C(3)	0.576(1)	0.157(1)	0.132(2)	6.5(7)
C(4)	0.642(1)	0.190(1)	0.022(2)	6.5(7)
C(5)	0.590(1)	0.1874(9)	0.174(2)	4.9(5)
C(6)	0.4685(9)	0.1548(7)	0.171(1)	3.9(4)
C(7)	0.416(1)	0.1527(8)	0.336(1)	4.7(5)
C(8)	0.206(1)	0.214(1)	0.507(1)	6.1(6)
C(9)	0.089(1)	0.278(1)	0.513(2)	7.2(7)
C(10)	0.008(1)	0.172(1)	0.174(2)	5.7(6)
C(11)	0.032(1)	0.1634(8)	0.008(2)	5.1(5)
C(12)	0.272(1)	0.0915(7)	0.004(1)	4.3(4)
C(13)	0.193(1)	0.5170(8)	0.367(2)	6.1(6)
C(14)	0.131(1)	0.5120(8)	0.205(2)	5.4(5)
C(15)	0.172(1)	0.574(1)	0.077(2)	7.5(7)
C(16)	0.253(2)	0.508(1)	0.039(2)	8.4(9)
C(17)	0.320(2)	0.423(1)	0.027(2)	7.4(8)
C(18)	0.388(1)	0.439(1)	0.178(2)	7.7(8)
C(19)	0.403(2)	0.550(1)	0.298(3)	9(1)
C(20)	0.311(2)	0.577(1)	0.429(2)	11(1)
F(1)	0.8387(6)	0.0469(7)	0.6782(9)	7.3(4)
F(2)	0.8711(8)	0.0277(7)	0.398(1)	8.8(5)
F(3)	0.6881(7)	0.0518(7)	0.485(1)	8.3(4)
F(4)	0.822(1)	0.1865(7)	0.555(2)	13.3(7)
B(1)	0.808(1)	0.080(1)	0.531(2)	4.7(6)

Table A.4.6
Summary of Bond Distances and Angles for [Ir(COD)(TT[9]OC)][BF_4], (11)

Distances (Å)

Ir-S(1)	2.444(3)	Ir-S(2)	2.317(3)
C(8)-C(9)	1.52(2)	Ir-S(3)	2.375(2)
Ir-C(13)	2.12(1)	Ir-C(14)	2.12(1)
Ir-C(17)	2.17(1)	Ir-C(18)	2.20(1)
C(10)-C(11)	1.48(2)	S(1)-C(7)	1.84(1)
S(1)-C(8)	1.82(1)	S(2)-C(9)	1.81(1)
S(2)-C(10)	1.80(1)	S(3)-C(11)	1.81(1)
S(3)-C(12)	1.83(1)	C(1)-C(2)	1.40(1)
C(13)-C(14)	1.41(2)	C(1)-C(6)	1.40(1)
C(13)-C(20)	1.51(2)	C(1)-C(12)	1.51(1)
C(2)-C(3)	1.36(2)	C(14)-C(15)	1.52(2)
C(3)-C(4)	1.37(2)	C(15)-C(16)	1.45(2)
C(4)-C(5)	1.39(2)	C(16)-C(17)	1.48(2)
C(5)-C(6)	1.41(1)	C(6)-C(7)	1.48(1)
C(17)-C(18)	1.35(2)	C(18)-C(19)	1.51(2)
C(19)-C(20)	1.49(3)	F(1) -B(1)	1.35(1)
F(2) -B(1)	1.36(1)	F(3) -B(1)	1.38(1)
F(4) -B(1)	1.32(2)		

Angles (°)

S(1)-Ir-S(2)	86.7(1)	C(9)-S(2)-C(10)	102.3(6)
S(1)-Ir-S(3)	100.33(8)	Ir-S(3)-C(11)	103.9(4)
S(1)-Ir-C(13)	98.7(3)	Ir-S(3)-C(12)	112.9(3)
S(1)-Ir-C(14)	137.5(3)	C(11)-S(3)-C(12)	100.7(5)
S(1)-Ir-C(17)	117.6(5)	C(2)-C(1)-C(6)	120(1)
S(1)-Ir-C(18)	87.1(4)	C(2)-C(1)-C(12)	118(1)
S(2)-Ir-S(3)	85.8(1)	C(6)-C(1)-C(12)	121.7(9)
S(2)-Ir-C(13)	88.6(4)	C(1)-C(2)-C(3)	119(1)
S(2)-Ir-C(14)	88.1(4)	S(2)-Ir-C(17)	154.9(5)
S(2)-R-C(18)	165.5(5)	C(2)-C(3)-C(4)	122(1)
S(3)-Ir-C(13)	159.8(4)	S(3)-Ir-C(14)	121.3(3)
S(3)-Ir-C(17)	83.6(4)	C(3)-C(4)-C(5)	119(1)
S(3)-Ir-C(18)	108.2(5)	C(13)-Ir-C(14)	39.0(4)
C(13)-Ir-C(17)	93.6(5)	C(4)-C(5)-C(6)	121(1)
C(13)-Ir-C(18)	79.4(6)	C(14)-Ir-C(17)	78.3(6)
C(14)-Ir-C(18)	87.7(4)	C(1)-C(6)-C(5)	118(1)
C(17)-Ir-C(18)	36.0(5)	C(1)-C(6)-C(7)	123(1)
Ir-S(1)-C(7)	119.3(3)	C(5)-C(6)-C7)	119(1)
Ir-S(1)-C(8)	103.0(4)	S(1)-C(7)-C(6)	111.9(7)

C(7)-S(1)-C(8)	99.4(6)	Ir-S(2)-C(9)	104.3(5)
Ir-S(2)-C(10)	105.5(4)	S(3)-C(12)-C(1)	107.1(6)
S(1)-C(8)-C(9)	113.1(9)	Ir-C(13)-C(14)	70.5(6)
Ir-C(13)-C(20)	114(1)	S(2)-C(9)-C(8)	112.5(8)
C(14)-C(13)-C(20)	125(1)	Ir-C(14)-C(13)	70.5(6)
Ir-C(14)-C(15)	116.7(9)	S(2)-C(10)-C(11)	112.2(8)
C(13)-C(14)-C(15)	122(1)	C(14)-C(15)-C(16)	111(1)
S(3)-C(11)-C(10)	112.1(8)	C(15)-C(16)-C(17)	116(1)
F(1)-B(1)-F(2)	112(1)	F(1)-B(1)-F(3)	107(1)
Ir-C(17)-C(16)	111(1)	F(1) -B(1)-F(4)	111(1)
Ir-C(17)-C(18)	73.4(9)	F(2) -B(1)-F(3)	106(1)
F(2)-B(1)-F(4)	111(1)	C(16)-C(17)-C(18)	125(1)
F(3) -B(1)-F(4)	110(1)	Ir-C(18)-C(17)	70.6(9)
Ir-C(18)-C(19)	112(1)	C(17)-C(18)-C(19)	122(1)
C(18)-C(19)-C(20)	115(1)	C(13)-C(20)-C(19)	112(1)

Table A.4.7 Summary of Crystal Data, Intensity Collection, and Structure Refinement for [Rh(COD)(ODT[9]OC)][BF_4], (12)

formula	**$C_{20}H_{28}BF_4ORhS_2$**
fw	538.24
a, Å	9.173(2)
b, Å	24.173(6)
c, Å	9.907(3)
α, deg	
β, deg	94.14(3)
γ, deg	
cryst syst	monoclinic
space group	$P2_1/c$ (No. 14)
V, Å^3	2190(2)
ρ (calcd) g/cm^{-3}	1.632
Z	4
μ, cm^{-1}	9.914 (empirical)
avg trans factor	0.9879
diffractometer	Rigaku AFC6S
λ, Å	0.71069
T, °C	24
take-off angle, deg	6.0
detect-aper, mm	6.0 horiz, 6.0 vert
cryst to detect, cm	40
scan type	ω-2θ
speed, deg/min	32.0 omega
scan width, deg	1.05 + 0.30 tanθ
data collected	4233
data, $F_o^2>3\sigma(F_o^2)$	2312
variables	263
goodness of fit	1.85
$R(F_o)$, %	5.84
$R_w(F_o)$, %	6.87

* $R = \Sigma||F_o|-|F_c||/\Sigma|F_o||$, $R_w = (\Sigma w(|F_o|-|F_c|)^2/\Sigma wF_o2)^{1/2}$ and $w = 1/\sigma^2(F)$

Table A.4.8
Positional parameters and B(eq) for [Rh(COD)(ODT[9]OC)][BF_4], (12)

atom	x	y	z	B(eq)
Rh	0.12433(9)	0.09525(3)	0.26957(8)	2.73(3)
S(1)	0.1281(3)	0.0728(1)	0.2593(3)	3.9(1)
S(2)	0.1168(3)	0.1854(1)	0.1606(3)	3.3(1)
O(1)	0.0455(9)	0.0790(3)	0.0029(8)	4.5(4)
C(1)	0.075(1)	0.2129(5)	0.350(1)	3.7(5)
C(2)	0.012(1)	0.2420(5)	0.457(1)	4.7(6)
C(3)	0.042(2)	0.2312(6)	0.589(1)	6.0(8)
C(4)	0.139(2)	0.1925(6)	0.612(1)	5.4(7)
C(5)	0.206(1)	0.1606(5)	0.509(1)	4.8(6)
C(6)	0.174(1)	0.1701(4)	0.376(1)	3.1(5)
C(7)	0.242(1)	0.1343(5)	0.264(1)	4.4(6)
C(8)	0.174(1)	0.0463(5)	0.091(2)	5.8(7)
C(9)	0.109(1)	0.0773(6)	0.019(1)	5.9(8)
C(10)	0.113(1)	0.1213(6)	0.071(1)	5.5(7)
C(11)	0.081(1)	0.1797(6)	0.022(1)	5.1(7)
C(12)	0.038(1)	0.2278(5)	0.207(1)	4.5(6)
C(13)	0.398(1)	0.0313(6)	0.245(1)	5.8(7)
C(14)	0.354(1)	0.0915(6)	0.243(1)	4.7(6)
C(15)	0.340(1)	0.1222(4)	0.353(1)	3.4(5)
C(16)	0.375(2)	0.1032(6)	0.498(1)	6.2(8)
C(17)	0.244(2)	0.0810(7)	0.559(1)	6.8(9)
C(18)	0.135(1)	0.0529(5)	0.458(1)	4.6(6)
C(19)	0.166(1)	0.0165(5)	0.358(1)	4.3(6)
C(20)	0.318(1)	0.0049(5)	0.338(1)	5.6(7)
F(1)	0.528(1)	0.1080(5)	0.964(1)	13.1(9)
F(2)	0.653(1)	0.1856(5)	0.952(1)	14(1)
F(3)	0.581(2)	0.1434(6)	0.784(1)	16(1)
F(4)	0.422(1)	0.1841(5)	0.890(2)	17(1)
B(1)	0.538(2)	0.1544(8)	0.902(2)	5.2(9)

Table A.4.9
Summary of Bond Distances and Angles for [Rh(COD)(ODT[9]OC)][BF_4], (12)

Distances (Å)

Rh-S(1)	2.373(3)	C(8)-C(9)	1.48(2)
Rh-S(2)	2.431(3)	Rh-C(14)	2.15(1)
Rh-C(15)	2.19(1)	Rh-C(18)	2.12(1)
Rh-C(19)	2.12(1)	C(10)-C(11)	1.53(2)
S(1)-C(7)	1.82(1)	S(1)-C(8)	1.80(1)
S(2)-C(11)	1.82(1)	S(2)-C(12)	1.84(1)
O(1)-C(9)	1.42(1)	O(1)-C(10)	1.42(2)
C(1)-C(2)	1.37(1)	C(13)-C(14)	1.51(2)
C(1)-C(6)	1.41(1)	C(13)-C(20)	1.50(2)
C(1)-C(12)	1.52(2)	C(2)-C(3)	1.37(2)
C(14)-C(15)	1.34(2)	C(3)-C(4)	1.33(2)
C(15)-C(16)	1.52(2)	C(4)-C(5)	1.39(2)
C(16)-C(17)	1.49(2)	C(5)-C(6)	1.38(2)
C(6)-C(7)	1.50(1)	C(17)-C(18)	1.53(2)
C(18-C(19)	1.37(2)	C(19)-C(20)	1.51(2)
F(1)-B(1)	1.29(2)	F(2)-B(1)	1.36(2)
F(3)-B(1)	1.29(2)	F(4)-B(1)	1.28(2)

Angles (°)

S(1)-Rh-S(2)	100.9(1)	S(1)-Rh-C(14)	161.7(4)
S(1)-Rh-C(15)	159.5(3)	C(2-C(3)-C(4)	119(1)
S(1)-Rh-C(18)	84.8(3)	S(1)-Rh-C(19)	87.7(3)
S(2)-Rh-C(14)	88.8(3)	C(3)-C(4)-C(5)	122(1)
S(2)-Rh-C(15)	84.1(3)	S(2)-Rh-C(18)	145.1(4)
S(2)-Rh-C(19)	170.9(3)	C(4)-C(5)-C(6)	120(1)
C(1)-Rh-C(15)	36.0(4)	C(14)-Rh-C(18)	96.1(5)
C(14)-Rh-C(19)	82.1(5)	C(1)-C(6)-C(5)	119(1)
C(15)-Rh-C(18)	80.1(4)	C(1)-C(6)-C(7)	121(1)
C(15)-Rh-C(19)	88.8(4)	C(5)-C(6)-C(7)	120(1)
C(18)-Rh-C(19)	37.8(4)	S(1)-C(7)-C(6)	106.4(7)
Rh-S(1)-C(7)	111.9(4)	Rh-S(1)-C(8)	106.4(4)
C(7)-S(1)-C(8)	102.7(6)	Rh-S(2-C(11)	111.8(5)
Rh-S(2)-C(12)	112.7(4)	C(11)-S(2-C(12)	101.9(6)
S(1)-C(8)-C(9)	114.7(9)	C(9)-O(1)-C(10)	114(1)
C(2)-C(1)-C(6)	118(1)	C(2)-C(1)-C(12)	119(1)
C(6)-C(1)-C(12)	123(1)	C(1)-C(2)-C(3)	122(1)
O(1)-C(9)-C(8)	111(1)	Rh-C(14)-C(13)	107.3(8)
Rh-C(14)-C(15)	73.6(7)	O(1)-C(10)-C(11)	113.7(9)
C(13)-C(14)-C(15)	124(1)	Rh-C(15)-C(14)	70.5(6)

Rh)-C(15)-C(16)	113.2(7)	S(2)-C(11)-C(10)	111.2(9)
C(14)-C(15)-C(16)	125(1)	C(15)-C(16)-C(17)	112(1)
S(2)-C(12)-C(1)	109.5(7)	C(14)-C(13)-C(20)	116(1)
Rh-C(18)-C(17)	110.4(8)	Rh-C(18)-C(19)	70.8(7)
C(17)-C(18)-C(19)	127(1)	Rh-C(19)-C(18)	71.4(7)
Rh-C(19)-C(20)	113.4(8)	C(18-C(19)-C(20)	124(1)
C(13-C(20)-C(19)	112(1)	F(1)-B(1)-F(2)	112(2)
F(1)-B(1)-F(3)	107(2)	F(1)-B(1)- F(4)	117(1)
F(2)-B(1)-F(3)	99(1)	F(2)-B(1)-F(4)	110(2)
F(3)-B(1)-F(4)	110(2)		

Table A.4.10 Summary of Crystal Data, Intensity Collection, and Structure Refinement for [Ir(COD)(ODT[9]OC)][BF_4], (13)

formula	**$C_{20}H_{28}BF_4IrOS_2$**
fw	627.55
a, Å	9.677(3)
b, Å	13.142(6)
c, Å	8.996(2)
α, deg	107.48(3)
β, deg	92.87(3)
γ, deg	97.46(3)
cryst syst	triclinic
space group	*P*$\bar{1}$ (No. 2)
V, Å^3	1077.2(7)
ρ (calcd) g/cm^{-3}	1.930
Z	2
μ, cm^{-1}	64.510 (empirical)
avg trans factor	0.8173
diffractometer	Rigaku AFC6S
λ, Å	0.71069
T, °C	24
take-off angle, deg	6.0
detect aper, mm	6.0 horiz, 6.0 vert
cryst to detect, cm	40
scan type	ω-2θ
scan speed, deg/min	32.0 omega
scan width, deg	1.05 + 0.30 tanθ
data collected	4047
data, $F_o^2>3\sigma(F_o^2)$	3802
variables	262
goodness of fit	2.95
$R(F_o)$, %	7.38
$R_w(F_o)$, %	6.59

[a] $R = \Sigma||F_o|-|F_c||/\Sigma|F_o||$, $R_w = (\Sigma w(|F_o|-|F_c|)^2/\Sigma wF_o2)^{1/2}$ and $w = 1/\sigma^2(F)$

Table A.4.11
Positional parameters and B(eq) for [Ir(COD)(ODT[9]OC)][BF_4], (13)

atom	x	y	z	B(eq)
Ir	0.29059(9)	0.18521(7)	0.22036(9)	2.37(2)
S(1)	0.2161(5)	0.3592(4)	0.3161(6)	3.5(2)
S(2)	0.2943(6)	0.1666(5)	0.0472(6)	3.7(2)
F(1)	1.186(2)	0.725(2)	0.271(2)	12(1)
F(2)	0.984(2)	0.754(2)	0.357(2)	12(1)
F(3)	1.002(2)	0.614(2)	0.154(2)	10(1)
F(4)	1.075(3)	0.619(2)	0.389(2)	12(1)
O(1)	0.027(2)	0.156(1)	0.128(2)	4.3(6)
C(1)	0.440(2)	0.365(2)	0.024(2)	3.9(9)
C(2)	0.572(3)	0.347(2)	0.021(2)	5(1)
C(3)	0.696(2)	0.407(2)	0.080(3)	4(1)
C(4)	0.683(2)	0.475(2)	0.220(3)	5(1)
C(5)	0.548(3)	0.492(2)	0.271(2)	5(1)
C(6)	0.427(2)	0.430(2)	0.164(3)	4(1)
C(7)	0.291(2)	0.454(2)	0.217(2)	4.0(9)
C(8)	0.027(2)	0.346(2)	0.267(3)	5(1)
C(9)	0.042(3)	0.229(2)	0.233(3)	6(1)
C(10)	0.015(3)	0.165(2)	0.023(3)	7(1)
C(11)	0.116(3)	0.103(2)	0.125(2)	7(1)
C(12)	0.320(2)	0.297(2)	0.085(2)	4.1(9)
C(13)	0.486(2)	0.136(2)	0.203(3)	5(1)
C(14)	0.383(3)	0.051(2)	0.172(3)	5(1)
C(15)	0.359(3)	0.028(2)	0.275(3)	6(1)
C(16)	0.250(2)	0.018(2)	0.390(3)	4(1)
C(17)	0.245(2)	0.135(2)	0.420(2)	3.9(9)
C(18)	0.358(2)	0.222(2)	0.470(2)	5(1)
C(19)	0.510(2)	0.196(2)	0.485(3)	7(1)
C(20)	0.587(3)	0.181(3)	0.355(3)	10(1)
B(1)	1.060(4)	0.676(4)	0.298(4)	7(2)

Table A.4.12
Summary of Bond Distances and Angles for [Ir(COD)(ODT[9]OC)][BF_4], (13)

Distances (Å)

Ir-S(1)	2.407(6)	Ir-S(2)	2.348(5)
C(6)-C(7)	1.47(3)	Ir-C(13)	2.08(2)
Ir-C(14)	2.02(3)	Ir-C(17)	2.14(2)
C(8)-C(9)	1.54(3)	Ir-C(18)	2.20(2)
S(1)-C(7)	1.84(2)	S(1)-C(8)	1.84(2)
S(2)-C(11)	1.82(2)	S(2)-C(12)	1.83(2)
C(10)-C(11)	1.53(4)	F(1)-B(1)	1.36(4)
F(2)-B(1)	1.33(4)	F(3)-B(1)	1.36(4)
F(4)-B(1)	1.28(3)	O(1)-C(9)	1.40(3)
O(1)-C(10)	1.40(2)	C(1)-C(2)	1.39(3)
C(13)-C(14)	1.35(3)	C(1)-C(6)	1.31(3)
C(13)-C(20)	1.55(3)	C(1)-C(12)	1.49(3)
C(2)-C(3)	1.45(3)	C(14)-C(15)	1.59(3)
C(3)-C(4)	1.33(3)	C(15)-C(16)	1.56(3)
C(4)-C(5)	1.43(3)	C(16)-C(17)	1.48(3)
C(5)-C(6)	1.46(3)	C(17)-C(18)	1.42(3)
C(18)-C(19)	1.56(3)	C(19)-C(20)	1.40(3)

Angles (°)

S(1)-Ir-S(2)	100.8(2)	S(1)-Ir(1)-C(13)	133.1(7)
S(1)-Ir-C(14)	169.3(7)	C(2)-C(3)-C(4)	120(2)
S(1)-Ir-C(17)	96.2(6)	S(1)-Ir-C(18)	81.4(7)
S(2)-Ir-C(13)	85.0(6)	C(3)-C(4)-C(5)	121(2)
S(2)-Ir-C(14)	85.7(6)	S(2)-Ir-C(17)	156.0(6)
S(2)-Ir-C(18)	161.7(6)	C(4)-C(5)-C(6)	117(2)
C(13)-Ir-C(14)	38.4(9)	C(13)-Ir-C(17)	95.5(8)
C(13)-Ir-C(18)	80.5(9)	C(1)-C(6)-C(5)	122(2)
C(14)-Ir-C(17)	80.1(9)	C(1)-C(6)-C(7)	122(2)
C(14)-Ir-C(18)	89.8(9)	C(5)-C(6)-C(7)	115(2)
C(17)-Ir-C(18)	38.2(8)	S(1)-C(7)-C(6)	111(2)
Ir-S(1)-C(7)	112.7(7)	Ir-S(1)-C(8)	109.8(8)
C(7)-S(1)-C(8)	103(1)	Ir-S(2)-C(11)	102.4(7)
Ir-S(2)-C(12)	112.7(7)	C(11)-S(2)-C(12)	107(1)
S(1)-C(8)-C(9)	110(2)	C(9)-O(1)-C(10)	113(2)
C(2)-C(1)-C(6)	120(2)	C(2)-C(1)-C(12)	116(2)
C(6)-C(1)-C(12)	124(2)	C(1)-C(2)-C(3)	120(2)
O(1)-C(9)-C(8)	113(2)	C(14)-C(13)-C(20)	125(2)
Ir-C(14)-C(13)	73(2)	Ir-C(14)-C(15)	120(2)

O(1)-C(10)-C(11)	111(2)	C(13)-C(14)-C(15)	125(2)
C(14)-C(15)-C(16)	106(2)	S(2)-C(11)-C(10)	108(2)
C(15)-C(16)-C(17)	115(2)	S(2)-C(12)-C(1)	107(1)
Ir-C(17)-C(16)	112(1)	Ir-C(17)-C(18)	73(1)
Ir-C(13)-C(14)	69(2)	Ir-C(13)-C(20)	115(2)
C(16)-C(17)-C(18)	128(2)	Ir-C(18)-C(17)	69(1)
Ir-C(18)-C(19)	108(1)	C(17)-C(18)-C(19)	119(2)
C(18)-C(19)-C(20)	119(2)	C(13)-C(20)-C(19)	109(2)
F(1)-B(1)-F(2)	107(4)	F(1)-B(1)F(3)	104(2)
F(1)-B(1)-F(4)	112(3)	F(2)-B(1)F(3)	110(3)
F(2)-B(1)-F(4)	112(3)	F(3)-B(1)F(4)	111(4)

Table A.4.13 Summary of Crystal Data, Intensity Collection, and Structure Refinement for [Ir(COE)(CO)(TT[9]OC)][BPh_4], (17)

formula	**$C_{45}H_{50}BIrOS_3$**
fw	906.16
a, Å	23.338(5)
b, Å	24.646(9)
c, Å	13.805(5)
α, deg	
β, deg	
γ, deg	
cryst syst	orthorhombic
space group	*Pbca* (No. 61)
V, Å^3	7940(4)
ρ, g/cm^{-3}	1.516
Z	8
μ, cm^{-1}	35.348 (empirical)
avg trans factor	0.8830
diffractometer	Rigaku AFC6S
λ, Å	0.71069
T, °C	24
take-off angle, deg	6.0
detect aper, mm	6.0 horiz, 6.0 vert
cryst to detect, cm	40
scan type	ω-2θ
scan speed, deg/min	8.0 omega
scan width, deg	1.05 + 0.30 tanθ
data collected	6726
data, $F_o^2>3\sigma(F_o^2)$	1493
variables	176
goodness of fit	1.73
$R(F_o)$, %	7.68
$R_w(F_o)$, %	7.98

* $R = \Sigma||F_o|-|F_c||/\Sigma|F_o||$, $R_w = (\Sigma w(|F_o|-|F_c|)^2/\Sigma wF_o2)^{1/2}$ and $w = 1/\sigma^2(F)$

Table A.4.14
Positional parameters and B(eq) for [Ir(COE)(CO)(TT[9]OC)][BPh_4], (17)

atom	x	y	z	B(eq)
Ir	0.08778(8)	0.16344(7)	0.2011(1)	3.37(7)
S(1)	0.1882(5)	0.1682(5)	0.1688(8)	4.2(6)
S(2)	0.0866(7)	0.0821(5)	0.112(1)	6.2(8)
S(3)	0.0762(5)	0.1069(4)	0.3427(8)	4.1(7)
O(1)	0.097(1)	0.268(1)	0.305(2)	6.5(8)
C(1)	0.179(2)	0.127(2)	0.421(3)	3(1)
C(2)	0.172(2)	0.147(2)	0.514(4)	5(1)
C(3)	0.202(2)	0.193(2)	0.540(4)	8(2)
C(4)	0.241(2)	0.218(2)	0.476(3)	4(1)
C(5)	0.249(2)	0.197(2)	0.385(3)	3(1)
C(6)	0.219(2)	0.147(1)	0.362(3)	3(1)
C(7)	0.228(2)	0.129(2)	0.260(3)	4.5
C(8)	0.193(2)	0.126(2)	0.064(4)	7(1)
C(9)	0.159(2)	0.071(2)	0.070(4)	8(2)
C(10)	0.078(2)	0.029(2)	0.215(4)	7(1)
C(11)	0.047(2)	0.046(2)	0.299(4)	6(1)
C(12)	0.143(2)	0.081(2)	0.396(3)	5(1)
C(13)	0.091(2)	0.222(2)	0.265(3)	4(1)
C(14)	0.042(2)	0.192(2)	0.074(3)	5(1)
C(15)	0.038(2)	0.254(2)	0.061(3)	5(1)
C(16)	0.010(2)	0.267(2)	0.019(4)	8(2)
C(17)	0.070(2)	0.236(2)	0.001(4)	9(2)
C(18)	0.094(2)	0.253(2)	0.088(4)	7(1)
C(19)	0.099(2)	0.215(2)	0.171(3)	6(1)
C(20)	0.038(2)	0.204(2)	0.219(4)	6(1)
C(21)	0.000(2)	0.172(2)	0.151(3)	3(1)
B(1)	0.864(2)	0.018(2)	0.241(3)	2(1)
C(22)	0.924(1)	0.052(1)	0.268(2)	4(1)
C(23)	0.946(1)	0.049(1)	0.361(2)	6(1)
C(24)	0.997(1)	0.076(1)	0.384(2)	7(2)
C(25)	1.0248(9)	0.107(1)	0.314(3)	6(1)
C(26)	1.002(1)	0.1099(9)	0.220(2)	6(1)
C(27)	0.952(1)	0.083(1)	0.197(2)	7(1)
C(28)	0.809(1)	0.064(1)	0.233(2)	2.3(9)
C(29)	0.8190(8)	0.118(1)	0.213(2)	5(1)
C(30)	0.773(1)	0.1543(7)	0.208(2)	6(1)
C(31)	0.717(1)	0.136(1)	0.224(2)	4(1)
C(32)	0.7078(8)	0.081(1)	0.245(2)	5(1)
C(33)	0.754(1)	0.0449(7)	0.249(2)	4(1)
C(34)	0.872(1)	0.0155(8)	0.138(1)	3(1)
C(35)	0.8214(9)	0.036(1)	0.098(2)	3(1)

C(36)	0.8237(9)	0.068(1)	0.015(2)	3(1)
C(37)	0.876(1)	0.0791(8)	0.028(1)	4(1)
C(38)	0.9267(8)	0.058(1)	0.011(2)	3(1)
C(39)	0.9244(9)	0.0265(9)	0.095(2)	3(1)
C(40)	0.854(1)	0.0259(9)	0.327(2)	3(1)
C(41)	0.878(1)	0.078(1)	0.321(2)	4(1)
C(42)	0.873(1)	0.1133(7)	0.399(2)	4(1)
C(43)	0.843(1)	0.097(1)	0.483(2)	4(1)
C(44)	0.819(1)	0.046(1)	0.488(2)	4(1)
C(45)	0.824(1)	0.0100(8)	0.410(2)	5(1)

Table A.4.15
Summary of Bond Distances and Angles for [Ir(COE)(CO)(TT[9]OC)][BPh_4], (17)

Distances (Å)

Ir-S(1)	2.39(1)	Ir-S(2)	2.35(1)
Ir-S(3)	2.41(1)	Ir-C(13)	1.70(4)
Ir-C(14)	2.17(5)	Ir-C(21)	2.18(4)
S(1)C(7)	1.85(4)	S(1)-C(8)	1.78(5)
S(2)-C(9)	1.82(6)	S(2)-C(10)	1.94(5)
S(3)-C(11)	1.76(5)	S(3)-C(12)	1.84(5)
O(1)-C(13)	1.27(5)	C(1)-C(2)	1.38(6)
C(14)-C(15)	1.55(6)	C(1)-C(6)	1.33(6)
C(14)-C(21)	1.53(6)	C(1)-C(12)	1.45(6)
C(2)-C(3)	1.40(7)	C(15)-C(16)	1.60(7)
C(3)-C(4)	1.41(7)	C(8)-C(9)	1.59(7)
C(10)-C(11)	1.44(7)	C(16)-C(17)	1.62(8)
C(4)-C(5)	1.37(6)	C(5)-C(6)	1.47(5)
C(17)-C(18)	1.41(8)	C(6)-C(7)	1.49(6)
C(18)-C(19)	1.49(7)	C(34)-C(39)	1.40(3)
C(35)-C(36)	1.40(3)	C(19)-C(20)	1.59(7)
C(36)-C(37)	1.40(3)	C(37)-C(38)	1.40(3)
C(38)-C(39)	1.40(3)	C(20)-C(21)	1.51(6)
C(40)-C(41)	1.40(3)	C(40)-C(45)	1.40(3)
C(41)-C(42)	1.40(3)	C(42)-C(43)	1.40(4)
B(1)-C(22)	1.66(5)	C(43)-C(44)	1.40(4)
B(1)-C(28)	1.70(5)	C(44)-C(45)	1.40(3)
B(1)-C(34)	1.65(5)	B(1)-C(40)	1.63(5)
C(22)-C(23)	1.40(4)	C(22)-C(27)	1.40(4)
C(23)-C(24)	1.40(4)	C(24)-C(25)	1.40(4)
C(25)-C(26)	1.40(4)	C(26)-C(27)	1.40(4)
C(28)-C(29)	1.40(4)	C(28)-C(33)	1.40(3)
C(29)-C(30)	1.40(3)	C(30)-C(31)	1.40(4)
C(31)-C(32)	1.40(4)	C(32)-C(33)	1.40(3)
C(34)-C(35)	1.40(3)		

Angles (°)

S(1)-Ir-S(2)	87.5(5)	C(6)-C(1)-C(12)	123(4)
S(1)-Ir-S(3)	106.8(4)	S(1)-Ir-C(13)	91(2)
S(1)-Ir-C(14)	108(1)	S(1)-Ir-C(21)	149(1)
C(2)-C(3)-C(4)	121(5)	S(2)-Ir-S(3)	85.9(4)
S(2)-Ir-C(13)	178(2)	S(2)-Ir-C(14)	81(1)
C(3)-C(4)-C(5)	120(4)	S(2)-Ir-C(21)	85(1)
S(3)-Ir-C(13)	94(1)	S(3)-Ir-C(14)	142(1)

C(4)-C(5)-C(6)	117(4)	S(3)-Ir-C(21)	102(1)
C(13)-Ir-C(14)	100(2)	C(13)-Ir-C(21)	97(2)
C(1)-C(6)-C(5)	121(4)	C(14)-Ir-C(21)	41(2)
C(1)-C(6)-C(7)	125(4)	Ir-C(13)-O(1)	173(4)
Ir-C(14)-C(15)	117(3)	Ir-S(1)-C(7)	110(1)
C(5)-C(6)-C(7)	113(4)	Ir-S(1)-C(8)	101(2)
S(1)-C(7)-C(6)	115(3)	C(7)-S(1)-C(8)	102(2)
Ir-S(2)-C(9)	107(2)	Ir-S(2)-C(10)	101(1)
C(9)-S(2)-C(10)	103(2)	Ir-S(3)-C(11)	105(2)
Ir-S(3)-C(12)	115(1)	S(1)-C(8)-C(9)	115(4)
C(11)-S(3)-C(12)	100(2)	C(2)-C(1)-C(6)	121(4)
C(2)-C(1)-C(12)	115(4)	S(2)-C(9)-C(8)	110(3)
Ir-C(14)-C(21)	70(2)	C(15)-(14)-C(21)	111(3)
C(14)-C(15)-C(16)	109(4)	S(2)-C(10)-C(11)	116(3)
C(15)-C(16)-C(17)	114(4)	S(3)-C(11)-C(10)	109(3)
C(16)-C(17)-C(18)	109(5)	S(3)-C(12)-C(1)	109(3)
C(1)-C(2)-C(3)	118(4)	C(17)-C(18)-C(19)	121(4)
C(28)-B(1)-C(34)	111(3)	C(28)-B(1)-C(40)	112(3)
C(34)-B(1)-C(40)	107(3)	B(1)-C(22)-C(23)	120(3)
B(1)-C(22)-C(27)	120(3)	C(18)-C(19)-C(20)	111(4)
C(23)-C(22)-C(27)	120(2)	C(22)-C(23)-C(24)	120(2)
C(19)-C(20)-C(21)	110(4)	C(23)-C(24)-C(25)	120(2)
C(24)-C(25)-C(26)	120(2)	Ir-C(21)-C(14)	69(2)
C(25)-C(26)-C(27)	120(2)	Ir-C(21)-C(20)	114(3)
C(14)-C(21)-C(20)	131(4)	C(22)-C(27)-C(26)	120(2)
B(1)-C(28)-C(29)	122(2)	B(1)-C(28)-C(33)	118(2)
C(22)-B(1)-C(28)	108(3)	C(29)-C(28)-C(33)	120(2)
C(22)-B(1)-C(34)	111(3)	C(22)-B(1)-C(40)	107(3)
C(28)-C(29)-C(30)	120(2)	C(37)-C(38)-C(39)	120(2)
C(29)-C(30)-C(31)	120(2)	C(34)-C(39)-C(38)	120(2)
B(1)-C(40)-C(41)	121(2)	C(30)-C(31)-C(32)	120(2)
B(1)-C(40)-C(45)	119(2)	C(41)-C(40)-C(45)	120(2)
C(31)-(32)-C(33)	120(2)	C(40)-C(41)-C(42)	120(2)
C(28)-C(33)-C(32)	120(2)	B(1)-C(34)-C(35)	116(2)
C(41)-C(42)-C(43)	120(2)	B(1)-C(34)-C(39)	124(2)
C(35)-C(34)-C(39)	120(2)	C(42)-C(43)-C(44)	120(2)
C(34)-C(35)-C(36)	120(2)	C(43)-C(44)-C(45)	120(2)
C(35)-C(36)-C(37)	120(2)	C(40)-C(45)-C(44)	120(2)
C(36)-C(37)-C(38)	120(2)		

Table A.4.16 Summary of Crystal Data, Intensity Collection, and Structure Refinement for [Ir(COD)(NO)(TT[9]OC)][BF_4]$_2$·H_2O, (24)

formula	$C_{20}H_{30}B_2F_8IrNO_3S_2$
fw	744.37
a, Å	18.821(6)
b, Å	9.611(5)
c, Å	14.225(8)
α, deg	
β, deg	
γ, deg	
cryst syst	orthorhombic
space group	*Pnma* (No. 62)
V, Å^3	2573(2)
ρ (calcd) g/cm^{-3}	1.921
Z	4
μ, cm^{-1}	53.97 (empirical)
avg trans factor	0.9954
diffractometer	Rigaku AFC6S
λ, Å	0.71069
T, °C	24
take-off angle, deg	6.0
detect aper, mm	6.0 horiz, 6.0 vert
cryst to detect, cm	40
scan type	w/2θ
scan speed, deg/min	32.0 omega
scan width, deg	1.05 + 0.30 tanθ
data collected	2603
data, $F_o^2>3\sigma(F_o^2)$	1180
variables	152
goodness of fit	1.79
$R(F_o)$, %	5.11
$R_w(F_o)$, %	4.83

[a] $R = \Sigma||F_o|-|F_c||/\Sigma|F_o||$, $R_w = (\Sigma w(|F_o|-|F_c|)^2/\Sigma wF_o2)^{1/2}$ and $w = 1/\sigma^2(F)$

Table A.4.17
Positional parameters and B(eq) for [Ir(COD)(NO)(TT[9]OC)][BF_4]$_2$·H_2O, (24)

atom	x	y	z	B(eq)
Ir	0.36216(7)	1/4	0.15916(8)	2.34(4)
S(1)	0.3006(3)	0.0580(5)	0.2262(3)	3.6(2)
F(1)	0.143(1)	1/4	0.596(2)	9(1)
F(2)	0.196(1)	0.140(2)	0.487(1)	12(1)
F(3)	0.252(2)	1/4	0.588(2)	16(3)
F(4)	0.451(1)	1/4	0.599(2)	12(2)
F(5)	0.418(2)	1/4	0.738(3)	9(4)
F(6)	0.513(2)	0.151(5)	0.692(4)	15(4)
F(7)	0.462(3)	0.129(4)	0.731(3)	10(3)
F(8)	0.562(4)	1/4	0.681(6)	18(7)
O(1)	0.281(2)	0.311(3)	0.007(2)	6(2)
O(2)	0.404(1)	1/4	0.330(2)	5(1)
O(3)	0.278(2)	1/4	0.771(3)	14(3)
N(1)	0.292(1)	1/4	0.054(2)	5(2)
C(1)	0.095(1)	0.178(2)	0.052(1)	5.5(6)
C(2)	0.135(1)	0.103(2)	0.118(1)	4.2(4)
C(3)	0.169(1)	0.177(2)	0.183(1)	4.3(5)
C(4)	0.210(1)	0.094(2)	0.258(2)	5.3(5)
C(5)	0.340(1)	0.028(2)	0.338(2)	5.8(5)
C(6)	0.389(2)	0.125(3)	0.370(2)	10(1)
C(7)	0.519(1)	0.172(2)	0.155(2)	6.4(6)
C(8)	0.450(1)	0.102(2)	0.140(1)	3.7(4)
C(9)	0.413(1)	0.100(2)	0.058(1)	4.0(4)
C(10)	0.444(1)	0.170(3)	0.028(2)	7.1(7)
B(1)	0.190(3)	1/4	0.538(3)	6(3)
B(2)	0.473(3)	1/4	0.688(3)	5(3)

Table A.4.18
Summary of Bond Distances and Angles for $[Ir(COD)(NO)(TT[9]OC)][BF_4]_2 \cdot H_2O$, (24)

Distances (Å)

Ir-S(1)	2.378(5)	C(1)-C(1')	1.39(4)
C(1)-C(2)	1.40(2)	Ir-N(1)	1.99(3)
C(2)-C(3)	1.33(2)	Ir-C(8)	2.20(2)
Ir-C(8)	2.20(2)	Ir-C(9)	2.25(2)
C(3)-C(4)	1.54(3)	S(1)-C(4)	1.79(2)
S(1)-C(5)	1.78(2)	F(1)-B(1)	1.21(5)
C(5)-C(6)	1.39(3)	F(2)-B(1)	1.29(2)
F(3)-B(1)	1.37(6)	F(4)-B(2)	1.34(4)
F(5)-F(7)	1.42(5)	F(5)-F(7)	1.42(5)
C(7)-C(7)	1.49(4)	F(5)-B(2)	1.26(6)
C(7)-C(8)	1.47(2)	F(6)-F(7)	1.13(5)
F(6)-F(8)	1.34(6)	F(6)-B(2)	1.21(5)
C(8)-C(9)	1.36(2)	F(7)-B(2)	1.33(4)
F(8)-B(2)	1.68(9)	C(9)-C(10)	1.52(3)
O(1)-O(1')	1.18(6)	O(1)-N(1)	1.07(3)
C(10)-C(10)	1.53(5)	O(2)-C(6)	1.36(3)
O(2)-C(6)	1.36(3)		

Nonbonded Distance

Ir...O1 2.87(3)Å

Angles (°)

S(1)-Ir-S(1)	101.8(3)	F(7)-F(5)-B(2)	59(3)
S(1)-Ir-N(1)	88.8(5)	F(7)-F(6)-F(8)	141(6)
S(1)-Ir-C(8)	85.1(5)	F(7)-F(6)-B(2)	69(4)
S(1)-Ir-C(8)	156.6(5)	F(8)-F(6)-B(2)	82(5)
S(1)-Ir-C(9)	88.1(5)	F(5)-F(7)-F(6)	112(5)
S(1)-Ir-C(9)	163.8(5)	F(5)-F(7)-B(2)	54(4)
F(6)-F(7)-B(2)	58(4)	F(6)-F(8)-F(6')	91(5)
F(6)-F(8)-B(2)	46(3)	S(1')-Ir-C(9)	88.1(5)
O(1)-O(1')-N(1)	56(2)	N(1)-Ir-C(8)	113.8(7)
C(6)-O(2)-C(6)	124(3)	N(1) Ir-C(9)	78.4(7)
Ir-N(1)-O(1)	137(2)	O(1)-N(1)-O(1')	67(4)
C(8)-Ir-C(8)	81(1)	C(1)-C(1')-C(2)	121(1)
C(8)-Ir-C(9)	35.6(6)	C(8)-Ir-C(9)	90.9(7)
C(1)-C(2)-C(3)	117(2)	C(8)-Ir-C(9)	35.6(6)
C(9)-Ir-C(9)	80(1)	Ir-S(1)-C(4)	114.5(8)
C(2)-C(3)-C(3)	123(1)	Ir-S(1)-C(5)	106.4(7)

C(2)-C(3)-C(4)	116(2)	C(4)-S(1)-C(5)	101(1)
C(3)-C(3)-C(4)	121(1)	F(7)-F(5)-F(7)	109(6)
S(1)-C(4)-C(3)	114(1)	F(7)-F(5)-B(2)	59(3)
Ir C(9)-C(8)	70(1)	Ir-C(9)-C(10)	113(1)
S(1)-C(5)-C(6)	117(2)	C(8)-C(9)-C(10)	119(2)
C(9)-C(10)-C(10)	116(1)	O(2)-C(6)-C(5)	126(3)
F(1)-B(1)-F(2)	117(3)	C(7)-C(7)-C(8)	117(1)
F(1)-B(1)-F(3)	105(3)	F(2)-B(1)-F(2)	111(3)
F(2)-B(1)-F(3)	102(4)	F(2)-B(1)-F(3)	102(4)
F(4)-B(2)-F(5)	106(5)	F(4)-B(2)-F(6)	104(4)
Ir-C(8)-C(7)	110(1)	Ir-C(8)-C(9)	74(1)
F(4)-B(2)-F(7)	113(3)	C(7)-C(8)-C(9)	126(2)
F(4)-B(2)-F(8)	105(5)	F(5)-B(2)-F(6)	119(4)
F(5)-B(2)-F(7)	67(4)	F(5)-B(2)-F(8)	149(5)
F(6)-B(2)-F(6)	104(8)	F(6)-B(2)-F(7)	53(2)
F(6)-B(2)-F(7)	140(6)	F(6)-B(2)-F(8)	52(4)
F(7)-B(2)-F(7)	122(6)	F(7)-B(2)-F(8)	101(4)

Table A.5.1
Summary of Crystal Data, Intensity Collection, and Structure Refinement for $RuCl_2(PPh_3)(ODT[9]OC)Cl(CH_2)_2Cl$, (25)

formula	$C_{32}H_{35}Cl_4RuOS_2P$
fw	773.60
a, Å	7.912(1)
b, Å	22.419(5)
c, Å	18.794(3)
α, deg	
β, deg	101.12(1)
γ, deg	
cryst syst	monoclinic
space group	$P2_1/c$ (No. 14)
V, Å^3	327(1)
ρ (calcd), g/cm^{-3}	1.571
Z	4
μ, cm^{-1}	10.08 (empirical)
avg trans factor	0.9387
diffractometer	Rigaku AFC6S
λ, Å	0.7107
T, °C	23.0
take-off angle	6.0
detect aper, mm	6.0 hor; 6.0 vert
cryst to detect, cm	40
scan type	ω-2θ
scan speed, deg/min	16.0 omega
scan width, deg	1.05 + 0.30 tanθ
data collected	3459
data, $F_o^2>3\sigma(F_o^2)$	1809
variables	2.11
goodness of fit	2.18
$R(F_o)^a$, %	5.52
$R_w(F_o)^a$, %	5.63

$^a R = \Sigma||F_o|-|F_c||/\Sigma|F_o||$, $R_w = (\Sigma w(|F_o|-|F_c|)^2/\Sigma wF_o2)^{1/2}$ and $w = 1/\sigma^2(F)$

Table A.5.2 Selected Positional Parameters and B(eq) for $RuCl_2(PPh_3)(ODT[9]OC)\cdot Cl(CH_2)_2Cl$, (25)

atom	x	y	z	B(eq)
Ru	0.0939(1)	0.25593(6)	0.67040(6)	1.91(5)
Cl(1)	0.3134(5)	0.2621(2)	0.5964(2)	3.2(2)
Cl(2)	0.2615(5)	0.1838(2)	0.7510(2)	3.2(2)
S(1)	-0.0220(5)	0.3353(2)	0.5990(2)	2.5(2)
S(2)	-0.0750(4)	0.2523(2)	0.7565(2)	2.3(2)
P(1)	-0.0434(5)	0.1812(2)	0.60616(2)	1.9(2)
O(1)	0.228(1)	0.3294(4)	0.7391(5)	2.6(5)
C(1)	-0.283(2)	0.3580(6)	0.7349(8)	2.3(3)
C(2)	-0.310(2)	0.3898(7)	0.7967(9)	4.0(4)
C(3)	-0.318(2)	0.4514(8)	0.795(1)	4.3(4)
C(4)	-0.306(2)	0.4819(8)	0.734(1)	4.7(4)
C(5)	-0.285(2)	0.4529(7)	0.6722(9)	3.8(4)
C(6)	-0.274(2)	0.3890(6)	0.6724(8)	2.5(3)
C(7)	-0.243(2)	0.3594(7)	0.6047(8)	3.3(4)
C(8)	0.`02(1)	0.3979(7)	0.6420(8)	2.9(4)
C(9)	0.265(2)	0.3775(7)	0.6956(8)	3.1(4)
C(10)	0.141(2)	0.3491(7)	0.7952(8)	2.7(3)
C(11)	0.057(2)	0.2960(6)	0.8256(8)	2.9(3)
C(12)	-0.281(2)	0.2924(6)	0.7383(8)	2.5(3)
C(13)	-0.208(2)	0.2068(6)	0.5255(7)	1.9(3)
C(14)	-0.378(2)	0.1895(7)	0.5139(8)	3.1(3)
C(15)	-0.497(2)	0.2095(7)	0.4544(9)	4.0(4)
C(16)	-0.446(2)	0.2491(9)	0.4091(8)	4.3(4)
C(17)	-0.278(2)	0.2683(7)	0.4187(8)	3.3(4)
C(18)	-0.156(2)	0.2462(7)	0.4765(7)	2.6(3)
C(19)	0.081(2)	0.1310(6)	0.5529(7)	1.7(3)
C(20)	0.000(2)	0.1029(6)	0.4908(8)	2.2(3)
C(21)	0.091(2)	0.0594(7)	0.4560(9)	3.6(4)
C(22)	0.258(2)	0.0456(7)	0.487(1)	4.0(4)
C(23)	0.338(2)	0.0725(7)	0.5501(9)	3.6(4)
C(24)	0.250(2)	0.1164(7)	0.5832(8)	2.7(3)
C(25)	-0.149(2)	0.1267(6)	0.6526(8)	2.0(3)
C(26)	-0.072(2)	0.0736(6)	0.6721(8)	2.7(3)
C(27)	-0.138(2)	0.0341(7)	0.7160(8)	3.0(4)
C(28)	-0.280(2)	0.0494(7)	0.7472(9)	3.1(4)
C(29)	-0.356(2)	0.1038(7)	0.7259(8)	3.3(4)
C(30)	-0.293(2)	0.1424(7)	0.6815(8)	2.7(3)
C(31)	1.081(3)	0.106(1)	0.893(1)	9.2(7)
C(32)	1.236(3)	0.128(1)	0.938(1)	8.9(7)
Cl(3)	0.965(1)	0.0616(3)	0.9346(4)	13.0(6)
Cl(4)	1.384(1)	0.0735(4)	0.9723(6)	20.1(8)

Table A.5.3
Selected Bond Distances and Angles For $RuCl_2(PPh_3)(ODT[9]OC)Cl(CH_2)_2Cl$, (25)

Distances (A)

Ru-Cl(1)	2.429(4)	C(5)-C(6)	1.43(2)
Ru-Cl(2)	2.428(4)	C(6)-C(7)	1.50(2)
Ru-S(1)	2.309(4)	C(8)-C(9)	1.54(2)
Ru-S(2)	2.290(4)	C(10)-C(11)	1.53(2)
Ru-P(1)	2.262(4)	C(13-C(14)	1.38(2)
Ru-O(1)	2.232(9)	C(13)-C(18)	1.9(2)
S(1)-C(7)	1.85(2)	C(14)-C(15)	1.39(2)
S(1)-C(8)	1.81(1)	C(15-C(16)	1.34(2)
S(2)-C(11)	1.79(1)	C(16)-C(17)	1.38(2)
S(2)-C(12)	1.84(1)	C(17)-C(18)	1.39(2)
P(1)-C(13)	1.83(1)	C(31)-C(32)	1.44(3)
P(1)-C(19)	1.85(1)	C(29)-C(30)	1.36(2)
P(1)-C(25)	1.85(1)	C(28)-C(29)	1.38(2)
O(1)-C(9)	1.42(2)	C(19)-C(20)	1.37(2)
O(1)-C(10)	1.43(2)	C(19)-C(24)	1.38(2)
C(1)-C(2)	1.41(2)	C(20)-C(21)	1.44(2)
C(1)-C(6)	1.38(2)	C(21)-C(22)	1.37(2)
C(1)-C(12)	1.47(2)	C(22)-C(23)	1.38(2)
C(2)-C(3)	1.38(2)	C(23)-C(24)	1.42(2)
C(3)-C(4)	1.35(2)	C(25)-C(26)	1.35(2)
C(4)-C(5)	1.37(2)	C(25)-C(30)	1.40(2)
C(26)-C(27)	1.38(2)	C(27)-C(28)	1.41(2)
Cl(3)-C(31)	1.65(2)	Cl(4)-C(32)	1.73(2)

Angles (°)

Cl(1)-Ru-Cl(2)	91.7(1)	C(19)-P(1)-(C25)	101.0(6)
Cl(1)-Ru-S(1)	82.6(1)	Ru-O(1)-C(9)	110.8(8)
Cl(1)-Ru-S(2)	170.2(1)	Ru-O(1)-C(10)	114.3(8)
Cl(1)-Ru-P(1)	91.9(1)	C(9)-O(1)-C(10)	112(1)
Cl(1)-Ru-O(1)	88.7(3)	C(2)-C(1)-C(6)	119(1)
Cl(2)-Ru-S(1)	169.6(2)	C(2)-C(1)-C(12)	118(1)
Cl(2)-Ru-S(2)	81.9(1)	C(6)-C(1)-C(12)	123(1)
Cl(2)-Ru-P(1)	90.4(1)	C(1)-C(2)-C(3)	120(2)
Cl(2)-Ru-O(1)	89.4(3)	C(2)-C(3)-C(4)	121(2)
S(1)-Ru-S(2)	102.6(2)	C(3)-C(4)-C(5)	121(2)
S(1)-Ru-P(1)	98.4(1)	C(4)-C(5)-C(6)	119(2)
S(1)-Ru-O(1)	81.8(3)	C(7)-S(1)-C(8)	100.9(7)
S(2)-Ru-P(1)	95.5(2)	C(1)-C(6)-C(5)	119(1)
S(2)-Ru-O(1)	83.9(3)	C(1)-C(6)-C(7)	123(1)

P(1)-Ru-O(1)	179.4(3)	C(5)-C(6)-C(7)	117(1)
Ru-S(1)-C(7)	117.7(5)	C(11)-S(2)-C(12)	103.7(7)
Ru-S(1)-C(8)	102.5(5)	S(1)-C(7)-C(6)	119(1)
Ru-S(2)-C(11)	98.9(5)	C(13)-P(1)-C(19)	99.8(6)
Ru-S(2)-C(12)	118.0(5)	C(13)-P(1)-C(25)	106.9(6)
Ru-P(1)-C(13)	113.9(5)	S(2)-C(12)-C(1)	120(1)
Ru-P(1)-C(19)	119.3(5)	S(1)-C(8)-C(9)	112(1)
Ru-P(1)-C(25)	114.0(5)	P(1)-C(13)-C(14)	124(1)
P(1)-C(13)-C(18)	118(1)	O(1)-C(9)-C(8)	111(1)
C(14)-C(13)-C(18)	118(1)	C(14)-C(15)-C(16)	119(2)
O(1)-C(10)-C(11)	110(1)	C(15)-C(16)-C(17)	122(2)
C(16)-C(17)-C(18)	120(1)	S(2)-C(11)-C(10)	113(1)
C(13)-C(18)-C(17)	120(1)	P(1)-C(19)-C(20)	119(1)
C(20)-C(19)-C(24)	120(1)	C(19)-C(20-C(21)	120(1)
C(28)-C(29)-C(30)	123(2)	C(20)-C(21)-C(22)	119(2)
C(25)-C(30)-C(29)	120(1)	C(21)-C(22)-C(23)	121(2)
Cl(3)-C(31)-C(32)	115(2)	C(22)-C(23)-C(24)	120(2)
Cl(4)-C(32)-C(31)	114(2)	C(19)-C(24)-C(23)	120(1)
P(1)-C(25)-C(26)	120(1)	P(1)-C(25)-C(30)	121(1)
C(25)-C(25)-C(30)	118(1)	C(25)-C(26)-C(27)	122(1)
C(26-C(27)-C(28)	121(1)	C(25)-C(26)-C(27)	122(1)
C(26)-C(27)-C(28)	121(1)	C(27)-C(28)-C(29)	115(2)

Table A.5.4
Summary of Crystal Data, Intensity Collection, and Structure Refinement for $RuCl_2$(DMSO)(TT[9]OC)

formula	**$C_{16}H_{28}Cl_2RuO_2S_4$**
fw	608.69
a, Å	19.590(5)
b, Å	16.849(4)
c, Å	13.149(4)
α, deg	-
β, deg	-
γ, deg	-
cryst syst	orthorhombic
space group	*Pbca* (No. 61)
V, Å^3	4340(4)
ρ (calcd), gcm^{-1}	1.863
Z	8
μ, cm^{-1}	14.64 (empirical)
avg trans factor	0.9697
diffractometer	Rigaku AFC6S
λ, Å	0.7107
T, °C	23.0
take-off angle	6.0
detect aper, mm	6.0 hor; 6.0 vert
cryst to detect, cm	40
scan type	ω-2θ
scan speed, deg/min	32.0 omega
scan width, deg	1.05 + 0.30 tanθ
data collected	4282
data with $F_o^2>3\sigma(F_o^2)$	2473
variables	234
goodness of fit	2.30
$R(F_o)^a$, %	3.68
$R_w(F_o)^a$, %	4.86

$^a R = \Sigma||F_o|-|F_c||/\Sigma|F_o||$, $R_w = (\Sigma w(|F_o|-|F_c|)^2/\Sigma wF_o2)^{1/2}$ and $w = 1/\sigma^2(F)$

Table A.5.5
Positional Parameters and B(eq) for $RuCl_2$(DMSO)(TT[9]OC)

Atom	x	y	z	B(eq)
Ru	0.46760(3)	0.12433(4)	0.23179(4)	1.66(2)
Cl(1)	0.4249(1)	0.1492(1)	0.4042(1)	3.0(1)
Cl(2)	0.4275(1)	-0.0136(1)	0.2432(2)	2.8(1)
S(1)	0.4998(1)	0.2550(1)	0.2382(2)	2.2(1)
S(2)	0.3617(1)	0.1682(1)	0.1713(2)	2.6(1)
S(3)	0.4925(1)	0.0870(1)	0.0685(1)	1.9(1)
S(4)	0.5696(1)	0.0746(1)	0.2893(2)	2.9(1)
S(5)	0.246(1)	-0.026(2)	0.205(3)	7.1(3)
O(1)	0.6071(3)	0.0193(4)	0.2201(4)	4.4(3)
O(2)	0.2528(4)	-0.0174(8)	0.198(2)	17(1)
C(1)	0.5949(5)	0.1912(5)	0.0185(6)	2.6(5)
C(2)	0.6539(6)	0.1567(6)	-0.0148(7)	4.0(6)
C(30	0.7162(6)	0.1844(7)	0.020(1)	5.4(7)
C(4)	0.7191(6)	0.2474(8)	00857(9)	5.4(7)
C(5)	0.6599(6)	0.2832(6)	0.1196(7)	4.2(6)
C(6)	0.5974(5)	0.2567(5)	0.0863(6)	2.8(5)
C(7)	0.5335(5)	0.2989(4)	0.1213(6)	2.8(4)
C(8)	0.4184(4)	0.3067(4)	0.2426(6)	2.6(4)
C(9)	0.3695(5)	0.2764(5)	0.1662(7)	3.7(5)
C(10)	0.3625(5)	0.1433(5)	0.0364(6)	3.0(5)
C(11)	0.4081(4)	0.0746(5)	0.0146(6)	2.5(4)
C(12)	0.5264(5)	0.1605(5)	-0.0176(6)	2.9(4)
C(13)	0.6320(5)	0.1449(5)	0.3246(7)	4.3(6)
C(14)	0.5633(5)	0.0244(5)	0.4073(6)	4.8(6)
C(15)	0.2634(6)	0.0224(7)	0.3316(9)	5.5(7)
C(16)	0.2415(7)	-0.0962(7)	0.252(1)	7.5(8)

Table A.5.6 Bond Distances and Angles for $RuCl_2$(DMSO)(TT[9]OC)

Distances (Å)

Ru-Cl(1)	2.453(2)	C(4)-C(5)	1.38(1)
Ru-Cl(2)	2.458(2)	C(5)-C(6)	1.38(1)
Ru-S(1)	2.292(2)	C(6)-C(7)	1.51(1)
Ru-S(2)	2.342(2)	C(8)-C(9)	1.48(1)
Ru-S(3)	2.294(2)	C(10)-C(11)	1.49(1)
Ru-S(4)	2.296(2)	S(1)-C(7)	1.829(8)
S(1)-C(8)	1.817(8)	S(2)-C(9)	1.832(9)
S(2)-C(10)	1.824(8)	S(3)-C(11)	1.809(8)
S(3)-C(12)	1.817(8)	S(4)-O(1)	1.494(6)
S(4)-C(13)	1.763(9)	S(4)-C(14)	1.771(9)
S(5)-O(2)	0.21(5)	S(5)-C(15)	1.89(3)
S(5)-C(16)	1.34(4)	C(1)-C(2)	1.37(1)
C(1)-C(6)	1.42(1)	C(1)-C(12)	1.51(1)
C(2)-C(3)	1.38(1)	C(3)-C(4)	1.37(1)

Angles (°)

Cl(1)-Ru-Cl(2)	89.81(7)	Ru-S(4)-C(14)	113.7(4)
Cl(1)-Ru-S(1)	83.98(8)	O(1)-S(4)-C(13)	103.8(4)
Cl(1)-Ru-S(2)	87.58(8)	O(1)-S(4)-C(14)	105.7(4)
Cl(1)-Ru-S(3)	170.28(8)	C(13)-S(4)-C(14)	98.0(4)
Cl(1)-Ru-S(4)	93.14(8)	O(2)-S(5)-C(15)	88(10)
Cl(2)-Ru-S(1)	173.78(8)	O(2)-S(5)-C(16)	146(9)
Cl(2)-Ru-S(2)	92.03(8)	C(15)-S(5)-C(16)	89(2)
Cl(2)-Ru-S(3)	81.88(7)	S(5)-O(2)-C(16)	29(9)
Cl(2)-Ru-S(4)	85.02(8)	C(2)-C(1)-C(6)	120.1(9)
S(1)-Ru-S(2)	87.33(8)	C(2)-C(1)-C(12)	120.3(9)
S(1)-Ru-S(3)	104.27(8)	C(6)-C(1)-C(12)	119.5(9)
S(1)-Ru-S(4)	95.69(8)	C(1)-C(2)-C(3)	120(1)
S(2)-Ru-S(3)	87.68(8)	C(2)-C(3)-C(4)	120(1)
S(2)-Ru-S(4)	176.96(9)	C(3)-C(4)-C(5)	120(1)
S(3)-Ru-S(4)	91.16(8)	C(4)-C(5)-C(6)	120(1)
Ru-S(1)-C(7)	117.2(3)	C(1)C(6)-C(5)	118.9(9)
Ru-S(1)-C(8)	102.7(3)	C(1)-C(6)-C(7)	121.9(8)
C(7)-S(1)-C(8)	98.6(4)	C(5)-C(6)-C(7)	119.2(9)
Ru-S(2)-C(9)	104.6(3)	Ru-S(2)-C(10)	104.4(3)
C(9)-S(2)-C(10)	101.1(4)	Ru-S(3)-C(11)	101.7(3)
Ru-S(3)-C(12)	117.8(3)	C(11)-S(3)-C(12)	99.4(4)
Ru-S(4)-O(1)	117.1(3)	Ru-S(4)-C(13)	116.4(3)
S(1)-C(7)-C(6)	111.4(6)	S(3)-C(12)-C(1)	111.4(6)
S(1)-C(8)-C(9)	112.4(6)	S(2)-C(9)-C(8)	111.9(6)
S(2)-C(10)-C(11)	111.8(6)	S(3)-C(11)-C(10)	113.0(6)

References

1. Meadow, J.R.; Reid, E. E. *J. Am.Chem. Soc.* **1934**, *56*, 2177.

2. Pedersen, C. J. *J. Am. Chem. Soc.* **1967**, *89*, 7017.

3. Pedersen, C. J. *Angew. Chem. Intl. Ed. Engl.* **1988**, *27* 1021.

4. a) Lehn, J-M. *Struct. Bonding* **1973**, *16*, 1-70; b) Lehn, J-M.*Angew. Chem. Intl. Ed. Engl.* **1988**, *27*, 89. c) Lehn, J-M.; Pine, S.H.; Watanabe, E.; Willard, A. K. *J. Am. Chem. Soc.* **1977**, *99*, 6766. d) Lehn, J-M. *Acc. Chem. Res.* **1978**, *11*, 49.

5. a) Schultz, R. A.; Dishong, D. M.; Gokel, G. W. *J. Am Chem. Soc.* **1982**, *104*, 625. b) Gokel, G. W. *Chem. Soc. Rev.* **1992**, *21*, 39.

6. a) Cram, D. J. *Angew Chem. Intl. Ed. Engl.* **1988**, *27* 1009. b) Timko, J. M.; Moore, S. S.; Walba, D. M.; Hiberty, P. C.; Cram, D. J. *J. Am. Chem . Soc.* **1977**, *99*, 4207. c) Cram, D. J.; Kaneda, T.; Helgeson, R. C.; Lein, G.M. *J. Am. Chem. Soc.* **1979**, *101*, 4987. d) Moran, J. R.; Karbach, S.; Cram, .D. J. *J. Am. Chem. Soc.* **1982**, *104*, 5826. e) Cram, D. J.; Dicker, I. B.; Lein, G. M.; Knobler, C. B.; Trueblood, K. N. *J. Am. Chem. Soc.* **1982**, *104*, 6827.

7. a) Gutsche, D. B.; Dhawan, B.; No, K. H.; Muthukrishnan, R. *J. Am. Chem. Soc.* **1981**, *103*, 3782. b) Gutsche, D. B.; Levine, J. A. *J. Am. Chem. Soc.* **1982**, *104*, 2652. c) Gutsche, C. D. *Calixarenes.* The Royal Society of Chemistry: Cambridge, **1989**.

8. Vögtle, F.; Sieger, H.; Muller, W. M. *Top. Curr. Chem.* **1981**, *98*, 107. b) Vögtle, F. *Liebigs Ann. Chem.* **1976**, 891.

9. Deitrich-Buchecker, C. O.; Sauvage, J-P.; Kern, J-M. *J. Am. Chem. Soc.* **1984**, *106*, 3043. b) Cesario, M.; Dietricj-Buchecker, C. O.; Guilheim, J.; Pascard, C.; Sauvage, J-P. *J. Chem. Soc., Chem Comm.* **1985**, 244.

10. Rosen, W.; Busch, D. H. *J. Am. Chem. Soc.***1969**, *91*, 4694-4697. b) Rosen, W.; Busch, D. H. *Inorg. Chem.* **1970**, *9*, 262.

11. Murray, S.G.; Hartley, F.R. *Chem. Rev.* **1981**, *81*, 365-414, and references therein.

12. a) Colman, P. M.; Freeman, H. C.; Guss, J. M.; Murata, M.; Norris, V. A.; Ramshaw, J. A. M.; Venkatappa, M. P. *Nature* **1978**, *272*, 319. b) Guss, J. M.; Freeman, H. C. *J. Mol. Biol.* **1983**, *169*, 521.

13. Adman, E. T.; Stenkamp, R. E.; Sieker, L. C.; Jensen, L. H. *J. Mol. Biol.* **1978**, *123*, 35.

14. Cooper, S.R. *Acc. Chem.Res.* **1988**, *21*, 141-146.

15. Cooper, S.R.; Rawle, S.C. *Struct. Bonding* **1990**, *72*, 1-72.

16. Blake, A.J.; Schröder, M. *Adv. Inorg. Chem.* **1990**, *35*, 1-80.

17. Ochrymowycz, L. A.; Mak, C-P.; Michna, J. D. *J. Org. Chem.* **1974**, *39*, 2079-2084.

18. Setzer, W. N.; Ogle, C. A.; Wilson, G. S.; Glass, R. S. *Inorg. Chem.* **1983**, *22*, 266.

19. a) Buter, J.; Keliogg, R.M. *J. Chem. Soc., Chem. Comm.* **1980**, 466-467. b) Buter, J.; Kellogg, R.M. *J. Org. Chem.* **1981**, *46*, 4481-4485.

20. Dijstra, G.; Kruizinga, W. H.; Kellogg, R. M. *J. Org. Chem.* **1987**, *52*, 4230.

21. Wolf, R. E.; Hartman, J. R.; Ochrymowycz, L. A.; Cooper, S.R. *Inorg. Synth.* **1989**, *25*, 122.

22. Aldrich Chemical Co. Ltd. *Handbook of Fine Chemicals*, Milwaukee, **1993-94**.

23. a) Sellman, D.; Zapf, L. S. *Angew. Chem. Intl. Ed. Engl.* **1984**, *23*, 807. b) Sellman, D.; Zapf, L. S. *J. Organomet. Chem.* **1985**, *289*, 57.

24. a) Sellmann, D.; Frank, P. *Angew. Chem. Intl. Ed. Engl.* **1986**, *25*, 1107. Sellmann, D.; Frank, P.; Knoch, F. J. *J. Organomet. Chem.* **1988**, *339*, 345.

25. Sellmann, D.; Knoch, F.; Wronna, C. *Angew. Chem. Intl. Ed. Engl.* **1988**, *27*, 691-692, and references therein.

26. Edema, J. J. H.; Stock, H. T.; Buter, J ; Kellogg, R. M. Smeets,; W. J. J.; Spek, A. L.; van Bolhuis, F. *Angew. Chem. Intl. Ed. Engl.* **1993**, *32*, 436.

27. a) Dale, J. *Isr. J. Chem.* **1980**, *20*, 3, and references therein. b) Dale, J. *J. Acta. Chem. Scand.* **1973**, *27*, 115.

28. Wolf, R.E.; Hartman, J.R.; Storey, J.M.E.; Foxman, B.M.; Cooper, S.R. *J. Am. Chem. Soc.* **1987**, *109*, 4328-4335.

29. De Simone, R. E.; Glick, M. D. *J. Am. Chem. Soc.* **1976**, *98*, 762.

30. a) Christensen, J.J.; Eatough, D.J.; Izatt, R.M. *Chem. Rev.* **1974**, *74*, 351. b) Izatt, R.M.; Bradshaw, J.S.; Nielson, S.A.; Lamb, J.D.; Christensen, J.J. *Chem. Rev.* **1985**, *85*, 271. c) Izatt, R.M.; Terry, R.E.; Hansen, L.D.; Avondet, A.G.; Bradshaw, J.S.; Dalley, N.K.; Jansen, T.E.; Christensen, J.J.; Haymore, B.L. *Inorg. Chem. Acta.* **1978**, *30*, 1. d) Izatt, R.M.; Eatough, D.J.; Christensen, J.J.

Struct. Bonding (Berlin) **1973**, *16*, 161. e) Izatt, R.M.; Pawlak, K.; Bradshaw, J.S.; Breuning, R.L. *Chem. Rev.* **1991**, *91*, 1721.

31. De Simone, R. E.; Gick, M. D. *J. Am. Chem. Soc.* **1975**, *97*, 942.

32. Glass, R.S.; Wilson, G.S.; Setzer, W.N. *J. Am. Chem. Soc.* **1980**, *102*, 5068-5069.

33. a) Wieghardt, K.; Küppers, H-J,; Weiss, J. *Inorg. Chem* **1985**, *24*, 3067. b) Wieghardt, K.; Küppers, H-J,; Raabe, E.; Krüger, C. *Angew. Chem. Intl. Ed. Engl.* **1986**, *25*, 1101. Küppers, H-J,; Neves, A.; Pomp, C.; Ventur, D.; Wieghardt, K.; Nuber, B.; Weiss, J. *Inorg. Chem* **1986**, *25*, 2400.

34. Blake, A. J.; Gould, R. O.; Holder, A. J.; Lavery, A. J.; Schröder, M. *Polyhedron,*, **1990**, *24*, 2919.

35. Blower, P.J.; Clarkson, J.A.; Rawle, S.C.; Hartman, J.A.R.; Wolf, R.E.; Yagbasan, R.; Bott, S.G.; Cooper, S.R. *Inorg. Chem.* **1989**, *28*, 4040-4046.

36. Blake, A. J.; Gould, R. O.; Halcrow, M. A.; Schröder, M. *J. Chem. Soc., Dalton Trans.* **1993**, 2909.

37. Blake, A. J.; Halcrow, M. A.; Schröder, M. *J. Chem. Soc., Chem. Comm.* **1991**, 253.

38. Blake, A. J.; Holder, A. J.; Hyde, T. I.; Roberts, Y. V.; Lavery, A. J.; Schröder, M. *J. Organomet. Chem.* **1987**, *323*, 261.

39. Blake, A. J.; Gould, R. O.; Holder, A. J.; Hyde, T. I.; Lavery, A. J.; Odulate, M. O.; Schröder, M. *J. Chem. Soc., Chem. Comm.* **1987**, 118.

40. Blake, A. J.; Gould, R. O.; Greig, J. A.; Holder, A. J.; Hyde, T. I.; Schröder, M *J. Chem. Soc., Dalton Trans.* **1989**, 118.

41. Kano, S. K.; Glass, R. S.; Wilson, G. S. *J. Am. Chem. Soc.* **1993**, *115*, 592.

42. Blake, A. J.; Gould, R. O.; Holder, A. J.; Hyde, T. I.; Reid, G.; Schröder, M. *J. Chem. Soc., Dalton. Trans.* **1990**, 1759.

43. Küppers, H-J.; Wieghardt, K.; Tsay, Y-H.; Kruger, C.; Nuber, B.; Weiss, J. *Angew. Chem. Intl. Ed. Engl.* **1987**, *26*, 575-576.

44. Clarkson, J.A.; Yagbasan, R.; Blower, P.J.; Cooper, S.R. *J. Chem. Soc., Chem. Comm.* **1989**, 1244-1245.

45. Bent, H. A. In *Organic Chemistry of Sulphur*; Oae, S., Ed; Plenum: New York, **1977**, p. 30.

46. a) Penfield, K. W.; Gerwith, A. A.; Solomon, E. *J. Am. Chem. Soc.* **1985**, *107*, 4519. b) Ashby, M. T. Ph.D. Dissertation, University of Arizona, **1986**

47. Ashby, M. T.; Enemark, J. H.; Lichtenberger, D. L.; Ortega, R. B. *Inorg. Chem.* **1986**, *25*, 3154.

48. Setzer, W. N.; Ogle, C. A.; Wilson, G. S.; Glass, R. S. *Inorg Chem.* **1983**, *22*, 266.

49. de Groot, B.; Loeb, S.J. *Inorg. Chem.* **1990**, *29*, 4084-4090.

50 de Groot, B.; Hanan, G.S.; Loeb, S.J. *Inorg. Chem.* **1991**, *31*, 4644-4647.

51. Giesbrecht, G.R.; Hanan, G.S.; Kickham, J.E.; Loeb, S.J. *Inorg. Chem.* **1992**, *31*, 3286-3291.

52. a) Hanan, G. S.; Kickham; J. E.; Loeb, S.J. *J. Chem. Soc., Chem. Comm.* **1991**, 893. b) Hanan, G. S.; Kickham; J. E.; Loeb, S.J. *Organometallics*, **1992**, *11*, 3063-3068.

53. a) Kickham, J. E.; Loeb, S. J. *J. Chem Soc., Chem. Comm.* **1993**, 1848. b) Kickham, J. E.; Loeb, S. J.; Murphy, S. L. *J. Am. Chem. Soc.* **1993**, *115*, 7031-7032. c) Kickham, J. E.; Loeb, S. J. *Inorg. Chem.* in the press.

54. a) de Groot, B.; Giesbrecht, G.R; Loeb, S.J.; Shimizu, G.K.H. *Inorg. Chem.* **1991**, *30*, 177-182. (Me_2TT[9]OC was also prepared following this method by A. Malats i Riera, visitng scientist to the University of Windsor, August, 1992.) b) de Groot, B.; Loeb, S. J. *J. Chem Soc. Chem. Comm.* **1990**, 1775.

55. Loeb, S.J.; de Groot, B. *Inorg. Chem.***1989**, *28*, 3573-3578.

56. Jenkins, H.A.; Loeb, S.J. *Organometallics* **1994**, *13*, 1840-1850.

57. Blake, A.J.; Gould, R.O.; Radek, C.; Schröder, M. *J. Chem. Soc., Chem. Comm.* **1994**, 985-986, and references therein.

58. de Groot, B.; Jenkins, H.A.; Loeb, S.J. *Inorg. Chem.* **1992**, *31*, 203-208.

59. Jordan, R.F.; Echols, S.F. *Inorg. Chem.* **1987**, *26*, 383-386.

60. TEXSAN-TEXRAY Structure Analysis Package, Molecular Structure Corp., 1985.

61. Cromer, D.T. *International Tables for X-ray Crystallography*; Kynoch Press: Birmingham, U.K., 1974; Vol. IV, Table 2.3.1.

62. Ibers, J.A.; Hamilton, W.C. *Acta. Crystallogr. A* **1964**, *17*, 781.

63. Cromer, D.T.; Waber, J.T. *International Tables for X-ray Crystallography*; Kynoch Press: Birmingham, U.K., 1974; Vol. IV, Table 2.2A.

64. a) Desper, J.M.; Powell, D.R.; Gellman, S.H. *J. Am. Chem. Soc.* **1990**, *112*, 4321-4324. b) Juaristi, E. *J. Chem. Educ.* **1978**, *56*, 438-441, and references therein.

65. Blake, A.J.; Gould, R.O.; Holder, A.J.; Hyde, T.I.; Schröder, M. *Polyhedron* **1989**, *8*, 513-518.

66. Clarkson, J.; Yagbasan, R.; Blower, P.J.; Rawle, S.C.; Cooper, S.R. *J. Chem. Soc., Chem. Comm.* **1987**, 950-951.

67. de Groot, B.; Loeb, S.J. *Inorg. Chem.* **1991**, *30*, 3103-3105.

68. Blake, A.J.; Collison, D.; Gould, R.O.; Reid, G.; Schröder, M. *J. Chem. Soc., Dalton Trans.* **1993**, 521-531.

69. Blake, A.J.; Reid, G.; Schröder, M. *J. Chem. Soc., Dalton Trans.* **1991**, 615-620, and references therein.

70. Blake, A.J.; Reid, G.; Schröder, M. *J. Chem. Soc., Chem. Comm.* **1992**, 1074-1076.

71. Saito, K.; Murakami, S.; Muromatsu, A. *Polyhedron* **1993**, *12*, 1587-1591.

72. Cotton, F.A.; Wilkinson, G. *Advanced Inorganic Chemistry 5th ed.*; Wiley-Interscience: New York, 1988.

73. Blake, A.J.; Gould, R.O.; Reid, G.; Schröder, M. *J. Chem. Soc., Chem. Comm.* **1990**, 974-976.

74. Lucas, C.R.; Liu, S.; Newlands, M.J.; Charland, J-P.; Gabe, E.J. *Can. J. Chem.* **1990**, *68*, 644-649.

75. Edema, J.J.H.; Buter, J.; Schoonbeek, F.S.; Kellogg, R.M.; van Bolhuis, F.; Spek, A.L.; *Inorg. Chem.* **1994**, *33*, 2448-2452.

76. Porterfield, W.W. *Inorganic Chemistry, a Unified Approach.* Addison-Wesley: Menlo Park, California, **1984**, p.92.

77. For reviews and leading references, see: a) Pierre, J-L.; Baret, P. *Bull. Soc. Chim. Fr. II* **1983**, 367-380. b) Schmidtchen, F.P. *J. Am. Chem. Soc.* **1986**, *108*, 8249-8255. c) Hawthorne, M.F.; Yang, X.; Zheng, Z. *Pure Appl. Chem.* **1994**, *66*, 245-354. d) Verboom, W.; Rudkevich, D.M.; Reinhoudt, D.N. *Pure Appl. Chem.* **1994**, *66*, 679-686. e) Beer, P.D.; Graydon, A.R. *J. Organomet. Chem.* **1994**, *466*, 241-247.

78. Valiyaveettil, S.; Engbersen, J.F.J.; Verboom, W.; Reinhoudt, D.N. *Angew. Chem. Intl. Ed. Engl.* **1993**, *32*, 900-901.

79. de Groot, B. M.Sc. Thesis, University of Manitoba, 1989.

80. a) Loeb, S.J.; Shimizu, G.K.H. *J. Chem. Soc., Chem. Comm.* **1991**, 1119-1121. b) Loeb, S.J.; Shimizu, G.K.H. *Synlett.* **1992**, 823-824. c) Loeb, S.J.; Shimizu, G.K.H. *Inorg. Chem.* **1993**, *32*, 1001-1006.

81. Shimizu, G.K.H. Ph.D. Dissertation, University of Windsor, 1993.

82. Loeb, S.J. Shimizu, G.K.H. *Can. J. Chem.* **1994**, *72*, in the press.

83. Loeb, S.J.; Shimizu, G.K.H. *J. Chem. Soc., Chem. Comm.* **1993**, 1395-1397.

84. (a) Bianchini, C.; Meli, A.; Peruzzini, M.; Vizza, F.; Zanobini, F. *Coord. Chem. Rev.* **1992**, *120*, 193-208, and references therein. (b) Bianchini, C.; Farnetti, E.; Graziani, M.; Kaspar, J.; Vizza, F. *J. Am. Chem. Soc.* **1993**, *115*, 1753-1759. (c)

Barbaro, P.; Bianchini, C.; Meli, A.; Peruzzini, M.; Vacca, A.; Vizza, F. *Organometallics*, **1991**, *10*, 2227-2238.

85. (a) Janowicz, A. H.; Bergman, R. G. *J. Am. Chem. Soc.* **1983**, *105*, 3929-3939. (b) Hoyano, J. K.; McMaster, A. D.; Graham, W. A. G. *J. Am. Chem. Soc.* **1983**, *105*, 7190-7191. (c) Jones, W. D.; Feher, F. J. *J. Am. Chem. Soc.* **1986**, *108*, 4856-4867. (d) Jones, W. D.; Feher, F. J. *Acc. Chem. Res.* **1989**, *22*, 91-100, and references therein.

86. (a) Ghosh, C. K.; Graham, W. A. G. *J. Am. Chem. Soc.* **1987**, *109*, 4726-4727. (b) Ghosh, C. K.; Graham, W. A. G. *J. Am. Chem. Soc.* **1989**, *111*, 375-376. (c) Jones, W. D.; Hessel, E. T. *J. Am. Chem. Soc.* **1992**, *114*, 6087-6095.

87. Blake, A. J.; Halcrow, M. A.; Schröder, M. *J. Chem. Soc. Chem. Comm.* **1991**, 253-256.

88. Yoshida, T.; Ueda, T.; Adachi, T.; Yamamoto, K.; Higuchi, T. *J. Chem. Soc., Chem. Comm.* **1985**, 1137-1138.

89. Blake, A. J.; Holder, A. J.; Hyde, T. I.; Küppers, H. J.; Schröder, M.; Stotzel, S.;Wieghardt, K. *J. Chem. Soc., Chem. Comm.*, **1992**, 1600-1602.

90. Hanton, L. R.; Kemmitt, T. *J. Chem. Soc., Chem. Comm.* **1991**, 700-702.

91. Giordano, G. *Inorg. Synth.* **1979**, *19*, 218-220.

92. Uson, R.; Oro, L. A.; Cabeza, J. A. *Inorg. Synth.* **1985**, *23*, 126-128.

93. van der Ent, A.; Onderdelinden, A. L. *Inorg. Synth.* **1974**, *14*, 94-95.

94. Collman, J. P.; Hegedus, L. S. *Principles and Applications of Organotransition Metal Chemistry*. University Science Books: Mill Valley California, **1988**.

95. Louie, B.M.; Rettig, S.J.; Storr, A.; Trotter, J. *Can. J. Chem.* **1984**, *62*, 633-637.

96. a) Lecomte, J-P.; Lehn, J-M.; Parker, D.; Guilhem, J.; Pascard, C. *J. Chem. Soc., Chem. Comm.* **1983**, 296-298. b) Parker, D. *J. Chem. Soc., Chem. Comm.* **1985**, 1129-1131.

97. Gordon, G.; DeHaven, P.W.; Weiss, M. C.; Goedken, V.L. *J. Am. Chem. Soc.* **1978**, *100*, 1003-1005.

98. Martin, A. E.; Bulkowski, J.E. *J. Organomet. Chem.* **1981**, *217*, C29-C33, and references therein.

99. a) Pandey, K. K. *Coord. Chem. Rev.* **1983**, *51*, 69-98. b) McCleverty, J. *Chem. Rev.* **1979**, *79*, 53-76. c) Enemark, J. H.; Feltham, R. D. *Coord. Chem. Rev.* **1974**, *13*, 339. d) Caulton, K. G. *Coord. Chem. Rev.* **1975**, *14*, 317.

100. (a) Collman, J. P.; Farnham, P. H.; Dolcetti, G. *J. Am. Chem. Soc.* **1971**, *93*, 1789-1790. (b) Brock, C. P.; Collman, J. P.; Dolcetti, G.; Farnham, P. H.; Ibers, J. A.; Lester, J. E.; Reed, C. A. *Inorg. Chem.* **1973**, *6*, 1304-1313.

101. Jardine, F.H. *Prog. Inorg. Chem.* **1984**, *31*, 265-370.

102. 5a) Cannadine, J. C.; Hector, A.; Hill, A. F. *Organometallics* **1992**, *11*, 2323-2324. b) Hill, A. F.; Alcock, N. W.; Cannadine, J. C.; Clark, G. R. *J. Organomet. Chem.* **1992**, *426*, C40-C43. c) Alcock, N. W.; Cannadine, J.C.; Clark, G. R.; Hill, A. F. *J. Chem. Soc., Dalton Trans.* **1993**, 1131-1135.

103. Bennett, M. A.; Goh, L. Y.; Willis, A.C. *J. Chem. Soc., Chem. Comm.* **1992**, 1180-1182.

104. 8a) Sellmann, D.; Kappler, O. *Angew. Chem. Intl. Ed. Engl.* **1988**, *27*, 689-691.

105. Hallman, P. S.; Stephenson, T. A.; Wilkinson, G. *Inorg. Synth.* **1970**, *12*, 237-239.

106. Hallman, P. S.; McGarvey, B. R.; Wilkinson, G. *J. Chem. Soc. (A)* **1968**, 3143-3150.

107. Bell, M. N.; Blake, A. J.; Schröder, M.; Kuppers, H-J.; Wieghardt, K. *Angew. Chem. Intl. Ed. Engl.* **1987**, *26*, 250-251.

108. de Groot, B.; Loeb, S. J., unpublished results. The complex $RuCl_2(DMSO)(TT[9]OC)$was prepared by refluxing a DMF solution of $RuCl_2(DMSO)_4$ and TT[9]OC in a 1:1 ratio. After removal of solvent under reduced pressure, $RuCl_2(DMSO)TT[9]OC)$ was isolated in 65%. Yield Anal. Calcd for $C_{14}H_{22}Cl_2S_4ORu$: C: 33.19; H: 4.39. Found: C: 33.10; H:4.37. Yellow crystals of the complex suitable for X-ray diffraction were obtained by diffusion of diethyl ether into a DMSO solution of the complex; data collection parameters, positional, and bonding parameters are listed in Tables A.5.4, A.5.5, and A.5.6 respectively.

109. a) Haymore, B. L.; Ibers, J. A. *Inorg. Chem.* **1975**, *14*, 3060-3067. b) McCleverty, J. A. *Chem. Rev.* **1979**, *79*, 53-76.

110. Nixon, J. F.; Pidcock, A. *Ann. Rev. NMR Spectrosc.* **1969**, *2*, 245.

111. Hoffman, P. R.; Caulton, K. G. *J. Am. Chem. Soc.* **1975**, *97*, 4221-4228.

Vita Auctoris

Personal Information:

Name:	Hilary Anne Jenkins
Year of Birth:	1962
Place of Birth:	Winnipeg, Manitoba, Canada

Education:

University of Winnipeg, Winnipeg, Manitoba
1980-1985 Bachelor of Science

University of Manitoba, Winnipeg, Manitoba
1985-1988 Master of Science

Publications:

7. H. A. Jenkins, S. J. Loeb "Thiacyclophane Complexes of Rhodium and Iridium. Synthesis, Structure and Reactivity of $[M(COD)(L)][BF_4]$, (M = Rh, Ir) and (L = 2,5,8-Trithia[9]-*o*-cyclophane, TT[9]OC, 5-Oxa-2,8-dithia[9]-*o*-cyclophane, ODT[9]OC)" *Organometallics* **1994**, *13*, 1840-1850.

6. B. de Groot, H. A. Jenkins, S. J. Loeb "Exodentate Versus Endodentate Coordination of a Crown Thioether Ligand in Silver(I) Complexes of 2,5,8-Trithia[9]-*o*-benzenophane (TT[9]OB). Structures of $[Ag(TT[9]OB)_2][X]$ (X = ClO_4, BPh_4, CF_3SO_3)." *Inorganic Chemistry* **1992**, *31*, 203-208.

5. H. A. Jenkins, S. J. Loeb, D. G. Dick, D. W. Stephan "Dihydride Formation Versus H_2-Loss in the Protonation of the Heterobimetallic FePt Complex $(CO)_3Fe(\mu\text{-}H)(\mu\text{-}PCy_2)Pt(PEt_3)_2$." *Canadian Journal of Chemistry* **1990**, *68*, 869-874.

4. H. A. Jenkins, S. J. Loeb, "Synthesis and Reaction Chemistry of the Heterobimetallic FeIr Complexes $(CO)_3(PPh_3)Fe(\mu\text{-}PCy_2)Ir(PPh_3)(CO)_2$ and $(CO)_4Fe(\mu\text{-}PCy_2)Ir(1,5\text{-}COD)$." *Canadian Journal of Chemistry* **1989**, 67, 1230-1235.

3. H. A. Jenkins, S. J. Loeb, D. W. Stephan "Synthesis and Reaction Chemistry of the Coordinatively Unsaturated Heterobimetallic Complexes $(CO)_3(PPh_3)Fe(\mu\text{-}PCy_2)Rh(PPh_3)(CO)$ and $(CO)_4Fe(\mu\text{-}PCy_2)Rh(1,5\text{-}COD)$. Crystal

*Taylor is my previous surname.

and Molecular Structure of $(CO)_3(PPh_3)Fe(\mu\text{-}PCy_2)Rh(PPh_3)(CO)$." *Inorganic Chemistry* **1989**, *28*, 1998-2003.

2. H. A. Jenkins, S. J. Loeb, N. T. McManus, "$(CO)(PEt_3)ClIr(\mu\text{-}PCy_2)_2IrCl(PEt_3)(CO)$, A Phosphido-Bridged Bimetallic Ir(II) Complex." *Inorganica Chimica Acta* **1989**, *159*, 83-86.

1. S. J. Loeb, H. A. Taylor*, L. Gelmini, D. W. Stephan "Heterobimetallic Dicyclohexylphophido-Bridged Complexes of MoNi, MoPd, MoPt, WNi, WPd, and WPt. Crystal and Molecular Structure of $(CO)_4Mo(\mu\text{-}PCy_2)_2Pd(PPh_3)$." *Inorganic Chemistry* **1986**, *25*, 1977-1982.

Conference Presentations

7. H.A. Jenkins, S.J. Loeb "Crown Thioether Complexes of Ru(II)." *77th Canadian Chemical Conference and Exhibition*, Winnipeg, Manitoba, **1994**.

6. H.A. Jenkins, S.J. Loeb "Crown Thioether Complexes of Rhodium and Iridium." *Inorganic Discussion Weekend*, Guelph, Ontario, **1993**.

5. H.A. Jenkins, S.J. Loeb "Crown Thioether Complexes of Rhodium and Iridium." *74th Canadian Chemical Conference and Exhitibion*, Hamilton, Ontario, **1991**.

4. H.A. Jenkins, S.J. Loeb "Structural Diversity in Silver Complexes of the Crown Thioether Ligand TT[9]OB." *74th Canadian Chemical Conference and Exhibition*, Hamilton, Ontario, **1991**.

3. H.A. Jenkins, S.J. Loeb "Structural Diversity in Silver Complexes of the Crown Thioether Ligand TT[9]OB." *American Chemical Society, Joint Central-Great Lakes Regional Meeting*, Indianapolis, USA, **1991**.

2. H.A. Jenkins, S.J. Loeb "Binuclear Dicyclohexylphosphido-Bridged FeRh and FeIr Complexes." *70th Chemical Institute of Canada Conference*, Quebec City, Quebec, **1987**.

1. S.J. Loeb, H.A. Taylor* "Binuclear Dicyclohexylphosphido-Bridged MoNi, MoPd, and MoPt Complexes." *XIIth International Conference on Organometallic Chemistry*, Vienna, Austria, **1985**.

*Taylor is my previous surname.